DESIGN, FABRICATION AND CHARACTERIZATION OF AN APPROPRIATE SOLAR THERMAL ELECTRICITY GENERATING SYSTEM

MILLIEN KAWIRA ERASTUS

DOCTOR OF PHILOSOPHY

(Energy Technology)

JOMO KENYATTA UNIVERSITY OF AGRICULTURE AND TECHNOLOGY

2015

Design, Fabrication and Characterization of an Appropriate Solar Thermal Electricity Generating System

Millien Kawira Erastus

A Thesis Submitted in Partial Fulfillment for the Degree of Doctor of Philosophy in Energy Technology in the Jomo Kenyatta University of Agriculture and Technology

2015

DECLARATION

This thesis is my original work and has not been presented for a degree in any other university.

Signature…….. Date…….

Millien Kawira Erastus

This thesis has been submitted for examination with our approval as the university supervisors.

Signature:…… Date……..

Prof. Robert Kinyua

JKUAT, Kenya

Signature:…… Date:…….

Dr. J. Ngugi Kamau

JKUAT, Kenya

DEDICATION

To my dear mother, Beatrice Ciakathia for the support and encouragement.

ACKNOWLEDGEMENT

This research work consists of contributions from many people. I take this opportunity to express my special gratitude to:

1. JKUAT fraternity as whole and in particular my supervisors Prof. Robert Kinyua and Dr. J Ngugi Kamau for their moral, material, financial and exemplary guidance and visionary suggestions throughout the research period. Their technical expertise and knowledge were very useful in meeting the objectives of the study. I also thank them for sacrificing and being present whenever an issue arose and the expediency with which they addressed the task at hand, especially at the research site. They were a source of motivation throughout the course.
2. IEET and BPS for providing checks and balances and support during undertaking of the research.
3. Physics Department for lending me measuring equipment and to all the members of the Physics Department for their useful contribution in various ways. I also thank Mr. Olume, Mr. Mwangi and Mr. Adenya of the Physics Department for their technical assistance.
4. Finally, I thank my family and friends for their support during the research undertaking.

TABLE OF CONTENTS

LIST OF TABLES

LIST OF FIGURES

LIST OF APPEDINCES

LIST OF ABBREVIATIONS

ASHRAE	American Society of Heating, Refrigerating and Air Conditioning Engineers
ASME	American Society of Mechanical Engineers
CSP	Concentrated Solar Power
GI	Galvanized Iron Pipe
NBS	National Bureau of Standards
NREL	National Renewable Energy Laboratory
PTSC	Parabolic Trough Solar Concentrator
PPR	Polypropylene
SEGS	Solar Energy Generating Station
SWERA	Solar and Wind Resource Assessment
TEMA	Tubular Exchangers' Manufacturers Association
ETSAP	Energy Technology Systems Analysis Program

NOMENCLATURE

$\boldsymbol{\theta}$	Angle between incident flux beam and normal to a plane surface (^{o})
$\boldsymbol{\theta_z}$	Zenith angle (^{o})
$\emptyset$	Latitude (^{o})
$\emptyset_{\boldsymbol{r}}$	Rim angle of concentrator (^{o})
$\boldsymbol{\delta}$	Declination (^{o})
$\boldsymbol{\varphi}$	Surface azimuth angle (^{o})
$\boldsymbol{\omega_t}$	Hour angle (^{o})
$\boldsymbol{\omega}$	Distance from the center of zone of solar image (m)
$\boldsymbol{d}$	Half width aperture of concentrator (m)
$\boldsymbol{\beta}$	Angle of inclination or slope (^{o})
$\boldsymbol{r_b}$	Tilt factor for beam radiation
$\boldsymbol{r_d}$	Tilt factor for diffuse radiation
$\boldsymbol{I_b}$	Incident flux beam (Wm^{-2})
$\boldsymbol{I_T}$	Solar flux falling on a surface (Wm^{-2})
$\boldsymbol{I_d}$	Diffuse flux beam (Wm^{-2})
$\boldsymbol{I_{\lambda s}}$	Wavelength dependent specular reflected intensity (Wm^{-2})
$\boldsymbol{I_{\lambda j}}$	Wavelength dependent incident intensity (Wm^{-2})
$\boldsymbol{I_g}$	Flux on a horizontal surface (Wm^{-2})
$\boldsymbol{I_{max}}$	Maximum flux density (Wm^{-2})
$\boldsymbol{I}$	Radiative flux density at radial position from axis r/R (Wm^{-2})
$\mathbf{I}(\boldsymbol{\omega})$	Radiant flux density (Wm^{-2})
$\boldsymbol{r_r}$	Radiation shape factor
$\boldsymbol{\gamma_r}$	Rim radius (m)
$\boldsymbol{r}$	Radius in focal plane from axis (m)
$\boldsymbol{R}$	Rim radius of concentrator (m)
$\boldsymbol{CR}$	Concentration ratio

$\boldsymbol{\rho}$	Spectral reflectance
$\boldsymbol{F}$	Focal length (m)
$\boldsymbol{F''}$	Collector flow factor
$\boldsymbol{F'}$	Collector efficiency factor
$\boldsymbol{F_R}$	Collector heat removal factor
$\boldsymbol{a}$	Aperture (m)
$\boldsymbol{\dot{m}}$	Mass flow rate (kgs^{-1})
$\boldsymbol{q_u}$	Concentrator useful heat gain (J)
$\boldsymbol{A_c}$	Collector area (m^2)
$\boldsymbol{A_b}$	Calorimeter base
$\boldsymbol{A_a}$	Aperture area (m^2)
$\boldsymbol{A_r}$	Area of receiver (m^2)
$\boldsymbol{A_s}$	Surface area of reflector (m^2)
$\boldsymbol{T_2}$	Outlet temperature of heat transfer fluid (^oC)
$\boldsymbol{T_1}$	Inlet temperature of heat transfer fluid (^oC)
$\boldsymbol{T_m}$	Mean temperature of heat transfer fluid (^oC)
$\boldsymbol{H_b r_b}$	Solar flux intensity (Wm^{-2})
$\boldsymbol{\alpha}$	Spectral absorptance
$\boldsymbol{\tau}$	Transmittance
$\boldsymbol{L}$	Length of collector (m)
$\boldsymbol{U_L}$	Heat loss coefficient (Wm^{-2})
$\boldsymbol{\gamma}$	Intercept factor (Wm^{-2})
$\boldsymbol{T_a}$	Ambient temperature (^oC)
$\boldsymbol{S}$	Absorbed solar radiation (Wm^{-2})
$\boldsymbol{Q_u}$	Total heat gain by receiver (Jm^{-2})
$\boldsymbol{\dot{Q}_{elec}}$	Rate of electricity power use (Ws^{-2})
$\boldsymbol{Q_{av}}$	Average heat absorbed by receiver (J)
$\boldsymbol{\eta_c}$	Collector efficiency (%)
$\boldsymbol{\eta_{opt}}$	Optical efficiency (%)

$\boldsymbol{h}$	Normal flux distribution coefficient (Wm^{-2})
$\boldsymbol{\sigma}$	Standard deviation of the normal distribution curve (m^2W^{-1})
$\boldsymbol{\lambda}$	Wavelength (m)
$\boldsymbol{\varepsilon}$	Emissivity
$\boldsymbol{\Delta f}$	Energy increment (J)
$\boldsymbol{P}$	Pressure (Nm^{-2})
$\boldsymbol{m}$	Mass (kg)

ABSTRACT

The sun provides an abundant and clean source of energy. However the supply of this energy is periodic following yearly and diurnal cycles, intermittent, unpredictable and it is diffused. Its density is low compared to the energy flux densities found in convectional fossil energy sources like coal or oil. There have been attempts to produce solar thermal power using parabolic trough technology as was demonstrated by Luz Company which built a solar electricity generating station with a power output of 354 MW in USA. Also the largest solar power plants in the world using parabolic trough technology are the Andasol 1 to 3 which are established in Spain. Therefore it was necessary to undertake design and fabrication of a solar thermal electricity generating system consisting of a collector, steam storage system, heat exchanger, turbine and generator as a local solution for power production. The design layouts were done using auto cad. The testing of the steam storage system and the heat exchanger were done using TEMA (Tubular Exchangers Manufacturers Association Standard and ASME (American Society of Mechanical Engineers). Locally produced heat transfer fluids (water, saline solutions, vegetable oils and engine oils) were tested for their suitability in solar power production using guidelines obtained from National Renewable Energy Laboratories. Some of the parameters investigated included mass flow rates, power output, efficiency, steam flow rate, heat absorbed, heat emitted, evaporation ratio, proportion of flash steam, number of heat transfer units among others. The efficiencies of the concentrator when using the heat transfer fluids were in the range of 48.8% to 60.1% for closed collector and in the range of 46.7% to 56.6% for the open collector. The length of complete discharge for the steam storage system ranged from 4.4 hrs to 6.9 hrs. The power output for the heat transfer fluids were in the range of 287.9 W to 467 W. The steam storage was found to have an efficiency of 93.5 % and a thermal capacity of 4.54×10^{3} kJ. The rate of heat transfer was an average of 68.4 $Js^{-1}kg^{-1}$ to 46.3 $Js^{-1}kg^{-1}$. The thermal efficiency for the heat transfer fluids was in the range of 0.85 to 0.66. Available power from the impulse type turbine was 478.4 Watts, isentropic efficiency was 83.5 %, cycle power output was 497.8 W, turbine output was 468.2 W

and gear efficiency was 87.9 % and generator efficiency of 86.9 %. The overall efficiency of the system was 34.97%. Coupling of the steam storage system and the heat exchanger increased the capacity of steam storage to 4.15×10^3 KJ, at a maximum temperature of 249.5 °C and at a pressure of 7.2×10^5 Nm^{-2}. Coupling of the steam storage system and the heat exchanger increased the capacity of steam storage to 4.15×10^3 kJ, at maximum temperatures of 249.5 °C and at a pressure of 7.2×10^5 Nm^{-2}. A single stage impulse turbine was fabricated which had an average efficiency of 61.6% and a maximum power output of 498 W. The solar thermal characterization and collection was done in solar intensities of the average range 700 Wm^{-2} to 1100 Wm^{-2}. In Coolidge irrigation facility, a thermocline storage tank has a capacity of 19.8 GJ and operates at a temperature of 288 °C. The thermal capacity of the storage system used in this study was 4.15×10^3kJ and was operating at a temperature of 249.9 °C.

CHAPTER ONE

INTRODUCTION

1.1 Background

Parabolic trough solar concentrators provide a sustainable way of generating power from the sun. Technical use of solar energy presently poses problems primarily because of inefficient collection and storage (Bayon *et al.,* 2010). Enhancement of technologies that generate power from renewable energy and alternative sources are a dependable way of cutting down on dependency on carbon based fuels and negative environmental impacts of acid rain, reduced ozone layer and global warming. Solar trough technologies are the most widely used solar thermal technologies.

(Patrick *et al.,* 2013). Solar technologies have the potential of lowering the cost of power generation since the sun is the most abundant source of renewable energy over the centuries (Ercan, 2006).

Direct steam generation and production of power from organic heat transfer fluids by use of parabolic trough solar concentrator and a storage system is a possible technology for producing electricity for all uses (Kruger, 2008). There are three forms of energy used in industrial processes which are electricity, direct fired heat and steam (SWERA, 2010). Electricity is applied in mechanical drive, heating and electrochemical processes among other uses. Direct fired energy is applied to directly transfer heat of fuel to a process while steam provides process heat, mechanical drive, component separation and a source of water for many reactions (Solar power, 2011). The advantages of steam in delivering energy are: - nontoxic nature, transportability, high efficiency, higher heat capacity and a lower cost compared to other alternative means of producing power. Steam holds between 1050 – 1312 kJ/kg of heat that can be extracted as mechanical work through a turbine or as process heat (ETSAP, 2013). In 2006, United States manufacturers used about 5000 trillion kilojoules of steam which represents about 40 % of the total energy used in industrial process applications for product output. Forest

products used 2222.85 trillion kJ of energy accounting for 76% of the total onsite energy, excluding feed stocks used in this industry. Chemical industry used 1579.2 kJ of energy to generate steam which represents about 47 % of the onsite energy excluding feedstock. Petroleum refining industry used about 960.75 trillion kJ of energy to generate steam which accounts for about 28 % of this industry's total onsite energy use (Kearney *et al.,* 2002). Developing efficient and less expensive energy storage devices is as important as developing new sources of energy (Bayon, 2010). Figure 1.1 shows that more than three quarters of electricity consumed in the world comes from fossils fuels. The environmental pollution has been increasing with their use. However renewable energy resources are gaining command of energy market share that has potential of reducing the use of fossil fuels with time.

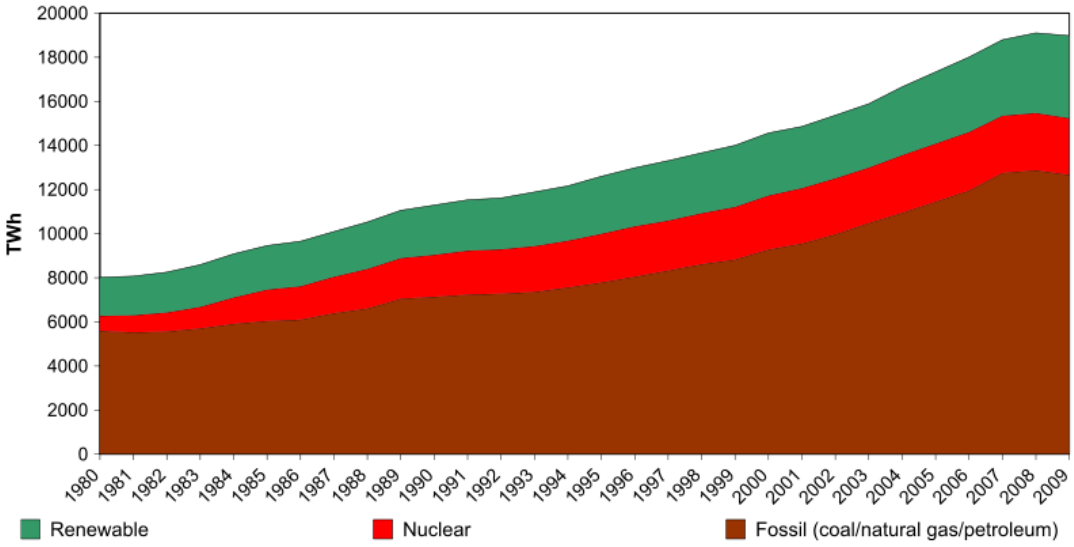

Figure 1. 1: Annual net electricity generation in the world (SWERA, 2009)

The main parts of a solar thermal plant are therein covered in sections 1.2 through 1.6. However in the direct steam generation the heat exchanger is not part of the system since the heat transfer fluid is the one which is used to turn the turbine blades.

1.2 Heat exchanger

There are various types of heat exchangers that include tube and shell, plate tube exchangers' among others (Gawande *et al.*, 2007). The choice of heat exchanger to use depends on the intended application. A heat exchanger transfers thermal energy from one fluid to another. In a heat exchanger steam transfers some of its heat content to a process fluid. The basic heat exchanger design property relates the rate of heat transfer between two fluids in the heat exchanger, overall heat transfer coefficient, heat transfer surface area and the logarithmic mean temperature difference. The heat transfer rate is calculated from the flow of one of the fluids, its heat capacity and the required temperature change. The flow of heat in a heat exchanger is from a liquid at a higher temperature to one at a lower temperature. The larger the heat transfer surface area the higher the cost of the heat exchanger. Besides the permissible pressure drop is evaluated to approximate the cost to be incurred. The performance of a heat exchanger can be found by the percentages losses or gains. If the exchanger is well insulated the heat emitted by the hot stream is equivalent to the heat absorbed by the water at ambient temperature stream. The temperature efficiency is found by comparing the maximum temperature difference between the two fluid streams for a heat exchanger of infinite size.

1.3 Steam Turbine

In a steam turbine the kinetic energy of steam is converted to mechanical work that drives shaft of a generator. The condensed steam is recycled in energy recovery process. Steam expands in volume with great velocity as compared to water. For higher efficiency a steam turbine should operate at a very high speed (Hewitt, 2002). The kinetic energy of steam provides energy of rotation of the shaft and the blades. The reduction in internal energy of steam is transformed into mechanical energy from acceleration of the particles of steam. Some essential parts of a steam turbine include nozzle, blades, shaft and the outer casing. Steam flows and expands through the nozzle. The temperature of steam drops as kinetic energy is gained from it. The steam impacts

on the blades and the blade wheel on which blades are fixed rotates with the frequency of the shaft. The blades are mounted on the blade wheel. The shaft carries the blade wheel and turns the rotor of the generator. The outer casing confines the steam to the area of the turbine. Bearings support the shaft. The sealing prevents the steam from leaking. Multistage turbines extract more heat from steam since each stage extracts a small amount of thermal energy which is converted to kinetic energy. In a single turbine where the entire conversion takes place at once, the rotation speed of the turbine becomes excessive and energy is lost (Jachen, 1996). Steam turbines are used in powering of ships, generation of nuclear power, fuel powered boilers, power machines, pumps, compressors, electricity generation etc.

1.4 Generator

It provides electrical power output from the input of mechanical power at a fixed voltage and frequency. Examples of three phase circuits include delta three phases and three phases. It is necessary for a three phase circuit to have a neutral wire. An electric generator generates currents that are the same frequency but out of phase by 120^{o} to provide three phases. Bringing a three phase circuit to a rack has the following effect on distribution, which are advantageous when compared to a single phase distribution. These are the lowering of the material and installation costs, lower installation time with fewer whips to pull, use of less wire under the floor which improves air flow and reduces wiring confusion and mistakes and finally it enables simplified load balancing with all the phases available in the rack (Minassians *et al.*, 2004). The balance at the rack has positive effect on the entire facility. A three phase system with a total of 15 kW load and a conductor current of 42 A has significantly less amperage than the 125 A required for a conductor of a single phase system (Stevenson *et al.*, 2001).

1.5 Parabolic Trough Solar Collector

Parabolic trough solar technology is the most proven with the lowest cost, large scale solar power technology available today given the example of the nine large commercial

scale solar power plants that are operating in California, Mojave desert (Hank *et al*., 2002).

Parabolic trough plants are the most popular concentrators for solar plant applications with increased maximum operational temperatures of 400 ^{o}C to 500 ^{o}C and hence thermal efficiency (Murphy & Kenneth, 2001). A practical feasibility of direct steam in parabolic steam power generation technology has been proven in recent years, reaching temperatures of 400 ^{o}C at pressures of 1.0×10^{7} Nm^{-2} (Eck *et al*., 2003). The need for thermal power by various industries varies between low temperature thermal energy used for space heating to high temperature thermal energy required for metal processing. Saturated steam is used because it provides large amounts of heat at constant temperature (World Bank, 2010). A parabolic trough solar collector consists of optical reflecting system, receiver that collects the solar thermal energy and passes it to a heat transfer fluid, glass cover on the collector itself or on the evacuated receiver, storage and thermal power conversion units. The receiver tracks the sun to ensure all radiation normal to the collector aperture is collected. The collector tracks the sun on a single axis aperture. Figure 1.2 shows the essential components of a cylindrical solar collector.

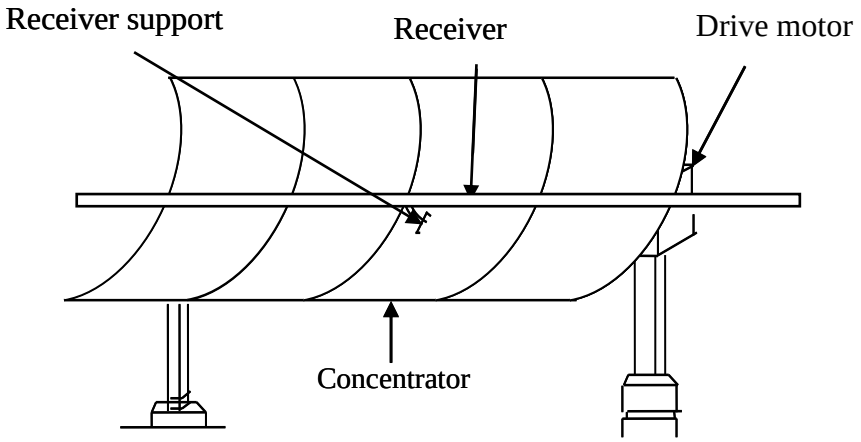

Figure 1. 2: Cylindrical parabolic concentrating collector

Steam is generated in parabolic trough solar concentrator and pressurized in the steam storage system. In the coupled system it is generated and pressurized in both the steam storage system and in the heat exchanger. Parabolic trough solar concentrator (PTSC) power production is gaining acceptance as a major source of steam to drive turbines for electricity production compared to other sources concentrated power (Duffie & Beckman, 2005). Parabolic trough solar concentrator constitutes a proven source of thermal energy for power generation and industrial process heat (Stine *et al.*, 2001). The Sudan PTSC had the following characteristics:- length, 5 m, aperture width 2.35 m, rim angle of 72^{o}, focal length of 0.78 m, receiver diameter of 4.67 m, geometric concentration ratio of 50.3 and collector height of 0.42 m (Eltahir *et al.*, 2012). Both evacuated glass shielded receiver and an unshielded receivers were tested in South Africa and peak thermal efficiencies obtained were 53.8 % and 52.2 % respectively (Brooks *et al.*, 2006). Receiver efficiency is defined as the ratio of the average power absorbed by the working fluid to the average power incident on the receiver evaluated over a defined period under a steady state condition. The purpose of characterization tests in the case of Brooks and others was to measure the performance of steam

generation system and the electric power generation system over a range of power loads and their inlet temperatures under steady conditions.

Other types of solar collectors include:

Compound parabolic collectors: These are non-imaging concentrators which are capable of reflecting all the incident radiation within wide limits. They accept incoming radiation over relatively wide range of angles. Multiple internal reflections are utilized for concentration of solar flux

Linear Fresnel reflector: An array of mirror strips concentrate light onto a fixed receiver mounted on a linear tower. The array of the mirrors does not need to be in form of a parabola. Large absorbers are usually constructed and the absorber does not require moving.

Parabolic dish reflector: This is a point focus collector that tracks the sun in two axes. Solar flux is concentrated onto a receiver located at the focal point of the dish.

Heliostat field collector: This collector is used for high input of solar energy. Many flat mirrors known as heliostats that us altazimuth mounts are used to reflect incident direct solar radiation on to a common absorber.

1.6 Steam Storage System

A storage system is used for storing excess steam when the demand is less than the supply in solar power generating systems. In this study water was initially put in the storage system before charging of the steam storage system. During the charging phase the incoming steam from the collector raised the heat content and the temperature of the steam in the storage system. In this system when there is cloud cover and the solar power intensity reduces, the reduction of pressure in the storage system causes flashing of steam in the system and hence there is a continuous supply of power depending on the demand needs. The development of a thermal storage system and increase of operational temperature of a parabolic trough solar concentrator and consequently electricity generated reduces the cost of electricity and hence increasing its accessibility (Arnold, 2010). Energy storage and its conversion to electrical power is an important step in solar

thermal technologies. The storage system enhances efficient use of solar thermal power from the sun and ensures optimization of solar energy (Earcan, 2006). There is a challenge of identifying and developing a new heat transfer and thermal storage fluids that would improve economics and operational characteristics for parabolic trough electric systems (Pacheo, 2002). Thermal storage is not a new concept and has been used for centuries. Energy storage can reduce time or rate of mismatch between energy supply and energy demand by load levelling. Johnson and Johnson system currently used in Sherman, Texas has a large flash tank system that provides energy storage (Solar Steam Power, 2011). The system uses solar energy collected by a field of parabolic trough collectors to produce steam for gauze bleaching process. The collector field is 1070 m^2. The parabolic trough solar concentrator (PTSC) uses pressurized water from the collector field which is pumped through a throttle valve, reducing the pressure slightly and then into the flash boiler storage tank. Water is pumped from the bottom of the storage tank into the field to receive additional heating. When the pressure is needed, the pressure of the flash boiler is reduced slightly to the saturation pressure of water in the storage. The water in the tank then boils and is pushed through a throttle valve into the plant steam lines.

Storage systems consisting of a mixture of crushed rock, sand and caloria HT-43 heat transfer fluid and another one made of a 2.5Mh backed bend thermocline with binary molten salt and a quartzite rock sand as a filler material were demonstrated at Sandia National Laboratories (Sandia National Laboratory, 2004). In Berlin Island grid, a power plant producing 50 MW electric power was operated which had steam accumulators of 67 MW storage capacity (Beckmann & Gilli, 1984).

The present study intends to design, fabricate, test and characterize a solar thermal storage system, a solar thermal turbine and generator, heat exchanger, a solar collector and test and characterize various thermal storage fluids.

1.7 Objectives

1.7.1 Main Objective

To design, fabricate and characterize an appropriate solar thermal electricity generating system.

1.7.2 Specific Objectives

1. To design and characterize a solar thermal steam storage system.
2. To design and fabricate a solar thermal steam turbine.
3. To design and fabricate an appropriate electrical generator.
4. To perform thermal characterization of saline solutions, vegetable oils, used engine oil and unused engine oil and examine their suitability as heat transfer fluids in terms of amounts of heat absorbed and emitted by each.
5. To study performance of a prototype parabolic trough solar collector using vegetable oils, used and unused engine oil and saline solutions.

1.8 Statement of the Problem

Over dependence on fossil fuels to supply high voltage power has resulted to environmental pollution and global warming. Means to supply high voltage power from the sun besides ensuring reliability will ensure that environmental pollution and global warming are reduced. Solar flux is readily available and the technology to harness solar power is the limiting factor. Large scale fabrication of solar thermal power transducers will demystify production of solar power giving it more acceptances for use. In this study locally available materials such as black iron sheets will be used for fabrication of power production components such as collector, steam storage system, heat exchanger, turbine and some parts of the generator. This will reduce the amount of greenhouse gases accumulating in the atmosphere and reduce environmental pollution and global warming.

1.9 Justification

The fabrication of turbine, generator and heat exchanger using locally available materials and also improving the efficiency of a parabolic trough solar concentrator provides a means of producing power at a lower cost. The improvement of the performance of the collector was achieved by use of an optical system of higher efficiency i.e. 0.92. The materials are locally available and hence there is potential of production of large scale power to provide electricity to remote areas that are off grid. Lack of technical knowledge on use of locally available materials has hindered the growth of this kind of undertaking. Besides ensuring energy security, this way of producing power shall prevent tons of carbon dioxide emissions annually reducing negative climatic changes and also reducing accumulation of greenhouse gases in the atmosphere.

CHAPTER TWO

LITERATURE REVIEW

2.1 Introduction

In this section previous work related to heat exchanger, steam storage, solar collector and power generation is presented. The main equations and some design considerations as given by the scholars are given.

2.2 Heat Exchanger

In a study conducted by Valan and Sornakumart (Valan & Sornakumart, 2006, thermal design considerations in the design of the shell and tube heat exchanger includes determination of heat transfer area, number of tubes, tube length and diameter, tube lay out, number of shell and tube passes, type of heat exchanger, tube pitch, number of baffles, type and size and pressure drop. Tube and shell heat exchangers are typically used for high pressure application of 3.0×10^7 Nm^{-2} and temperatures greater than 260 ^oC (Srinivasa *et al.,* 2014). Wang and Wen, 2008, observed that extension of design can be done by considering uncertainty distributions other than Gaussian where a simulation can be used to find additional area of heat exchanger that will compensate for uncertainties in theoretical heat transfer coefficients, tube wall thermal conductivity and the tube diameters. The technology was scalable and the cost came down significantly especially for plants producing around 10 MW (Kroger, 1988). Studies show that only 48.9 % of the available solar radiation was used for steam generation and that the rest is lost either as collector or thermal losses (Kalogirou, 2004). It was observed that the vibration analysis of shell and tube heat exchanger helps in achieving optimization in design by prevention of tube failure was shown to cause flow induced vibration as a result of increased size of the heat exchanger (Gawande *et al.,* 2007). According to Vera Garcia *et al*., 2010, a manufacturer's catalogue on heat exchanger contains several tested

parameters known as catalogued working conditions which include condensation temperature or evaporation temperature depending on the case

There are various types of heat exchangers that include: - double pipe exchanger, shell and tube exchanger, plate exchangers, plate fin exchangers, spiral heat exchangers, air cooled exchangers, direct contact exchangers, agitated vessels and fired heaters among others.

In a heat exchanger where two fluids flow and are separated by a thin wall of copper metal, the heat transfer fluid provides the heat that is absorbed by another fluid so that it vaporizes or increases its enthalpy. The other liquid‘s (duty fluid) energy is used to produce motion in a prime mover and consequent production of power. The first law of thermodynamics applies to heat exchanger design activities. For two fluids flowing in a heat exchanger the overall energy balance can be represented as shown in equation 2.1

$$m_h c_{ph}(T_{1h} - T_{2h}) = m_c c_{pc}(T_{1c} - T_{2c}) \quad \text{(2.1)}$$

Where m_h is the mass of the heat transfer fluid,

c_{ph} is the specific heat capacity of the heat transfer fluid,

T_{1h} is the inlet temperature of the heat transfer fluid,

T_{2h} is the outlet heat transfer fluid after it has lost the heat to a liquid flowing in the shell side of the heat exchanger,

T_{1c} is the inlet temperature of the water at ambient temperature heat transfer fluid,

T_{2c} is the outlet temperature of heat transfer fluid after it has lost the heat the liquid flowing on the shell side of the heat exchanger. Less viscous fluid is more suitable for shell side due to larger passage area and higher pressure drop (Incopera *et al.*, 2007).

According to Kuppan, 2000, during the design of heat exchangers the basic equations applied relate the rate of heat transfer between the two fluids in the heat exchanger, overall heat transfer coefficient and heat transfer surface area the logarithmic temperature difference. The logarithmic temperature difference of a heat transfer fluid is the logarithmic average of the temperature difference between the hot and the water at ambient temperature feeds at each end of the double pipe heat exchanger. From Kaka

and Liu, 2000, the heat transfer rate can be obtained from the flow rates of one of the fluids, heat capacity and the required temperature change.

2.3 Effectiveness, ε

The heat exchanger effectiveness is a measure of the magnitude of the amount of heat that was actually transferred between the fluids of the heat exchanger. The effectiveness, ε; of a heat exchanger is given by Equation 2.2 (Shah & Senkuli, 2003).

$$effectiveness = \frac{Actual\ heat\ transfer}{Theoretical\ maximum\ heat\ transfer} \quad \text{..... (2.2)}$$

Work on heat exchangers indicates that the increase in surface area and use of exotic material is cited as one of the factors that increase the cost of a heat exchanger (Saunders, 1988).

Heat absorbed by the water at ambient temperature fluid q_a is given by Equation 2.3;

$$q_a = m_c . c_{pc} (T_{c2} - T_{c1}) \quad \text{..... (2.3)}$$

Heat emitted by the hot fluid is given by Equation 2.4;

$$q_e = m_h . c_{ph} (T_{h2} - T_{h1}) \quad \text{..... (2.4)}$$

The heat lost, Q_l is by Equation 2.5;

$$Q_l = q_a - q_e \quad \text{..... (2.5)}$$

The rate of heat transfer for the heat exchanger is given by Equation 2.6;

$$\dot{Q} = \dot{m} c_p (T_{in} - T_{out}) \quad \text{..... (2.6)}$$

Where q_a is the amount of heat absorbed, m_c is the mass of water at ambient temperature water, c_{pc} is the specific heat capacity of water at ambient temperature water, T_{c2} is the outlet temperature of water at ambient temperature water, T_{c1} is the inlet temperature of water at ambient temperature water, q_e is the amount of heat emitted, m_h is the amount of heat emitted, c_{ph} is the specific heat capacity of hot water, T_{h2} is the outlet temperature of hot water, $T_{h1}$is the inlet temperature of hot water, $\dot{m}$ is the mass flow rate of heat transfer fluid, c_p is the specific heat capacity, T_{in} is the inlet temperature and T_{out} is the outlet temperature of heat transfer fluid.

2.4 Number of Heat Transfer Units

The number of heat transfer units (**NTU**) and the heat capacity ratio of a heat exchanger are given by Equation 2.7 and 2.8 respectively (Kaka & Liu, 2000).

$$NTU = \frac{UA}{(\dot{m}c)_{min}} \quad \text{..... (2.7)}$$

Where $(\dot{m}c)_{min}$ is the smaller heat capacity rate,

UA is the overall conductance,

U is the overall heat transfer coefficient ($Wm^{-2}\,{}^{0}C^{-1}$),

Ω is the fluid heat capacity ratio given by Equation 2.8:-

$$\omega = \frac{W_{min}}{W_{max}} \quad \text{..... (2.8)}$$

Where W_{min} is the smaller heat capacity rate,

W_{max} is the higher of the heat capacity rates.

The hot heat transfer fluid flows on the tube side of a heat exchanger while the water at ambient temperature heat transfer fluid flows on the shell side. The overall heat transfer coefficient is given by Equation 2.9 (Hewitt, 2002).

$$U = \frac{W_{min}}{A} . NTU \quad \text{..... (2.9)}$$

Heat transfer coefficient, U is given by Equation 2.10:-

$$U = \frac{qe}{A\,\Delta t_{lm}}\ W/m^2K \quad \text{..... (2.10)}$$

Where A is the heat transmission surface area,

Δt_{lm} is the logarithmic temperature difference.

Calculations of U obtained account for all other factors that affect thermal performance.

The magnitude of the heat flow rate is given by Equation 2.11

$$\dot{Q} = W_h(T_{h,in} - T_{h,out}) = W_c\,(T_{c,out} - T_{c,in}) = UA \times \Delta t \quad \text{..... (2.11)}$$

Where W_h and W_c is the water at ambient temperature and hot stream heat capacity rate respectively, $T_{h,in}$ is the inlet temperature of the hot fluid flow and $T_{h,out}$ is the out let temperature of the water at ambient temperature fluid flow respectively.

The logarithmic temperature difference is given by Equation 2.12 (Shah & Sekuli, 2003);

$$T_{MTD} = \frac{(T_{1,in} - t_{2,out}) - (T_{2,out} - t_{1,in})}{In \frac{T_{2,in} - t_{2,out}}{T_{2,out} - t_{1,in}}} \quad \text{.....} \quad (2.12)$$

Where $T_{1,in}$ is the hot fluid inlet temperature and $T_{2,out}$ is the hot fluid outlet temperature. The required heat transfer surface for design is given by Equation 2.13. (Kaka & Liu, 2000)

$$A = \frac{Q}{U.\Delta T_f} \quad \text{.....} \quad (2.13)$$

The mean temperature efficiency for the fluid transmitting heat to the water at ambient temperature fluid is given by Equation 2.14 (Saunders, 1988)

$$\eta_T = \frac{T_{2,1} - T_{2,O}}{T_{2,i} - T_{1,i}} \times 100 \quad \text{.....} \quad (2.14)$$

Energy efficiency of the heat exchanger is given by Equation 2.15 (Singh, 1989):

$$\eta_e = \frac{energy\ exchanged}{total\ energy\ supplied} \times 100 \quad \text{.....} \quad (2.15)$$

The difference in temperature efficiency and energy efficiency was as result of other losses that occurred during transmission of heat transfer fluid from one component to another.

2.5 Steam Storage System

Thermal energy storage systems help balance energy demand and supply. They increase the overall efficiency of the energy systems. The storage of thermal energy from renewable energy sources can replace energy from fossil fuels. In Europe it has been estimated that around 1.4 million GWh per year could be saved and 400 million tons of carbon dioxide emission be avoided by use of storage systems (Price & Kearney, 1999). The selection of a steam storage system is guided mainly by the inlet temperature and the out let temperature of the storage system. The required thickness of the material for use is determined by elastic analysis and by consideration of the allowable stress to withstand the pressure of operation and observation of safety (Maan, 2001). In a study by Bowels, 1966, the main components of a steam storage were named as; a safety valve which keeps the steam storage system from exceeding maximum allowed

working pressure, a steam- pressure control valve which regulates the amount of steam entering the steam store and maintains constant pressure, a non-return valve which is a combination of shut off and check valve that allows steam out of the tank but prevents back flow when the pressure drops, a steam flow meter which tracks the amount of steam produced by the system and a feed water control valve which moves up and down in response to water level.

Various studies show that the purpose of a performance test of a steam storage system is to find out the efficiency of the steam storage system and the evaporation ratio of the fluids (Wu *et al.*, 2009) as shown Equations in 2.16 and 2.17 respectively.

$$Efficiency = \frac{Heat\ output}{Heat\ input} \times 100 \quad \text{..... (2.16)}$$

$$Evaporation\ ratio = \frac{Quantity\ of\ steam\ generation}{Quantity\ of\ heat\ input} \quad \text{.....(2.17)}$$

According TEMA, 1993, the tubular exchange manufacturers Association a steam storage system is tested at 130 % of the rated pressure.

Experiments on Load levelling show that levelling is achieved by use of pressure maintaining valves. In these studies the pressure is set to be less than the highest control pressure to prevent interference of the surplus valve and is set high enough to maintain the pressure in the steam storage at a safe level (Rabl, 1985).

The mean value of load was used to size the steam storage system because this prevents unnecessary oversizing of the storage system. During the sizing it is necessary to consider mean off peak load which is the load below maximum rating (Solar concentrators, 2011).According to a study on power overload, to find the mean value of overload and off peak load interrogation of patterns of load demands made on a chart to get the mean loads and the time over which they occur is done (Suhas, 1992). A steam storage system is required to meet a peak demand by releasing steam when required. Storing steam as a dry gas is not practical due to enormous storage volume required at normal pressures vessel ratings.

Steam capacity of a storage system is obtained from Equation 2.18 (Ganapathy, 1994):-

$$Steam\ storage\ capacity = \frac{Difference\ in\ enthalpy\ of\ water \times mass\ of\ water}{Enthalpy\ of\ evaporation\ at\ lower\ pressure} \quad \text{..... (2.18)}$$

The proportion of flash steam produced from a steam storage system is given by Equation 2.19 (Wang *et al*., 2008).

$$\text{Proportion of flash steam} = \frac{[h_f(P_1) - h_f(P_2)]}{h_{fg}(P_2)} \quad \text{..... (2.19)}$$

Where h_f and h_{fg} are enthalpies of steam at the pressure P_1 and P_2.

The leaks and flaws in welding are observed during the test. Stiffening of the steel case is usually done to avoid collapse of vessel when pressure fall below atmospheric pressure. This is done for high pressure vessels in the excess of 1.0×10^8 Nm^{-2}. Thermal energy storage based on sensible heat storage offer a storage capacity ranging from 10 -50 $kWhs^{-1}$ and power efficiencies of 50 – 90 % depending on thermal insulation technology (Sandia Laboratories, 2004). The Luz trough plant which was used in Solar Energy (SEGS 1) included a direct two tank thermal energy system with three hours of fluid load storage capacity (NREL, 2000). The mass of saturated steam that can be produced by a steam storage system can be obtained from equation 2.20 (Ganapathy, 1994):

$$m_s h_f = m_l c_l\ (t_{sat}\ (P_1) - t_{sat}(P_2)) \quad \text{..... (2.20)}$$

Where m_s is the mass of steam,

h_f is the latent heat of vaporization of water

, c_l is the specific heat capacity of water,

$t_{sat}\ (P_1)$ is the temperature at an initial pressure and

$t_{sat}(P_2)$ is the temperature at a final pressure.

The mass of saturated steam obtained for charging process from pressure P_1 to pressure P_2 is given by Equation 2.21 (Wu *et al.*, 2009).

$$m_s = \frac{M_l C_l B\left(\frac{1}{A - \ln P_i} - \frac{1}{A - lnP_2}\right)}{\Delta h_f \left(1 - \left(\frac{\left(\frac{B}{A - \ln P_m} - C + 273.15\right)/647}{(1 - (t_{ref} + 273.15/647))}\right)^{0.38}\right)} \quad \text{..... (2.21)}$$

Where A, B and C are constants (Kuppan, 2000), whose values are: - A = 11.9, B = 3985, C= 234.1

c_l is the specific heat capacity of liquid phase,

Δh_f is the heat of vaporization.

m_l is the mass of liquid phase in vessel,

m_s is the mass of steam during discharge,

P_1 is the initial pressure at the discharge,

P_2 is the final pressure at the discharge,

P_m is the pressure of saturated steam and t_{ref} is the reference temperature of steam.

Equation 2.20 and equation 2.21 represent two different approaches which are used to find the mass of discharged steam. They provide a basis of comparing the results obtained in the experimental work.

The amount of heat transferred during the discharge is given by Equation 2.22.

$$Q = \frac{c_p\, dt\, m}{t} \quad \text{.....} \quad (2.22)$$

Where Q is the rate of heat transferred (Js^{-1}),

mt^{-1} is the mass flow rate,

c_p is the specific heat capacity of water and dt is the change in the temperature of the fluid. The amount of steam is given by Equation 2.23.

$$m_s = \frac{q}{h_e} \quad \text{.....} \quad (2.23)$$

Where m_s is the mass of steam (kgs^{-1}), q is the heat transfer and h_e is the enthalpy of evaporation of steam (Jkg^{-1}). Evaporation energy for different steam pressures is determined by use of the steam tables which give the enthalpies of steam at various temperatures (Cecil, 2010).

The efficiency of a system is given as shown in Equation 2.24.

$$\eta = \frac{Heat\ out\ put}{Heat\ input} \times 100 \quad \text{.....} \quad (2.24)$$

Evaporation ratio for a storage system is given by Equation 2.25 (Duffie & Beckman, 2005)

$$\text{Evaporation ratio} = \frac{Heat\ in\ steam\ out\ put}{Heat\ in\ electrical\ input} \times 100 \quad \text{..... (2.25)}$$

The steam flow rate $\dot{m}_s$ is given in Equation 2.26 (Geyer, *et al.*, 1991)

$$\dot{m}_s = 12\ K_v\ P_1\sqrt{(1 - 5.67\ (0.42 - \chi)\ )^2} \quad \text{..... (2.26)}$$

Where $\dot{m}_s$ is the steam flow rate (kgh^{-1}), k_v is the capacity index factor/ valve flow rate coefficient = 100 m^3h^{-1}, P_1 is the boiler pressure bar and χ is the pressure drop ratio $\Delta\ P/P_1$.

The pressure drop ratio is given as shown in Equation 2.27

$$\chi = \frac{P_1 - P_2}{P_1} \quad \text{..... (2.27)}$$

2.6 Steam Turbine

There are two general types of steam turbines: - reaction turbines and impulse turbines. In a reaction turbine, rotation of the blades is as a result of reactive force of steam. The expansion of steam in the rotating blades causes reaction force that drives them. In the impulse turbine the thermal energy of steam is converted to kinetic energy in the turbine nozzle. The kinetic energy is converted to blade mechanical energy and transferred to the shaft and coupling and to the load. In the reaction turbine there is no nozzle to convert steam to mechanical energy. It has been shown that moving blades work to differential pressure of steam between the front and at behind of moving blades (Lamberson & Moll, 2002). This turbine is not a standalone but works on along with impulse turbine. Most of the commercial turbines are a combination of the two types of turbines. An extraction type turbine releases steam at various stages of the turbine and it is used for industrial heat process needs or the steam is sent to the boiler feed water heaters to improve overall cycle efficiency. The flow of steam from the turbine stages during extraction may be controlled or not. In US patent number US 3452132 A by

Gilbert, 1969, super-heated steam at a temperature of 300 ^{o} C and a manifold pressure of 1.0×10^{10} Nm^{-2} was impinged asymmetrically on the yarn at an angle of 30^{o}C and this was the angle that produced the best results. Small single stage turbines can have efficiencies as low as 50 % (NREL, 2006). According to Chenduran *et al*., 2004, about 90% of all the electricity produced in the United States of America is produced by use of steam turbines. An ideal steam turbine is considered to undergo an isentropic process in which the entropy of steam entering the turbine is equal to the entropy of the steam leaving the turbine. It was observed that there is no steam turbine that is truly isentropic and the isentropic efficiencies range from 20 % to 90 % based on the application (API Standard 612, 1995).

In a study conducted by the World Bank in 2011, the thermodynamic cycle for the steam turbine is the Rankine cycle (World Bank, 2011). The cycle consists of a heat source such as a boiler that converts water to high pressure steam.

The steam turbine isentropic efficiency is the ratio of power actually generated from the turbine to what would be generated from a perfect turbine with no internal losses using steam at the same inlet conditions and discharging at the same pressure. The electrical generating efficiency of a power plant is the ratio of net power to total heat input to the cycle. The steam turbine thermodynamic efficiency is a measure of how efficiently the turbine extracts the power from the steam itself and is useful in identifying the conditions of the steam as it exits from the turbine and in comparing the performance of different turbines.

From Ecoworld, 2000, the electrical efficiency of a turbine is given as shown in Equation 2.28

$$Electrical\ efficiency = \frac{Net\ electricity\ energygenerated}{total\ energy\ input} \quad \text{..... (2.28)}$$

Steam turbine thermodynamic efficiency is a measure of how efficiently the turbine extracts power from steam itself. A study conducted by Schetz & Fuhs, 1996, showed that this efficiency ranges from 65 % for small turbines to 90 % for bigger commercial ones and that the centripetal force, F, on a turbine blade is given by Equation 2.29

$$F = \rho A\omega^2 \left(\frac{r_2{}^2 - r_1{}^2}{2}\right) \quad (2.29)$$

Where ρ is the density of the material,

A is the cross sectional area of the blade,

ω is the angular velocity of the rotating blade,

r_1 is the radius of the rotor disc and

r_2 is the distance between the center of the rotor disc and the tip of the blade.

In an earlier study it was found that the nominal stress σ on the blade root is given by Equation 2.30 (Lambertson & Moll, 2002)

$$\sigma = \frac{F}{A_{root}} \quad (2.30)$$

Where F is the centripetal force and A_{root} is the cross sectional area of the blade root

The turbine efficiency is given by Equation 2.31 (Jachen, 1996).

$$Turbine\ efficiency = \frac{power\ output\ by\ turbine}{power\ supplied\ to\ turbine} \quad (2.31)$$

The angular velocity ω is given by Equation 2.32 (Fre'chette *et al.*, 2004)

$$\omega = \frac{r.p.m \times 2\pi}{60} \quad (2.32)$$

The efficiency of the turbine is given by Equation 2.33 (Stevenson & Williams, 2001)

$$\eta = \frac{Net\ out\ put\ of\ shaft\ work}{Work\ input} \quad (2.33)$$

Torque on the shaft is given by Equation 2.34 (Church, 1987)

$$torque = \frac{Power\ in\ Watts}{2\pi \times Rotational\ speed} \quad (2.34)$$

In a study conducted on micro turbines, a micro turbine that was fabricated consisted of a stack of five wavers and was fabricated by micro electro mechanical system technology using photolithography and bonding process with the first second fourth and fifth layers containing plumbing and hydrostatic axial thrush bearings of turbine. The third wafer contained the turbines stator, rotor and hydrodynamic journal bearings (Byung, 2005). The configuration for a complete micro rankine power source consisted of a heat source, a cooling mechanism, MEM's based micro rankine device and power electronic that was designed and fabricated. In such a study the device consisted of a

steam driven turbine that entrained a liquid pump and an integrated generator along with a compact evaporator and a condenser (Fre'chette *et al.*, 2004). In the study, there was a challenge in design of a turbine to cater for low power demand of 50 W while it had to operate at high supply pressure of 5.0 to 6.0 × 10^5 Nm^{-2}. It was shown that to meet the industrial demand, the study indicated that a high speed turbine and a generator of 45000 r.p.m and a small blade span of 200×10^{-6} m which minimized the mass flow while achieving highest possible turbine performance were used (Satos *et al.*, 2011).

2.7 Blade Path Design

A study conducted on successive expansion of steam showed that for steam turbines with a number of stages, successive expansion processes in alternate stationary and rotating blades enable the conversion of thermal energy to mechanical energy (EEAR, 2008). Figure 2.1 shows the velocity triangles involved in blade path design. The velocities relative to the rotor blade are related to the stator velocities and to the wheel as shown in the figure. Absolute velocities are denoted by V and relative velocities by W. In the design transposition of these velocities and accompanying steam conditions are used.

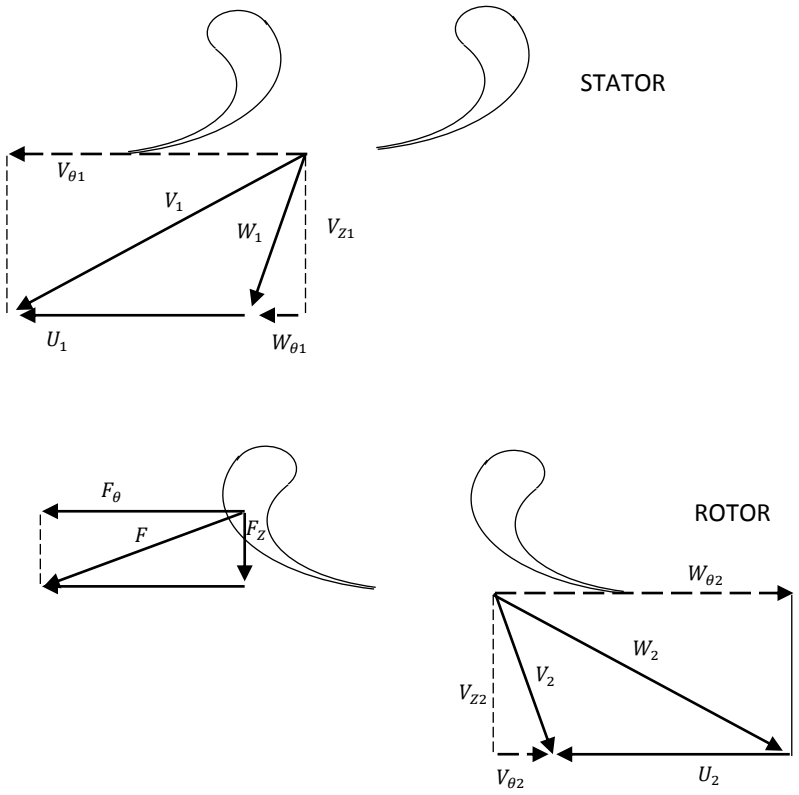

Figure 2. 1: Components of steam velocity at inlet and at outlet of the stream tube

From Newton's laws, the change of momentum by the fluid in a tangential direction and the force exerted on the fluid are equal. It was shown that when the flow is assumed steady and the velocity components assumed constant within the stream tube in the upstream and downstream the force on the fluid is given by Equation 2.35 (Jachen, 1996)

$$F = \frac{\dot{M}}{g}(V_{\theta 2} - V_{\theta 1}) \quad \text{(2.35)}$$

Where F is the force,

$\dot{M}$ is the rate of fluid flow,

$V_{\theta 2}$ and $V_{\theta 1}$ are the components of velocity and

g is the gravitational field strength.

A study showed that considering that the stream tube entering and leaving radii are the same, the power developed by the moving blade is given by Equation 2.36 (Fre'chette *et al*., 1991).

$$P = \frac{\dot{M}}{g} r\omega(V_{\theta 2} - V_{\theta 1}) \quad \text{(2.36)}$$

Where r is the radius and ω is the angular velocity.

In a study on turbine design, thermodynamic interactions within the turbine are evaluated by finding the values of enthalpy and the entropy of the steam. In the study, the case of a turbine with many stages, the thermodynamic interactions are determined for all the stages and enthalpy at the wheel and the nozzle are quantified at the pressures of operation (Jachens, 1996).

The importance of rotor balancing was studied and it revealed that the rotor balancing over the design operating range during assembly is an important undertaking to ensure rotations are kept to a minimum (Barret *et al*., 1986). Further study showed that when a rotor is balanced the critical speed and the natural frequency of vibration of the rotor coincide with that of stator producing a state of balance for the whole assembly (Bethel *et al*., 1993).

2.8 Generator

A study on selection of a prime mover for a generator showed that the selection of suitable size of the prime mover for an a.c generator is governed by electrical power output supplied to the load and efficiency of the a.c generator. The drive in put for the generator is given by Equation 2.37 (Valan & Sornakumart, 2006)

$$Kw\ drive\ input = \frac{k\ W\ output}{\eta} \quad \text{(2.37)}$$

where kW the drive input is the prime mover rating in kilowatts, kW the output is the electrical power supplied and η is the efficiency.

Bowel, 1966, showed that the kVA for a three phase power supply is given by Equation 2.38 (Bowel, 1996).

$$kVA = \frac{\sqrt{3\times}\, volts \times current}{1000} \times p.f \quad \text{(2.38)}$$

Where p.f is the power factor.

It was shown that three phase power provides more power for the same current than a single phase circuit. They are used in power distribution systems due to the following reasons; they produce higher power transmission for the same electric current, less copper is required for the same power transmission and that safe or lower voltages transmitted due to the multiple phases and that the input power is produced by the prime mover (Stevenson, 2001). This is higher than the electrical output of single phase a.c generator. It was shown that the efficiency of the generator is given by Equation 2.39 (Zarza *et al.*, 2001).

$$\eta = \frac{Electrical\ output}{input\ power\ of\ prime\ mover} \quad \text{.....} \quad (2.39)$$

According to a study on power systems by Leyzerovich, 2005, a generator must rotate at constant synchronous speed with respect to the frequency of the source of power. In this work the most common speeds are 3000 rpm for 50 Hz systems, and 3600 rpm for 60 Hz systems installations with high speed system output as is found in nuclear power stations.

2.9 Solar radiation geometry

In order to establish the beam energy falling on a surface of any orientation, the value of beam flux coming from the direction of the sun to the collector is converted to an equivalent value corresponding to the normal direction to the surface. There are relations that make this conversion possible. Suppose θ is the angle between an incident beam of flux I_{bn} and the normal to a plane surface. Then the equivalent flux normal to the surface is given by $I_{bn}\cos\theta$. The angle θ is related through a general equation to latitude $\emptyset$, zenith angle θ_z, declination δ, surface azimuth angle φ , hour angle ω and+ slope β as given in Equation 2.40 (Duffie & Beckmann , 2005).

$$\cos\theta = \sin\emptyset(\cos\delta\cos\beta + \cos\delta\cos\varphi\cos\omega\sin\beta) + \cos\emptyset(\cos\delta\cos\omega\cos\beta - \sin\delta\cos\varphi\sin\beta)$$

$$+(\cos\delta \sin\varphi \sin\omega \sin\beta) \quad \text{.....(2.40)}$$

For a horizontal surface β = 0 and Equation 2.39 becomes Equation 2.41:

$$\cos\theta = \sin\emptyset \sin\delta - \cos\emptyset \cos\delta \cos\omega \quad \text{..... (2.41)}$$

Figure 2.2 shows the relationship between the angles and the sun.

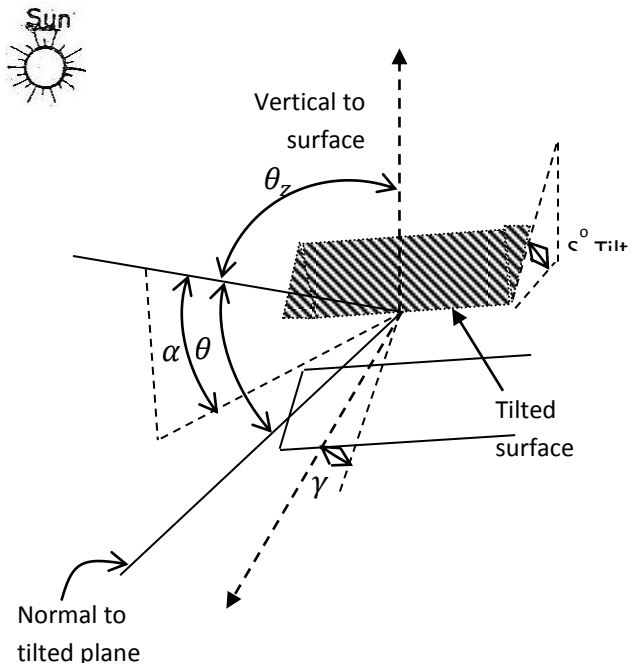

Figure 2. 2: Relationship between various sun collector angles

The hour angle corresponding to sunrise or sunset (ω_s) on a horizontal surface is given by Equation 2.42, (Twidel, 1986), for β = 0

$$\cos\theta = \sin\phi\sin\delta + \cos\phi\cos\delta\cos\omega \quad \text{..... (2.42)}$$

The hour angle as bt Twindwel 1986 is given in Equation 2.43 as

$$\omega_s = \cos^{-1}(-\tan\phi\tan\delta) \quad \text{..... (2.43)}$$

From Equation 2.43, ω_s is positive in the morning and negative in the afternoon. 15^o of hour angle is equivalent to 1 hour. The time used for calculating the hour angle ω is the local apparent time. This is obtained from the standard time observed on a clock by applying two corrections. The first correction arises because of the difference between the longitude of a location and the meridian on which the standard time is based. It has a correction of 4 minutes for every degree difference in longitude. The second correction, called the equation of time, arises as a result of the earth's orbit and rate of rotation subject to small fluctuations.

2.10 Solar radiation on tilted PTSC surface

The ratio of beam radiation falling on a tilted surface to that falling on a horizontal surface r_b is given in Equation 2.44 (Rai, 1987) as.

$$r_b = \frac{\cos\theta}{\cos\theta_z} = \frac{\sin\delta\sin(\phi-\beta)+\cos\delta\cos\omega\cos(\phi-\beta)}{\sin\phi\sin\delta+\cos\phi\cos\delta\cos\omega} \quad \text{.....} \quad (2.44)$$

Where $\cos\theta$ and $\cos\theta_z$ are shown in Equations 2.45 and 2.46 respectively

$$\cos\theta = \sin\delta\sin(\emptyset-\beta)+\cos\delta\cos\omega\cos(\emptyset-\beta) \quad \text{.....} \quad (2.45)$$

$$\cos\theta_z = \sin\emptyset\sin\delta + \cos\emptyset\cos\delta\cos\omega \quad \text{.....} \quad (2.46)$$

The solar flux I_T falling on a tilted surface at any instant consists of both beam and diffuse radiations as shown in Equation 2.47 (Kaligirou, 1997) as.

$$I_T = I_b r_b + I_d r_d + (I_b - I_d) r_r \quad \text{.....} \quad (2.47)$$

where

$I_b r_b$ is the beam radiation, $I_d r_d$ represents diffuse radiation and I_T represents total radiation on a surface:

The tilt factor for diffuse radiation is given by Equation 2.48;

$$r_b = \frac{1+\cos\beta}{2} \quad \text{.....} \quad (2.48)$$

The radiation shape r_r factor for a tilted surface with respect to the sky tilt factor for diffuse radiation is obtained using Equation 2.49

$$r_r = \rho\left(\frac{1-\cos\theta}{2}\right) \quad \text{.....} \quad (2.49)$$

Ratio of the flux on a tilted surface, I_T at any instant to that on a horizontal surface, I_g is given by Equation 2.50

$$\frac{I_T}{I_g} = \left(1 - \frac{I_d}{I_g}\right) r_d + \frac{I_d}{I_g} r_d + r \quad \text{.....} \quad (2.50)$$

2.11 Parabolic trough collector and Nomenclature

A section of a linear parabolic concentrator showing major dimensions is shown in Figure 2.3. The principal focus lies on an axis along the parabola. This is where the rays incident on the optical system are concentrated to heat the heat transfer fluid The principal focus may be projected out of the parabola if it is insulated against heat losses by covering it with an envelope of evacuated glass. The vacuum is achieved by mechanical removal of air by suction on a sealed treated glass envelop that is eventually sealed at both ends.

In figure 2.3, *a*, is the aperture and f is the focal length. If a radiation beam from the sun's disk is incident on the reflector at point B on the rim where radius is maximum at r_r, the angle $\varnothing_r$ is the rim angle which is given in Equation 2.51.

The most important parts of a parabolic trough solar concentrator can be summarized as shown in Figure 2.3.

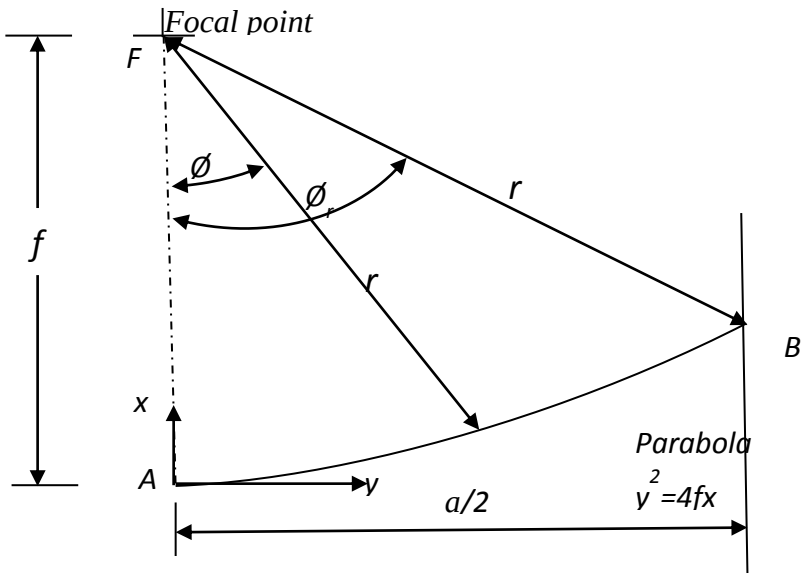

Figure 2. 3: Main dimensions of a parabolic trough solar concentrator

$$\emptyset_r = \tan^{-1}\frac{8\left(\frac{f}{a}\right)}{16\left(\frac{f}{a}\right)^2 - 1} \quad \text{..... (2.51)}$$

. A study on solar concentration on receiver showed that not all rays are brought to receiver by the optical system because some are lost at the edges and others are scattered by irregularities on the optical system (Algoul *et al.*, 2005).

Testing of the parabolic trough collector was by Duffie and Beckman, 2005, done using a standard testing and rating practice i.e. ASHRAE 93–77 provides an equitable basis for comparing efficiencies of different types of collectors and an essential basis for design and selections of equipment. Procedures to use as described here have been widely used and were initially proposed by the National Bureau of Standards (NBS) and the American Society of Heating Refrigerating and Air Conditioning Engineers (ASHRAE). An incident beam of solar radiation is a cone as shown in Figure 2.4

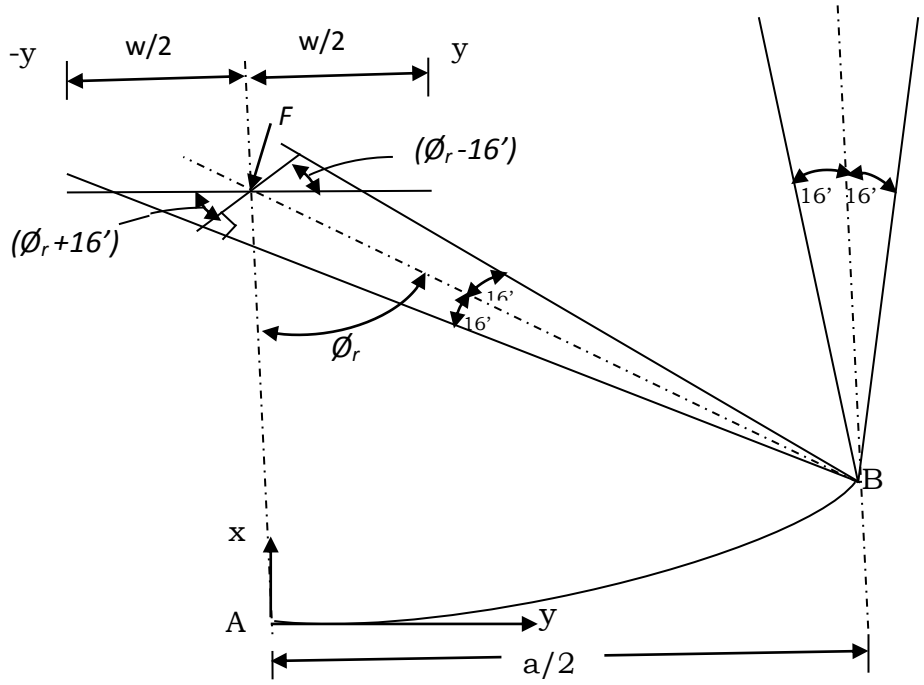

Figure 2. 4: Reflection of a beam of the sun at collector angle

The efficiency of the solar collector, η_i is given by Equation 2.52 (Duffie & Beckman, 2005).

$$\eta_i = \frac{q_u}{A_c I_T} = \frac{\dot{m} c_p (T_{2-} T_1)}{A_c I_T} \quad \text{..... (2.52)}$$

where q_u is the useful gain in heat,

$\dot{m}$ is the mass flow rate,

I_T is the beam radiation intensity,

A_C is the collector area,

c_p is the specific heat capacity of heat transfer fluid,

T_2 is the outlet temperature of heat transfer fluid,

T_1 is the inlet temperature of heat transfer fluid.

The data used was recorded under steady state conditions.

It was shown that parabolic trough solar collectors are the preferred type of collectors used for steam generation due to their ability to work at high temperatures with high efficiencies (Bakos *et al.*, 2001). Heat transfer runs through the tube in the line focus absorbing concentrated sunlight in the collector with an efficiency of 60 – 80 % (Umar *et al.*, 2013).

An energy balance equation provides heat gain per unit collector length L as shown in Equation 2.53 (Duffie & Beckman, 2005).

$$Q_u = \frac{A_a}{L} H_b r_b \rho \gamma (\alpha\tau)_b - \pi D_O U_l (T_m - T_a) \quad \text{(2.53)}$$

D_o represents external diameter of absorber,

A_a represents area of aperture,

$H_b r_b$ represents solar flux intensity,

ρ represents reflectance,

α represents absorptance,

τ represents transmittance,

L represents *l*ength,

U_l represents heat loss coefficient,

T_m represents mean temperature of heat transfer fluid, and

γ represents intercept factor.

The heat gain q_u is given by Equation 2.54 (Gillet and Moon, 1985).

$$q_u = \frac{A_a}{L} H_b r_b \rho \gamma (\alpha\tau)_b - \pi D_o U_l (T_m - T_a) \quad \text{(2.54)}$$

The collector efficiency factor, q_u can be obtained from equation 2.54. It refers to the efficiency with which thermal heat is being absorbed,

where, $H_b r_b$ is the solar beam intensity,

A_a is the aperture area,

L is the length of collector, S is the absorbed radiation,

$(T_m - T_a)$ is the temperature difference,

$(\alpha\tau)$ is the absorptance transmittance product,

U_l is the heat loss coefficient,

ρ is the reflectance and

γ is the intercept factor.

Equation 2.53 and 2.54 represent the same physical quantity that is being obtained in the two ways given by the equations.

The collector heat removal factor F_R is defined as the ratio of the actual heat gain of collector to the gain if collector surface were at inlet temperature of the heat transfer fluid which is given by Equation 2.55 (Duffie & Beckman, 2005).

$$F_R = \frac{\dot{m}c_p(T_{fo}-T_{fi})}{\frac{A_a}{A_r}S-U_l(T_{fo}-T_{fi})} \quad \text{(2.55)}$$

where $\dot{m}$ is the mass flow rate of heat transfer fluid,

c_p is the specific heat capacity of heat transfer fluid,

F_R is the heat removal factor of collector,

U_l the heat loss coefficient,

A_r is the receiver tube outer diameter,

F' is collector efficiency factor,

S is absorbed solar radiation energy.

In a study by Duffie and Beckman, 2005 and Rai, 1987, to determine the heat gain, collector flow factor, collector efficiency and optical efficiency, Equations 2.56, 2.57, 2.58 and 2.59 show the variables respectively.

The total heat gain is given by Equation 2.56

$$Q_u = F_R A_a \left[\frac{A_r U_l}{A_a}(T_1 - T_a)\right] \quad \text{(2.56)}$$

The collector flow factor F'' is given by Equation 2.57 (Duffie & Beckman, 2005).

$$F'' = \frac{F_R}{F'} = \frac{\dot{m}c_p}{A_r U_l F'}\left[1 - e^{\frac{F' A_r U_l}{mc_p}}\right] \quad \text{(2.57)}$$

Collector efficiency and the optical efficiencies are given by Equation 2.58 and 2.59 respectively (Rai, 1987).

$$\eta_c = \frac{Q_u}{H_b r_b A_a} \quad \text{(2.58)}$$

Optical efficiency η_{opt} is given by Equation 2.59.

$$\eta_{opt} = \rho\gamma\langle\alpha\tau\rangle \quad \text{..... (2.59)}$$

where ρ is the reflectance loss for the material under consideration which was evaluated using radiation tables (Dunkle & Devovosky, 1961). It can be determined experimentally. $\alpha\tau$ is the absorptance- transmittance product of the collector receiver and cover respectively and the γ is the intercept factor is the amount of the solar flux reaching the absorber. For parabolic trough system, the normal distribution curve for intercept factor can be expressed by use of Equation 2.60 (Rai, 1987).

$$\frac{I}{I_{\max}} = e^{-h^2\left[\frac{\omega}{W}\right]^2} \quad \text{..... (2.60)}$$

The value of *h* is obtained from Equation 2.61

$$I_{max} = \frac{1}{\sigma\sqrt{2\pi}} = \frac{h}{\omega\sqrt{\pi}} \quad \text{..... (2.61)}$$

I_{max} is the highest amount of flux reaching the absorber or the maximum flux density, ω is the distance from the center of the zone of convergence of the solar flux accessing the absorber, *d* is the half – width (aperture) of concentrator, *h* is the normal flux distribution coefficient and σ represents the standard deviation of the normal distribution curve.

For parabolic trough concentrator which is being tracked, the distribution function is obtained from Equation 2.62 and 2.63 (Algou *et al.*, 2005).

$$\frac{I}{I_{\max}} = e^{-h^2\left(\frac{r}{R}\right)^2} \quad \text{..... (2.62)}$$

and

$$I_{\max} = \frac{1}{\sigma\sqrt{2\pi}} = \frac{h}{R\sqrt{\pi}} \quad \text{..... (2.63)}$$

where *I* is the radiative flux density at radial position from axis *r/R*, *r* is the radius in focal plane from axis and *R* is the concentrator rim radius

The intercept factor γ is given by Equation 2.64 (Kalogirou, 1997). This physical quantity provides the fraction of solar flux that actually coincides with the receiver for solar thermal extraction.

$$\gamma = \frac{I_{\max}\int_0^{\left(\frac{r}{R}\right)} e^{-h^2\left(\frac{r}{R}\right)^2} 2\pi\left(\frac{r}{R}\right) d\left(\frac{r}{R}\right)}{I_{\max}\int_0^{\infty} e^{-h^2\left(\frac{r}{R}\right)^2} 2\pi\left(\frac{r}{R}\right) d\left(\frac{r}{R}\right)} \quad \text{...} \quad (2.64)$$

Integration between the given limits in Equation 2.64 gives equation 2.65.

$$\gamma = 1 - e^{-h^2\left(\frac{r}{R}\right)^2} \quad \text{..} \quad (2.65)$$

The variations in objectives, summarized methodology, results obtained in related studies are as presented as follows: Solar thermal parabolic trough collectors can be used to provide heat for desalination, cooling electricity generation and thermal processing even up to 200 ^{o}C with pressurized water which has low radiative and convective losses (Kruger, 2008). In California, Mojave desert nine solar electricity generating systems (SEGS I – IX) have a total peak power output of 354 MW which is supplied to the grid. In this project, synthetic oil is used as the heat transfer fluid that is heated from 290 ^{o}C to 311 ^{o}C in the collectors and superheated steam of 1.0×10^7 Nm^{-2} at 370 ^{o}C is produced (Kearney & Cohen, 1997).

Organic oil based heat transfer fluids, air, water and molten salts have been used for transferring heat in solar concentrating plants. The inorganic salts maintain stability at high temperatures, but solidify easily at temperatures of 230 ^{o}C (Sarada K., 2012). Graphite is preferred for improving the thermal properties of a storage system because it has high thermal conductivity, good process ability and chemical inertness to provide storage of solar heat for high temperature applications such as process heat and solar thermal power (Rogelio *et al.*, 2014). In study by Laing *et al.*, 2006, on concrete it was found out that the advantage of concrete storage is low cost, high strength, easy to handle, readily availability and offers favorable sensible heat storage. More research on

the same revealed that high temperature concrete is suitable for solar thermal power plants (Hurtado and Kast, 1984). It was shown that in solar power generation using heat transfer fluids the organic based heat transfer fluids breakdown temperature is currently 400 ^{o}C (Fathollahneyad *et al.*, 1993).

In a study conducted by Slocum *et al*., 2011, and other scholars, a concentrated solar power plant with integral storage was constructed where heliostat mirrors were mounted to direct sunlight into a volumetric absorption molten salt receiver either near the base of the hill where sunlight could directly penetrate the salt or at the top of the hill where the light was directed off the lid of the receiver before it entered the salts. In most solar power applications the concentration ratio ranges from 30 to 80 depending on concentrator and the heat transfer fluid can reach a temperature of 400 ^{o}C that depends on the concentration ratio, solar intensity, heat transfer flow rate among other parameters (Mohammad *et al*., 2013). It was found that one achievement by the parabolic trough concentrator is the 80 MW solar thermal electric power plants set up by Luz in California with the following dimensions and characteristics:- Aperture width: 5.76 m, length: 95.2 m, curved reflecting surface of glass mirror area: 224 m^2, reflectivity: 0.94, glass covers transmitivity: 0.965, outer absorber tube diameter: 0.003 m, tube surface absorptivity: 0.97, tube surface emissivity: 0.15, optical efficiency: 0.772, peak collection efficiency: 0.68 and annual collection efficiency:0.53 (Suhas, 1991).

The Euro trough model 150 had the following characteristics: Focal length; 1.71 m, absorber radius; 0.035 m, aperture width; 5.77 m, aperture area; 817.5 m^2, collector length: 148.5 m, number of glass facets: 336, mirror reflectivity: 0.94 and weight of steel structures, 18.5 kg.

Another Euro trough model collector consists of 12 m long collector modules. Nine commercial solar electric generating systems (SEGS), designed, constructed and operated by Luz international operate in Mojave Desert of Southern California. (World Bank, 2010). The largest solar power plants in the world are Andasol 1 to 3 located in Spain.

In the collector designs that have been used in the plant described above, reflectors are made of back silvered glass, low iron float glass panels which are shaped over parabolic forms, metallic and lacquer protective coatings are applied to the back of the silvered surface and a measurable degradation of the reflective surface has been observed, the glass is mounted on truss structures, with the position of large arrays of modules adjusted by the hydraulic drive motors, receivers are 0.07 m diameter steel tubes and 0.003 m in diameter with cermet selective surfaces surrounded by a vacuum glass jacket, which is achieved by removing air around the receiver and sealing the ends of the receiver, the surfaces have an absorptance of 0.96 and emittance of 0.19 at 380 ^{o}C, reflectance of mirrors is 0.94 when clean and the total mirror area is 1.35 x 10^{6} m^{2}. Cleaning by use of a machine is done every two weeks. Synthetic heat transfer fluid is utilized (NREL, 2008). In order to improve solar thermal collection liquid metals have been explored to increase temperatures of operation of parabolic trough concentrators. However they are risky since most react with moisture. A study by NREL, 2009, showed that the current operational temperatures of 785 ^{o}C for Sodium – Potassium at atmospheric pressure can be increased to temperatures exceeding
1100 ^{o}C with moderate pressurization

It was shown that the conditions of operation for these concentrators are such that the operating temperatures are higher; edge effects are more significant, conduction terms are quite high and radiation flux on receivers is also quite high compared to flat plate collectors (NREL, 1999). There may be no obvious general method of estimating thermal loses. However generalized analysis of a focusing collector system is very similar to that of flat plate collectors (Close, 1988).

The variations of objectives, approaches to arriving at physical parameters and findings from various power generation projects around the world have been presented.

In summary from the literature review, studies have been carried out on design considerations of steam storage, heat exchanger, steam turbine and generator designs and fabrication considerations for power production. Various performance parameters have been investigated such as efficiency and the technologies involved were presented.

The gaps identified from the studies include inefficient solar thermal collection and storage technologies, need for alternative heat transfer fluids, need for availability of heat transfer fluids with a higher temperature limit of the power cycle and that there was need to lower the cost of kWh by generating more green power to mitigate global environmental pollution and climatic change.

The new knowledge therefore expected is based on the study of alternative heat transfer fluids and steam storage and heat exchanger power generation technology that will be expected to lower the cost of power when used on a large scale. Local technology and materials studies are presented in this work

CHAPTER THREE

MATERIALS AND METHODS

3.1 Introduction

In this section the materials and methods that were used in obtaining data are described. The design and characterization of a solar thermal storage system for storing steam, design and fabrication of a solar thermal steam turbine, design and fabrication of a locally made electrical generator, a study of performance of a prototype parabolic trough solar collector using vegetable oils, used and unused engine oil and saline solutions and performance thermal characterization of saline solutions, vegetable oils, used engine oil and unused engine oil and examination of their suitability as heat transfer fluids was done.

A vegetable oil is a triglyceride extracted from a plant (Sauro, *et al.*, 2103). It can be extracted from a seed or form a nut. In this study vegetable oil 1 was extracted form a seed, refined and sold in the local market. Vegetable oil 2 was an extract form a nut and was refined and sold in a local market. Vegetable oil 1 is an extract from a nut (O'Brien, 1988). In an oil refining study it was observed that vegetable oil 2 had a thermal conductivity of 0.1564 $Wm^{-1}K^{-1}$ and a specific heat capacity of 2.857 $KJkg^{-1o}C$ at 300 ^{o}C (Chempro Technovation, 2013).

Various test parameters pertaining to each of the study components were measured as described. The measuring instruments that were used were: - a digital multimeter, a Bourdon tube gauge, a digital thermometer, a digital water flow meter and a solar power intensity meter.

3.2 General Fabrication Procedures

The following processes were undertaken during fabrication of solar thermal components; laying out, cutting, bending, forming and welding. During the laying out, measurements and markings along which cutting and welding was done, were made on

the black sheets. A scriber was used for drawing lines on the sheet metal. A flat steel square was used for marking parallel lines. A protractor was used for drawing angles other than 45° and 90°. To mark the beginning and end of a line a prick punch was used. Dividers were used to scribe arches for small circles for temperature and pressure sensor terminals. Trammel points were used to scribe circles of the cylindrical parts of the components.

To cut along the marked lines of cylindrical sheets, compound lever shears and oxy fuel torch were used; chisels were used for smaller cuts. Straight snips were used to cut along straight lines. The solid punch was used to cut the small diameter holes for the temperature sensor probes. The cylindrical and hemispherical shapes were formed using the slip roll forming machine and drill presses. The cut pieces were joined by welding. The welding machine was adjusted for metal thickness and electrode selected and used. The final assembly was made using some manual hammering, welding, riveting, threading and fastening.

The selection of materials which were used for fabrication of the steam storage system, heat exchanger and the turbine was guided by American iron and steel guidelines (AISI, 2001), American Society of Mechanical Engineers (ASME, 2002b), Tubular exchangers manufacturers association (TEMA, 1993), American petroleum institute 612 (API, 1995), steam plant calculations manual (Ganapathy, 1994), Thermodynamics of steam engine and other heat engines (Cecil, 2011), Physical data book in SI units (Hanssan, 1972), Heat Exchanger Hand Book (Hewitt, 2002). Fundamentals of Heat and Mass Transfer (Incopera, 2007), Steam turbines – their construction, Selection and Operation (Jachen, 1996) and Theory and design of plate and shell structures (Maan, 1994). The TEMA, API, and manuals provided guidance for the design specification ranges regarding the stress, modulus of elasticity, pressures of operation and temperature were provided. The Physical data book provided the values of specific heat capacities and other physical quantities regarding the materials that were used in this study. Thermodynamics of steam engines provided the specific enthalpies of steam with regard to temperature, density and pressure.

3.3 Measuring Apparatus

The apparatus that were used in this study were:-

A digital multimeter model MY – 64. The brand name is Oem digital multimeter made in China. It had an accuracy of 0.5 $\pm$ 1. Power output from the generator was determined using the readings of voltage and current that would be displayed by the meter. The current corresponding to the voltage was measured for every change in current.

A Bourdon tube gauge shown was used for pressure measurement; It consisted of a formed tube with one fixed end and the other end free to deflect under pressure. This gauge had an accuracy of $\pm$ 0.25 %.

Figure 3. 1: Bourdon tube gauge

A Digital thermometer. The digital thermometer was used for measuring temperature. The probes were made of Nickel – Chromium alloy and Nickel metals. During calibration the fixed points of ice i.e melting point of ice of 0 ^{0}C and boiling point of 100 ^{o}C were used to find the voltage increase per each degree of temperature rise. The accuracy was found to be 1 % $\pm$ 1.

A Solar power intensity meter model BTU W/m^2 auto tester; the radiation energy tester auto range had four buttons, two of which were to enable display

of solar power intensity in terms of BTU units and in W/m^2. The other two were for setting it. It would be placed at the plane of the solar concentrator to measure the direct beam radiation intercepted by the collector. The accuracy of the meter was $\pm$ 10 W/m^2. Figure 3.2 shows solar power intensity measurement meter which was used in this study.

Figure 3. 2: Solar power intensity meter

A Digital water flow meter. The solar power intensity meter was manufactured by India mart manufacturers of India. It was made of aluminium and nylon housing. It would display instantaneous flow rate. There were reset buttons to enable measurement of different flows. The accuracy of the readings displayed was $\pm$ 1%. Figure 3.3 shows the digital flow meter that was used in measurement of liquid flow rate.

Figure 3. 3: Digital water flow meter

3.4 Steam Storage System

3.4.1 Introduction

In this section design, fabrication and testing of the steam storage system is presented. The component was designed using auto cad. The component was used in solar thermal harvesting using the following heat transfer liquids:- water, Vegetable oil 2, vegetable oil 1, used engine oil, unused engine oil, 2 M, 4 M and 6 M sodium chloride solutions. The testing of the named component was carried out using the named heat transfer fluids which heated water to steam so that it would be possible to assess their suitability as solar thermal storage fluids during the collection of solar thermal energy. Figure 3.4 shows the cross section of the steam storage system. The pressure gauges Po and P_i and the digital thermometers T_o and T_i that were fixed on entry and exit of the heat transfer fluid into and out of the steam storage system were used to take the pressure and temperature of the heat transfer fluids respectively. The heat transfer fluids were put in the storage system each on its turn and were heated. The thermostat was used to set the temperatures of the heat transfer fluids. The saline solutions were tested in the temperatures of 100 ^oC, 150 ^oC, 200 ^oC, 250 ^oC and 290 ^oC. The used engine oil was tested in the range of 100 ^oC, 150 ^oC, and 200 ^oC. The unused engine oil was tested in the range of 100 ^oC, 150^oC, 200 ^oC, 250 ^oC. Water was tested in the range of 100 ^oC, 150^oC, 200 ^oC, 250 ^oC and 290 ^oC. Vegetable oil 1 was tested in the range of 100 ^oC to 135 ^oC and the vegetable oil 2 was tested in the range of 100 ^oC and 125 ^oC. Plate 7 on appendix A shows the thermostat and the electrical switch which were used in this test. On being heated they were passed through the heat exchanger and the water which flowed on the shell side turned into steam. The thermostat maintained the temperature of the heat transfer fluid at the set temperature during the test. The hot heat transfer fluid heated water which flowed on the shell side of the heat exchanger to make steam. A three dimensional auto Cad diagram of the steam storage system is presented in appendix P.3.

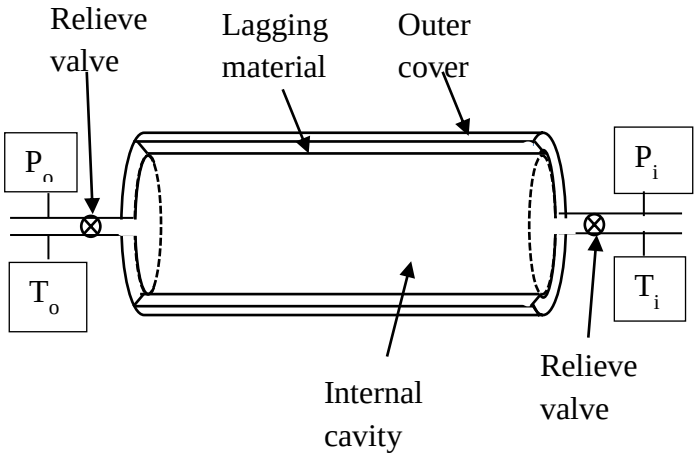

Figure 3. 4: Main parts of the steam storage system

The steam storage system was used in the steam generation system where the steam could be stored during sunshine duration and the excess stored for balancing the load demand during peak demand hours. The peak demand point was the maximum discharge of the steam storage system that would be set at 1.0×10^6 Nm^{-2} and 60 kgs^{-1}. It was determined by adjusting the steam exit valve of the storage system to the maximum of discharge of 60 kgs^{-1}. The essence of fabrication of a steam storage system was to test supply of steam reliability by release of flash steam when the demand was greater than the ability to supply. It could accept steam when the demand was low. Low demand was arrived at by adjusting the discharge valve to minimum corresponding to 3 kgs^{-1} steam discharge at a pressure of 1.0×10^6 Nm^{-2}. Heat transfer fluids flow rates, steam flow rates, temperatures of fluids, heat transfer fluids' specific heat capacity and density were measured and used in the designing the steam storage system. A design trial value of steam mass flow rate which was used was 9.0 kgs^{-1} at a temperature of 300 ^oC and a pressure of 1.0×10^6 Nm^{-2} for the water/steam storage mixture. During the testing the steam was being provided by a 0.02 m^3 boiler powered by 6 Kw electrical heater.

During the solar thermal collection the steam was provided by the sun flux incident on the collector plane.

3.4.2 Design and Fabrication of steam storage system

The design pressure storage system that was designed and fabricated was between 1.0×10^5 Nm^{-2} to 1.2×10^6 Nm^{-2}. It operated at a minimum inlet temperature of 25^oC and a maximum outlet temperature of 380 ^oC for the heat transfer fluids that were used. Two black sheets of thickness 0.005 m for inner casing and the same for the outer surface were cut out according to the auto cad design. Other dimensions of the storage system were; External radius was 0.45 m, internal radius was 0.35 m, length of storage volume was 0.68 m, inlet hole diameter was 0.03 m and outlet hole diameter was 0.026 m. The black sheets were bent and cut by use of dimensions on the Auto Cad lay outs. The inlets and the outlets were made from steel pipe nipples that were secured on the inside using back nuts. Figure P.1 in the appendix shows the design of the steam storage system that was used. The metal sheets were shaped using shears and drill presses. They were cut into desired sizes using oxy fuel torch and its parts were ground to shape for fitting together. The various pieces of storage system were fitted and tack welded together using electric arc welding equipment. Some cutting was also done using chiseling and band saws that had hardened blades. Bending was done using manual hammering. The whole assembly was done by welding, riveting, threading, fastening and bending inform of crimped seam.

To prevent warping, the welded parts were covered with sand during cooling and straightening operations which were carried out after welding. Straightening was carried out using oxy-acetylene flame. The heat was selectively applied to the black sheets in a slow, linear sweep.

Annealing was carried out to reduce residual stress on the welded parts. Storage system breather valve joints and flow curves were prepared by cutting and finishing. Slots for temperature sensors and pressure gauges were prepared by drilling the holes of 0.001 m into the sides of the storage system.

The required thickness of the black sheet was determined by elastic analysis (Maan, 2011), considering allowable stress of σ; 2.0×10^6 Nm^{-2}, pressure p; 1.0×10^7 Nm^{-2}, radius, a radius of a; 1.27 m, elastic modulus E; 1.7×10^6 Nm^{-2} and poisons ratio μ; 0.5

Maximum moment, M was obtained using Equation 3.1 (Baker, *et al.*, 1994).

$$M = \frac{\sigma_y t^2}{4} \quad \text{(3.1)}$$

Thickness, t, of the plate was obtained using Equation 3.3 (Maan, 2011).

$$t = \sqrt{\frac{6M}{\sigma}} \quad \text{(3.2)}$$

The required thickness of the curved shell, estimated to be spherical was obtained using Equation 3.3 (Maan, 2011).

$$t = \frac{P_r}{2\sigma} \quad \text{(3.3)}$$

The longitudinal bending stress σ_l, of the curved storage tank was obtained using Equation 3.4:-

$$\sigma_l = \frac{6M_o}{t^2} \quad \text{(3.4)}$$

The longitudinal stress, σ_h for the hemispherical part was obtained using Equation 3.5 (Goulds, 1998).

$$\sigma_h = \frac{p_r}{2t} + \frac{6M_o}{t^2} \quad \text{(3.5)}$$

The buckling of cylindrical structure under lateral and axial pressure in elastic range was found using Equation 3.6 (Kollar & Dalacska, 1992).

$$P_{cr} = \frac{2.42E}{(1-\mu^2)^{\frac{3}{4}}} \quad \text{(3.6)}$$

The optimum insulation at maximum heat flux was determined using Equation 3.7 (Jawad, *et al.*, 2003).

$$\frac{dQ}{dr_o} = \frac{T_i - T_\infty}{\left(\frac{1}{2\pi r_o \hbar} + \ln\frac{(r_o/r_i)}{2\pi K}\right)^2}\left(-\frac{1}{2\pi r_o^2 \hbar} + \frac{1}{2\pi K r_o}\right) = 0 \quad \text{(3.7)}$$

Insulation beyond critical value increases the heat loss instead of reducing it. Equation 3.7 was solved for $r_o = r_{crit}$ at which R_t was minimum to obtain

$B_i = 1 = \frac{\hbar r_{crit}}{K}$ at maximum heat flux: Where

$r_{crit}-$ Critical radius of insulation, $\hbar-$ average heat transfer resistant, $K-$ thermal conductivity, $dQ-$ heat flux, B_i- Biot number, r_o- outside area, r_i- inside area, $U-$ heat loss coefficient.

Equation 3.8 by Kalogirou, 1997, was used to estimate total mass of saturated steam, M_s which was stored in the fabricated steam storage system.

$$M_s = \frac{M_l C_l B\left(\frac{1}{A-\ln P_i}-\frac{1}{A-lnP_2}\right)}{\frac{\Delta h_{evap}\left(1-\left(\frac{B}{A-\ln P_m}-C+273.15\right)/647\right)}{(1-(t_{ref}+273.15/647))^{0.38}}} \quad \text{(3.8)}$$

Where $ABC-$ are Antoine equation constants, C_l- specific heat capacity of liquid phase, P_l- pressure at beginning of discharge process, P_2- pressure at end of discharge process and $\Delta h_{evap}-$ heat of vaporization, P_m- pressure and $t_{ref}-$ reference temperature of operation.

3.4.3 Measurement of Mass Flow Rate

The digital mass flow rate meter was calibrated against the mass flow rate of the fluid when connected to the flow circuit. The flow rate was quantified by diverting the water in the flow circuit into a twenty liters container and the time taken to fill the container was measured using a stop watch. The amount of liquid flow per second was then calculated. The mass flow rate of the heat transfer fluids was measured using a digital flow meter that displayed the mass of the fluid passing the meter at any time. Measurement of the mass flow rate of water which was flowing on the shell side of the heat exchanger was also measured.

3.4.4 Measurement of Pressure

The bourdon pressure gauges were calibrated against a mercury manometer. The pressure of the steam at the inlet and outlet of the steam storage system was measured

using the tube bourdon pressure gauge. Also the outlet and inlet pressures of the heat exchanger and turbine were measured by reading the pressures shown on the pressure gauge (Plate 4). The pressures of the heat transfer fluids and the water before turning to steam was measured using a U – tube manometer. Mercury was used as the liquid in tube so that a shorter tube was used.

3.4.5 Measurement of Power Output

The power output produced during the testing and during the solar thermal collection was obtained by reading and recording the values of voltage and current displayed by the multimeter and then magnitude of power was obtained by use Equation 3.59. The multimeter probes would be placed at the output terminals of the three phase generator. The values of the alternating current and the corresponding voltage were recorded for each of the heat transfer fluids during and the testing and during the solar thermal collection. The testing was repeated three times and a value for each of the heat transfer fluids was determined (Appendix 1).

3.4.6 Measurement of Efficiency

The efficiency of the steam storage system was measured by determining the heat content of heat transfer fluids before entering the steam storage system and the heat content on exiting the steam storage system. The difference in the heat contents expressed as a ratio of heat in the heat transfer fluid before entering the storage system was expressed as a percentage. The mass of condensed steam was measured using an electronic beam balance shown in Figure 3.5.

Figure 3. 5: The Electronic balance used in the study.

The accuracy of the beam balance was 0.0001 kg. It was manually calibrated by comparing the calibration mass against its value on a triple beam balance. It was reset by pressing down the reset buttons simultaneously for one second. Mass flow rate for the hot heat transfer fluid was determined by collection of the fluid in an insulated metallic container of mass 5 kg and time period for the collection would be recorded before and after the entry into the storage system. The temperature difference was obtained from readings of digital thermometers installed at the entrance and exit of the steam storage system and was used in the evaluation of the heat absorbed and heat emitted by the heat transfer fluid. The probes of the digital thermometers were drilled into the pipe system so that they were in contact with the liquid being measured.

3.4.7 Measurement of Temperature

Mercury in glass thermometer graduated at 0.05 ^{o}C intervals was used to calibrate the digital thermometers which were used as temperature sensors. These temperature were readily available and provided an accuracy of ±0.01 ^{o}C. During installation good thermal contact between fluid and terminals of the digital thermometers was ensured by sinking their contacts deep inside the liquid flow pipe through the 0.001 m holes that were drilled in the piping system. The temperature values were read directly from the digital thermometers. They were placed before and after the liquid entry into the storage

system, heat exchanger and the collector. They were also used to measure the temperature of the fluid entering the turbine and the one leaving.

3.4.8 Measurement of Mass of Steam flow rate

The amount of steam obtained from the steam storage system was obtained from condensing the steam in a container of known mass and the time period when it was collected was measured. The mass of the copper calorimeter and jacket and the condensed steam was measured using a beam balance. Water at ambient temperature water of known mass was put into the copper calorimeter for condensing the steam. The steam was fed into the water in the calorimeter for 30 s. The temperature difference was obtained by reading the values of the digital thermometer at steam entry into calorimeter and after cooling of calorimeter and its contents to room temperature. Lagging of the steam storage system was done using cotton wool to minimize heat losses from the system. Plate 1 shows the steam storage system before lagging. The mass flow rate of steam generated by the water on the shell side of the heat exchanger was also measured. During coupling of the steam storage system and the heat exchanger, the steam which was formed by water on the shell side of the heat exchanger changing into steam after absorbing heat from the heat transfer fluids which flowed in the tube side of the heat exchanger was also measured. The steam trapped in the calorimeter with water at ambient temperature water was measured within the time of collection to find the steam flow rate (Plate 13). The time interval was measured using a stop watch.

The mass of saturated steam, m_s produced was evaluated by use of Equation 3.9:

$$m_s h_f = m_l c_l \, (t_{sat}\,(P_1) - t_{sat}(P_2)) \quad \text{..... (3.9)}$$

Where h_f is the enthalpy of the water at evaporation, m_l is the mass of water, c_l is the specific heat capacity of the liquid at saturation temperature, P_1 and P_2 are the initial and final pressures at the saturation temperatures.

The amount of heat that was transferred during the discharge was quantified by use of Equation 3.10.

$$\dot{Q} = \frac{c_p\, dt\, m}{t} \quad \text{..... (3.10)}$$

Where $\dot{Q}$ is the rate of heat transferred (J/s), m/t is the mass flow rate c_p is the specific heat capacity of water and dt is the change in the temperature of the fluid. The amount of steam obtained was determined by use of Equation 3.11.

$$m_s = \frac{q}{h_e} \quad \text{..... (3.11)}$$

Where m_s the mass of steam (kgs^{-1}), q is is the heat transfer and h_e is the enthalpy of evaporation of steam (Jkg^{-1}). Evaporation energy for different steam pressures was found using the steam tables (Cecil, 2010). The heat transfer fluid flowed at constant rate for different temperatures and pressures.

3.4.9 Measurement of Heat Absorbed and Emitted

The heat absorbed or emitted by the heat transfer fluid was obtained from the measurement of the mass of heat transfer fluid, inlet and outlet temperatures of the heat exchanger and specific heat capacities of the heat transfer fluids using Equation 3.10. This was done for the heat transfer fluids passing through steam storage system, heat exchanger and the collector each on its own. The amounts of heat absorbed and emitted for water were obtained and compared well to those found in steam tables (Cecil, 2011).

3.4.10 Testing of the Steam Storage system

The testing of the steam storage was carried out using international boiler and pressure vessel code guidelines (ASME, 2002b) and American Society of Mechanical Engineers guidelines (ASME) pressure vessel code – alternate rules (ASME, 2002) with and adaptation of locally available materials. The steam storage system was tested at a pressure of 1.5×10^6 Nm^{-2} which was 130 % testing pressure required by the ASME standards. The material used for the pressure vessel fabrication was of the standards of SA516 Grade 70 PVQ. The steam storage system experiments during its cycles of charging and discharging were carried out. Figure 3.6 shows the testing loop that was used during the testing. During the charging the steam storage exit valve was closed and

at the same time the valve supplying the steam to the storage system was open. The steam storage system was three quarter way filled with water before charging could start. Incoming steam from the boiler first heated the water in the steam storage system.

The boiler steam valve would be set at $1.0\times 10^{6}\ Nm^{-2}$. The pressure control exit valve was closed when the pressure in the steam storage system was building up to the set level and steam charging began.

The valve was set to open at intervals of $1.0\times 10^{5}\ Nm^{-2}$ and increasing up to$1.0 \times 10^{6}\ Nm^{-2}$ for each experiment. During the discharge process the steam from the storage system flowed in to the turbine and power would be produced by the generator.

The following measurements were taken: temperatures of inlet and outlet steam, inlet and outlet pressure from the steam storage system, mass flow rates of both water and the heat transfer fluid and period of time for the collection of steam. Plate 7 on appendix A shows the power source and the thermostat which were used during the testing. Plate 2 also shows the steam storage testing loop used. The power source provided electricity for the heater to make steam while the thermostat was used to set temperatures of the heat transfer fluids during testing. During solar thermal collection the heater and the thermostat were removed. The sun provided the power to heat the heat transfer fluids which in turn heated water into steam.

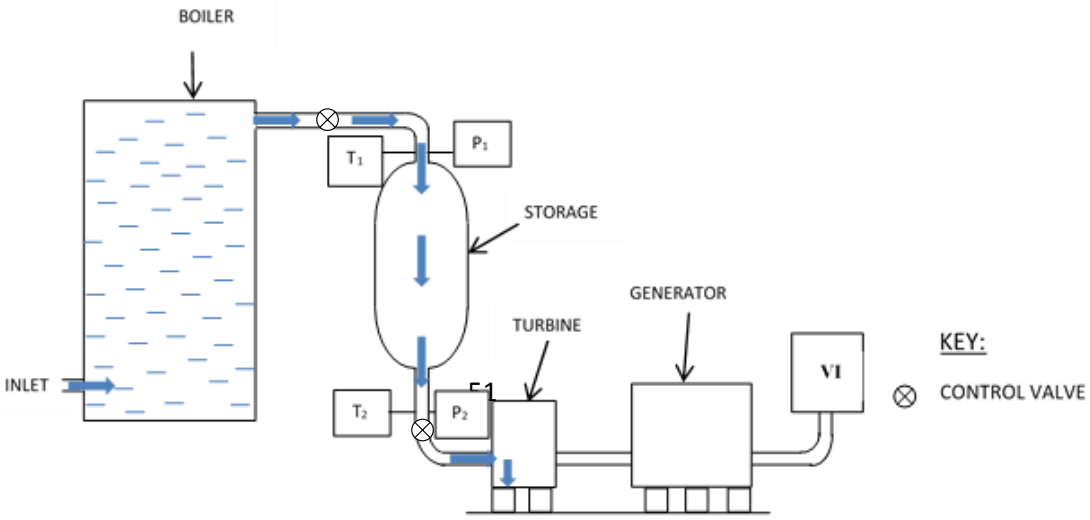

Figure 3. 6: Steam storage testing loop

3.4.11 Sizing of Steam Storage system

The sizing of the prototype steam storage system was undertaken by estimation of the following design parameters; Maximum continuous rating of 40 kgs^{-1}, pressure between 1.0×10^5 Nm^{-2} to 1.0×10^6 Nm^{-2}, Maximum instantaneous demand which corresponded to maximum steam exit valve adjustment, the mean value of overload steam flow rate, mean off peak load steam flow rate which corresponded to minimum steam exit valve adjustment, steam storage capacity and proportion of flashing steam. The maximum instantaneous demand, mean value of overload and the off peak load were measured by use steam inlet and steam outlet valves of the storage system. The steam storage capacity was obtained by use of equation 3.12 (Duffie & Beckman, 2005).

$$Steam\ storage\ capacity = \frac{difference\ in\ enthalpy\ of\ water \times mass\ of\ water}{enthalpy\ of\ evaporation\ at\ lower\ pressure} \ldots\ldots (3.12)$$

3.4.12 Estimation of mean overload and off peak outputs of the storage system

The steam storage system was operated at pressures in the range of 1.0×10^5 Nm^2 and 9.0×10^6 Nm^2 and solar power intensities in the range of 700 Wm^{-2} and 1100 Wm^{-2}. The maximum discharge rate, the time cycle over which it occurred and the length of time the discharge occupied were determined. To measure the maximum instantaneous demand the steam exit valve to the turbine was adjusted to its maximum steam discharge. The rate of the steam discharge was measured and recorded. The amount of discharged steam was measured as described in section 3.4.8.

To determine the maximum continuous rating of the steam storage system for the pressures of operation between 1.0×10^5 Nm^2 and 9.0×10^6 Nm^2 and the solar

intensities of range of 700 Wm^{-2} and 1100 Wm^{-2} the steam mass flow rate was monitored and the values recorded for any changes of pressure and solar power intensities. The amount of flash steam was determined using equation 3.16. The discharge which was the highest after full charge was recorded with the steam storage exit control valve at maximum discharge. The lowest steam discharge when the steam exit valve was adjusted to minimum discharge was also determined.

3.4.13 Charging and Discharge Process

The testing of the steam storage system set up was done as shown in plate 2. The steam storage system was three quarter way filled with water. The steam from the 0.02 m^3 capacity boiler was fed into the steam storage system during testing. The steam control valve was opened and steam allowed into the steam storage at different pressures in the range of $1.0\times 10^5\ Nm^{-2}$ and $9.0\times 10^5\ Nm^{-2}$ and temperatures in the range of 100 ^oC and 300 ^oC. The rate of steam supply and the corresponding power output from the generator was recorded. It was observed when pressure in the steam storage system increased beyond $3.0\times 10^5\ Nm^2$ after 20 minutes the boiler pressure remained constant and the supply of steam was constant despite decrease in solar power intensity. This was attributed to the fact that the water in the steam storage system was under pressure and pressure drop in the storage system caused flashing of steam. The steam pressure valves were set to allow accumulation of pressure in the steam storage system as the charging took place. During this time the steam discharge was allowed at the same time with minimum exit valve adjustment. The steam storage exit valve was set at a mean discharge rate of 18.5 kgh^{-1} and the non-return valve prevented any back flow of steam once it entered the steam storage system. The rate of steam charging was greater than the rate steam discharge during the day. During the steam discharge, the exhaust valve was opened to release the steam to the turbine and during charging it was closed or adjusted to minimum steam discharge to allow accumulation of steam into the steam storage system. The steam pressure control valve regulated the amount of steam entering the storage system.

During overcast and at times when the solar intensity reduced, flashing of steam would take place and the pressure remained at the set point. The non-return valve allowed the steam to proceed into the steam storage system but prevented back flow of the steam from the steam storage system when pressure in the steam storage dropped. The feed water was manually controlled. The mass flow rate of the water at ambient temperature fluid was read from the automatic flow meter and amount of condensed steam was determined by trapping steam in 0.02 kg of water at ambient temperature which was contained in a calorimeter of mass 5 kg within 30 s. The difference between the original mass of the trapped steam and contents of container and the final mass of container and contents provided the mass of steam within 30 s which was measured using a stopwatch. The steam storage efficiency was determined from calculating heat content in steam output by use of the steam tables (Cecil, 2010) and finding the heat content in fluid exiting from turbine expressed as a percentage of the original heat contetnt. The evaporation ratio was determined by measuring the heat quantity of steam generated in 60 s as a ratio of heat from collector input which was expressed as a percentage.

Load levelling was done by the help of the manual steam control valve which was fitted on the steam storage system outlet; it was set to produce steam per unit time when the solar power intensity was of range 950 Wm^{-2} and 1100 Wm^{-2}. The exit pressures and the corresponding power output values were recorded.

Thermal losses of the storage system were determined when discharge was taking place and the rate of change in temperature was found. This was done at night when there was no heat supply form the sun. The temperatures were recorded at intervals of one hour. During testing of thermal losses the temperatures of inlet and outlet temperatures of the heat transfer fluids were measured. These were used to find the amount of heat lost or gained by the steam storage system. Approximation of the content of saturated steam /water mixture inside the storage system was done by use of heat transfer mass flow rates. This process was repeated for the steam storage system and heat exchanger coupled system. During solar thermal collection the storage system and heat exchanger coupled system was connected to the solar thermal collection loop as shown in Plate 13.

The measurements of heat transfer fluid mass flow rate and temperature for the determination of the thermal losses of the storage system were done when charging and discharging was taking place.

3.4.14 Measurement of steam entry and Steam exit Pressure

The entry pressure and exit pressure were measured by use of a bourdon tube pressure gauge that was positioned at the entry and exit of the turbine inlet and outlet respectively. The turbine outlet was providing the exit for the steam – water mixture that was passing to the turbine blades. It represented expanded steam from which kinetic energy of the steam had been extracted to turn the blades. The testing loop for the steam store was as shown in plate 2 of Appendix A.

3.4.15 Measurement of efficiency and evaporation ratio

The measurement of the efficiency of the steam storage system was carried out by quantifying the amount of heat output content and the heat input content of the heat transfer fluids expressed as percentage as shown in Equation 3.13.

$$\eta = \frac{Heat\ out\ put}{Heat\ input} \times 100 \quad \text{(3.13)}$$

To find the evaporation ratio, the heat in steam output and the heat supplied by the electrical heater during testing or heat supplied by the collector during solar thermal collection was quantified. The values obtained were used in Equation 3.14.

$$\text{Evaporation ratio} = \frac{Heat\ in\ steam\ out\ put}{Heat\ from\ collector\ input} \times 100 \quad \text{(3.14)}$$

The steam flow rate was obtained by use of Equation 3.15 (Barret *et al*., 1986).

$$\dot{m}_s = 12\ K_v\ P_1 \sqrt{(1 - 5.67\ (0.42 - \chi)\ )^2} \quad \text{(3.15)}$$

Where $\dot{m}_s$ is the steam flow rate (kgh^{-1}), k_v is the capacity index factor/ valve flow rate coefficient = 100 m^3h^{-1}, P_1 is the boiler pressure bar and χ is the pressure drop ratio $\Delta P/P_1$. The pressure drop ratio was obtained from Equation 3.16.

$$\chi = \frac{P_1 - P_2}{P_1} \quad \text{..... (3.16)}$$

3.4.16 Measurement of proportion of flash steam

The proportion of flash steam, $S_{f,}$ was determined by setting the charging pressure by use of pressure control valve and the discharge pressure was measured using the pressure gauge. Equation 3.17 was used to calculate the proportion of flash steam (Church, 1987).

$$S_f = \frac{\left(h_f(P_1)\right) - \left(h_f(P_2)\right)}{h_g(P_2)} \quad \text{.....(3.17)}$$

Where h_f, h_g are heat coefficients at pressure P_1 and P_2 respectively. Steam tables were used in the evaluation of the proportion of flash steam. The heat coefficients of steam at various temperatures was obtained from steam tables (Cecil, 2010).

3.4.17 Measurement of Physical parameters.

The physical properties that were studied and approximated were axial strain, axial stress, modulus of elasticity load and thickness. The axial strain was measured at a pressure of 1.0×10^6 Nm^{-2}. Two lines of thickness 0.001 m and 0.01 m apart were drawn axially on the steam storage system when there was no steam. Then steam was put in the storage system until the pressure gauge read a pressure of 1.0×10^6 Nm^{-2}. The distance between the two lines was measured again using a Vernier scale and the axial strain was determined as the ratio of change in length to original length. The percentage strain was obtained for various parts of the storage system. This was done by repeating the procedure above on different parts of the storage system and calculating the percentage.

The modulus of elasticity was measured by putting the steam in the steam storage system up to a set pressure of 1.0×10^6 Nm^{-2} which was the maximum pressure of operation for the design. The force produced by the steam was obtained from equation 3.18

$$F = P \times A \quad \text{.....3.18}$$

The area of the steam storage under the impact was measured.

The stress was measured in terms of pressure. The stress magnitudes tested were 1.0×10^5 Nm^{-2}, 2.0×10^5 Nm^{-2}, 3.0×10^5 Nm^{-2}, 4.0×10^5 Nm^{-2}, 5.0×10^5 Nm^{-2}, 5.0×10^5 Nm^{-2},
6.0×10^5 Nm^{-2}, 7.0×10^5 Nm^{-2}, 8.0×10^5 Nm^{-2} and 9.0×10^5 Nm^{-2}.
The modulus of elasticity was obtained by use of Equation 3.19

$$E = \frac{\sigma}{\varepsilon} \quad \text{..... (3.19)}$$

Where E is the modulus of elasticity, σ is the stress and ε strain. The loading was done in terms of pressure. The pressure control valve was adjusted to the pressures shown and the change in the distance between the axial lines was measured.

3.5 Heat Exchanger

A heat exchanger was designed for use in transmitting the heat from heat transfer fluids to water. This was because the heat transfer fluids could not be fed directly into the turbine. The material which was used for separating the hot heat transfer fluid and the water was copper. Copper is a good conductor of heat and hence it conducted heat from the hot heat transfer fluids to water.

3.5.1 Introduction

The purpose for designing a heat exchanger was to extract heat from the heat transfer fluids. The rates of heat transfer were determined to examine the heat transfer fluids suitability for use in production of power that can be used by areas which are hindered from connection to the grid. The shell and coiled tube heat exchanger was considered for design and fabrication since it gives a large surface area in a small volume, provides a good shape for pressure operation, uses well established fabrication techniques and can be constructed from a wide range of materials.
In the design of the coiled tube and shell tube exchanger the following was put to account; duty was defined for the heat exchanger in terms of heat transfer rate, rates of fluid flows and their temperatures, specific heat for the heat transfer fluids and density.

A trial value of overall heat transfer coefficient, U of 350 $Wm^{-2o}C$ was used, the mean temperature difference was calculated, the heat transfer surface area was calculated and the least area was obtained by minimization, the heat exchanger lay out was made on auto cad, the calculated overall heat transfer coefficient was compared with the trial value and found to be 361.7 $Wm^{-2o}C$, the heat exchanger pressure drop was calculated and the smallest area that was giving the above was obtained. The tube used for the heat exchanger was made of copper as shown in Plate 3. Figure P.2 of the appendix shows the design that was used for the heat exchanger fabrication.

Tube and shell heat exchanger was designed using Auto Cad and fabricated since it provides a large ratio of heat transfer area /olume and weight compared to other types of heat exchangers (Incopera, 2007). Fabrication guidelines for the process are presented in section 3.2. To make the shell, a 0.005 m black sheet was machined and rolled. The design equations that guided the 0.09 m^3 shell volume capacity was determined by considering overall heat transfer coefficient among other factors. Figure 3.7 and 3.8 respectively show the coiled tube parameters of heat exchanger and the arrangement of the inlet and outlet flows of fluids.

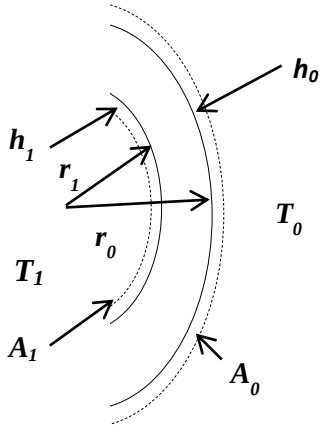

Figure 3. 7: Coiled tube parameters.

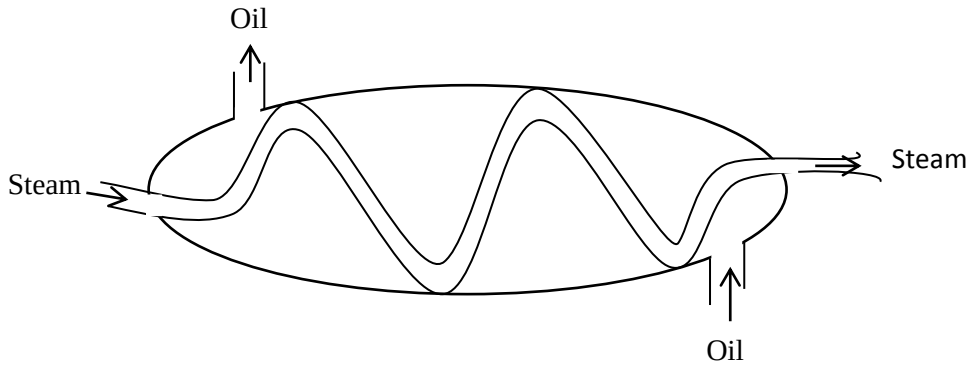

Figure 3. 8: Flow of fluids in the coiled tube heat exchanger

Figure 3.7 gives the following parameters; T_i , is the temperature of the liquid surrounding the tube, r_o and r_i is the outer and inner radii of the tube, T_o, is the temperature of fluid surrounding the tube on the out let side. A_i and A_o are the inner and outer heat transfer surface areas respectively. U_o, the overall heat transfer coefficient for the outer surface area was obtained using Equation 3.20 (Maan, 2004).

$$U_o = \frac{1}{\frac{A_o}{h_i A_i}+\frac{R_{fi}A_o}{A_i}+\frac{A_o \ln(r_o|r_i)}{2\pi L K_w}+R_{fo}+\frac{1}{h_o}} \quad \text{..... (3.20)}$$

For the inner surface the corresponding heat transfer coefficient U_i was obtained using Equation 3.21:-

$$U_i = \frac{1}{\frac{1}{h_i}+R_{fi}+\frac{A_i \ln(r_o|r_i)}{2\pi L K_w}+\frac{R_{fo}A_i}{A_o}+\frac{A_i}{h_o A_o}} \quad \text{..... (3.21)}$$

The design equation was solved by defining mean temperature difference and the design area was obtained using Equation 3.22 (Collier, 1994).

$$A = \frac{Q_t}{U_x(MTD)} \quad \text{.....} \quad (3.22)$$

Where Q_t – Heat exchanger, A - area of heat transfer, U_x – heat loss coefficient, MTD mean temperature difference for counter current cooling. The mean temperature difference was obtained using Equation 3.23 (Saunders, 1998).

$$MTD = \frac{(T_i - t_0) - (T_0 + t_i)}{In\left(\frac{(T_i - t_0)}{(T_0 + t_i)}\right)} \quad \text{.....} \quad (3.23)$$

Where T_i is the inlet temperature of the hot fluid, t_o is the outlet temperature of the water at ambient temperature fluid, T_o is the outlet temperature of the hot fluid and t_i is the inlet temperature of the water at ambient temperature fluid.

The heat exchanger was designed to operate at a temperature of 350 ^{o} C, at a heat transfer rate of 85.0 J s^{-1} kg^{-1}, with a steam flow rate of 12.0 kgs^{-1}. The trial value of overall heat coefficient was 350 W/ m^{2o}C. For the purpose of design the mean temperature difference was calculated. The heat exchanger surface area which was the smallest area that could be used for the heat transfer for the duty defined was determined. The pressure drop on the tube side and the pressure drop on the shell side was also determined.

To make the shell, its lay out on auto cad was marked on the black sheets and cut out. The design equations that guided the 0.0098 m^3 shell volume capacity was determined by considering overall heat transfer coefficient. A coiled copper tube which was 5 m in length and 0.013 m in diameter was fixed in the shell of the heat exchanger. The tube was supported by 0.05 m $\times$ 0.028 m galvanized cast iron bars that acted as baffles. The shell side fluid was water and the tube side fluid was heat transfer fluids. The shell was circular in cross-section and was made by machining, rolling and bending 0.015 m thick black sheet into a cylindrical structure and the longitudinal joint was welded. The top and bottom parts of the heat exchanger consisted of hemispherical parts of radius 0.028 m.

3.5.2 Heat Exchanger Testing

The American Tubular Exchanger Manufacturers Association (TEMA) standards (TEMA, 1993) were applied. In these standards the design and manufacturing tolerances, corrosion allowances, recommended design stresses for materials of construction and the pressure code for the shell were used. During the testing of the heat exchanger, the steam temperatures with a range of 100 °C, 150 °C , 200 °C,250 °C and 300 °C was fed to the heat exchanger from a boiler. The temperatures were set using a thermostat. Water at ambient temperature flowed on the shell side of the heat exchanger and on absorbing the heat it would turn to steam. The steam produced was fed into the turbine where mechanical energy of rotation was generated that was transformed to electrical power in the generator.

The testing loop shown in Figure 3.9 was used in testing of the heat exchanger. Plate 7 shows the power source and the thermostat used during the testing.

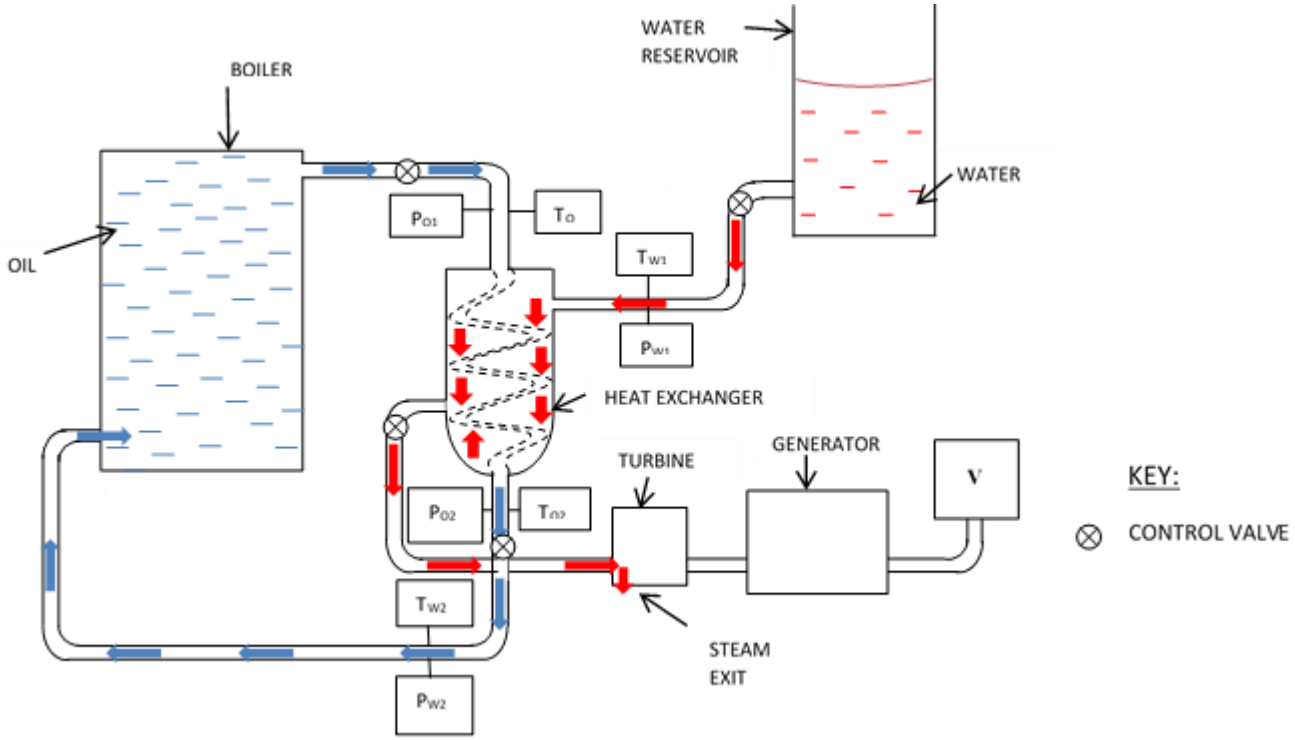

Figure 3. 9: Heat exchanger testing loop

The system was allowed to reach steady state i.e. state where the mass flow rate, pressure, and steam discharge were constant. The readings of pressure and temperature were taken three times at different intervals to ensure that steady state had been achieved whereby the readings obtained for the parameters varied by less than 1 %. Plate 7 shows the power source and the thermostat that were used during the testing. The power source provided electricity for the heater to make steam while the thermostat was used to set temperatures of various tests. The pressure control valve was used to set pressures between 1.0×10^5 Nm^{-2} and 1.0×10^6 $Nm^{-2.}$ After the testing the coiled heat exchanger was used in solar thermal collection.

3.5.3 Heat Absorbed and Heat Emitted

Heat absorbed by the water at ambient temperature fluid q_a was obtained using Equation 3.24:-

$$q_a = m_c . c_{pc} (T_{c2} - T_{c1}) \quad \text{(3.24)}$$

Heat emitted by the hot fluid was obtained using Equation 3.25:-

$$q_e = m_h . c_{ph} (T_{h2} - T_{h1}) \quad \text{(3.25)}$$

Heat transfer coefficient, U was obtained using Equation 3.26:-

$$U = \frac{qe}{A\,\Delta t_{lm}} \; W/m^2K \quad \text{(3.26)}$$

Where A is the heat transmission surface area, Δt_{lm} is the temperature difference.

The energy balance equation for the two fluid heat exchanger was obtained using Equation 3.27:-

$$m_2 c_{p2}(T_{2,in} - T_{2,out}) = m_1 c_{p1}(T_{1,out} - T_{1,in}) \quad \text{(3.27)}$$

It was assumed that the overall heat transfer coefficient (U), the isobaric specific heat of fluid and (c_p) were constant.

Heat losses were assumed negligible and that flow rates of the fluids were constant.

The rate of heat transfer for the heat exchanger was obtained by use of Equation 3.28

$$\dot{Q} = \dot{m} c_p (T_{in} - T_{out}) \quad \text{(3.28)}$$

The rate of heat produced by the heat transfer fluid, $\dot{Q}_e$, was obtained by use of Equation 3.29

$$\dot{Q}_e = \dot{m}_h \, c_{p,h}\left(T_{2,i} - T_{2,o}\right) \quad (3.29)$$

Where $T_{2,i}$ and $T_{2,o}$ was the inlet and outlet temperatures of the hot heat transfer fluid, $\dot{m}_h$ was the hot heat transfer mass flow rate and $c_{p,h}$ was the specific heat capacity of the hot fluid.

The rate of heat absorption, Q_c, by the water at ambient temperature fluid that converted to steam was obtained by use of Equation 3.30.

$$\dot{Q}_c = \dot{m}_c c_{p,c}\left(T_{1,i} - T_{1,o}\right) \quad (3.30)$$

Where $\dot{m}_c$ was the mass flow rate of the stream of water at ambient temperature fluid flow, $c_{p,c}$ was the specific heat capacity of the water at ambient temperature flow fluid and $T_{1,i}$ and $T_{2,o}$ are the inlet and outlet temperatures of the water at ambient temperature fluid flow respectively.

The rate of heat loss Q_l was obtained by use of Equation 3.31

$$\dot{Q}_l = \dot{Q}_e - \dot{Q}_c \quad (3.31)$$

The overall heat loss coefficient, U, was obtained by use of Equation 3.32

$$Q = W_h(T_{h,in} - T_{h,out}) = W_c\,(T_{c,out} - T_{c,in}) = UA \times \Delta t \quad (3.32)$$

Where W_h and W_c is the water at ambient temperature and hot stream heat capacity rate respectively, $T_{h,in}$ is the inlet temperature of the hot fluid flow and $T_{h,out}$ is the out let temperature of the water at ambient temperature fluid flow respectively.

The highest temperature rise was taken as the difference between the temperatures of the two entering streams. The highest temperature rise was obtained with the fluid with the least capacitance by use of Equation 3.33.

$$Q = UA\Delta T_t \quad (3.33)$$

Q is the quantity of heat, U is the heat transfer coefficient, A was the heat transfer area and ΔT_t is the total temperature difference or the overall driving force for the process.

3.5.4 Measurement of Mass Flow Rate

Mass flow rate of the tube flow of the heat exchanger was measured by collecting the hot fluid flowing into a 5 kg copper container. A beam balance was used to find the mass of the heat transfer fluid. The period within which the fluid was collected was measured using a stop watch. The mass flow rate on the shell side was measured using of a digital flow meter which showed the flow rate. The volume control valve was adjusted to allow more water at ambient temperature water to flow during high demand i.e when valve was adjusted to maximum discharge and a limited amount to flow during off peak demand (minimum valve discharge adjustment). High demand was estimated by opening the exit valve to a maximum discharge of 50 kgh^{-1} while the off peak was estimated by adjusting the valve to a discharge 10 kgh^{-1} of steam. On absorbing heat from the hot fluid flowing in the tube side the water in the shell side of the heat exchanger changed into steam.

3.5.5 Measurement of Power Output

When heat transfer fluids from the collector passed through the tube side of the heat exchanger the water on the shell side of the heat exchanger absorbed heat and turned into steam. The steam pressure built up in the heat exchanger when the heat exchanger steam exit valve was closed. The steam from the shell side of the heat exchanger flowed in to the turbine when the exit valve was open. The multimeter probes were put on the output terminals of the generator and values of voltage and current were read directly from the multimeter. The power output was obtained from Equation 3.59.

3.5.6 Measurement of Efficiency

The efficiency of the heat exchanger was determined in terms of the amount of heat extracted by the water at ambient temperature water from the hot fluid flow and the initial amount of heat for the hot fluid before entry into the heat exchanger expressed as a percentage. The total amount of heat absorbed by the water in the water at ambient

temperature flow stream was calculated from mass flow rate of the water at ambient temperature flow, temperature change and specific heat capacities of the heat transfer fluids. The mass flow rate of the hot fluid was also determined and the temperature drop was determined from the digital thermometers located at the entry and exit of fluid to and from the heat exchanger. Equations 3.28 and 3.29 were used to determine the amounts of heat.

The mean temperature efficiency for the fluid transmitting heat to the water at ambient temperature fluid was obtained by use of Equation 3.34

$$\eta_T = \frac{T_{2,1} - T_{2,O}}{T_{2,i} - T_{1,i}} \times 100 \quad \text{..... (3.34)}$$

Energy efficiency of the heat exchanger was obtained by use of Equation 3.35

$$\eta_e = \frac{energy\ exchanged}{total\ energy\ supplied} \times 100 \quad \text{..... (3.35)}$$

3.5.7 Measurement of Temperature

The temperature of heat transfer fluid was measured before it entered the heat exchanger and on leaving the heat exchanger. The pressure of the heat absorbing liquid in the heat absorber was also measured. The temperature of the steam leaving the heat exchanger and going into the steam turbine was measured. The temperature and pressure of the fluid from the turbine was measured by checking the readings on the digital thermometer and the pressure gauges.

3.5.8 Measurement of heat exchanger effectiveness

The heat exchanger effectiveness was a measure of magnitude of amount of heat that was actually transferred between the heat transfer liquid and the liquid transporting the heat to the turbine and the generator. The actual energy change for the heat transfer fluid was obtained using Equation 3.29. The heat exchanger effectiveness was obtained by use of Equation 3.36

$$\varepsilon = \frac{Actual\ energy\ change}{greatest\ theoretical\ energy\ change} \quad \text{.....(3.36)}$$

3.5.9 Number of heat transfer units

The number of heat transfer units can be used as a measure of size of heat exchanger. The number of heat transfer units was evaluated from Equation 3.37 (Srinivasa, 2014).

$$NTU = \frac{UA}{W_{min}} \quad \text{.....} \quad (3.37)$$

Where W_{min} is the smaller heat capacity rate, UA is the overall conductance, A is the total heat transfer surface area (m^2) and U is the overall heat transfer coefficient ($W/m^2\ ^0C$). The overall conductance was determined from the values of overall heat transfer coefficient for the different heat transfer fluids and the heat transfer area.

The fluid heat capacity ratio, ω, was obtained by use of Equation 3.38(Vera, 2010)

$$\omega = \frac{W_{min}}{W_{max}} \quad \text{.....} \quad (3.38)$$

Where W_{min} is the lower heat capacity of the two streams and W_{max} higher heat capacity. In the inner copper tube of the heat exchanger, hot heat transfer liquid temperature was reduced by the water at ambient temperature fluid flowing in its surrounding and the overall heat transfer coefficient involved was obtained by use of Equation 3.39.

$$U = \frac{W_{min}}{A} . NTU \quad \text{.....} \quad (3.39)$$

The calculations of U obtained accounted for all other factors that affected thermal performance.

3.5.10 Measurement of Steam Output

The shell side of the heat exchanger produced steam that would proceed to the turbine for energy conversion. The steam formed from the shell side was trapped in a 5 kg copper container with 2 kg mass of water at ambient temperature water. The mass of the steam was calculated per unit time of collection. During steam collection the steam outlet control valve was closed and the temperature and pressure were read and recorded.

In testing the heat exchanger the boiler pressures was set up between pressures of 1.0×10^5 Nm^{-2} and $1.0\times 10^6\, Nm^{-2}$ and the inlet temperatures were set using a thermostat. The heat transfer fluid was allowed to circulate for twenty minutes to obtain a steady state operating conditions whereby:-

$\dot{Q} = \dot{m}c_p(T - T_a)$ was held constant. Where $\dot{m}$ was the mass of the flowing heat transfer fluid, T was the temperature of operation and T_a was the ambient temperature. To ensure a constant mass flow rate, a constant amount of fluid was supplied to the heat exchanger. This was made possible by adjusting the volume control valve of inlet flow. The thermostat would be set at the desired test temperatures to ensure a constant temperature for a particular flow rate. The temperature range was set between 100 ^oC to 300 ^oC.

Non return valve would close down when the steam flow reduced in the heat exchanger. The volume control valves were used to regulate the amount of water at ambient temperature water flowing into the shell side of the heat exchanger and the boiler feed pipe.

The inlet and out let temperatures of heat transfer fluids was measured. The quantities that were determined to find the percentage of losses or gains were; magnitude of heat emitted from hot liquid and magnitude of heat absorbed by the water at ambient temperature liquid, mass flow rates of hot and water at ambient temperature fluids respectively, inlet and outlet enthalpies of hot fluids respectively, inlet and outlet enthalpies of water at ambient temperature fluids respectively, inlet and outlet temperatures of hot fluid, inlet and outlet temperatures of the water at ambient temperature fluid, and specific heats of water at ambient temperature and hot fluids. The temperature efficiency of the streams was determined by finding the temperature changes in each of the fluid stream and was compared with the maximum temperature difference between the two fluid streams. Temperature efficiencies were also obtained from the temperature measurements taken. The heat lost and the heats gained were evaluated using the measurements obtained above.

3.5.11 Testing of Coupled Steam Storage and Heat Exchanger

Before the start of the charging process, five liters of water were put in the steam storage tank and 0.003 m^3 of water were put on the shell side of the heat exchanger and the system was coupled as shown in figure 3.10. The steam outlet valve of the steam storage system was closed to enable charging that was taking place as a result of the steam that was flowing from the heat exchanger. The steam storage system and the heat exchanger were being charged simultaneously by the boiler. When the pressure was set at 2.0 $\times 10^5$ Nm^{-2}, it took half an hour for the pressure of the system to be constant at the set pressure. The rate of steam discharge of the boiler was 1.3 kgs^{-1}. When discharging the feed water would be opened at intervals of five minutes and then closed. The continuous discharge rate for the steam was 1.1 kgs^{-1}. Each of the heat transfer fluids was passed through the heat exchanger each turn.

The coupled system was then charged using the solar collector as shown in plate 13 of appendix A. The temperature of inlet and outlet steam was measured using digital thermometer. The inlet and outlet pressures were estimated using tube bourdon gauge. The mass flow rate of water was measured using a digital water flow meter. The amount of power output was measured as shown in appendix A. Plate 15 of appendix A shows the power source and the thermostat that were used during the testing. The power source provided electricity for the heater to make steam while the thermostat was used to set temperatures of various tests. The test temperatures used were 100 ^oC, 150 ^oC, 200 ^oC, 300 ^oC.

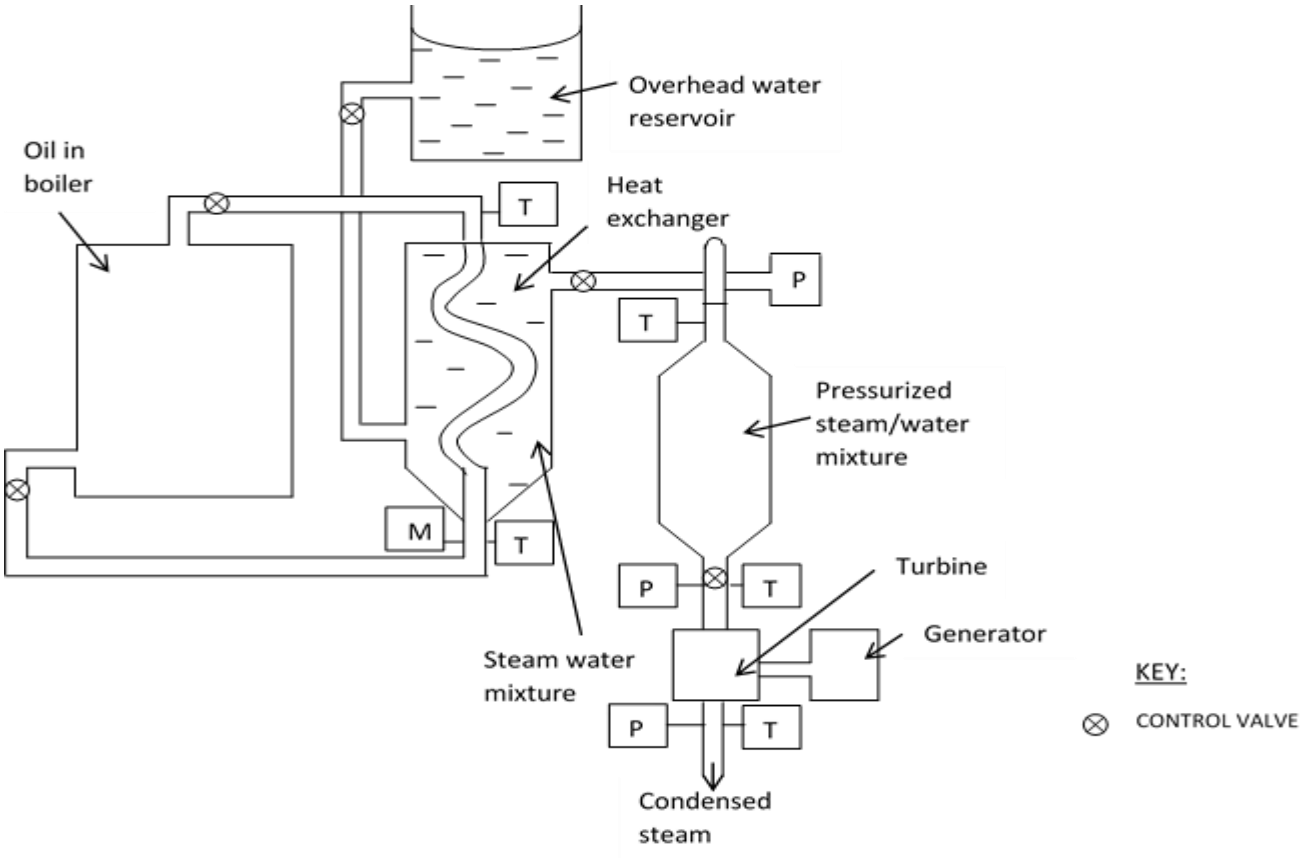

Figure 3. 10: Testing loop for the coupled heat exchanger and steam storage system

During the solar thermal collection using the steam storage and heat exchanger coupled system, the system was set up as shown in figure 3.10.

3.5.12 Investigating a Prototype Heat Exchanger for Steam Storage

Heat Exchanger Storage System

In order to investigate the coiled tube counter flow heat exchanger the following was done; the parameters as per the design of the storage system, were defined as follows: - heat exchanger operational temperature of 350 ^{o} C, at a heat transfer rate of 85.0 Js^{-1} kg^{-1}, with a steam flow rate of 12.0 kg s^{-1} and a capacity of 0.01 m^3 was used. The logarithmic temperature difference was evaluated using Equation 3.40

$$\Delta T_m = \frac{(T_{i,h} - T_{o,c}) - (T_{o,h} - T_{i,c})}{In\frac{(T_{i,h} - T_{o,c})}{T_{o,h} - T_{i,c}}} \quad \text{.....(3.40)}$$

Where $T_{i,h}$ is the hot fluid inlet temperature, $T_{o,h}$ is the hot fluid outlet temperature, $T_{i,c}$ is the water at ambient temperature fluid inlet temperature and $T_{o,c}$ is the water at ambient temperature fluid outlet temperature.

Heat transfer surface area was obtained using Equation 3.41

$$Q = UA\Delta T_m \quad \text{.....(3.41)}$$

Where Q is the magnitude of heat transferred, U is the overall heat transfer coefficient and ΔT_m is the mean temperature difference. A was the smallest area that could be used for the heat transfer for the duty defined by optimization. In the shell side water turned into steam on absorbing the heat from the heat transfer fluid that flowed in the copper coiled tube.

3.5.13 Fabrication of Heat Exchanger

The design of the heat exchanger was done by use of Kerns method (Kuppan, 2000). To make the shell, its layout was made on AutoCAD 2010 software and its measurements were used to cut the black iron sheets. It consisted of two hemispheres which were welded to the cylindrical structure. The dimensions of the heat exchanger steam storage shell were: External diameter of 0.47 m, internal diameter of 0.43 m, length of storage volume of 0.51 m, mass of 49.9 kg ,volume capacity of 0.018 m^3, inner coiled copper tube's external diameter and internal diameter was 0.013 m and 0.015 m respectively, length of coiled copper tube was 1.2 m, shell dome length was 0.019 m, heat transfer fluids inlet tube diameter and the outlet tube diameters were 0.002 m each respectively and the tube inlet and outlet diameters for water were 0.002 m and 0.015 m respectively. The diameter of the water outlet tube was smaller than that of the heat transfer fluids' outlet tube to retain water in the shell for longer period of time. This enhanced the absorption of heat by the water from the heat transfer fluid to make steam. The copper

coils spacing was 0.15 m. During fabrication the coiled copper tube of length 1.2 m and diameter 0.013 m was positioned in the shell side.

The tube was supported by 0.05 m × 0.028 m galvanized cast iron bars that acted as baffles. They supported the coiled tubes in position and reduced the momentum of the coiled tubes under the influence of heat transfer fluid induced eddies. The shell side fluid was water and the tube fluid was heat transfer fluids. Two black iron sheets which were 0.5 m by 0.6 m and 0.015 m were laminated into one sheet using Loctite glue. It was folded into a circular cross-section and was made by machining, rolling and bending into a cylindrical structure and the longitudinal joint was welded. The shell dome was also welded on to the cylindrical structure. Bonnets with threaded connection for the side tube piping were fabricated by machining of seamless galvanized iron pipe. Insulation of the heat exchanger was done using 0.04 m of cotton wool. The heat transfer fluid flowed in the tube since it was at a higher pressure.

The shell side pressure drop was obtained by use of Equation 3.42 (Singh, 1989).

$$\Delta Pa = \frac{2f_c G_s^2 (N_B + 1)}{\rho D_e \left(\frac{\mu}{\mu_s}\right)^{0.14}} \quad \text{..... (3.42)}$$

Where f_c is the friction factor for flow on the shell side of shell side as obtained from TEMA guide lines (TEMA, 1993),

G_s is the mass velocity on the shell side,

D_e is the inside diameter of the shell,

N_B was the number of baffles,

ρ was the density of the fluid flowing on the shell side of the heat exchanger,

l was the tube length and

D was the equivalent diameter.

The tube side pressure drop was obtained using Equation 3.43 (Stevenson and William, 2001)

$$\Delta Pa = f_c \frac{L}{D}\left(\frac{1}{2}\rho V^2\right) \times NP \quad \text{..... (3.43)}$$

Where NP was the number of passes.

The number of heat transfer units was obtained by use of Equation 3.36. The overall heat transfer conductance, UA was obtained as shown in Equation 3.32. Thermal conductivity of copper tube used was 26 Wm^{-1} K^{-1} (Hewitt, 2002). Effectiveness of the heat exchanger was the measure of the amount of heat that was transferred between the hot fluid and the water at ambient temperature fluid which were normalized with the maximum possible enthalpy change, considering no losses. The effectiveness,ε of the heat exchanger was hence obtained by use of Equation 3.44

$$\varepsilon = \frac{Actual\ heat\ transfer}{Maximum\ possible\ heat\ transfer} \quad \text{..... (3.44)}$$

The steam formed exited from the shell through side outlet connection to the turbine. Heat transfer coefficients for the heat transfer fluids were calculated by use of values obtained from fluids coefficients tables (Medrano *et al.*, 2010). Area of baffles was 0.0003 m^2, Tube spacing was 0.05 m and the heat transfer fluid average velocity was 8.0 ms^{-1}. Temperature efficiencies of the heat exchanger streams are an important measure of performance of a heat exchanger. The temperature efficiency of the hot stream was obtained by use of Equation 3.45 (Shah & Senkuli, 2003).

$$\eta_{ht} = \frac{T_{i,h} - T_{o,h}}{T_{i,h} - T_{i,c}} \times 100 \quad \text{..... (3.45)}$$

Where η_{ht} was the efficiency of the hot fluid,

$T_{o,c}$ was the outlet temperature of the fluid at ambient temperature stream,

$T_{i,h}$ was the inlet temperature of the hot stream,

T_{ih} was the inlet temperature of the hot stream and

$T_{i,c}$ was the inlet temperature of the fluid at ambient temperature stream.

The temperature efficiency of the water at ambient temperature fluid was obtained using Equation 3.46 (TEMA, 1993);

$$\eta_{cd} = \frac{T_{o,c} - T_{i,c}}{T_{i,h} - T_{i,c}} \times 100 \quad \text{(3.46)}$$

Where $T_{o,c}$ was the outlet temperature of the water at ambient temperature sream, $T_{i,c}$ was the inlet temperature of water at ambient temperature stream, $T_{o,h}$ was the outlet temperature of the hot stream and $T_{i,h}$ was the inlet temperature of the hot stream.

3.5.14 Heat Exchanger Steam Storage System Charging and Discharging

The heat exchanger steam storage system was charged during the day and was discharged on demand. It required three and half hours to be charged to a capacity of 3.26×10^3 kJ at a maximum temperature of 249.4 ^{o}C and a pressure of 7.2×10^5 Nm^{-2} at solar irradiance of 1097 Wm^{-2}. The safety valve was installed on the heat exchanger storage steam inlet tube to ensure that it does not exceed the set pressure. During charging 0.004 m^3 of water at ambient temperature water was put in the shell and the steam exit valve to the turbine was closed. Hot heat transfer fluid from the solar collector flowed in the tube side of the heat exchanger and heated the water to steam. Steam pressure was allowed to build up to the set pressure after which the steam control discharge valve was opened. The steam was proceeding to the main storage system where it was pressurized further. When there was over cast weather and the heat exchanger storage was fully charged, discharge was producing lower pressure in the shell side. The pressure drop caused flashing of steam from the shell side and hence more steam would be discharged for the turbine thermal energy conversion. The sizing of the heat exchanger steam storage system was undertaken by consideration of the following design parameters: - Maximum continuous rating of 60 kg h^{-1}, the working pressure between 1.0 $\times 10^5$ Nm^{-2} and 1.0×10^6 Nm^{-2}, maximum instantaneous demand of 50 kg h^{-1} and mean value of overload used to size the heat exchanger storage system was 30 kg h^{-1}. The mean off peak load was approximated from the anticipated users of the power at 500 W load and used in off peak sizing calculation. The steam storage capacity was calculated using Equation 3.47.

$$C_{st} = \frac{Q_d \times m_w}{Q_e} \quad \text{.....} \quad (3.47)$$

Where C_{st} was the steam storage capacity, Q_d was the difference in enthalpy of water, m_w was the mas of water and Q_e was the enthalpy of evaporation at lower pressure.

3.5.15 Coupled Heat Exchanger Storage System

The testing loop shown in Figure 3.10 was used in testing of the heat exchanger storage system. Plate 4 also shows the heat exchanger performance testing. The system was allowed to reach steady state. The readings of pressure and temperature were taken three times at half hour intervals to ensure that steady state had been achieved whereby the readings obtained for the parameters varied by less than 1 %. TEMA guide lines (TEMA, 1993) were considered during the testing. In the testing of the heat exchanger storage system, the boiler was set at a pressure of 5.0 $\times 10^6$ Nm^{-2} and the inlet temperatures of operation was fixed using a thermostat to 300 ^oC. The heat transfer fluid was circulated for thirty minutes to obtain steady state operating conditions using Equation 3.48.

$$\dot{Q} = \dot{m} c_p (T - T_a) \quad \text{.....} \quad (3.48)$$

Where $\dot{Q}$ was the rate of heat transfer, $\dot{m}$ was the mass flow rate, T was the temperature of operation, T_a was the ambient temperature and c_p specific heat capacity of storage fluid. The thermostat was set at the inlet test temperatures of 150 ^oC, 200 ^oC, 250 ^oC, 250 ^oC and 300 ^oC to ensure a constant temperature for a particular flow rate.

At steady state it was assumed that the rate of heat flow was constant for the heat exchanger storage system. This was done since insulation kept heat loses to a minimum. The steady position of the system ensured that variations and errors of measurements were minimum. Non return valve closed down when the steam flow stopped to flow in the heat exchanger storage system hence preventing back flow of steam to the parabolic solar collector during solar thermal collection. The inlet and outlet temperatures of heat transfer liquids were measured. The quantities that were used to find the percentage

losses and gains were amount of heat emitted from hot liquid and amount of heat absorbed by the water at ambient temperature liquid. The following were also measured: mass flow rates of hot and water at ambient temperature heat transfer fluids respectively, inlet and outlet enthalpies of the water at ambient temperature and hot fluids were calculated respectively, inlet and outlet temperatures of hot and water at ambient temperature fluids respectively, specific heats of water at ambient temperature and hot fluids and the steam flow rates and enthalpy of the steam produced.

The characteristic properties of the heat exchanger storage system were obtained from the measurements that were taken from the set up. These were heat absorbed, heat emitted, inlet temperatures, outlet temperatures, inlet pressures and outlet pressures. The temperature efficiencies of the streams were obtained by measuring the temperature changes in each of the fluid stream which was compared with the maximum temperature difference between the two fluid streams. The heat lost and the heat gained was obtained by using the temperature measurements obtained. The heat exchanger was feeding the main steam storage system with steam that was supplied to the turbine for power generation. The heat transfer fluids flowed in the tube side of the exchanger and they heated the water on the shell side during charging and discharge. The steam exit valve allowed the steam to move into the turbine during discharge when it was opened.

3.5.16 Measurement of Physical Parameters

The approximation of the physical parameters such as strain, stress, modulus of elasticity, load and thickness were obtained as described in section 3.4.17

3.6 Turbine

The steam turbine extracted thermal energy from pressurized steam and transformed it into mechanical energy of rotating a shaft. The mechanical energy was in turn transformed into electrical power by a generator. Plate 11 of Appendix A shows the four pole magnet on the shaft.

3.6.1 Design and fabrication

Plate 6 shows the turbine after assembly. The turbine fabricated was a direct drive turbine with a single stage blade wheel system. The steam was expanded in a nozzle inside the turbine and the pressure remained constant as it passed over the blade row. The impulse concept was utilized since the blade height was 0.005 m. Figure P.3 of the appendix shows the design of the turbine shaft and the blade. Euler's turbine equation which is shown in Equation 3.49 was used in the blade design (Jachen, 1966)

$$V = h_{1+} + \frac{V_1^{\,2}}{2g} - h_2 - \frac{V_2^{\,2}}{2g} - \frac{U}{g}\,(W_{\theta 1} - W_{\theta 2}) \quad \text{.....} \quad (3.49)$$

Where h is enthalpy of steam, $V_1$and V_2 are velocity components, W is relative velocity, U is internal energy and g is the gravitational field strength. Plate 5 shows the turbine blades welded to the shaft. The blades were cut from a 0.015 m galvanized black sheet. The design layout was made by use of AutoCAD. The cutting was made using the layout marks that were made on the black sheet. Figure P.3 of the appendix shows the turbine shaft and blade design.

The mass of the shaft was 2.5 kg, radius of 0.02 m and a length of 0.5 m. The turbine was designed to produce a rotor speed of 2800 r.p.m. The steam turbine was connected to a single gear box coupled to a three phase generator. Fabricated turbine technical data was: Output: 500 W, Inlet pressure; 2.0×10^6 Nm^{-2}, 4 Pole generator. The blades were fabricated individually and attached to the wheel disc. The moving blade tips were riveted to a cover-band which acted as a labyrinth was fabricated and it braced the moving blades to reduce the vibration. The radial clearance was 0.1 m. The rotor was balanced both statically and dynamically after assembly of the blades. Each blade was balanced individually before assembly. In the static balancing the weight was displaced parallel to rotor axis until the blade balanced. In the dynamic balancing the mass axis was not coincidental with the rotational axis and hence the imbalances were corrected by removal of material from the rotor by drilling and milling and also by adding material to the light position by bolting and welding balance weight. The rotor was tested at a speed of 500 r.p.m. which was then increased to 800 r.p.m., 1200 r.p.m., 1600 r.p.m., 2000

r.p.m., 2400 r.p.m., and 2800 r.p.m. Figure 3.11 shows the turbine blades riveted to the rotor.

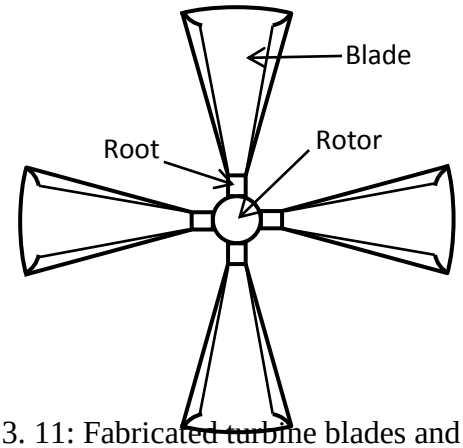

Figure 3. 11: Fabricated turbine blades and setting

The blades were made of galvanized black iron. The shaft was made of steel alloy. Its end contained an integral coupling gland seal and bearing area for the ball bearings. The steel alloy was used since it had a good creep resistance and withstood high temperature and had high fracture toughness.

The rotor was balanced dynamically at a low speed with weight adjustments made in two planes, one at each end of the rotor. Provision was made to vary screwed plugs in tapped holes. Four pedestals were fabricated from galvanized iron rods of diameter 1 mm and length 0.3 m. They supported the turbine via the bearings in a fixed axial relationship such that gland clearances were maintained.

The bearings used were of 0.01 m with length – diameter ratio of 0.1. They were fixed on the shaft-line. They were made of mild-steel. The bores of bearings were elliptical to provide geometry for hydrodynamic lubrication. Circular bores were machined with shims in horizontal split. During operation, oil would be poured manually into the bearing via lead-in ports at two diametrically opposite points on the horizontal center line.

The rotating component consisted of a solid single piece integrally forged rotor shaft with hydrodynamic tilting pad bearings and flexible element couplings.

The rotor design depended on the flow path and the size of inlet which was 0.001 m. The nozzles were fabricated such that its cross-section varied from 0.008 m to 0.001 m and was put at an angle of 30^0 to the blade. The angle used compared well with US Patent number US 3452132 (Pitzl, 1969). The nozzle end diameter was 0.001 m, so that the flow of steam through the nozzle was an adiabatic expansion. A control valve was threaded to the nozzle to control steam flow into the turbine.

The steam casing was made from 0.0025 m thick galvanized cast iron sheet. The half pieces were bolted together and rubber seals put in between the half cases to prevent leakage of steam from the steam chamber.

3.6.2 Estimation of Measurement of Rotor Speed

The angular velocity of the rotor or shaft was estimated from measurements of magnitude of how much the angle changed with time using a white line reference mark made on it. The larger the angular velocity the greater was the velocity of the rotor.

The speed of rotation of shaft as a design parameter was obtained from the product of number of generator pole pairs and rotational speed. The magnitude of change of angle was recorded.

3.6.3 Measurement of Blade Centripetal Force

The following measurements were made in order to find the centripetal forces on the blades: cross sectional area of the blade was measured by measuring the length and width of the blade using a tape measure, measurement of blade tip radius and radius of rotor disc using tape measure and measurement of angular velocity. The density of the material from which the blades was made from was confirmed by an experiment where the mass of a 0.0005 m^2 was measured using a beam balance and its volume was determined using displacement method. Figure 3.12 shows the force which acts on the turbine wheel during operation.

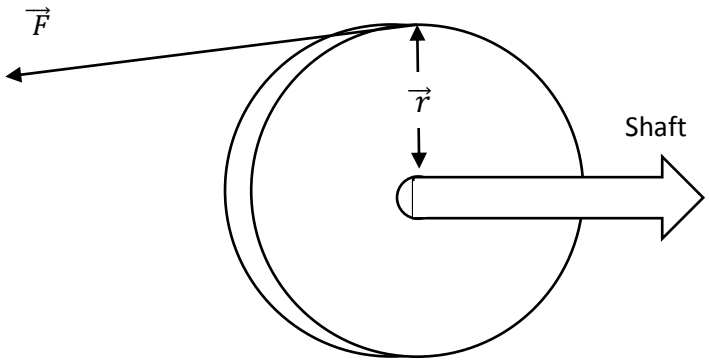

Figure 3. 12: Force acting on the wheel of the turbine

The blade centripetal force, F, was obtained by use of Equation 3.50

$$F = \rho A \omega^2 \left(\frac{{r_2}^2 - {r_1}^2}{2}\right). \quad \text{(3.50)}$$

Where ρ is the density of the material the blade is made of (steel), A is the blade cross sectional area, ω is the angular velocity and r_2 is the blade tip radius and r_1 is the radius of the rotor disc.

3.6.4 Measurement of Shaft Torque

The torque of the shaft was determined by obtaining the power of the turbine in watts and the rotational speed which were used as shown in Equation 3.51.

$$torque = \frac{Power\ in\ Watts}{2\pi \times Rotational\ speed} \quad \text{(3.51)}$$

3.6.5 Estimation of Angular Velocity

A white line 0.01 m and 0.01m in thickness was marked on the shaft. A protractor was placed against it. At initial position angular displacement was zero and time lapse was also zero. A steam valve to produce steam which turned the blades on the shaft was opened fully and at the same time a stop watch was started and then stopped after five seconds. The steam valve was opened again and was closed after ten seconds. The angular velocities at these two positions were evaluated from the angular displacement

observed. The angular acceleration was determined as the rate of change of angular displacement with time by use equation 3.49. In the five seconds the line turned through an angle evaluated by use of Equation 3.52.

$$\Delta\theta = \omega_i \Delta t + \frac{1}{2}\alpha(\Delta t)^2 \quad \text{.....(3.52)}$$

Angular velocity, ω, was obtained by converting the rotations per minute to angular velocity by use of Equation 3.53

$$\omega = \frac{rpm \times 2\pi}{60} \quad \text{.....(3.53)}$$

Where rpm is the number of rotations per minute for the shaft.

3.6.6 Measurement of Efficiency

Calculation of the enthalpy of steam at the turbine was done using the steam tables by Cecil, 2010. The isentropic efficiency of turbine was determined using equation 3.54 The ratio of the enthalpies under the conditions of pressure was used to calculate efficiency of the impulse turbine by use of Equation 3.54.

$$\eta = \frac{(h_{Ti} - h_{Te})}{h_{T,i} - h_{Te,y}} \quad \text{..... (3.54)}$$

Where h_{Ti} is the enthalpy of steam at turbine inlet, h_{Te} is the specific enthalpy of steam at the turbine exhaust, $h_{Te,y}$ is the specific enthalpy of steam at turbine exhaust pressure after isentropic expansion. Electrical and a general efficiency of the turbine were obtained by determining the following quantities: Net electricity that was generated, the total energy input, the power output by the turbine and the power supplied to the turbine. These were used in Equation 3.55 and 3.56 to find the electrical efficiency and turbine efficiency respectively.

$$Electrical\ efficiency = \frac{Net\ electricity\ generated}{Total\ energy\ input} \times 100 \quad \text{..... (3.55)}$$

The turbine efficiency was obtained by use of Equation 3.56

$$Turbine\ efficiency = \frac{power\ output\ by\ turbine}{power\ supplied\ to\ turbine} = \frac{Net\ out\ put\ of\ shaft\ work}{Work\ input} \quad \text{.....(3.56)}$$

3.6.7 Measurement of Frequency of Rotation

The frequency of rotation was obtained from the product of number of generator pole pairs and the rotational speed as 60 HZ. The magnet that was used for the generator fabrication was four pole magnetic by design. The frequency of rotation was obtained by use of Equation 3.57.

$$f = \frac{r.p.m \times 2\pi}{60} \times no.of\ poles \quad \text{(3.57)}$$

The shaft was in form of a cylindrical rod of radius 0.02 m. Its moment of inertia I was obtained from: $\frac{1}{3}Ml^3$. Where M was the mass of the shaft and l was the length of the shaft that was 0.68 m.

3.6.8 Testing of the Turbine

The testing of the turbine was done using ASME PTC 6 2004 testing guidelines. The turbine was operated at a first pressure of 1.0×10^5 Nm^{-2} set by the steam valve and the first shaft output was determined. The steam was generated from a boiler powered by a 10 Kw electric heater. The thermostat was set at temperature of 300 ^{0}C. The turbine was afterwards set at a second pressure of 8.0×10^5 Nm^{-2} by use of the pressure control valve and the second shaft output was obtained. This was repeated for the following temperatures and pressures: 200 ^{O}C, 150 ^{0}C and 100 ^{0}C with pressures of 6.0×10^5 Nm^{-2}, 5.0×10^5 Nm^{-2}, 4.0×10^5 Nm^{-2} and 3.0×10^5 Nm^{-2} respectively. The following measurements were recorded: generator output as shown in Plate 7, turbine inlet steam pressure, turbine exit steam pressure, turbine exhaust steam pressure, maximum power at shaft, electrical power output per minute, electrical power supplied by heater.

The revolutions per minute of the shaft were 2800 r.p.m by design. The power output of the turbine was determined from measuring the output current and voltage of the generator and use of Equation 3.59. To find out how much torque (how much force it could generate per radius of arm length), the power output in watts was determined from readings of the generator current and voltage and the rotational speed of the rotor was calculated. The frequency of rotation of the turbine was obtained from the angular

velocity of the disc, area of the disc, radius of the rotor disc, the distance between center of rotor disc and blade tip

The material that was used for fabrication of the shaft was carbon steel 40C8 with a tensile strength of 590.0×10^6 Nm^{-2} and yield strength 300.0×10^5 Nm^{-2} (EEAR, 2008). The efficiency of the turbine was calculated from power output by the turbine and power supplied to the turbine by the steam expressed as a percent. The power output and the power input were determined from of heat content.

The moving blades were fabricated individually and were attached to the wheel disc that was part of the rotating shaft.

During rotor assembly balancing was done so that the rotor was well balanced over the operating range, the blade row was driven starting at the center and working out towards the shaft ends. The steam turbine casing was fabricated with a diameter of 0.25 m and a height of 0.05 m. This was due to considerations of steam pressures of 1.2×10^6 Nm^{-2}, temperatures of 300 ^oC at a flow rate of 10 kgs^{-1} of steam.

3.6.9 Measurement of Physical Parameters

The approximation of the physical parameters such as strain, stress, modulus of elasticity, load and thickness were obtained as described in section 3.4.17.

3.7 Generator

The rotation of a coil in magnetic field changes the magnetic flux through the coil and generates a voltage. In the prototype generator presented in this study the magnet providing the magnetic field was moving as the shaft rotated and the windings of copper coils were fixed.

3.7.1 Design and fabrication

The fabricated parts of the a.c generator consisted of static part (stator) and rotating part (rotor) which was driven by the prime mover (turbine). Plate 8 shows the positions of the stator and rotor in the generator. Production of a.c power needs an accurate speed

control of the rotation of the rotor (Whitaker, 2006). The stator was made of copper coils while the rotating part was made of a four pole magnet fixed to the shaft. Plate 9 shows the stator windings. To make four poles of the magnet two 0.1 m by 0.03 m bar magnet were cut into two, machined and bonded to the shaft by use of Loctite glue with alternate poles adjacent to one another. Figure 3.13 shows the four pole magnet used on the rotor. Plate 10 shows the terminal leads of the 3 phase power generator.

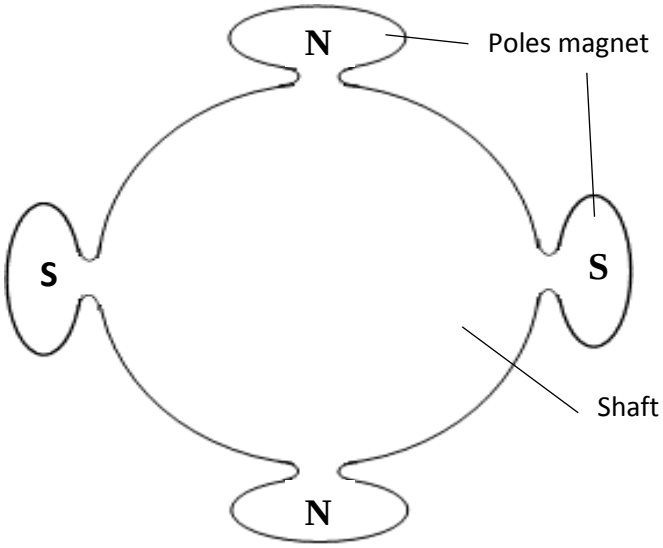

Figure 3. 13: Four pole magnet

The turbine shaft rotations of 2800 rotations per minute were matched to the generator by fixing the four pole magnet on the shaft to act as the rotor of the generator.

To cool the generator air was drawn from the outside directly into the bottom side of the generator and was discharged to the outside through a convection current that was built between the hot air in the generator and the water at ambient temperature air on the outside.

Technical data of the three phase power generator:- Span – 1- 7, Turns – 260, copper wire size – SWG 28, Connection – Top to bottom, Coils 6 × 2, Slots – 24. The span 1 -7 was for separating the three terminals. The turn bundles for the coils were 260. Metal to

metal bond glue locally called locktite was used to fix the magnet to the rotor. The connections of the generator was such that brown was neutral, blue the live and the body was earth of the generator.

Insulated copper wires of 28 gauge, 5.0 m in length were used for the coil on laminated galvanized iron structure. A 4 pole magnetic was used to provide magnetic field. Three phase power was obtained by wye connection. Plate 11 shows the 4 –pole magnet on the shaft. The generator output frequency is given by Equation 3.58

$$output\ frequency = \frac{driven\ speed\ (rev/min) X\ no.of\ magnetic\ poles}{120} \quad \ldots\ldots\ldots\ldots \quad (3.58)$$

A wye frame support at 120^0 angle separation for stator with a permanent magnet mounted on a steel shaft was fabricated. The three power supplies terminals had a phase difference of 120^0. Figure 3.14 shows the three wye phase power leads.

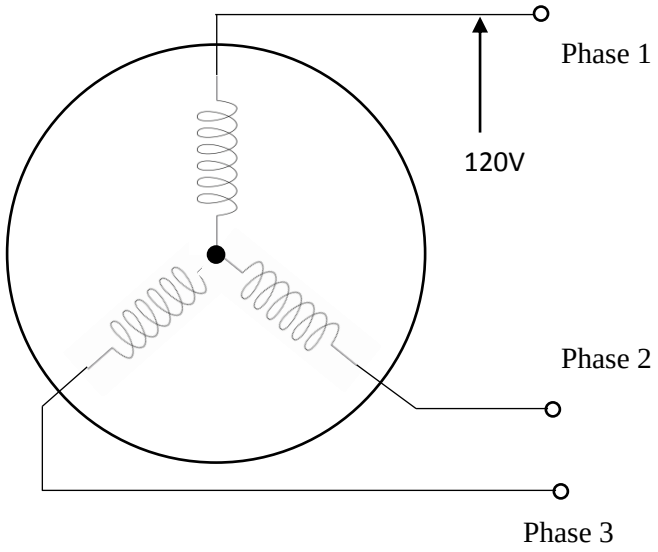

Figure 3. 14: Three phase power terminals

When in operation the temperature inside the generator was maintained at 20 ^oC by the air that flowed in and out by convection. The generator was tested by supplying steam to the turbine at temperature in the range of 100 °C and 270 °C and pressures in the range

of 1.0×10^5 Nm^{-2} and 1.0×10^6 Nm^{-2} . The generator output was measured as described in section 3.7.3. below.

3.7.2 Measurement of Frequency

The frequency of the generator was evaluated from number of generator poles which were four and the rotational speed. The frequency of the generator was obtained as the product of the two. Equation 3.57 was used in approximation of the frequency. The physical quantities that were measured and used were the shaft speed and the number of magnetic poles was as per the design of the field magnet.

3.7.3 Measurement of Power Output

The electrical power of the generator was obtained by use of current and voltage measurements that were given by the multimeter. The multimeter probes would be connected to the terminals of the three phase generator.

Mechanical power in watts produced by the generator was obtained by use of Equation 3.59

$$P = \omega T \quad \text{.....(3.59)}$$

Where ω is the speed in radians per second and T is the torque in newton meters.

3.7.4 Measurement of Efficiency

The efficiency of the generator was obtained by calculating the enthalpy of the fluid entering the turbine and the enthalpy of fluid leaving the turbine. The difference in the two enthalpies constituted the useful energy utilized in energy conversion to electric energy while the enthalpy at the input of the turbine constituted the energy input.

3.7.5 Measurement of Phase Power

The generator had six terminals for generation of electric power by design as shown in plate 10 of appendix A. The turbine was set at full steam discharge capacity and three

multimeters were each connected to the sets of the terminals simultaneously and the values of the current and the voltage were recorded. To obtain the phase power output (KVA) Equation 3.59 was used.

3.7.6 Generator Test

During the test of the generator, the steam exit valve was opened and the turbine was allowed to run. The generator was tested to find its performance in terms of its efficiency of conversion of mechanical power to electrical power using solar thermal energy. The efficiency of the generator was obtained by determining the net electricity generated and the total energy input. The net electricity generated was obtained by use of measurement of the current and voltage outputs of the generator while the total energy input was determined by measuring the amount of electricity that was used in vaporizing the amount of water that was collected as steam.

The output power for the generator was tested for the three phases. The frequency of rotation was plotted against the output power for both steam storage system and exchanger as standalone and when the two components are coupled.

Output frequency of the generator was obtained by use of the speed of the generator and the number of poles of the magnet by use of equation 3.58.

The KVA which gave the power output for the generator was obtained by use of Equation 3.60

$$KVA = \frac{\sqrt{3} \times V \times I}{1000} \times P.F \quad \text{..... (3.60)}$$

Where P.F is the power factor, V is the voltage and I is the current.

The kilowatts drive input was determined by use of Equation 3.61

$$\text{KW drive input} = \frac{\sqrt{3} \times Volts \times Current}{\eta_a} \quad \text{..... (3.61)}$$

Where η_a is the efficiency.

Amperage, A for the generator was obtained by the measurements of potential drop, power and power factor which was determined by use of Equation 3.62.

$$A = \frac{kW \times 1000}{V \times P.F} \quad \text{(3.62)}$$

The cost of power using direct steam was determined by finding the cost of one watt of power when neglecting the cost of heat exchanger. While the cost of power using the rest of the heat transfer fluids was determined with the cost of heat exchanger being inclusive. Equation 3.60 was used to find the magnitude of power.

3.8 Solar Collector

Parabolic trough technology is one of the main concentrating solar power commercially used today. The solar flux was concentrated at the linear focus of the parabolic trough where a pipe containing a heat transfer fluid was fixed. The heat was transported through the absorber to the heat exchanger. The steam produced was pressurized and stored in a steam storage system, where it was discharged into a turbine. The turbine converted the kinetic energy of steam to mechanical energy of shaft rotation. The shaft carried a four pole magnet that rotated in copper conducting wires. The cutting of the copper wires by magnetic flux lines of the magnet caused power to be generated in the three phase generator. The heat transfer fluids that passed through the absorber were; 6 M sodium chloride solution, 4 M sodium chloride solution, 2 M sodium chloride solution, used engine oil, Unused engine oil, Vegetable oil 1 and vegetable oil 2.

Figure P.4 of the appendix shows the Auto Cad design of the solar concentrator that was used in this study. The collector used in this study was designed and fabricated in a previous study (Kawira *et al.*, 2012). The modifications that were done were use of copper receiver of internal diameter of 0.013 m compared to one of 0.005 m of the same material in the earlier study and use of an aluminium sheet of solar reflectance of 0.92 compared to aluminium reflector of reflectance of 0.9 used in the previous study. The design equation used was given by Equation 3.63

$$y^2 = \frac{x}{4\,p} \quad \text{(3.63)}$$

Where *x* and *y* are Cartesian plane coordinates and *p* is the predetermined focal length. The solar collector was made using angle iron metallic bars 0.0015m, 4.8 m in length and 2.4 m in width. The bars were shaped in parabolic bends with a focal axis at 0.04 cm from the bottom of the trough. Black sheets of dimensions 4.8 m by 2.4 m by 0.0015 m were folded and welded onto the angle iron beams. The parabolic concentrator was laminated with anodized aluminium sheets of reflectance 0.92 of dimensions 4.8 by 2.4 m by 0.001 m. The collector was of length 5.8 m and of aperture width of 1.2 m. The receiver was painted dull black with dull black paint and was suspended at the focal axis of the parabolic trough solar collector. The internal diameter of the receiver was 0.013 m. The collector was covered with a 0.004 m thick glass. The aperture width was 2.4 m. The following heat transfer fluids were passed through the collector each in turn; water, vegetable oil 1 and Vegetable oil 2, used engine oil, unused engine oil, 2M sodium chloride solution, 4M sodium chloride solution and 6 M sodium chloride solution. Figure P.4 of the appendix shows the solar collector design that was used.

3.8.1 Determination of concentration ratio

The geometrical concentration ratio, *CR* was determined by use of Equation 3.64

$$CR = \frac{A_a}{2\pi rl} \quad \text{.....} \quad (3.64)$$

The circular absorber tube area, A_r was obtained from $A_r = \pi dl$. Where d represents the outer diameter of the absorber tube A_a was the aperture area and l represents length of the absorber tube. Rim angle ϕ_r was obtained as 79.38 ^{o} by use of Equation 3.65.

$$\phi_r = \tan^{-1}\left[\frac{8\left(\frac{f}{a}\right)}{16\left(\frac{f}{a}\right)^2 - 1}\right] \quad \text{.....} \quad (3.65)$$

where f is focal length of PTSC and a is the aperture of PTSC (parabolic trough solar collector).

Optical properties of the concentrator were used to obtain absorbed radiation, *S*, per unit area of exposed aperture. For higher reflectance aluminium sheet, the absorbed solar radiation was obtained as 1036.4 Wm^{-2} by use Equation 3.66 (Kalogirou, 1997).

$$S = I_b \rho \gamma \langle \alpha \tau \rangle \quad (3.66)$$

where, S is absorbed solar radiation; I_b is the solar beam radiation normal to collector aperture.

3.8.2 Measurement of Solar Irradiance

Solar irradiance was measured using the digital solar irradiance meter. The meter would be placed perpendicular to the plane of collector and the solar irradiance would be read when the reading stabilized. The characterization of the concentrator would be done when the variation of the solar irradiance did not exceed 50 Wm^{-2} (ASHRAE 93 -77). Plate 17 shows the solar irradiance meter in use for measurement of solar power intensity at the plane of the collector.

3.8.3 Tracking System

The tracking system consisted of a gear of a ratio of 1:50 which had a lever that was rotated anti clockwise while tracking the sun or anticlockwise while being reset in the evening. The lever was adjusted to ensure that the tracking pin did not cast a shadow. This meant that the lever was adjusted to align the collector to the normal solar beam from the sun. The pin was 0.004 m and diameter of 0.0015 m. Plate 14 and 16 shows manual gear tracker with the lever during the tracking. Plates 14 and Plate 16 show the tracker as was used for solar thermal power production.

3.8.4 Measurement of Absorptance/ Transmittance

Figure 3.15 shows the apparatus that was used in the determination of absorptance and transmittance of the 0.004 m thick glass that was used as a cover for the concentrator. The 0.004 m piece of glass measuring 0.003 m by 0.002 m was placed in the sample

space partition. The lamp was put on. The light from the lamp through the glass sample was analyzed by the spectrometer which gave the value of the glass of absorptance and transmittance respectively.

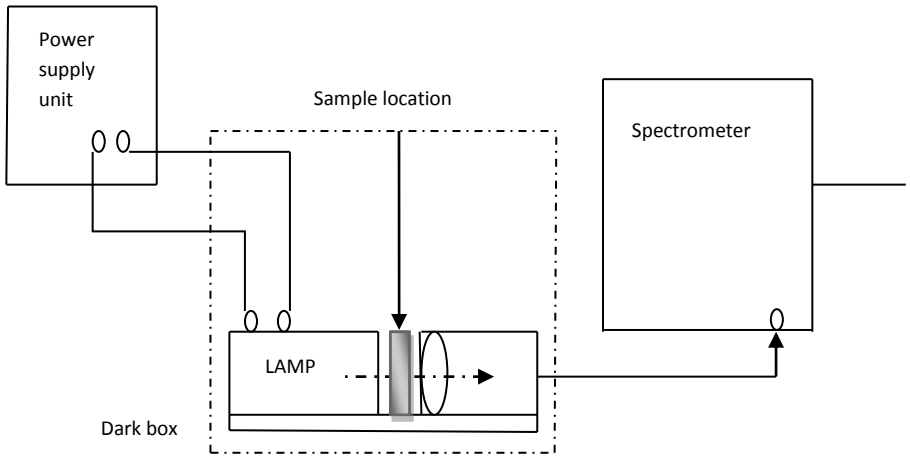

Figure 3. 15: Set up for determination of transmittance and absorptance

Figure 3.16 shows the set up that was used in determination of the reflectance of the aluminium sheet that was used in solar thermal collection. A small piece of the reflector was placed as shown in the figure and the lamp was put on. Direct rays from the lamp were blocked using the probe. The spectrometer gave a value of reflectance of the anodized aluminium that was used.

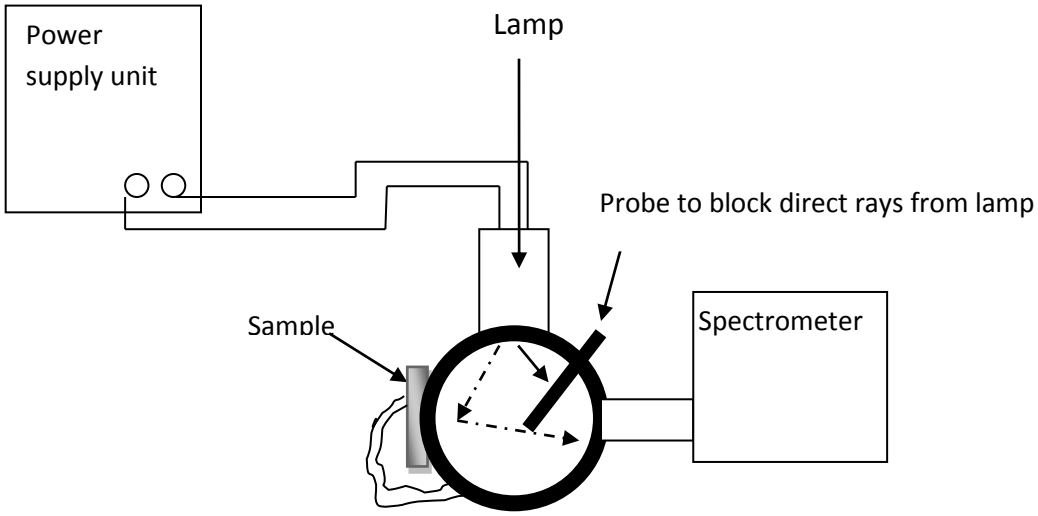

Figure 3. 16: Setup for determination of reflectance

3.8.5 Treatment of absorber

The receiver tube was made of a cylindrical copper pipe of external diameter, D_o= 0.0127 m when painted with black board paint of emissivity, ε = 0.1 and solar absorptance of 0.94. The paint coat had to be kept thin so that there was minimum resistance to flow of heat through the coat and through mass of the pipe to the heat transfer fluid, which was water. Plate 18 shows the position of the receiver in the collector system.

The internal diameter of the absorber pipe D_i was 0.0126 m and of effective length was 5.8 m .The collector was covered by glass of thickness 0.0004 m and whose transmitivity was 0.88. The cover reduced the rate of heat loss by conduction and convection, hence reducing the heat loss coefficient U_l. The transmittivity of the glass cover was obtained using the set up in figure 3.15.

This reduction was as a result of suppression of convections heat loss by interposition of a restriction of a long wave length thermal radiation in the collector chamber which was emitted back to the receiver. Plate 18 and 19 show the receiver position in the collector during the thermal collection for heat transfer fluids and the receiver at the focal axis of collector during thermal collection using salt solutions and the water respectively.

3.8.6 Absorber Efficiency

The efficiency of the absorber was obtained by computing the average power absorbed by the heat transfer fluids and the average power that was incident on the absorber. This was done over solar noon under steady state conditions of solar irradiance of $\pm$ 50 Wm^{-2} for irradiance of minimum value of 700 Wm^{-2} , a flow rate of $\pm$ 2.0 kgs^{-1}, temperatures of 100 ^{o}C, 150 ^{o}C, 200 ^{o}C, 250 ^{o}C and 300 ^{o}C.

3.8.7 Test installation and testing

The collector test was carried out in Juja, Kenya at latitude 1.1833 ° and 37.1167 ° in longitude. Collector mounting was done in a way not to obstruct the aperture of collector. An open mounting structure was made to allow free circulation of air. Closed loop testing was used involving gravity. The water reservoir was raised at a height of 1.5 m above the ground, control valves and other components were used to control fluid flow in the loop. Each of the heat transfer fluids i.e water, vegetable oil 1, vegetable oil 2, used engine oil, unused engine oil, 2 M sodium chloride solution, 4 M sodium chloride solution and 6 M sodium chloride solution were used each in turn. The carbon black pipe was used to lead the heat transfer fluid into and out of collector. The polypropylene pipe lead heat transfer fluid from the boiler to the heat exchanger since they are corrosion resistant during the testing. The pipe lengths between inlet and outlet of collector were kept as short as possible to reduce heat losses to the surroundings. Solar thermal collection by use of polypropylene pipes was as shown in Plate 12.

The pipe bends (mixing devices) were introduced upstream after 0.2 m from the collector on its both ends. A bypass loop and a control valve were used to provide flow control. This also assisted in stabilizing the mass flow rate of heat transfer fluid. During the solar thermal collection galvanized iron pipes were used as shown in Plate 13.

3.8.8 Steady state

The length required for steady state test period was determined from thermal capacity *C* (fluid thermal capacity per square meter) of collector and the thermal flow rate mc_f of the heat transfer fluid through the collector. To ensure that a steady state was attained, the test period was made about four times the period defined by C/mc_f (Gillet and Moon, 1985). Where c_f refers to specific heat capacity of heat transfer fluid. The time taken to attain steady state was found to be ten minutes. Collector fluid capacity was determined by filling the absorber with each of the heat transfer fluids. The mass of the fluid it contained was measured to be 3.04 kg for water, 3.42 for sodium chloride solutions and an average of 2.48 kg for the heat transfer oils. The steady state period was determined as 10 minutes for water and the sodium chloride solutions and 12.5 minutes for the heat transfer oils. The mass flow rate was determined by use of the readings from the flow meter.

3.8.9 Temperature control

To control temperatures during the testing period, calibrated temperature sensors were used. Mercury in glass thermometer graduated at 0.05 ^{o}C intervals was used to calibrate the digital thermometers which were used as temperature sensors. During installation good thermal contact between fluid and terminals of digital thermometer was ensured by sinking their contacts deep inside the liquid flow channel through the 0.001 m holes that were drilled on the carbon black pipe connectors. In order to prevent overheating of the bath during the testing the heat transfer fluid was pre-cooled before being fed to thermostatic bath by use of a fabricated heat exchanger. The water in the thermostat bath was removed after every ten minutes by siphon and fresh water at ambient temperature water added to enhance its cooling effect.

3.8.10 Measurement of Inlet and Outlet Temperatures

Digital thermometers were fixed at the inlet and outlet pipes of the boiler, steam storage and heat exchanger during the tests. Temperature of heat transfer fluid at the inlet and out let was measured to an accuracy of $\pm 0.1^{o}$C. The surrounding air temperature was measured to an accuracy of $\pm$ 0.5 ^{o}C. The pressure tapping were installed normal to the flow. A hole of diameter 0.001 m on each side of mixing devices was made for the trappings. A smooth straight piece of pipe was incorporated before pressure tapping at inlet and outlet sections of components under test. Collector aperture area in reference was the transparent area of collector normal to incident solar flux. The heat transfer fluid would flow from bottom to the top of collector during testing. Before each day's testing period was carried out, circulation of heat transfer fluid at a temperature of approximately 110 ^{o}C was done.

3.8.11 Collector test variables

Testing of the heat transfer fluids was carried out at their operating temperatures around solar noon. These temperatures were in the range of 100 ^{o}C to 290 ^{o}C. The tests produced data that was used in characterization of the solar collector. Data points of at least 4 fluid inlet temperatures spaced evenly over the operating range of the collector were used. The inlet temperatures of the heat transfer fluids were varied depending on the nature of the heat transfer fluid. The test times were taken symmetrically about noon as follows: 11.00, 11.30, 12.30 and 1.00 p.m. The tests were made under steady state conditions. The test period for a steady state data point typically contained a time of approximately 10 minutes with a set fluid inlet temperature. A thermostat with a range of temperatures between 50 ^{o}C to 300 ^{o}C was used for setting the inlet temperatures of the heat transfer fluids during the testing.

3.8.12 Collector testing loop

The collector testing was carried out at height of 3 m above the ground, on a building top. This was done to ensure economy of space usually utilized for agricultural activities. During the testing, the heat transfer fluids which were 6 M sodium chloride solution, 4 M sodium chloride solution, 2 M sodium chloride solution, used engine oil, unused engine oil, vegetable oil 1 and vegetable oil 2 were fed from the boiler at a set inlet temperature, and the following measurements were also taken: pressure drop across each component, mass flow rate and solar irradiance at the plane of the collector in the case of the solar thermal testing. These measurements were used in characterization where efficiencies, heat losses, heat loss coefficients and solar thermal steam pressures of different heat transfer fluids were obtained compared. The testing used was carried out using the National Bureau of Standards (NBS), the American Society of Heating, Refrigerating and Air Conditioning Engineers (ASHRAE) and American Society of Mechanical Engineers (ASME) guide lines. During the solar thermal collection the heat transfer fluid was heated by the solar flux as it passed through the collector. Figure 3.17 shows the collector testing loop for the solar collector. The heat transfer fluids were each used in characterization of the collector. Plate 19 shows the receiver at focal axis during solar thermal collection.

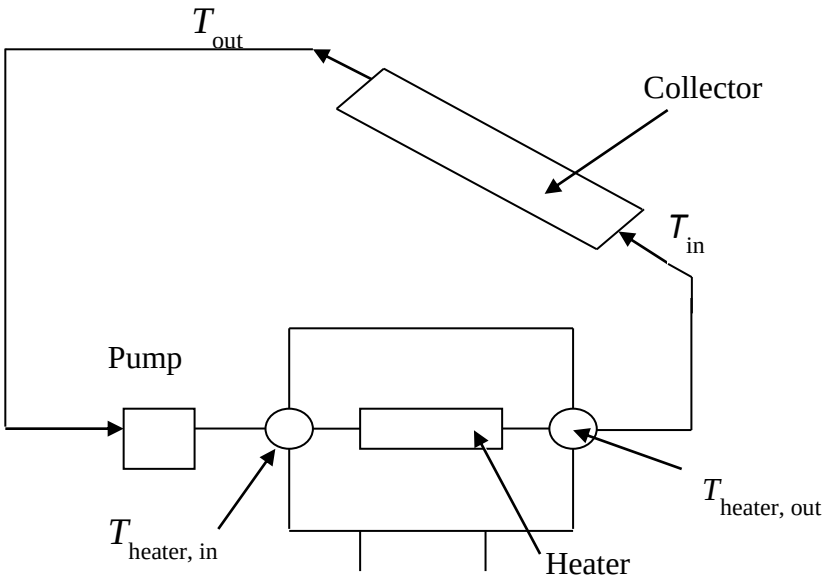

Figure 3. 17: Collector testing set up

3.8.13 Production of steam

The solar collector was used to harness solar thermal energy with all the heat transfer fluids that were being tested as shown in Figure 3.18. The heat transfer fluid flow through absorber pipe was controlled by use of a volume control valve positioned at the inlet of the collector. The flow rate of the heat transfer fluid was measured using a digital flow rate meter. For water flow, a non-return valve at the mixing joint prevented the back flow of steam when temperatures reduced and the beam radiation at the collector reduced. T_1 and T_2 were digital thermometers that were used for measuring heat transfer fluid's inlet and outlet temperatures respectively. The parabolic trough collector tracked the sun in a North-South orientation from the morning to the evening in this study. The steam pressure values obtained were directly read from pressure gauges placed at inlet and out let mixing joints of heat transfer liquid. The values of

temperatures of steam obtained were recorded along the pressure drop values. The rate of heat delivered by heat transfer fluids was computed by using equation 3.67 (Twidel, 1986).

$$\dot{Q} = \dot{m}\, c_p (T_2 - T_1) \quad \text{..... (3.67)}$$

where: $\dot{m}$ is the mass flow rate of heat transfer fluid, $\dot{Q}$ is the heat rate delivery by the receiver and $(T_2 - T_1)\ K$ is the temperature difference and c_p is the specific heat capacity of heat transfer liquid.

The solar power heat gain was determined by use of Equation 2.56. Thermal efficiency was calculated from the solar power intensity obtained from the power intensity meter and the heat gained by the heat transfer fluid. The parameters measured were: aperture area, receiver area, inlet temperature of the heat transfer fluid and the ambient temperature.

3.8.14 Measurement of Thermal Efficiency

To find the thermal efficiency of the collector temperatures of heat transfer liquids were measured during entry into the receiver and during exit using digital thermometers. The normal beam irradiance at the plane of the collector G_{bm} was measured using a solar irradiance meter. Equation 3.68 was used to find the thermal efficiency of the collector.

$$\eta = \frac{\int_{T_1}^{T_2} \dot{m} c_{p(T_2 - T_1)dt}}{A_a \int_{T_1}^{T_2} G_{bm}\, dt} \quad \text{..... (3.68)}$$

Where G_{bm} is the component of normal beam irradiance in the plane of the collector, T_1 and T_2 is the inlet and outlet heat transfer receiver temperatures; $\dot{m}$ is the mass flow rate of heat transfer fluid and A is the aperture area of the concentrator.

3.9 Coupled Heat Exchanger and the Storage System

Figure 3.18 shows the set up that was used during solar thermal collection for each heat transfer fluid.

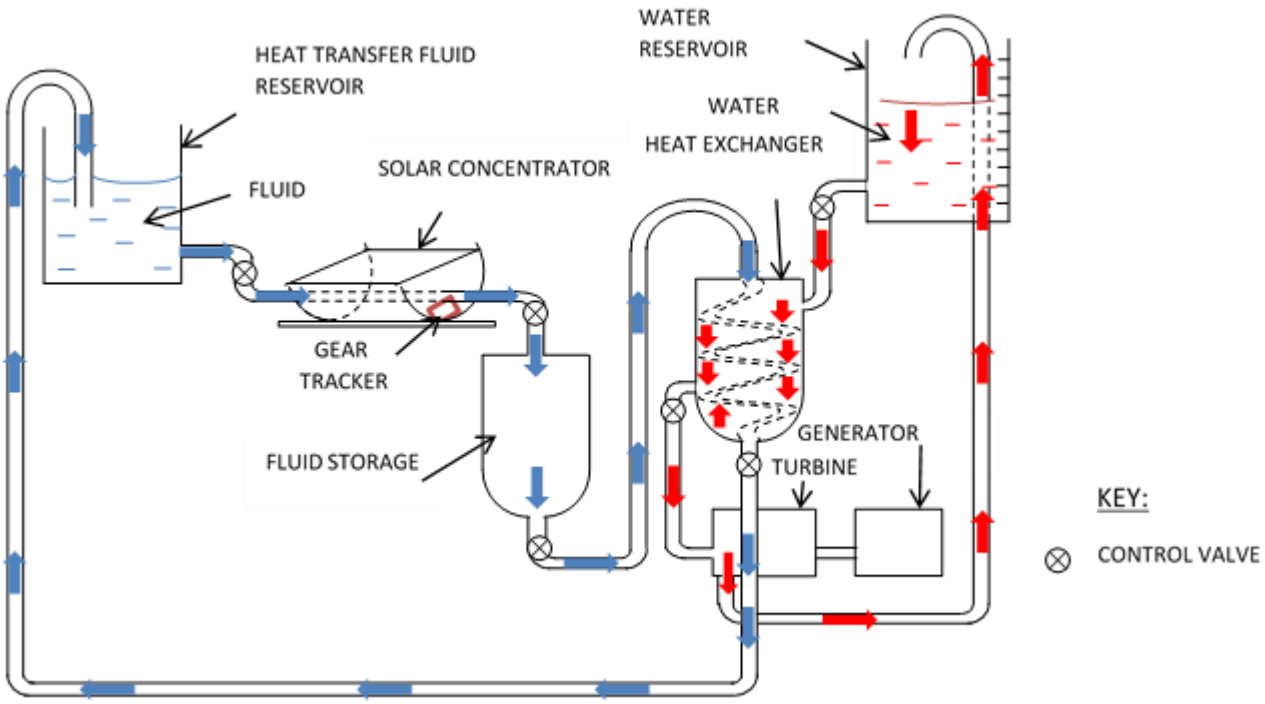

Figure 3. 18: Solar thermal collection loop

In this study solar thermal collection was done using the steam storage system and it was also done without the steam storage system during generation of steam for power production. For the set ups with and without steam storage system the inlet and outlet temperature of steam was measured, the mass of steam produced and pressures of operation were also measured. During charging the steam exit valve at the heat exchanger would be closed and the non-return valve at the steam entry of the storage system would prevent the steam formed from returning to the reservoir when pressure reduced. Reduction in steam pressure would be caused by overcast sky and changes of weather. Steam generation would start when the set discharge pressure would be reached. The test discharge pressures ranged between 1.0×10^5 Nm^{-2} to 9.0×10^5 $Nm^{-2.}$ In direct power production the set up in Figure 3.18 was used without the heat exchanger. The steam produced in the collector proceeded to the storage system for pressurization and then it was discharged to the turbine. Water was used as the heat transfer fluid for direct power production.

3.9.1 Measurement of Steam Flow Rate

The steam flow rate of the water that was absorbing heat from the heat transfer liquids was measured by collecting the steam from the steam storage system and condensing it. Its mass was determined per unit time. The process was repeated three times and an average obtained.

3.9.2 Measurement of Power Output

Power output from the generator was obtained by use of measurements given by digital multimeter that showed the values of voltage and current for the heat transfer liquids. The multimeter was calibrated before use to ensure no errors in the readings obtained. Equation 3.59 shows how the values of the voltage and current were used for finding the power output of the generator.

3.9.3 Measurement of Turbine Efficiencies

The amount of heat possessed in 2 kg of steam trapped in water at ambient temperature water before entry into the turbine and the heat possessed by the same amount of steam at exit of the turbine was determined using steam tables (Cecil, 2010). The masses of steam and the temperatures before it entered the turbine and after leaving the turbine provided means for evaluation of the efficiencies. The mass of steam before entering the turbine was found by condensing 0.2 kg of steam in water at ambient temperature water in a 5 kg copper container. The mass of steam after it had lost heat in the turbine was determined by cooling the condensate then measuring its mass using a beam balance. The temperatures were measured using a digital thermometer and the time lapse was determined using a stop watch.

3.9.4 Measurement of Heat Emitted by Heat Transfer Fluids

The heat that was emitted by the heat transfer fluids was obtained by measuring the mass of the heat transfer fluid over 120 s and the flow rate obtained from the digital flow rate

meter. The temperature at the beginning of the taking the flow meter reading and after were recorded for the heat transfer fluids as they flowed through the heat exchanger. The temperature, mass of the water absorbing the heat, and the duration of flow measured were determined.

3.9.5 Measurement of Pressure Drop

The pressure drop was measured using a U – tube manometer using mercury as the liquid in tube. The pressure due to steam would cause a head of column of mercury to be formed. The head of mercury column was measured using a meter rule. The pressure drop was then calculated using the density of mercury and the gravitational field strength. The U – tube would be positioned across the turbine. Other components whose pressure drop was determined were the collector and the coupled system.

When the system was in operation, as the kinetic energy of the steam was converted to energy of motion of turbine there was a pressure drop observed across the turbine. The pressure of the steam that was formed was higher before entry into the turbine compared to when it was coming out. The pressure drop ratio was calculated as the ratio of the difference in the entry and exit pressures and the initial or entry pressure.

3.9.6 Measurement of Efficiency of Generator

The efficiency of the generator was obtained as the ratio of the useful power that was obtained from the generator to the input power expressed as a percentage. Useful power was the product of voltage and the current that were read from the multimeter while the input power was obtained from the power developed by the shaft. The values of voltage and current provided the basis for determining power for the generator.

3.9.7 Measurement of Efficiency of Heat Transfer Fluids

The efficiency of the heat transfer fluids was found in terms of the amount of heat that was absorbed by the water to turn to steam and the initial amount of heat before entry into the heat exchanger. The heat emitted by the heat transfer fluids, heat absorbed by

the water and the heat absorbed by the heat transfer fluid from the sun were determined. The masses and the temperatures of the heat transfer fluids and the water that turned to steam were also measured. The temperatures were measured using digital thermometers and the masses were measured using the beam balance.

3.9.8 Measurement of the Efficiency of the Steam Storage

The efficiency of the steam storage system was determined by obtaining the amounts of heat that the heat transfer fluids had absorbed before entering the storage and the amount it had by the time it was leaving the steam storage in a span of 60 s of flow. The ratio of the heat absorbed by the steam before entry into the steam storage system and the amount of heat in the steam exiting the steam storage system expressed as a percentage gave the efficiency of the steam storage system.

3.10 Measurement of Receiver Heat Loss

The heat transfer fluids were circulated at a rate 0.005 m3s-1 through the receiver when there was no sun and the heat transfer fluid was cooling. The temperature of heat transfer fluid at the inlet and at the outlet of the collector was measured using a digital thermometer. The amount of heat lost by the receiver was determined using Equation 3.66. The heat loss per unit area was found by dividing the amount of heat lost by the surface area of the receiver. The amounts of heat losses gave the character of the receiver in terms of losing heat during operation. The magnitude of heat losses were recorded against operation temperatures for the receiver.

CHAPTER FOUR

RESULTS AND DISCUSSION

4.1 Introduction

In this section the results are presented and discussed for the performance of heat transfer fluids, tests and characterization for fabricated; steam storage, heat exchanger, turbine and generator. The characterization of the solar collector and solar thermal energy collection is also presented. The results obtained in this section compare well with those obtained by other researchers. The results obtained as follows: Solar collector: collector average steam discharge, inlet and outlet temperature and pressure, reflectance of optical system, transmission of glass cover among others. Steam storage system: inlet and outlet temperature and pressure with and without coupling, steam loads, steam flow rates, mass flow rates of the heat transfer fluids, storage capacity of the steam storage system, evaporation ratio of the storage system, maximum continuous rating for steam among others. Heat exchanger: inlet and outlet temperature and pressure, efficiency, overall heat transfer coefficient, NTU, temperature efficiency of the streams, mean temperature difference, pressure drop, stress, strain, elasticity among others. Turbine: inlet and outlet temperature and pressure, enthalpy of heat transfer fluid during entry and exit from the turbine, centripetal force acting on blade, frequency of rotation of shaft, angular velocity among others. Generator: Frequency of output power, efficiency, KVA, amperage among other parameters.

4.2 Parameters used in Fabrication

Table 4.1 shows the results obtained for the physical parameters that were tested for fabrication of steam storage system, heat exchanger and the turbine.

Table 4. 1: Summary of parameters of components used

PARAMETER	HEAT EXCHANGER	STEAM STORE	BLADE	SHAFT	TURBINE SHELL
Percent Axial strain (%)	2.1	1.8	2.0	1.5	2.2
Axial stress (Nm^{-2})	83.4×10^6	93.8×10^6	76.7×10^6	101.6×10^6	105.3×10^6
Modulus of elasticity (Nm^{-2})	1.87×10^6	2.24×10^6	1.58×10^6	3.20×10^6	2.19×10^6
Load (Nm^{-2})	1.0×10^6	1.0×10^6	1.0×10^6	1.0×10^6	1.0×10^6
Thickness (m)	0.0015	0.0003	0.001	0.0026	0.001
Moment (Nm)	0.0036.1	0.003	0.0037	0.00261	0.22

4.3 Performance of Heat Transfer Fluids

The following heat transfer fluids were used in solar thermal collection; vegetable oil 1, vegetable oil 2, used engine oil, unused engine oil, 2 M, 4 M and 6 M sodium chloride solutions.

The performance of heat transfer fluids was experimented on basis of the presented results obtained on how they emitted the heat to the fluid on the shell fluid of the heat exchanger, how they absorbed heat from the sun and how efficient they were in absorbing and emitting the solar thermal heat.

Figure 4.1 shows the efficiency with which the heat transfer fluids transmitted the heat they absorbed to water to from steam. The efficiency of each of the heat transfer fluid was as shown. The 6 M salt solution had the highest efficiency of transmitting heat to the water. For the 4 M salt solution and 2 M salt solution, efficiency decreased with concentration. The efficiency of Vegetable oil 2 was the poorest among the heat transfer

liquids that were tested. Water in which salt was added absorbed heat with a higher efficiency compared to water without salt added. The vegetable oils that were used absorbed heat less efficiently than the salt solutions. The used oil had less efficiency of absorbing the heat and passing it to water to form steam compared to unused oil. The performance of the unused oil was better because it did not contain the byproducts of combustion from the engine compared to the performance of used engine oil.

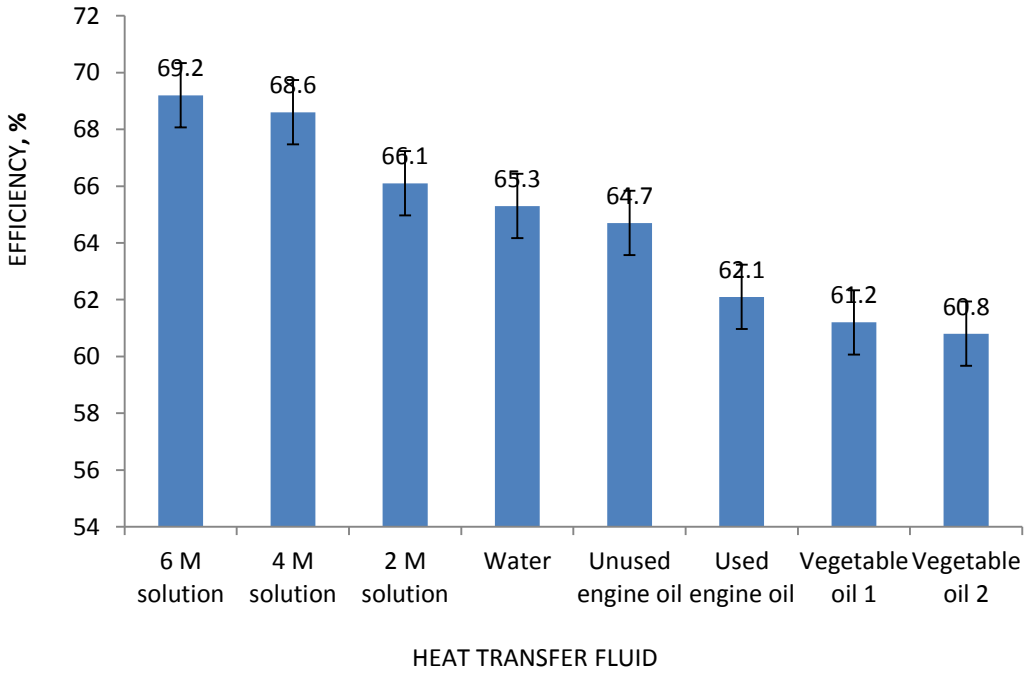

Figure 4. 1: Generator efficiency for the heat transfer liquids

The maximum power output for the heat transfer fluids for the steam that was generated from the heat transfer fluids ranged from 284.1 W to 458.5 W as shown in Figure 4.2. The vegetable oils power output was the lowest while the power output for salt solutions was the highest. The higher the concentration of the salts the better was the power output for the heat transfer fluid for the concentrations that were considered. Adding salt to the water therefore made water a better heat absorber and hence it made more heat available

for absorption in the shell side of heat exchanger by the water so as to form steam during solar thermal collection.

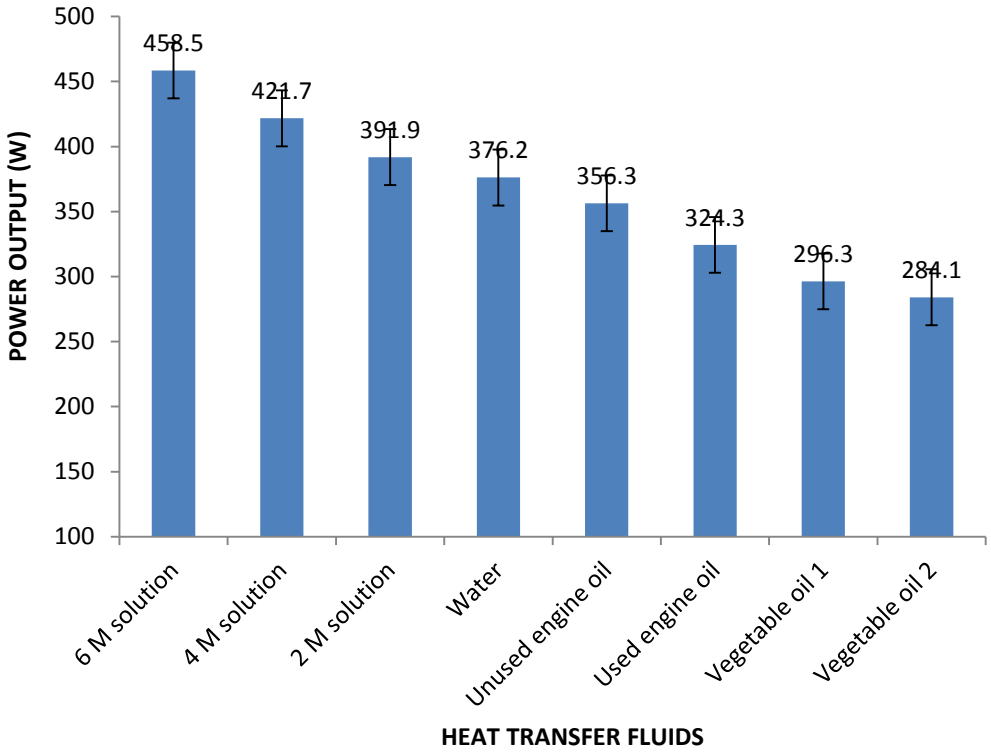

Figure 4. 2: Maximum power output for heat transfer fluids

The conditions under which the results in Figure 4.2 were obtained were 7.8×10^5 Nm^{-2} to 7.8×10^5 Nm^{-2} of pressure and temperatures in the range of 157.9 ^oC and 261.8 ^oC with average solar power intensity of 1100 Wm^{-2}.

Table 4.3 shows the heat absorbed, pressures of operation and the mass flow rates for water as heat transfer fluid at average solar power intensities of 1068 Wm^{-2}. The solar power intensities were in the range of 738.4 Wm^{-2} to 1100.4 Wm^{-2} during the data collection. There was a difference in the behavior of absorption of heat at the same pressure. Vegetable oil heat transfer fluids absorbed less heat compared to the salt solutions and so did the used oil and the unused oil. Water was a better absorber of solar thermal heat compared to the Vegetable oil 2 and the vegetable oil 1. The difference was

in that the heat was conducted by ions in the salt solutions while there are no ions in vegetable heat transfer fluids. The results for other heat transfer fluids are given in appendix H. A heat transfer fluid under pressure absorbed a higher amount of solar thermal heat as shown in the Tables 4.2 and appendix H. Solar thermal intensity ranged between 659.5 Wm^{-2} and 993.8 Wm^{-2} during the thermal collection.

Table 4. 2: Variation of heat absorbed with pressure and mass flow rate for water on 24.1.2014

Heat absorbed (J)	**11673.1**	**12789.3**	**13526.9**	**14307.5**	**15841.4**	**17368.0**	**18479.7**	**19128.6**
Pressure (× 10^5 Nm^{-2})	1.0	2.0	3.0	4.0	5.0	6.0	7.0	8.0
Mass flow rate (kgs^{-1})	3.1	3.4	3.9	4.3	4.7	5.3	5.6	6.1

It was observed that the heat absorbed increased with the increase in the amount of mass flow rate in table 4.2. The increase in mass flow rate was as a result of the effect of pressure. The higher mass flow rates delivered more energy than the lower mass flow rates. The effectiveness of each of the streams was an average of 0.87 for the heat transfer flow (tube side) and an average of 0.87 for the water that would absorb heat from heat transfer fluids to turn into steam (shell side) respectively.

The percentage heat losses for the hot heat transfer fluids at an average temperature of 161.4 ^oC were as shown in table 4.3. It was observed that the heat transfer fluids that absorbed more heat also had higher percentage losses of heat.

Table 4. 3: Percentage losses for the heat transfer fluids on 18.1.2014

Fluid	**Heat Absorbed (J)**	**Pressure (Nm^{-2})**	**Percentage Loss (%)**
Water	16005.8	5.3×10^5	5.4
Vegetable oil 2	16874.1	5.3×10^5	5.8
Vegetable oil 1	16572.9	5.3×10^5	5.7
Used Engine oil	16696.3	5.3×10^5	5.75
Unused Engine oil	16398.5	5.3×10^5	5.5
2M salt solution	16981.3	5.3×10^5	5.9
4M salt solution	172644.7	5.3×10^5	6.0
6M salt solution	17869.6	5.3×10^5	6.2

Table 4.4 shows the temperature efficiencies of the heat transfer fluids at an average temperature of 153.9 ^oC; pressure of 6.1×10^5 Nm^{-2} and a solar power intensity of an average of 1067.4
Wm^{-2}. The efficiencies increased with magnitude of the heat absorbed by the heat transfer fluids from the sun. The more the solar power intensity the salt solutions acquired higher temperature efficiencies than the rest of the heat transfer fluids because they absorbed more heat from the sun.

Table 4. 4: Temperature efficiency for the hot heat transfer fluids on 19.1.2014

Heat Transfer Fluid	**Average temperature of operation (^{o}C)**	**Temperature Efficiency (%)**
6 M Salt solution	193.1	92.4
4 M Salt solution	183.6	89.9
2 M Salt solution	176.9	85.6
Water	173.4	84.6
Unused engine oil	153.7	83.4
Used engine oil	132.2	81.9
Vegetable oil 1	128.1	78.6
Vegetable oil 2	121.5	78.1

The higher the temperature of operation achieved by the heat transfer fluid, the higher was the temperature efficiency. The heat transfer fluids that achieved high operational temperatures also absorbed more solar thermal radiation than the ones which achieved lower temperature efficiencies. Temperature efficiencies were used to measure performance of the heat transfer fluids in terms of temperatures achieved.

The heat coefficient for the heat transfer fluids and their corresponding flow rates were as shown in table 4.5. The steam flow rate increased with the increase in heat coefficient.

Table 4. 5: Variation of heat coefficient with steam flow rate on 4.2.2014 at an average of 953.7 Wm^{-2}

Fluid	**Heat Coefficient (W/ m^2 ^oC)**	**Steam Flow Rate (kgs^{-1})**
6 M Sodium chloride solution	321.6	0.054
4 M Sodium chloride solution	307.3	0.05
2 M Sodium chloride solution	292.8	0.048
Water	289.1	0.038
Unused engine oil	281.4	0.041
Used engine oil	277.6	0.40
Vegetable oil 1	266.1	0.36
Vegetable oil 2	250.5	0.031

The heat loss coefficient was related to the amount of heat absorbed by the heat transfer fluid in that the more the heat the heat transfer fluid absorbed the higher the heat coefficient. Figure 4.3 shows the heat emitted to the water to form steam by the heat transfer fluids with time of day at an average solar power intensity of 998 Wm^{-2}. The heat absorbed depended on the solar power intensity. Solar intensity increased with time of day and it is observed that it starts to decline from 2 p.m in the afternoon. There is an increase in the amount of solar heat that was released to the water to form steam with time of day. The salt solutions released and absorbed more heat energy compared to the vegetable oils that were used.

The heat that was emitted by the heat transfer fluids was determined and plotted against the time of day. The emission of the heat would be interrupted by some overcasting in the skies and hence non smooth curves. The solar irradiance during the solar thermal

collection ranged from 354.3 W/m^2 at 8.00 a.m. to 1098.4 W/m^2 at 2.00 p.m. The low solar thermal collection in the morning was due to the low amounts of direct beam at collector plane and hence the amount of beam radiation was in range of 0 – 30 % before 8. 00 a.m. in the morning. After 8.00 a.m the direct beam radiation reaching the collector increased up to 90 % at noon. After 2.00 p.m the amount of direct beam radiation reduced gradually from 90 % and reached 29.5 % at 5.00 p.m. Other Figures for the other heat transfer fluids are presented in appendix B.

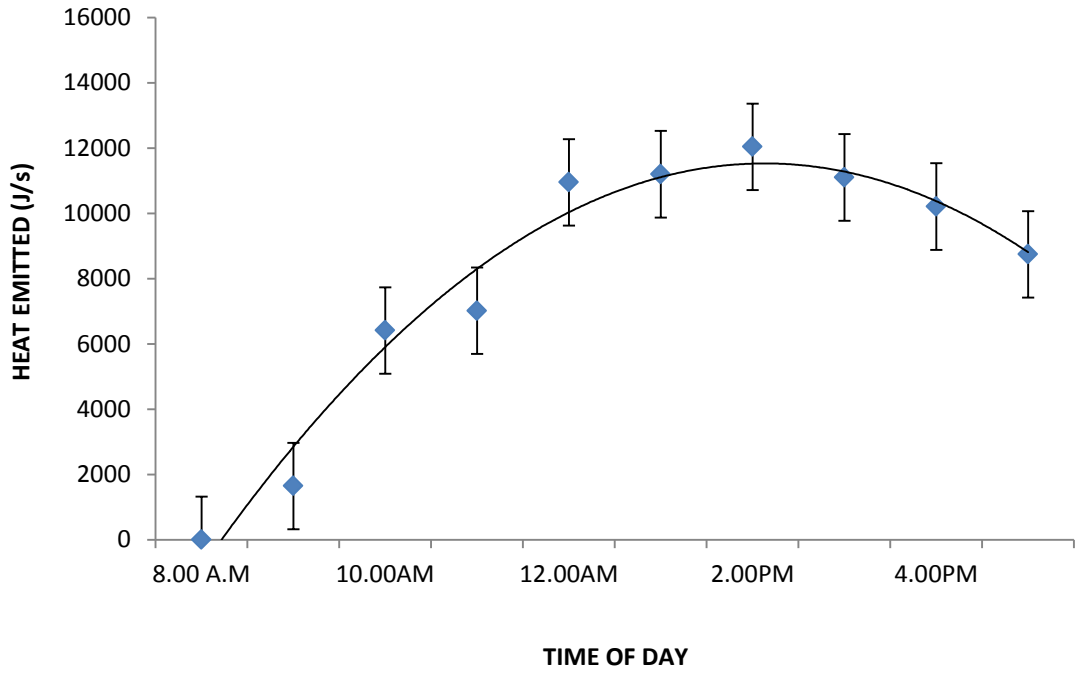

Figure 4. 3: Heat emitted by Vegetable oil 2 with time of day on 9.4.2014

The heat absorbed on hourly basis was as shown in Figure 4.4 at solar power intensities of 1032.3 Wm^{-2}. The figure gives the solar heat absorbed with time of day for Vegetable oil 2. The figures showing the heat absorption with time of day for the other heat transfer fluid are shown in appendix C.

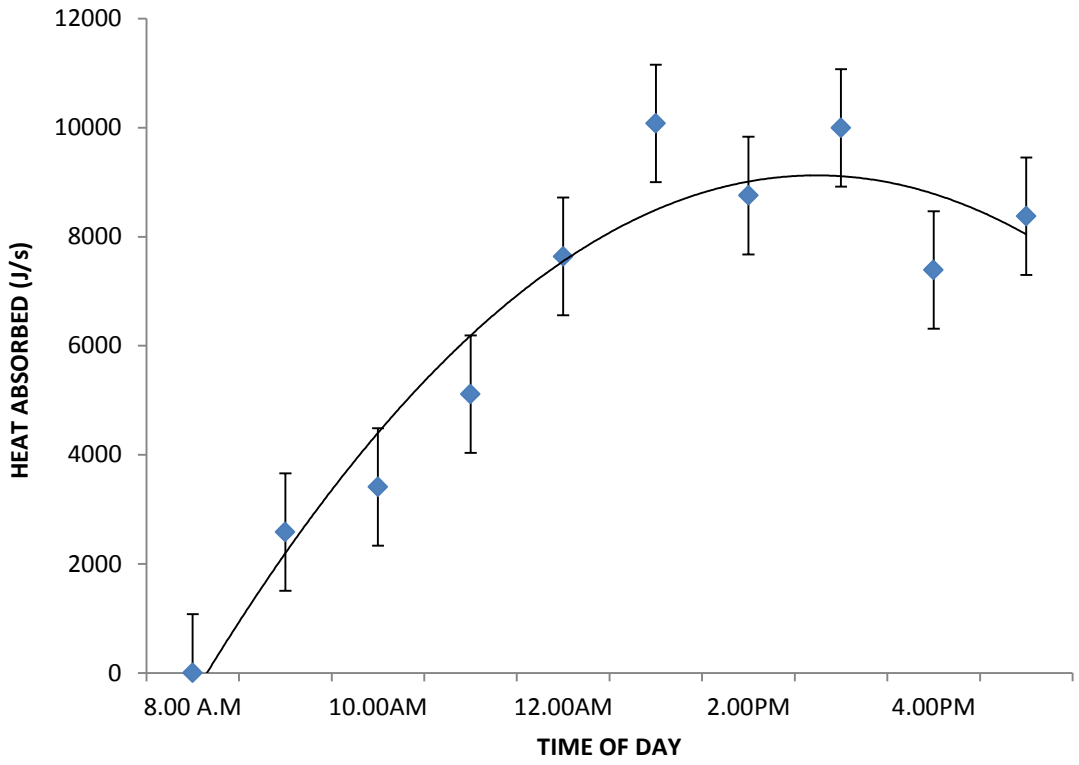

Figure 4. 4: Heat absorbed by Vegetable oil 2 heat transfer fluid on 19.1.2014

The heat transfer fluids absorbed the heat energy from the sun as they passed through the concentrator. In a study on mineral oil heat transfer fluid, water was heated into steam for a turbine with an efficiency ranging from 60 % to 80 % (Pradeep *et al*., 2013).

4.4 Direct Steam Power Generation

In direct steam power production, water was used as the heat transfer fluid and it was also used as the heat storage medium. Section 3.7.6 of the methodology describes the production of power using the three phase power generator used in this study. The cost of producing power without heat exchanger was obtained as Ksh 111.00 per 1000W and the cost of power when using a heat exchanger was obtained as 150.00 per 1000W. The cost of power by direct power production was less by an average of 7.4 % compared with the other heat transfer fluids which required a heat exchanger to heat water to

produce steam power. Thermal energy storage systems based on sensible heat storage offer a storage capacity ranging from 10 - 50 $KWhs^{-1}$ and storage efficiencies between 50 – 90 % depending on the thermal insulation technology (Zarza *et al.*, 2001).

Figure 4.5 shows the power output against the heat output by the heat transfer fluids. In the morning the power output was low due to low heat output from the heat transfer fluids due to low solar power intensity. This was due to diffusion of solar radiation in the morning by the horizons as the sun rises. In Figure 4.5, power output became steady in the afternoon because the steam storage system supplied steam by flashing when pressure inside it dropped as a result of decreasing solar intensity. In a study by Minassians *et al.*, 2004, a three phase stirling engine cycle produced 217 W of solar thermal power with an efficiency of 70 %. In this study a rankine engine cycle produced an average power of 362.1 W with a solar power efficiency of 65.4 %.

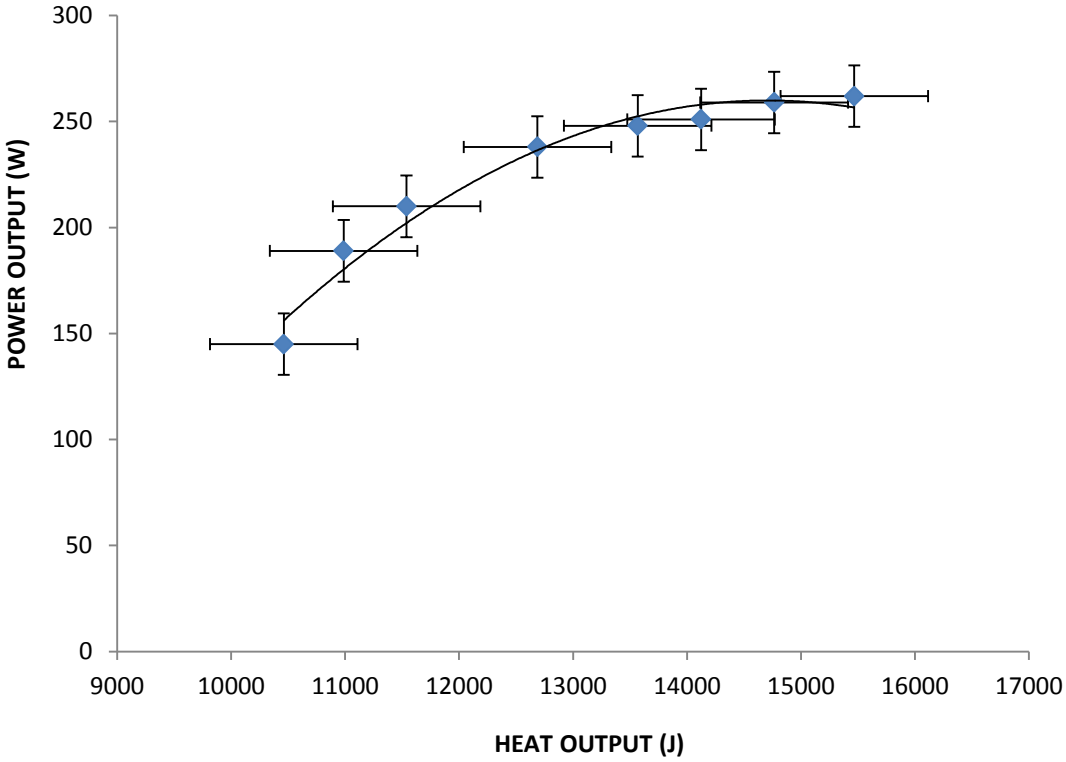

Figure 4. 5: Power output against heat output for direct steam generation on 18.1.2014

In Figure 4.6, the power output increased with the amount of heat absorbed by the heat transfer fluid. Direct steam generation power production by use of water as the heat transfer fluid and also as storage fluid was economical since there was no use of heat exchanger in heat transfer. This is compared to when heat transfer fluids other than water were used. Use of direct absorption solar collectors is being developed and is attractive since sunlight is directly absorbed into the working fluid and this eliminates the intermediate heat transfer step (Patrice *et al.,* 2013).

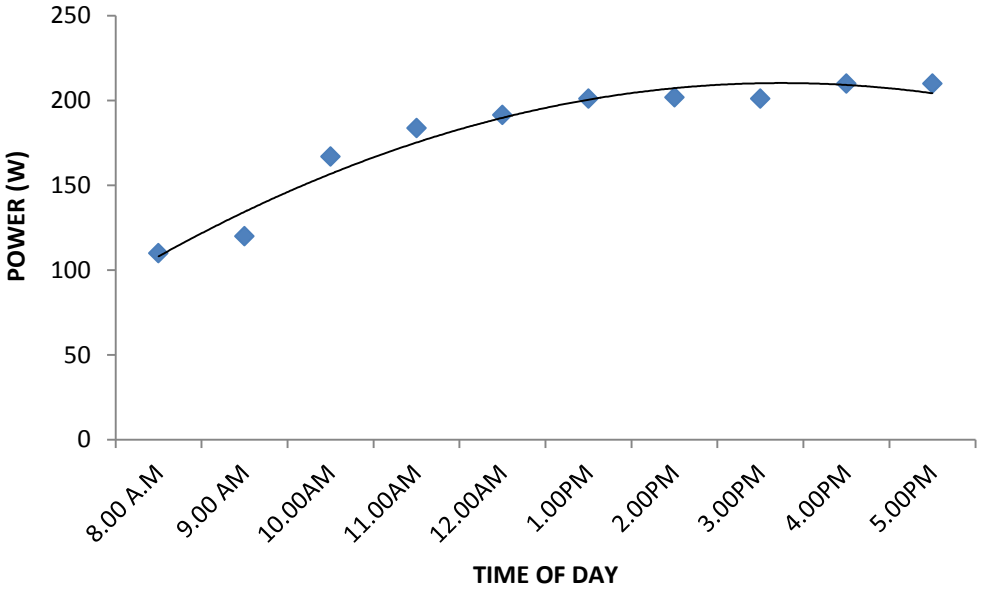

Figure 4. 6: Power output against time of day for water on 17.1.2014

4.5 Heat Exchanger

The heat exchanger that was designed and fabricated was a coiled tube counter flow heat

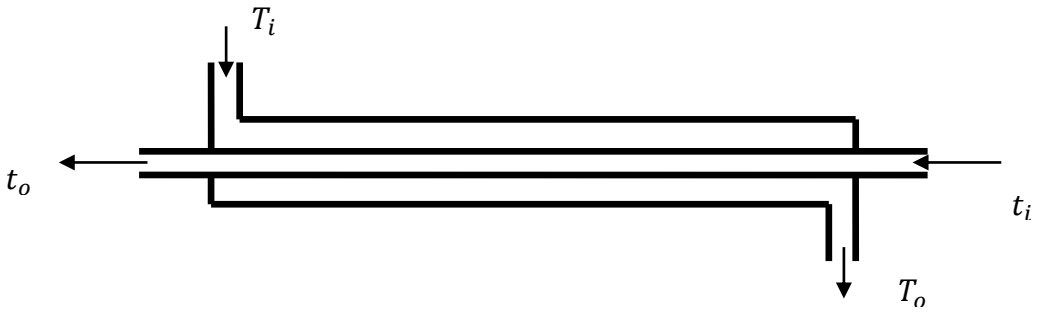

Figure 4. 7: Tubes of counter flow heat exchanger

exchanger. The following characteristics of the heat exchanger were determined and results herein presented: - the heat absorbed and the heat emitted by the heat transfers fluids, the heat transfer coefficient with respect to the heat transfer fluid under

consideration, the heat exchanger effectiveness, the number of heat transfer units transmitted, the efficiency, operating points, heat transfer conductance, and the heat absorbed during thermal solar collection by the heat transfer fluids.

4.4.1 Heat Exchanger Effectiveness, ε

The heat exchanger effectiveness was a measure of magnitude of amount of heat that was actually transferred between the heat transfer fluid and the liquid transporting the heat to the turbine and the generator. It was found to be in the range of 0.87 to 0.73. The variation in the effectiveness was attributed to the variation of solar power intensities of between 983.5 Wm^{-2} to 1094.2 Wm^{-2}. The heat exchanger effectiveness, ε, for 6 M sodium chloride solution, 4 M sodium chloride solution, 2 M sodium chloride solution, water, vegetable oil 1, Vegetable oil 2, unused engine oil and used engine oil was obtained as 0.91, 0.85, 0.84, 0.83, 0.76, 0.73, 0.81 and 0.79 respectively.

4.4.2 Heat Exchanger Operating Points

The heat exchanger operating points for the heat transfer fluids that were tested varied from one heat transfer liquid to the other. The measurements that were made in order to find the operating points of the heat exchanger were: - mass flow rate, volume flow rate, fluid pressure, density, specific heat, heat capacity, smoke point, heat transfer outlet temperature and the heat transfer inlet temperatures. The smoke point was the temperature when smoke would be observed to come out of the system when the heat transfer fluid was in study. The heat transfer fluids absorbed heat that was conducted by water to make steam. Table 4.6 shows the heat exchanger operating points for the different heat transfer fluids that were used in this study. The operating points for the other heat transfer fluids are presented in appendix J. A shell and tube heat exchanger with paper insulation was fabricated and operated at an effectiveness of 0.33 (Vindhya *et al*., 2014). The heat exchanger fabricated in this study performed better due its coupling with steam storage system which enhanced pressurization and hence effectiveness.

The heat exchanger operating points for the fabricated heat exchanger for solar irradiance of 1084 Wm^{-2} was obtained and are shown in Figure 4.6.

Table 4. 6: Operating points for vegetable oil 2 vs water fluids on 4.1.2014

Property	**Hot fluid (Vegetable oil 2)**	**Water at ambient temperature fluid(Water)**
Mass flow rate (kg/s)	4.2	3.2
Volume flow rate (m^3/s)	1.5	1.0
Fluid Pressure (Nm^{-2})	5.0	5.0
Density (kg/m^3)	915	1000
Specific heat, c_p ($Jkg^{-1o}C^{-1}$)	912.8	4170
$T_{2,out}$ **(^oC)**	35.0	143.7
$T_{1,out}$ **(^oC)**	150	24.1

The following is a summary of other characteristics of the heat exchanger that were determined in this study: The required heat transfer surface for design was determined as 0.75 m^{-2} from the variables that were obtained experimentally and used. Heat transfer fluid velocity was an average of 2.4 ms^{-1} for pressure drop of 1.4×10^4 Nm^{-2} on the tube side and pressure drop of 1.16×10^4 Nm^{-2} on the shell side.

The average overall heat transfer coefficient was calculated and was found to be 361.4 $W^0 m^{-2}C^{-1}$ for the steam to oil, 387.6 $W^0 m^{-2}C^{-1}$ for the steam to salt solutions and 548.9 $W^0 C^{-1}$ for water to water counter current flow. It was higher for salt solutions since they absorbed more solar thermal energy compared to the other heat transfer fluids.

The overall heat transfer conductance, UA W^0C^{-1} for the heat transfer fluids was 61.4 W $^0C^{-1}$ for 6 M sodium chloride solution, 57.2 W $^0C^{-1}$ for 4 M sodium chloride solution, 56.9 W $^0C^{-1}$ for 2 M sodium chloride solution, 36.8 W^0C^{-1} for water, 25.6 W^0C^{-1} for vegetable oil 1, 19.4 W $^0C^{-1}$ for Vegetable oil 2, 32.5 W $^0C^{-1}$ for unused engine oil and

28.5 W $^{0}C^{-1}$ for used engine oil. The organic vegetable oils achieved lower transfer conductance since they absorbed low amount of solar thermal heat. The number of heat transfer units for the heat transfer fluids were 1.12 for 6 M sodium chloride solution, 0.93 for 4 M sodium chloride solution, 0.91 for 2 M sodium chloride solution, 0.90 for water, 0.74 for vegetable oil 1 oil, 0.71 for Vegetable oil 2, 0.63 for unused engine oil and 0.79 for used engine oil. The salt solutions achieved higher number of heat transfer units because they conducted more heat to the second fluid of the heat exchanger which was water. The logarithmic temperature difference, LMTD for 6 M sodium chloride solution, 4 M sodium chloride solution , 2 M sodium chloride solution, water –, vegetable oil 1 , Vegetable oil 2, unused engine oil and used engine oil was obtained as 83.3, 81.4, 79.3, 68.7, 61.5, 59.2, 73.8 and 71.6 respectively. The logarithmic temperature ratio of performance showed that salt solutions were better in absorbing solar thermal energy compared to water, organic oils, used engine oil and the unused engine oil.

The heat transfer flow rate was obtained as 7890.9 Js^{-1} for 6 M sodium chloride solution, 7621.3 Js^{-1} for 4M sodium chloride solution, 7263.4 Js^{-1} for 2 M sodium chloride solution, 6938.7 Js^{-1} for water, 5231.7 Js^{-1} for, 5097.8 Js^{-1} for Vegetable oil 2, 4843.8 Js^{-1} for unused engine oil and 6348.2 Js^{-1} for used engine oil. The heat transfer flow rates were high for the heat transfer fluids that absorbed high solar thermal radiation. Hence the best heat transfer fluid for harnessing solar thermal energy among the fluids studied was 6 M sodium chloride solution.

4.5 Steam Storage System

The longitudinal stress for the hemispherical part was obtained as 2.1×10^{6} Nm^{-2} using design equations. The steam storage system could store solar energy inform of heat with an average loss of 5.6 %. Interrogation of the performance of the steam storage was done by quantifying the following; efficiency of the storage system, amount of heat transferred during discharge and the amount emitted during discharge, the power output for steam discharged to the turbine from the steam storage, amount of heat absorbed by

the heat transfer fluids at testing and during the solar thermal collection, steam flow rates, sizing of the steam store. The determined values of steam flow rate of 9.7 kgs^{-1}, output temperature of 385.3 ^{o}C and pressure of 9.32×10^{5} Nm^{-2} were compared with the trial values and were found to have deviations of 0.5, 10.0 and 1.0×10^{2} Nm^{-2} respectively. The pressure of 1.0×10^{6} Nm^{-2} set by use of a pressure control valve. The boiling point of water rose to a maximum of 284.3 ^{0}C at 1.0×10^{6} Nm^{-2} pressure.

Table 4.7 shows the variation of heat absorbed with pressure and the mass flow rate of steam obtained from solar thermal collection without steam storage as one of the components. The results of the other heat transfer fluids are presented in appendix I. The results of solar thermal collection with steam storage as one of the components are as well presented in appendix H.

Table 4. 7: Variation of heat absorbed, pressure and mass flow rate for 6 M sodium chloride solution on 15.3.2014

Heat absorbed (J)	**18251.7**	**19017.6**	**19395.9**	**19667.1**	**20241.2**	**20698.9**	**21130.3**	**21732.7**
Pressure $\times 10^5$ (Nm^{-2})	1.0	2.0	3.0	4.0	5.0	6.0	7.0	8.0
Mass flow rate (kgs^{-1})	3.2	3.8	4.6	5.2	5.9	6.4	6.8	7.9

It was observed that the steam storage system increased the efficiency of solar energy collection by 15.1 % and consequently steam was producing more solar thermal power. The power generation system had an efficiency of 34.97 % without the storage system and with the storage system the efficiency obtained for the whole system was 40.1 %. This provided higher discharge rate of 40 kgh^{-1} during the peak periods that corresponded to maximum valve discharge. The steam storage system was operated between pressures of 1.0×10^5 Nm^{-2} – 1.0×10^6 Nm^{-2}. When in operation and there was discharge of steam to the turbine the fluid in the steam store flashed and the pressure in the steam store remained constant for ten to fifteen minutes. During the day higher discharge rates were possible since the heat transfer fluids at higher sensible heat contents continuously supplied heat to the steam storage system with solar power collection. The steam storage system was limited by design capacity when the solar irradiance was an average of 1105 Wm^{-2}.

During the charging process, the mass in the volume of heat exchanger increased as a result of more incoming steam which exceeded the discharge since during this process the steam exit valve was closed or was set to discharge less steam than the incoming steam for the coupled system. During this process the temperature of heat transfer fluids increased from an average of 100 ^{o}C to an average of 268.7 ^{o}C. During the coupled system solar thermal collection the steam generated from the flow of heat transfer fluids exceeded the demand and the excess would be stored increasing the pressure of the heat exchanger and the steam storage system. The steam storage system and the heat exchanger coupled system would be discharged by lowering the pressure to produce the steam by flashing. In the heat exchanger thermal energy would be transferred from the heat transfer fluids to water. The pressurized water in the heat exchanger was used for storage of heat. The fluid exiting from the turbine was fed into the reservoir of water at ambient temperature water and then passed to the collector for recirculation.

Figure 4.8 shows the efficiency for the steam storage system against the inlet temperatures that were used. Increase in temperature of operation of the steam storage system reduced the efficiency of the steam storage system. Lower inlet temperatures for the heat transfer fluid led to higher efficiency of operation of the solar thermal collector. In flat plate collectors the thermal efficiency of the collector increases with the increase in heat transfer fluids (Ekramian *et al.,* 2104). This is because the temperatures of operation of the flat plate are relatively low (80 °C to 150 °C) compared to the temperatures of operation of concentrating collectors (100 °C to 400 °C) (Hank *et al.,* 2002).

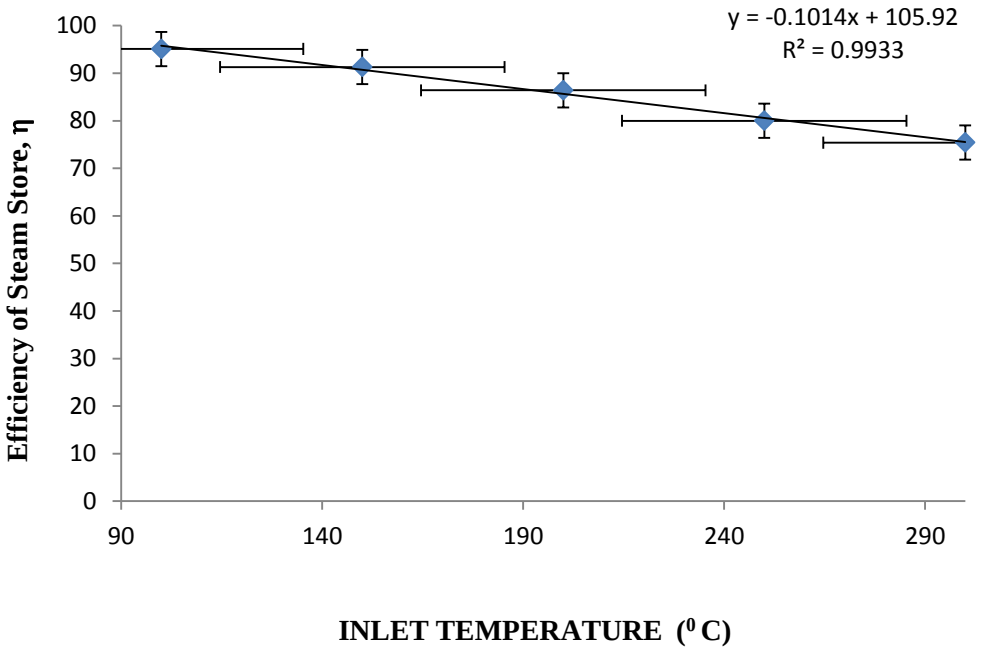

Figure 4. 8: Steam storage efficiency against inlet temperature on 19.1.2014

The steam storage system provided approximately 50 kg saturated steam per cubic meter of saturated steam storage volume. The pressure of 1.0×10^6 Nm^{-2} set by use of a pressure control valve kept the water in liquid phase despite the temperature being excess of 100 ^{0}C. The boiling point of water rose to a maximum of 284.3 ^{0}C at 1.0×10^6 Nm^{-2} pressure.

Evaporation energy for different steam pressures was found using the steam tables (Cecil, 2010) and used to obtain values of energy in appendix H and appendix I. The heat transfer fluid flowed at a constant rate for different temperatures and pressures.

Figure 4.9 shows the power output in watts obtained for 6 M sodium chloride solution for the operating pressures shown. Increase in pressure increased the boiling point at which the water absorbing heat from the heat transfer fluid turned into steam. The lower the output pressure the higher the amount of power output that was obtained. The output pressure was the pressure at which the mixture of steam and water left the turbine.

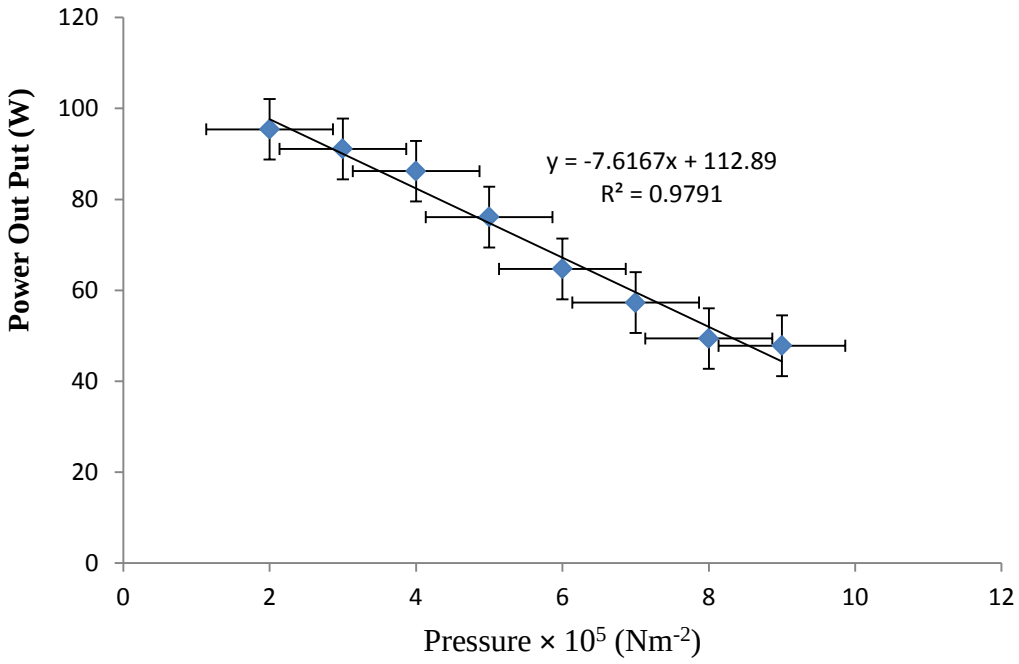

Figure 4. 9: Power output against output pressure for the steam storage system on 18.1.2014 Using 6 M sodium chloride solution

The operating pressure, the heat absorbed by the water from the heat transfer fluids, the mass flow rate of the heat transfer fluids and the mass of steam produced for each of the heat transfer fluids was as shown in appendix H and I. The amount of heat absorbed by water to produce steam increased with the increase in operating pressure. This is because pressure increase caused an increase in the boiling point of the water.

Table 4.8 shows how water absorbed heat at the shown conditions of pressure, mass flow rate, mass of steam obtained and the average solar power intensity. The study shows that water was a suitable heat transfer fluid for producing power by pressurization of steam.

Table 4. 8: Heat absorbed by water on 24.1. 2014

Pressure ($\times 10^5$) **Nm^{-2}**	**Q(J)**	**Temperature ^{o}C**	**Mass flow rate (kgs^{-1})**	**Mass of steam (kg)**	**Solar irradiance (Wm^{-2})**
2	14630.9	112.2	3.5	6.5	756.5
4	16720.4	146.1	4.0	7.3	804.7
6	18810.1	181.5	4.5	8.2	846.1
8	20900.5	219.7	5.0	9.0	932.5
10	22990.3	246.8	5.5	10.2	1027.4

4.5.1 Discharge Values of Temperature and Pressure

Table 4.7 shows that with an initial pressure of 9.0×10^5 Nm^{-2} the above values of gauge pressures and temperatures of steam output were obtained. The heat transfer vegetable oils achieved lower maximum temperatures of operation because they absorbed less heat from the sun. The operation temperature of the used oil kept fluctuating due to impurities and was less than that of the unused engine oil. The heat absorbed by the salt solutions was more than for the other heat transfer oils and this made them achieve higher operation temperatures at lower pressures.

Table 4.9 shows maximum temperatures achieved by the heat transfer fluids at the shown conditions of discharge pressure and solar irradiance.

Table 4. 9: Variation of maximum temperature and discharge pressure on 8.1.2014

Heat transfer fluid	Discharge Pressure (Nm^{-2})	Maximum temperature (^oC)	Solar irradiance (Wm^{-2})
Water	2.51×10^5	257.4	1064.9
Vegetable oil 2	2.37×10^5	157.7	986.3
Vegetable oil 1 oil	2.21×10^5	198.1	861.9
Used engine oil	3.5×10^5	207.9	957.4
Unused engine oil	2.41×10^5	275.2	945.8
2M sodium chloride solution	2.39×10^5	281.6	984.6
4M sodium chloride solution	2.34×10^5	284.9	994.1
6Msodium Chloride solution	2.31×10^5	289.6	976.5

The steam storage system efficiency was determined using Equation 3.13 and obtained as an average of 93.5 %. This shows that the heat losses from the stored steam amounted to 6.5% due to conduction, convection and radiation heat losses. The insulation of cotton reduced the heat losses to the environment.

Maximum temperatures obtained by the water that absorbed heat from the transfer fluids increased with the mass flow rate of the heat transfer fluid. The 6M salt solution had the highest rate of transmitting the heat it carried to the water to produce steam. The increase was as a result of increase in solar power intensity and further increase in heat absorption reduced due to increased resistance of addition of heat at temperatures in the range of 120 ° for vegetable oils and 200 °C for salt solutions.

4.5.2 Sizing of Steam Storage System

The steam storage capacity was obtained as 18.79 kgh^{-1} of steam as set in the design. When pressure dropped by 0.5×10^4 mN^{-2} the mean steam flow rate was 9.13 kgs^{-1}. This was because there was an initial amount of water in the storage system before charging the storage system. The proportion of flash steam obtained was 0.401 $kgkg^{-1}$ of water which was obtained by use of Equation 3.17. Therefore for every 0.401 kg of flash steam an initial amount of 1 kg of water had to be fed to the storage system before charging. The amount of water that was required at saturation temperature was 12.7 kg. The maximum steam release rate was 12.8 $kgm^{-3}s^{-1}$ at a pressure of 7.9×10^5 Nm^{-2} and solar irradiance an average of 1109 Wm^{-2}. The average collector maximum continuous rating was an average of 25.3 kgs^{-1} at a normal peak working pressure of 1.0×10^6 Nm^{-2} and solar power intensity of an average of 1100 Wm^{-2}. These were the maximum conditions under which the continuous rating could be achieved. Reduction in solar power intensity reduced the continuous rating. The mean value of overload corresponded to the maximum discharge in a cycle of 45 minutes for a period of 10 minutes at a solar power intensity of an average of 1105 Wm^{-2} at an average discharge rate of 11.5 kgs^{-1}. The off peak load corresponded to lowest steam discharge of an average of 3.2 kgs^{-1} at solar power intensity of an average of 752 Wm^{-2} from the storage system. The off peak load discharge corresponded to minimum steam exit valve adjustment. During the discharge process there was discharge of steam adequate to power the turbine even at a lower solar power intensity. The largest mean overload was obtained as an average of 40.2 kgh^{-1} at a pressure of 9.3×10^5 Nm^{-2} at a solar irradiance of an average of 1108 Wm^{-2}. A minimum vessel volume of 0.016 m^3 was required to satisfy the storage capacity of 18.79 kgh^{-1}. In solar two projects, molten salt at 565 ^oC is used to make steam for power production. The thermal storage medium consists of nitrate salt. The solar steam generated is at a pressure of 1.0×10^7 Nm^{-2} at an outlet temperature of 510 ^oC. The current maximum thermal storage temperature is 567 ^oC in direct salt storage in a central receiver tower (Medrano, *et al.*, 2010). In this study the thermal storage consists of steam at an average temperature of 247.4 ^oC at a pressure of

9.1×10^5 Nm^{-2}. This compares well with solar two because an improvement in performance of heat transfer fluid can improve the temperature of steam produced.

The average steam storage efficiency was determined from Equation 3.13 as 93.5%. Solar two power plant was using Heliostats with a receiver diameter of 0.07 m, storage of thermocline rock oil, granite sand and Caloria HT 43 oil, operating at a thermal capacity of 522 GJ, at a maximum temperature of 304 ^oC and operation time of four hours dispensing 7 MW of power (Stine & Harrigan, 1985). Molten salts have better thermal conductivities compared to oils. This is because the oils lack ions to conduct heat. The most prominent salt used for solar thermal storage is the solar salt that operates in the temperature range of 260 ^oC and 567 ^oC and that currently maximum operational steam conditions are 500 ^oC at a pressure of 1.2×10^7 Nm^{-2} (Pilkington Solar International, 1999). In this study the maximum range of temperatures for the heat transfer fluid was 207.9 ^oC to 289.6 ^oC.

4.6 Coupled Steam Storage and Heat Exchanger

The coupling system consisted of the heat exchanger and the steam storage system. During discharge flashing would occur in both the heat exchanger and the steam storage hence maintaining a constant pressure. This ensured that power production continued even if solar power was no longer available.

The following characteristics were determined for the system; efficiency, heat output for the heat transfer fluids, exit pressure, solar thermal power output among others. The coupled system was observed to produce more power compared to heat exchanger and steam storage system each on its own. Table 4.10 shows the magnitudes of average power produced by a steam storage and heat exchanger coupled system and for the system without coupling.

Table 4. 10: Comparison of power output for coupled system and non-coupled system

Heat Transfer Fluid	Coupled system power (W)	Non coupled system power (W)
Vegetable oil 1	321.6	312.4
Vegetable oil 2	341.3	333.7
Used engine oil	337.8	324.6
Unused engine oil	385.3	361.3
6 M sodium chloride solution	478.7	451.9
4 M sodium chloride solution	443.1	432.8
2 M sodium chloride solution	423.8	411.5
Water	401.6	387.9

Figure 4.10 shows heat output against operation pressure for the heat transfer fluids at an average solar power intensity of 1009.5 Wm^{-2}. It was observed that the higher the amount of heat absorbed by the heat transfer fluid the higher the pressure of operation. Pressurization of water caused increase in boiling point of water. The performance of the other heat transfer fluids was as shown in appendix D.

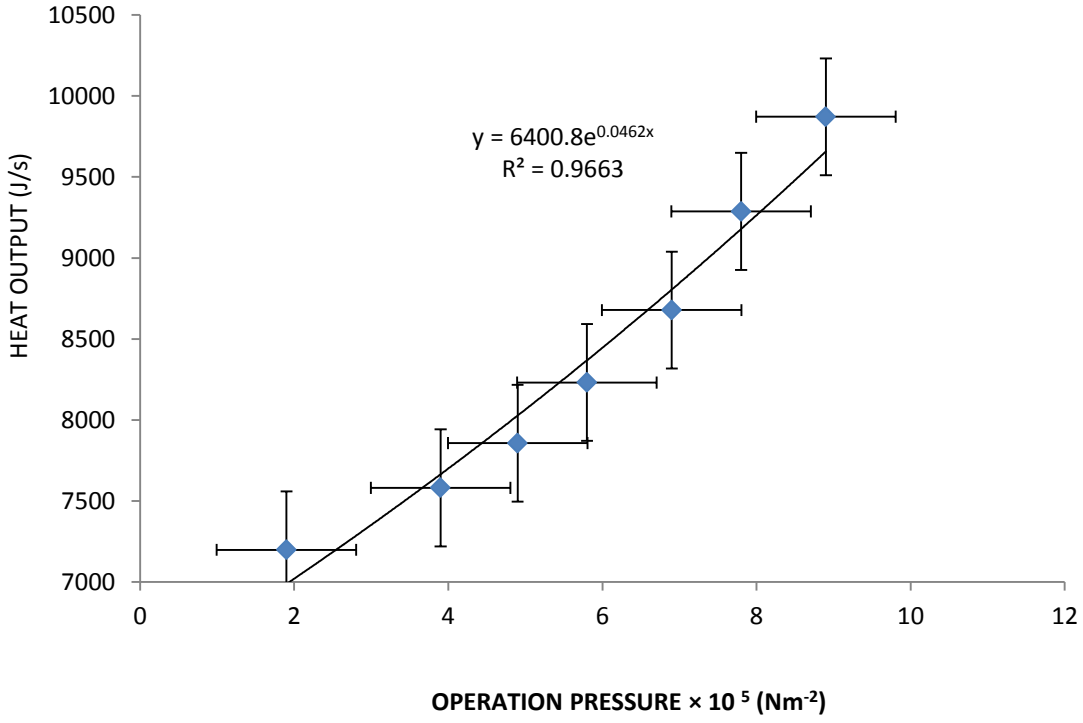

Figure 4. 10: Heat output against operation for Vegetable oil 2 on 8.1.2014

Average Power output of the coupled system was determined per hour for the heat transfer fluids and was plotted against the time of day. Figures 4.11 shows that the power output reduced very slowly even after irradiance began decreasing after two in the afternoon. The average solar power intensity during the study was 1051.6 Wm^{-2}. It was also noted that after solar intensity had been decreasing slowly for three consecutive hours it was possible to produce steady average power in excess of 250 W. The steam storage system was lagged with cotton and there was an average minimum loss of 6.2 % of heat to the surroundings by the coupled system. More heat was stored than was lost, flashing steam effect and hence the slowing up of power output reduction with time. The performance of the other heat transfer fluids was as shown in appendix E.

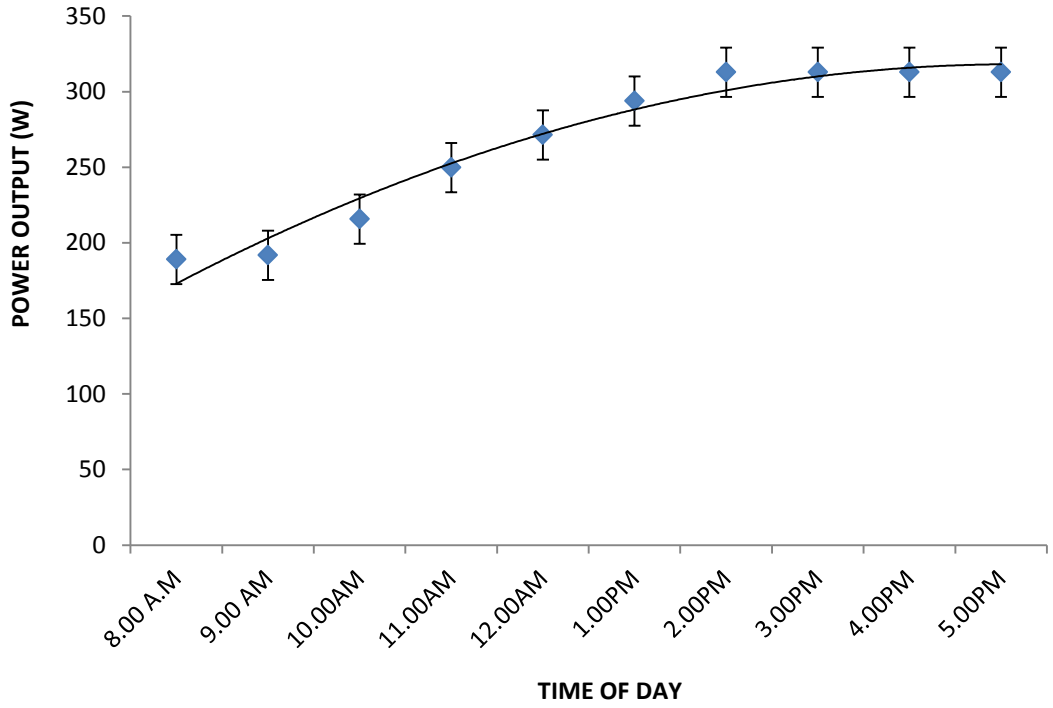

Figure 4. 11: Power output against time of day for 6 M sodium chloride salt solution

On 18.1.2014

Figure 4.12 shows relationships between the pressure drop ratio and the steam mass flow rate of the heat transfer liquids. The pressure drop ratio, $\chi = \frac{P_1 - P_2}{P_1}$ was observed to increase exponentially with the steam flow rate of the heat transfer fluid. For all the heat transfer liquids the bigger the pressure drop the higher the amount of steam that was obtained. The pressure drop at the turbine was related to the mass flow rate in that the more the pressure drop the more the steam flow rate of the heat transfer fluid. This was attributed to the fact that the heat transfer fluids lost the heat they absorbed from the sun to the water that changed its state to steam. The steam provided the energy that powered the turbine which caused power to be produced in the generator. The performance of the

other heat transfer fluids for the pressure drop ratio against steam flow rate was as shown in appendix K.

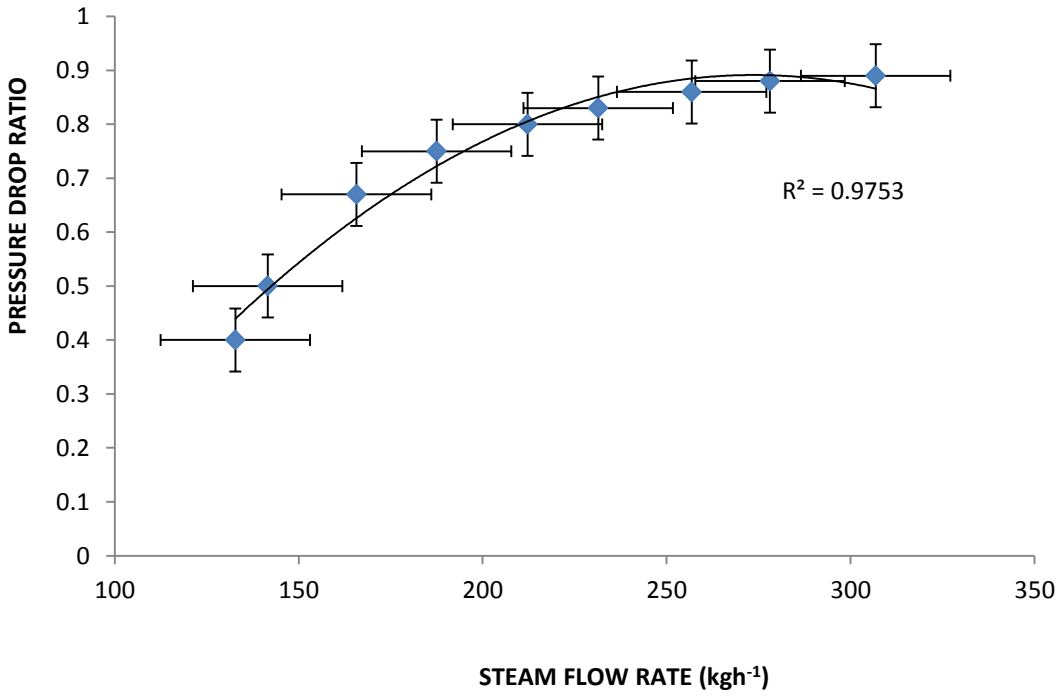

Figure 4. 12: Pressure drop against steam flow rate for Vegetable oil 2 on 4.2.14

4.7 Heat Exchanger Steam Storage System

The heat exchanger was tested for use as steam storage system. Figs. 4.13 through to 4.16 show the steam mass flow rates (kgs^{-1}) for the heat transfer fluids against steam temperatures obtained for the heat exchanger storage system. The temperature of steam discharged increased with the increase in the steam flow rate. Pressurization of the steam increased the enthalpy of water hence temperature increase for the steam. The steam obtained with inorganic solutions achieved higher temperatures compared to the one obtained from vegetable oils. This was because the inorganic fluids had higher degradation temperatures above 200 °C. The steam obtained from unused engine oil had

higher temperature compared to the one obtained from used engine oil. This was because the used engine oil underwent faster thermal degradation compared to the unused engine oil since the used engine oil is degraded oil containing carbon and other byproducts. The unused engine oil absorbed more heat from the sun compared to the used engine oil.

Fig. 4.13 shows the disparity between the 6M sodium chloride solution and 4 M sodium chloride solution transfer fluids. This was because the 6 M salt solution absorbed more heat from the sun compared 4 M salt solution and therefore more steam was generated when 6 M sodium chloride solution was used than when 4 M sodium chloride solution was used. Figure 4.16 shows the variations of steam flow rates between unused engine oil and water. Water has a higher specific heat capacity compared to the engine oil and therefore initially steam flow rate of Unused engine oil was higher than that of water. However as the temperatures of operation increased water achieved higher steam flow rates compared to unused engine oil. Figure 4.15 shows the comparison between the steam flow rates for vegetable oil 2 and used engine oil. The used engine oil achieved a higher steam flow rate compared to the vegetable oil 2. This was because vegetable oil 2 had lower heat absorption ability than used engine oil. Figure 4.14 shows the comparison between the steam flow rates for vegetable oil 1 and 2 M sodium chloride solution. The steam flow rates for the salt solution were higher than for vegetable oil 1. This was because the salt solution absorbed more heat from the sun and emitted to the water to make steam as compared to vegetable oil 1.

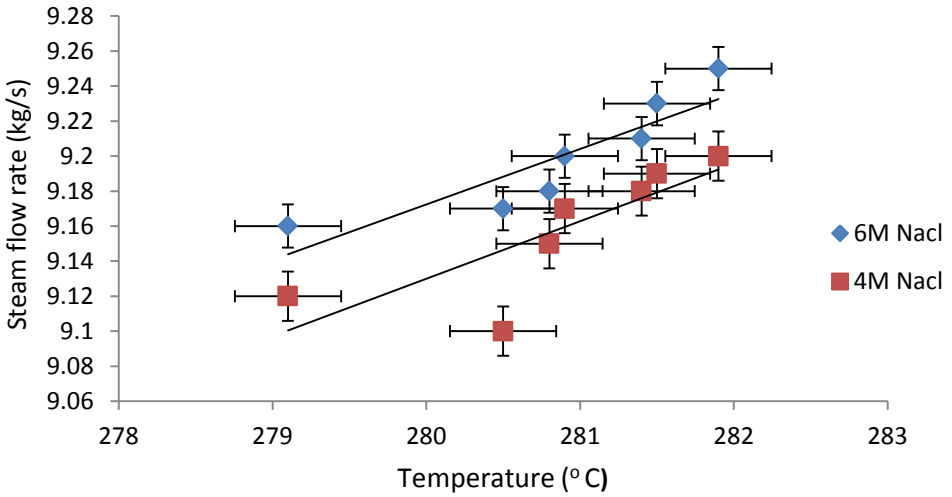

Figure 4. 13: Steam flow rate against temperature for 6 M and 4 M NaCl solution on17.1.2014

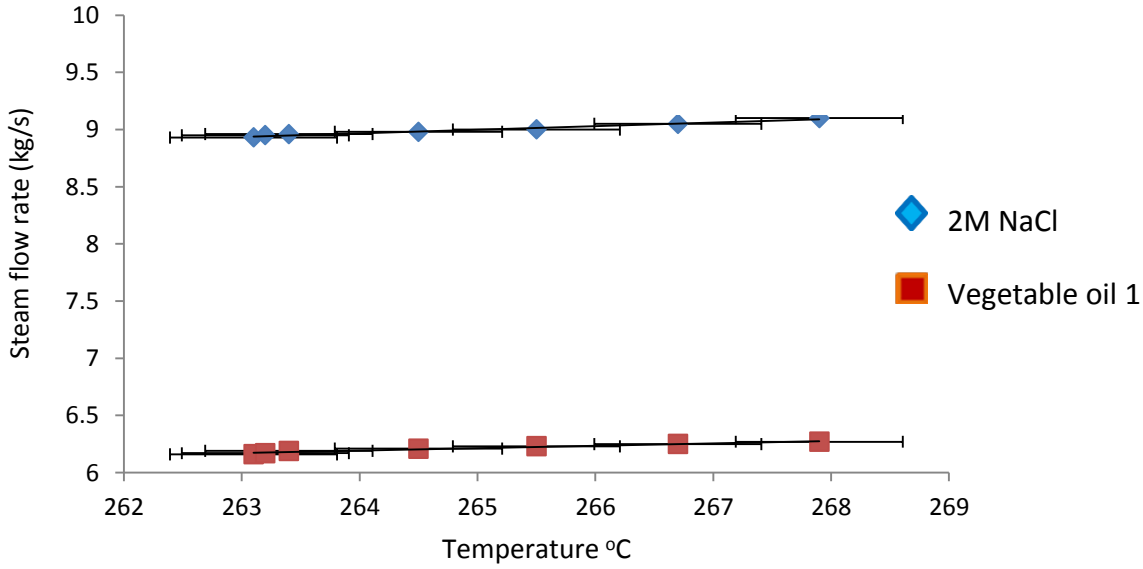

Figure 4. 14: Steam flow rate against temperature for 2 M NaCl solution and vegetable oil 1 on 19.1.2014

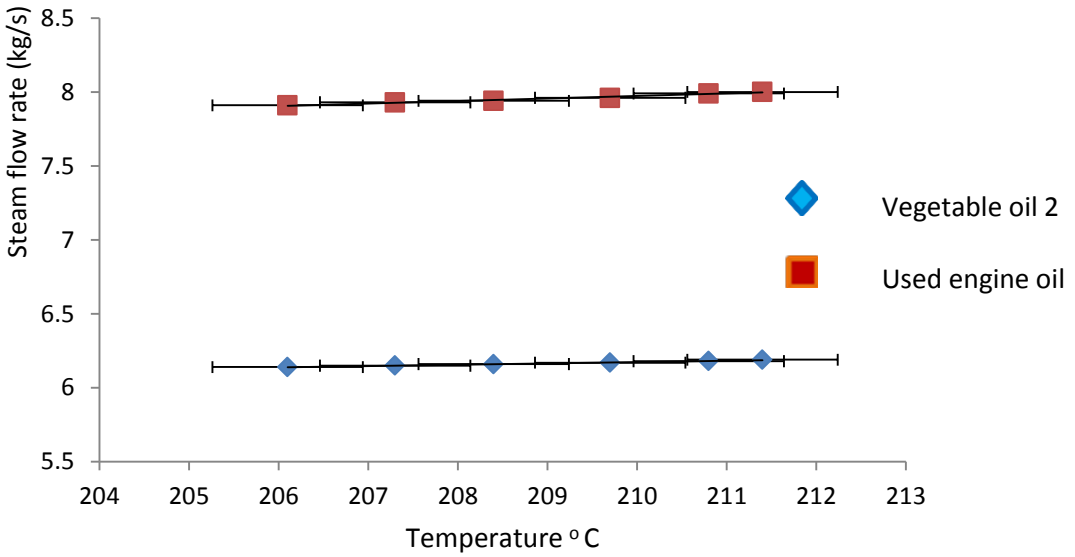

Figure 4. 15: Steam flow rate against temperature for Vegetable oil 2 and Used engine oil on 20.1.2014

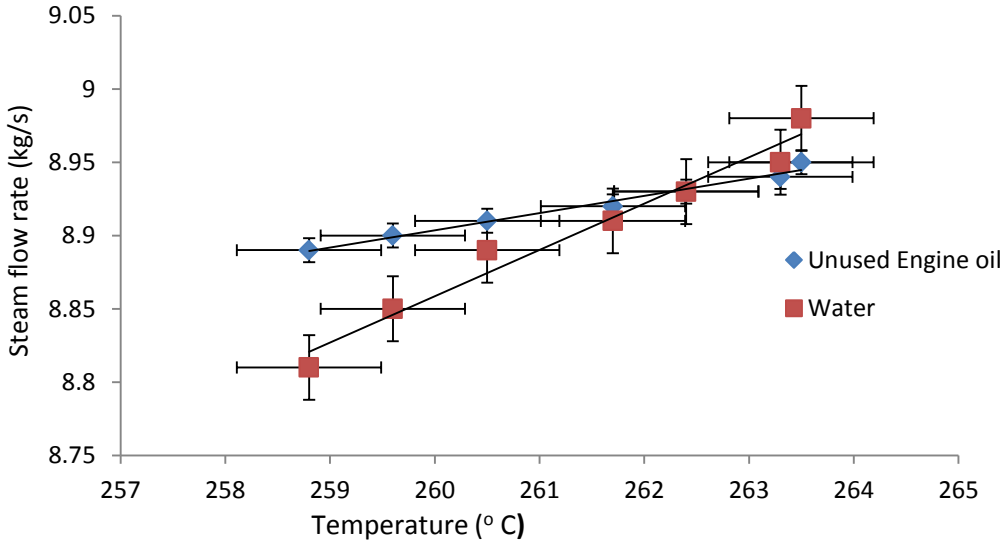

Figure 4. 16: Steam flow rate against temperature for Unused Engine oil and Water on 21.1.2014

A comparison of the findings of the study and other studies is summarized as follows:

The storage system in this study operated at a thermal capacity of 3.26×10^3 k J, maximum average temperature of 249.5 ^oC and a pressure of 7.2×10^5 Nm^{-2}. This compares well with a study on steam storage systems which showed that the current maximum thermal storage temperature is 567 ^oC in direct salt storage in a central receiver tower (Pilkington Solar International, 1999). The study used mineral heat transfer oil.

Thermal storage is necessary to cater for unpredictable transients in solar intensity due to overcast skies and at night time. Solar one power plant was using heliostats with a receiver diameter of 0.07 m, storage of thermocline rock oil, granite sand and Caloria HT 43 oil. It operated at a thermal storage capacity of 522 GJ, at a maximum temperature of 304 ^oC and a operation time of four hours dispensing 7 MW of power (NREL, 2011). The most prominent salt used for solar thermal storage is the solar salt that operates in the temperature range of 260 ^oC and 567 ^oC and that currently, the maximum operational steam conditions are 500 ^oC at a pressure of 1.2×10^7 Nm^{-2}. The heat exchanger storage system compared well with other storage system around the world such as Coolidge storage irrigation facility with a thermal capacity of 19.8 GJ and operating at a maximum temperature of 288 ^{o} C, Shenandoa Solar total energy project has thermal capacity of 1.33 GJ and operates at a maximum temperature of 363 ^{o} C, Invapah solar generating facility uses molten salt and has a storage efficiency of 98 % and Jonhson and Johnson solar total energy project has a thermal capacity of 29.3 GJ and an efficiency of 96.7 % (NREL, 1999). In this study the coupled system of steam storage system and the heat exchanger achieved thermal capacity of 4.15×10^3 k J at a maximum temperature of 249.5 ^oC and a pressure of 7.2×10^5 Nm^{-2}. The performance was lower due to small size of the test facility used for the study.

A means of reducing tube vibrations that are caused by eddying motion of the fluid in the wake of the tube needs to be investigated. This caused considerable wear and tear on the coiled tube heat exchanger.

4.8 Generator

A three phase generator was fabricated of the following technical data:- Span 1-7 to separate the 3 star connection terminals, 260 turn bundles, copper wires of gauge 4 by 8 AWG, connection – top to bottom, coils 6×2 at a length of 1524 m, 24 slots, a magnet of four poles and a star frame support.

The generator converted the mechanical energy of rotation of the shaft to electrical power. The following was quantified with respect to its performance: - output power, output frequency, the kilowatts drive input and its efficiency. The a.c generator shaft input power was the same as the turbine shaft output power as a matter of design which was in the range of an average of between 128 W and 489.1W . The three phase system was considered for power generation since it delivers more power with smaller gauge conductors than a single phase system of the same amperage (Leyzorovich, 2005). Mechanical power in watts as applied to a generator was obtained as 2.24×10^{4} Js^{-1}.

4.8.1 Characterization of Generator

Figure 4.17 shows the three wye phases of the generator that was fabricated. The figure shows that the power output increased with the rotations per minute. This was because the rotation of the magnet that was attached to the shaft caused change of magnetic flux linking the copper turns and a voltage was produced. The higher the number of rotations per minute the higher the power output that was realized.

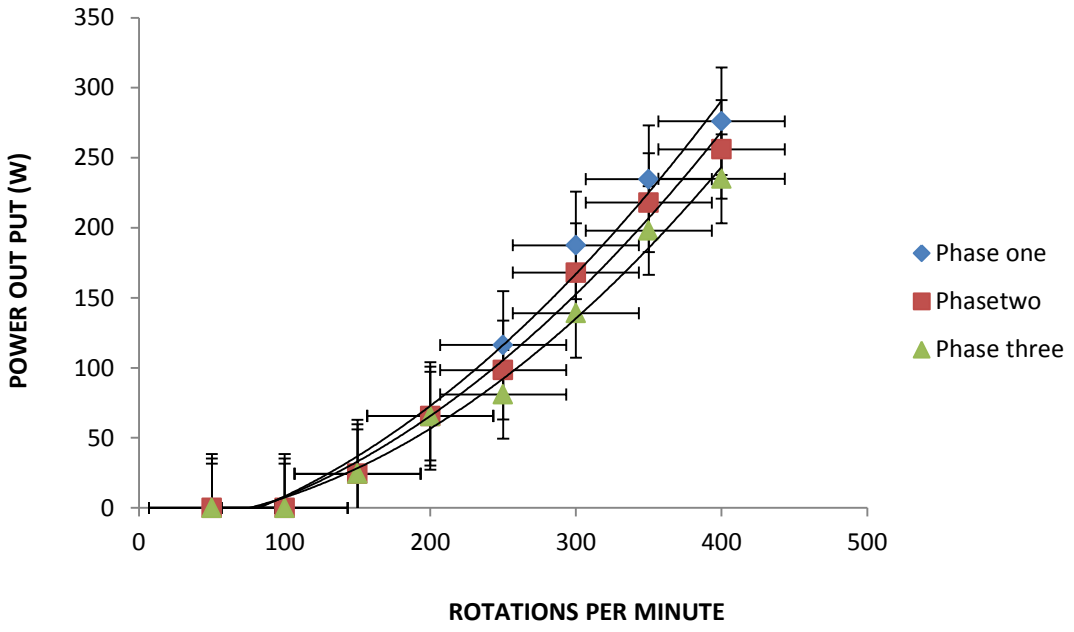

Figure 4. 17: Three phase power generation against rotation on 10.9.2013

The average output frequency of the generator was obtained as 59.6 Hz. This was obtained as described in section 3.6.2 and Equation 3.57 was used on determining the value.

The average KVA which gave the power output for the generator in terms of watts was obtained as 495.3 W. It was determined by use of Equation 3.59.

The kilowatts drive input was obtained as 0.5 kW. The selection of the shaft of the generator was governed by electrical power output supplied to the load and efficiency of the a,c generator as per the design variables. The efficiency of the generator depended on the heat transfer fluids used. The highest efficiency of the generator of 91.8 % which was obtained with 6 M sodium chloride solution and the lowest was with Vegetable oil 2 of 62.4 %. The difference was associated with the difference the amounts of heat absorbed by the heat transfer fluids. Salt solutions absorbed more solar heat compared to the other heat transfer fluids.

Amperage, A for the generator was found to be 9.8 A with use of a power factor of 0.9 (Stevenson, 2000). The kW drive input was taken as the shaft power in kilowatts while the kW output was taken as electrical power supplied to the load. The η_a was taken as the efficiency 'per unit 'of a.c generator. The efficiency of generator was determined and was plotted against quantity of heat absorbed by the heat transfer liquids.

Figure 4.18 shows the average efficiency of the generator in terms of converting the mechanical energy from solar heat to electrical power. Increase in the amount of heat absorbed by the heat transfer fluids increased the efficiency of the generator. The heat emitted by the heat transfer fluid was absorbed by water which turned into steam and turned a turbine and hence power was generated.

Average power output of the turbine was determined as 457.1 W and the power output by the generator was an average of 419.6 W. This produced an efficiency of 91.8 % of power conversion by the generator.

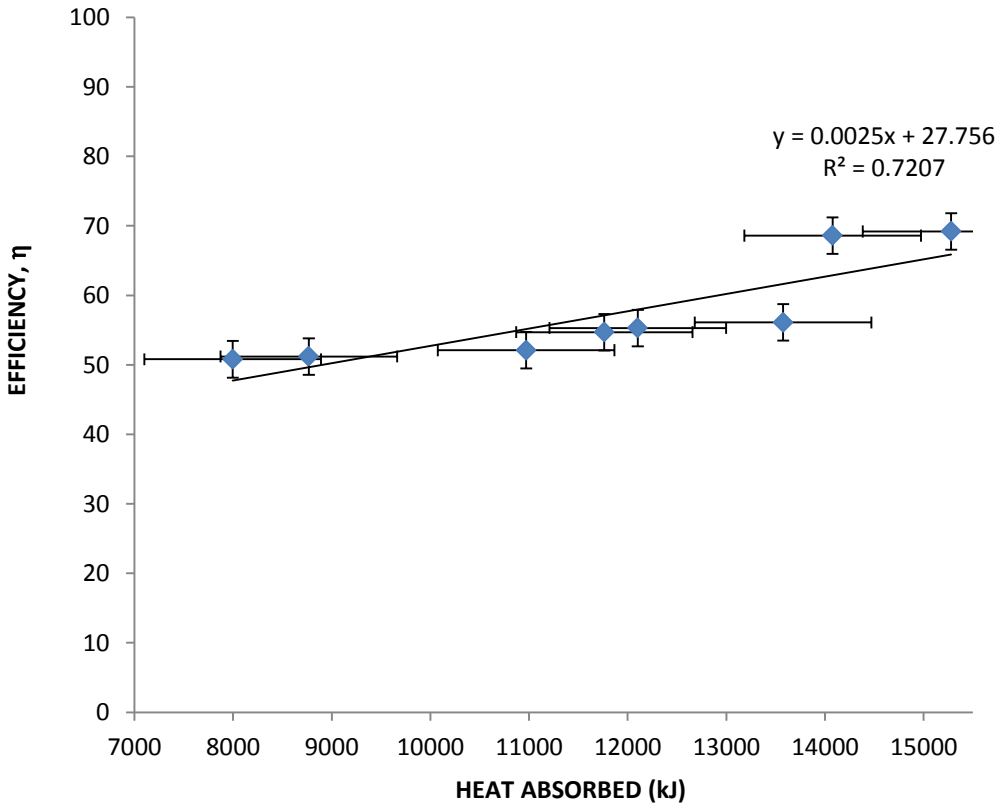

Figure 4. 18: Efficiency of generator against heat absorbed by heat transfer fluids

19.9.2014

4.9 Turbine

The following aspects of the single stage impulse turbine were approximated: - centripetal force on turbine blades, angular velocity of the shaft, efficiency of the turbine, torque developed by the shaft, heat absorbed by the heat transfer fluids with respect to power developed, electrical efficiency and turbine efficiency. Angular velocity for the rotor was found to be 43.6 $rads^{-1}$. The speed of rotation of the rotor was obtained from the product of the angular velocity and the radius of the rotor as 64.2 ms^{-1}. The angular velocity was estimated as an average of 102.6 $rads^{-1}$. A single stage impulse

turbine was fabricated where thermal energy of steam was converted to kinetic energy that was converted to mechanical energy through rotor shaft and coupling to the load. Total centripetal force acting on the blade was obtained from Equation 3.49 as 734.1 N per blade. The average angular velocity, ω of the disc was determined as 146.62 $rads^{-1}$. The blades were assumed to execute circular motion. The blade tip radius was found to be 0.048 m and the rotor disc radius was found to be 0.045 m. Blade cross sectional area was 0.0004 m^2. The average efficiency of the turbine was obtained as 61.6 %. The average torque on the shaft was obtained as 153.1 NM. Maximum shaft power was obtained as 434.7 W.

Figure 4.19 shows that centripetal force increased with heat absorbed by the water that produced steam to turn the turbine. Some power from the steam was used to provide the centripetal force on the turbine blades.

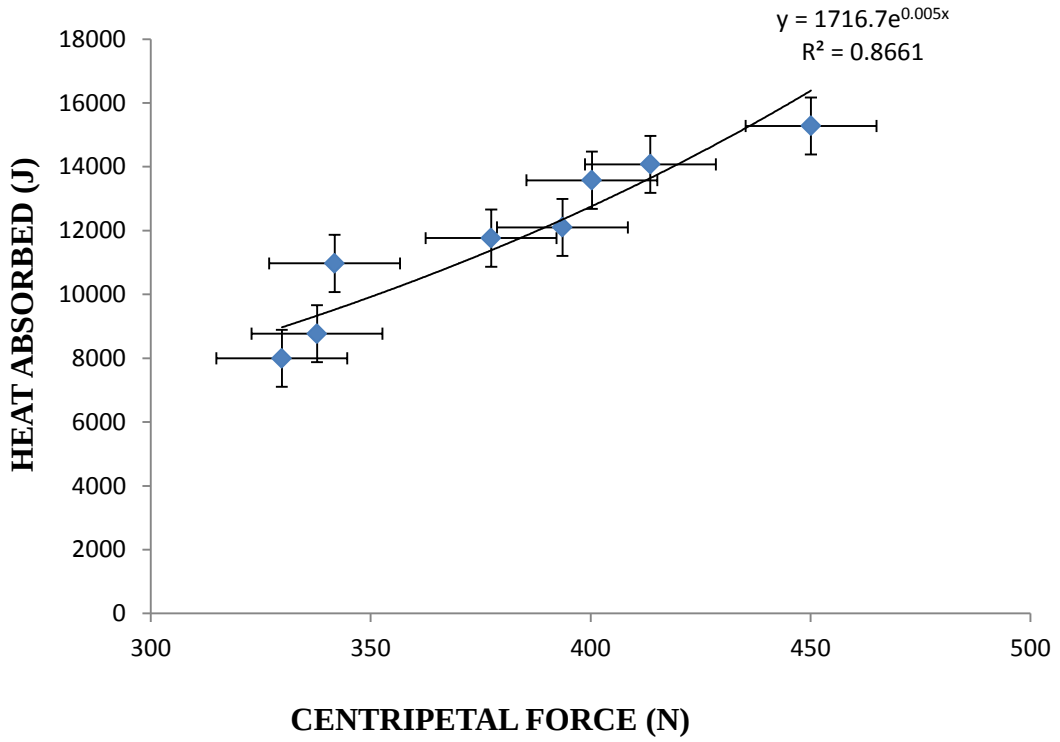

Figure 4. 19: Heat absorbed against centripetal force 15.9.2013

The thermodynamic cycle for the steam turbine is the rankine cycle that consists of a heat source that converts water to high pressure steam (Stine, 1985). The steam turbine thermodynamic efficiency was a measure of how efficiently the turbine extracted power from the steam itself and was found to be an average of 55 %. A study showed that thermodynamic efficiency ranges from 65 % for small turbines to 90 % for bigger commercial ones and small single stage turbines have efficiencies as low as 50 % (Schetz & Fuhs, 1996). The efficiency obtained in this study was lower due to the lower pressures of operation used compared to the ones in the quoted work. The Solar one power plant was using a power conversion cycle of rankine with a turbine inlet pressure of 1.01×10^{7} Nm^{-2} at a temperature of 510 ^{o}C and a thermal efficiency of 25 % (Stine & Harrigan, 1985).

The steam turbine shaft rotated had a speed of 2800 revolutions per minute. A summary of the characteristics of the turbine were: - The number of revolutions for the shaft per minute was 2800 r.p.m, angular velocity was 146.62 rads^{-1}, blade cross sectional area was 0.0009 m^2, material density was 8000kg/m^3, blade tip radius, r_2 was 1.2 m and blade root cross sectional area was 0.002 m^2 and angular velocity of the shaft was approximated as 138.7 rads^{-1}.

4.9.1 Characterization of Turbine

The performance characteristics of the turbine that was fabricated were obtained by use of information from ASME Turbine design manual. The following are the attributes of the single stage impulse turbine: average isentropic efficiency was 83.5 %, average cycle power output was 457.8 W, average turbine maximum power output was 498.2 W and average gear efficiency was 87.9 %. In a study on ac generators the torque is converted to power with efficiency higher than 90% (Whitaker, 2006). This observation compares well with the findings of this study. The efficiency in this study was lower than the quoted one due to more losses of flux linkage in the generator. Generator speed was 2800 r.p.m., turbine blade length was 0.05 m, Blade radius was 0.03 m, Nozzle diameter was 0.33 m, angle of nozzle was 30 ^{0}, shaft length was 0.5 m, shaft speed was 2800 r.p.m., inlet flow rate was 0.013 kgs^{-1}, design turbine wheel diameter was 0.15 m.

The turbine inlet conditions were as follows: pressure was 1.0×10^5 Nm^{-2} to 1.0×10^5 Nm^{-2}, average temperature was 234.8 ^{0} C, average steam flow rate was 0.014 kgs^{-1} and average enthalpy of 4570 Jkg^{-1}.

The turbine outlet conditions were as follows: average pressure 4.0×10^5 Nm^{-2}, average temperature was 84.3 ^{0}C. Average steam exit flow rate was 3.5 kgs^{-1} and at an enthalpy of 3256 Jkg^{-1}. Table 4.11 shows the turbine efficiency obtained with each of the heat transfer fluids. The higher the heat solar output for the heat transfer fluid, the higher was the efficiency of the turbine. The turbine produced the highest efficiency with 6 M sodium chloride solution, its heat output was the highest compared to the other heat transfer fluid.

Table 4. 11: Characterization of turbine between 16.9.2013 and 10.10.2013

Heat Transfer Fluid	Average Turbine Efficiency, %
6M sodium chloride solution	62.5
4 M sodium chloride solution	61.7
2 M sodium chloride solution	59.8
Water	55.4
Unused engine oil	54.8
Used engine oil	52.1
Vegetable oil 2	51.8
Vegetable oil 1	51.1

4.9.2 Turbine and Generator

The combined average efficiency of the turbine and generator was 74.2 %. The generator efficiency was higher than the turbine efficiency. To maximize the turbine efficiency the temperature of the working fluid had to be as high as possible. The temperature of steam entering the turbine had to be as high as possible and the temperature of the fluid leaving the turbine had to be as low as possible for maximum efficiency. In this study the temperature at which the fluid was leaving the turbine was not the lowest since the turbine used a single stage turbine and hence the fluid leaving carried some thermal heat with it as it exited. The lowest temperature of the exiting fluid was 109.5 °C

Figure 4.20 shows the variation of steam flow rate and power output for the heat transfer fluids at an average solar power intensity of 1103 Wm^{-2}. The steam flow rate was highest for the sodium chloride solutions and the organic oils had a lower steam flow rate. This was because the organic oils absorbed less solar heat compared to the inorganic salt solutions. The higher the amount of heat absorbed by the heat transfer

fluid the higher was the mass flow rate for the secondary fluid that was water. Figures on the other heat transfer fluids on steam flow rate against power output are found in appendix F.

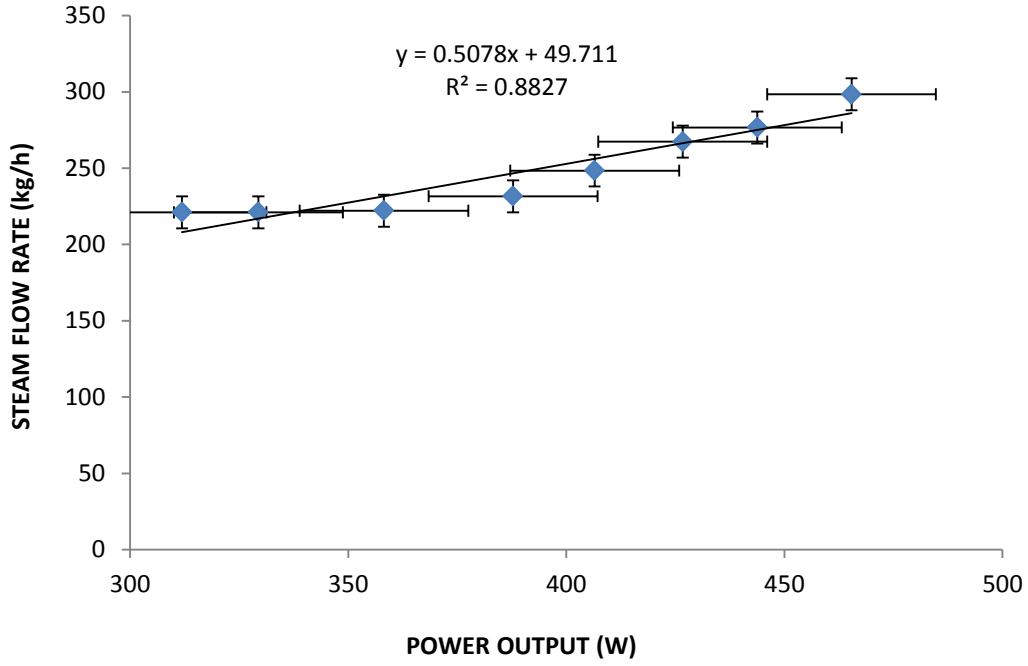

Figure 4. 20: Steam flow rate against power output for 6 M NaCl solution on 7.1.2014

4.10 Characterization of Collector

The testing conditions for the thermal performance were as follows: - the variation of collector inlet temperature of less than $\pm$ 0.1 ^{0}C, variation of ambient temperature of less than $\pm$ 0.1 ^{0}C, minimum difference temperature of 1.5 ^{0}C, average minimum beam irradiance of 700 W/m^2, incident angle of 27 ^{0}, variation of flow rate of less than 1 % and the spectrum weighted value for transmittance absorptance product at normal incidence not differing by 3% of the value when the standard spectrum was used. The collector was tested over average operating range of temperatures of 100 ^{o}C to 300 ^{o}C

for unused engine oil and the salt solutions and 100 ^{o}C to 250 ^{o}C for the used engine oil and the organic oils.

The collectors were covered with glass that was 0.0004 m thick. Due to the use a receiver use of a receiver of diameter 0.0127 m the open collector efficiencies obtained were relatively close to the efficiencies of the closed concentrators as shown in appendix G. The average solar power intensity during the test was 700 Wm^{-2} to 1152.1 Wm^{-2}. The closed collectors achieved higher efficiency due to due to the glass cover that prevented excessive heat loss to the surrounding. The geometrical concentration ratio of the concentrator was 81.9.

4.10.1 Solar Thermal Characterization

This section consists of results presentation and the general discussion of the parameters involved. Other documented findings are as well presented. The discussion with comparison form other works for the collectors is presented after the results presented in the ensuing section.

The following heat transfer fluids were used for collector characterization as follows:

4.10.2 Water

Figure 4.21 shows the characterization of closed concentrator using water as the heat transfer liquid. The figures on efficiency characterization of the collector for the other heat transfer fluids are found in appendix G. The efficiency of the solar collector was 56.4 %. This was due to use of reflector of reflectance of 0.92 and a receiver of radius 0.0127 m. Efficiency performance of the collector using the other heat transfer fluids is found on appendix G.

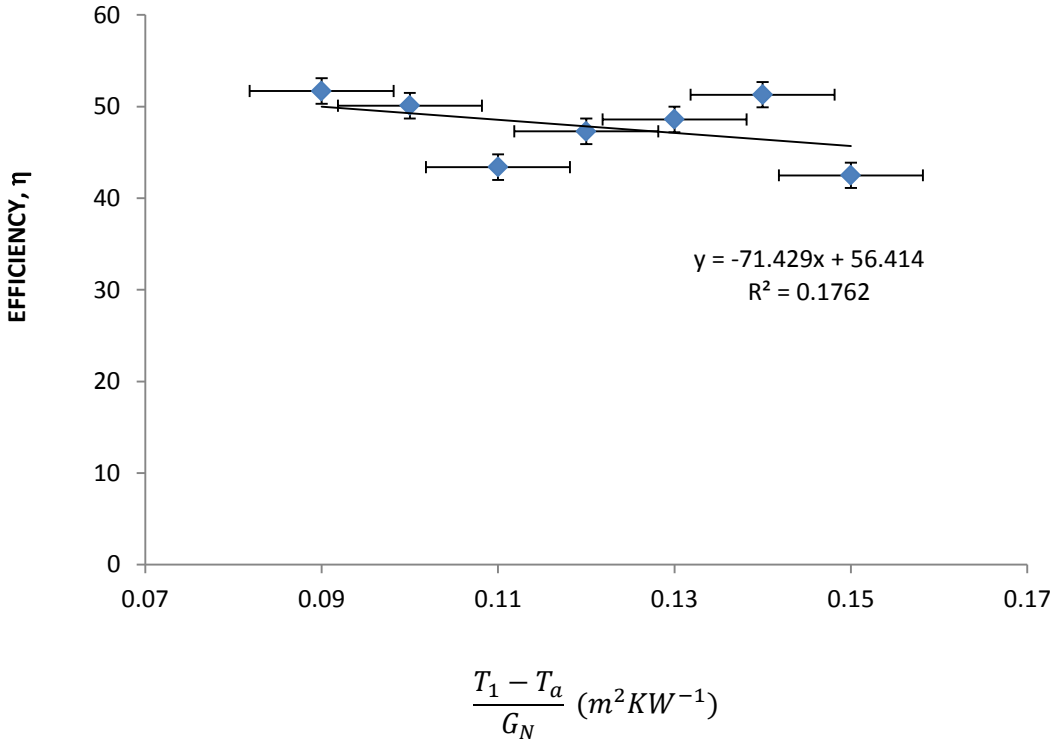

Figure 4. 21: Efficiency of closed solar collector using water on 16.10.13

The test conditions were: pressure of 9.0×10^9 Nm^{-2}, average flow rate of 9.4 kgs^{-1}, average ambient temperature of 22.5 ^oC, inlet temperature of water of 22.1 ^oC and an outlet temperature of 243.8 ^oC. The gradient of the slope provided the receiver heat loss. The y – intercept, $F_R\eta_o$ provided the highest achieved efficiency that the collector could achieved in operation. For the collector using water, the value of the slope, $-\frac{A_r U_l F_R}{A_c}$ was obtained as - 71.4. The collector overall heat loss coefficient, U_l was obtained as 840.12 $Wm^{-2}K^{-1}$. The collector heat removal factor, F_R was obtained as 0.901 and the maximum possible efficiency, $F_R\eta_o$ was obtained as 56.4 %. Characterization of open solar collector using water as the heat transfer fluid was also carried out. The collector was not covered and hence some heat was carried away from the receiver. The efficiency of the collector

was obtained as 54.1 %. The slope, $-\frac{A_r U_l F_R}{A_c}$ was obtained as - 51.8 and the overall heat coefficient for water as the heat transfer fluid was obtained as 745.81 $Wm^{-2}K^{-1}$

4.10.3 Vegetable oil 2

For the closed collector, the test conditions were: Pressure of 9.0×10^9 Nm^{-2}, average flow rate of 6.5.kgs^{-1}, average ambient temperature of 21.4 ^oC, inlet temperature of water of 21.1 ^oC and an outlet temperature of 110.3 ^oC The slope, $-\frac{A_r U_l F_R}{A_c}$, was obtained as – 64.6, U_l was the overall heat loss coefficient and it was obtained as 587.3 $Wm^{-2}K^{-1}$ and the efficiency that the collector using vegetable oil 2 heat transfer oil achieved was 48.8 % and F_R was obtained as 0.911. For the open vegetable oil 2 oil solar collector slope, $-\frac{A_r U_l F_R}{A_c}$ was obtained as – 57.14, U_l was obtained as 497.5 $Wm^{-2}K^{-1}$, $F_R$was obtained as 0.931 and the efficiency of operation was obtained as 46.7 %.

4.10.4 Vegetable oil 1

For the closed collector, the test conditions were: pressure of 9.0×10^9 Nm^{-2}, average flow rate of 7.0 kgs^{-1}, average ambient temperature of 22.1 ^oC, inlet temperature of water of 21.8 ^oC and an outlet temperature of 118.3 ^oC. The slope, $-\frac{A_r U_l F_R}{A_c}$, was obtained as - 65.4, U_l was obtained as 654.1 $Wm^{-2}K^{-1}$ and the efficiency that the collector using Vegetable oil 1 can achieved was 49.9 % and F_R was obtained as 0.931. For the open vegetable oil 1 heat transfer fluid the slope, $-\frac{A_r U_l F_R}{A_c}$ was obtained as – 52.5, U_l was obtained as 567.6 $Wm^{-2}K^{-1}$, $F_R$was obtained as 0.925 and the efficiency of operation was obtained as 46.5 %.

4.10.5 Used Engine Oil

The test conditions for the used oil solar collector were: - pressure of 9.0×10^9 Nm^{-2}, average flow rate of 8.9 kgs^{-1}, average ambient temperature of 21.3 ^oC, inlet temperature of water of 20.9 ^oC and an outlet temperature of 223.8 ^oC. For closed used oil solar heat

transfer fluid the slope, $-\frac{A_r U_l F_R}{A_c}$ was obtained as – 24.6, U_l was obtained as 593.8 $Wm^{-2}K^{-1}$, F_R was obtained as 0.939 and the achieved efficiency was obtained as 53.7 % while the slope for the open collector, $-\frac{A_r U_l F_R}{A_c}$ was obtained as – 71.4, U_l was 438.9 $Wm^{-2}K^{-1}$, F_R was obtained as 0.923 and the achieved efficiency was 49.9.

4.10.6 Unused Engine Oil

The test conditions for unused engine oil heat transfer fluid were:- pressure of 9.0×10^9 Nm^{-2}, average flow rate of 9.5 kgs^{-1}, inlet temperature of water of 20.7 ^oC, average ambient temperature of 20.9 ^oC and an outlet temperature of 251.1 ^oC.

For closed collector using unused oil the slope, $-\frac{A_r U_l F_R}{A_c}$ was obtained as – 53.9, U_l was obtained as 791.4 $Wm^{-2}K^{-1}$, F_R was obtained as 0.941 and the achieved efficiency was 57.6 % while for the open solar collector using unused engine oil the slope, $-\frac{A_r U_l F_R}{A_c}$ was obtained as – 58.5, U_l was obtained as 638.7 $Wm^{-2}K^{-1}$, F_R was obtained as 0.938 and the maximum achievable efficiency was obtained as 55.2 %.

4.10.7 2 M Sodium Chloride Solution

For closed 2 M sodium chloride solution heat transfer fluid, the test conditions were: - Pressure of 9.0×10^9 Nm^{-2}, average flow rate of 9.5 kgs^{-1}, average ambient temperature of 21.7 ^oC , inlet temperature of water of 21.5 ^oC and an outlet temperature of 258.9 ^oC. The slope, $-\frac{A_r U_l F_R}{A_c}$ was obtained as – 183.2, U_l was obtained as 878.7 $Wm^{-2}K^{-1}$, F_R was obtained as 0.945 and the attained efficiency was obtained as 58.7 % while for the open collector the slope, $-\frac{A_r U_l F_R}{A_c}$ was obtained as – 40.7, U_l was obtained as 761.2 W/m^2K, F_R was obtained as 0.949 and the efficiency of operation was obtained as 56.5 %.

4.10.8 4 M Sodium Chloride Solution

For 4 M sodium chloride solution heat transfer fluid, the test conditions were: - pressure of 9.0×10^9 Nm^{-2}, average flow rate of 9.6 kgs^{-1}, average ambient temperature of 22.1 ^oC, inlet temperature of water of 21.9 ^oC and an outlet temperature of 264.9 ^oC.

For closed 4 M sodium chloride solution the slope, $-\frac{A_r U_l F_R}{A_c}$ was obtained as – 87.1, U_l was obtained as 981.6 $W/m^{-2}K^{-1}$, F_R was obtained as 0.949 and the efficiency was obtained as 59.1 % while for the open collector the slope, $-\frac{A_r U_l F_R}{A_c}$ was obtained as – 40.7, U_l was obtained as 891.8 $Wm^{-2}K^{-1}$, F_R was obtained as 0.953 and the efficiency of operation was obtained as 58.3 %.

4.10.8 6 M Sodium Chloride Solution

For closed solar collector using 6 M sodium chloride solar solution the test conditions were: - pressure of 9.0×10^9 Nm^{-2}, average flow rate of 10.1 kgs^{-1}, average ambient temperature of 21.9 ^oC, inlet temperature of water of 21.6 ^oC and an outlet temperature of 271.5 ^oC. The slope, $-\frac{A_r U_l F_R}{A_c}$ was obtained as – 68.6, U_l was obtained as 1076.9 $Wm^{-2}K^{-1}$, F_R was obtained as 0.961 and the efficiency was obtained as 60.1 % while for the open collector the slope, $-\frac{A_r U_l F_R}{A_c}$ was obtained as – 55.9 , U_l was obtained as 973 $Wm^{-2}K^{-1}$, F_R was obtained as 0.943 and the efficiency was obtained as 58.6 %. The performance of the collector in this study compared well with the collectors in use in various parts of the world. However the collectors cited here have better performance due to higher inlet temperature heat transfer fluids that were used, superior treatment of the absorber pipe and high optical reflectance of the reflecting system. A study on IST collector obtained a maximum efficiency in the range of 76.3 to 70.8 % (Dudley *et al*., 1995).

Figure 4.22 shows the variation of collector efficiency and power output against the concentration of the salt solutions.

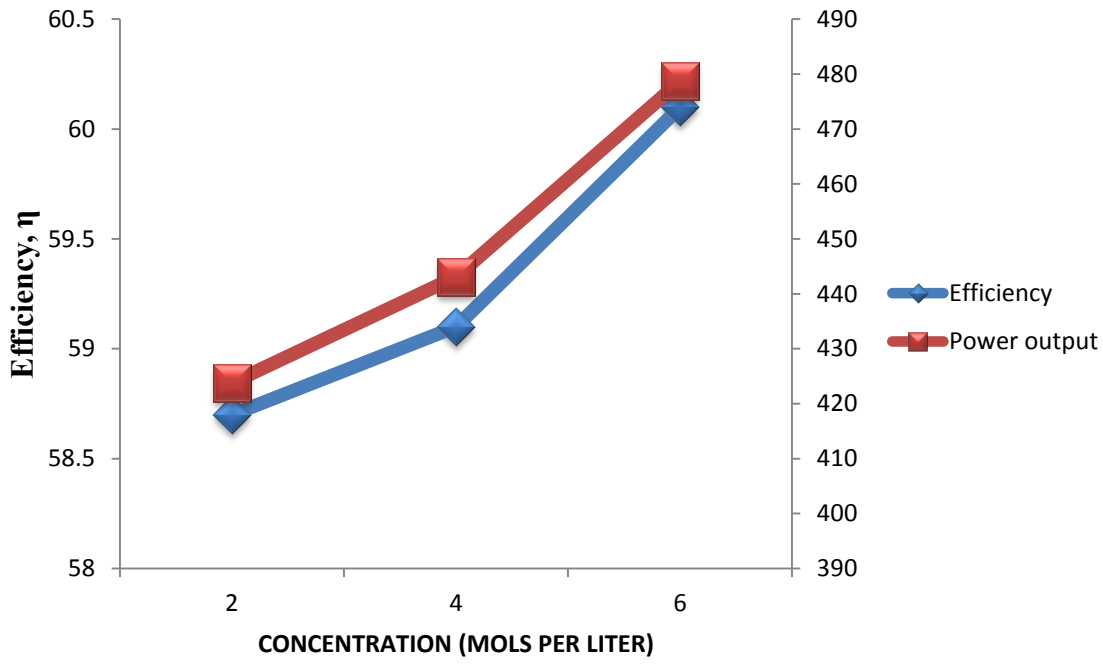

Figure 4. 22: Variation of collector efficiency and power output against concentration of salt solutions

An increase in concentration of the salt solutions caused an increase in the collector efficiency and the power output. This was so since the salt solution with higher concentration absorbed more heat from the sun compared to the one of lower concentration of the salt. It was observed that 6 M sodium chloride solution absorbed the highest amount of solar radiation and hence produced the highest collector efficiency and the highest power output. Therefore the 6 M sodium chloride is recommended in this study for power production.

In this study the efficiencies of the collector with the various heat transfer fluids was in the range of 48.8 % and 60.2 %. The most efficient collector was using 6 M sodium chloride solution. The collector used reflector of optical reflectance of 0.92 and a absorber with absorbance of 0.97. The efficiencies were lower because the receiver was

painted with a black paint which was an inferior surface treatment and was not evacuated as is the case with the quoted works however the results obtained compared well to those obtained in the quoted works. The most recent Eutrough collector has an approximate efficiency of 75 % (Geyer *et al*., 1995). The concentrator reflector was made of silvered glass whose optical efficiency was 0.99. The heat transfer fluids used were synthetic hence a higher solar thermal collection. Solargenix's collector modules produce 176 kW of energy at peak efficiency of 56 % (Cleaveland, 2005). In this study the range of power produced was 401.6W to 321.6 W for the coupled system with efficiency of 54.9 %. This was because the heat transfer fluid used in the quoted study was synthetic oil which could achieve higher temperatures compared to the heat transfer fluids used in this study.

In a study a parabolic trough collector gave a peak thermal efficiency of 53.8 % when open and 55.2 % with evacuated receiver tube (Brooks *et al*., 2006). In this study the efficiencies achieved for the closed collectors were 48.8% to 60.2 % and for the open collectors the range of efficiency was 46.5 % to 58.6 %. Therefore the results in this study compared well with the results obtained by Brook and his team and cleaveland.

The following various results are documented by Klause, 2008 and they compare well with the results in this study that have been presented: In Kuraymat, Egypt, a steam turbine produces an output power of 77 MW at an inlet pressure of 9.2×1.0^6 Nm^{-2} and at an inlet temperature of 560 ^oC. In Lebrija 1, Spain, a Parabolic Trough Solar Concentrator using oil as the heat transfer fluid has a steam turbine that produces 52 MW at an inlet pressure of 1.04×1.0^7 Nm^{-2} and an inlet temperature of 377 ^oC, in Andusalusiant plant, Gemasolar, a solar power tower uses molten salt as the heat transfer fluid and produces 19 MW at an inlet pressure of 1.05×1.0^7 Nm^{-2} at an inlet temperature of 542 ^oC, in Puerto Errado I, Spain, a linear Fresnel direct steam generation plant, a steam turbine produces 1.4 MW at an inlet pressure of 5.5×1.0^6 Nm^{-2} and at an inlet temperature of 270 ^oC and in Julich Solar Tower, Germany has a steam turbine that produces 1.6 MW at an inlet pressure of 2.7×1.0^6 Nm^{-2} and at an inlet temperature of 480 ^oC, In Andusalusiant plant, Gemasolar, a solar power tower uses molten salt as the

heat transfer fluid and produces 19 MW at an inlet pressure of 1.05×1.0^7 Nm^{-2} at an inlet temperature of 542 ^oC, in Puerto Errado I, Spain, a linear Fresnel direct steam generation plant, a steam turbine produces 1.4 MW at an inlet pressure of 5.5×1.0^6 Nm^{-2} and at an inlet temperature of 270 ^oC,

Julich Solar Tower, Germany has a steam turbine that produces 1.6 MW at an inlet pressure of 2.7×1.0^6 Nm^{-2} and at an inlet temperature of 480 ^oC, Invapah Solar Power Complex, USA, Direct power generation uses a steam turbine for first plant that produces 123 MW at an inlet pressure of 1.6×1.0^9 Nm^{-2} at an inlet temperature of 550 ^OC, Andasol 1 &2, Spain, a steam turbine produces 100 MW at an inlet temperature of 1.00×1.0^7 Nm^{-2} at an inlet temperature of 377 ^oC, Nevada Solar One, USA, a steam turbine produces 74 MW of power at an inlet pressure of 9.0×1.0^6 Nm^{-2} at an inlet temperature of 371 ^oC (Akan *et al.,* 2007).

4.10.9 Heat Absorbed Against OutPut Pressure

The heat output for the liquid absorbing heat from the heat transfer fluids i.e. water was determined and was plotted against the output pressure of the turbine. Figure 4.23 shows the relationship between the heat absorbed by heat transfer fluid and output pressure. Performance of the other heat transfer fluids on heat absorbed against output pressure is found on Appendix M. The 2M, 4M and the 6 M sodium chloride solutions absorbed more heat compared to the other heat transfer liquids that were studied and hence they availed more heat for water to absorb and turn to steam. The 2 M, 4 M and 6 M sodium chloride solutions absorbed in the range of 4 % to 4.5 % more heat compared to plain water. The salt solutions also absorbed 11.2 % to 15.7 % more heat compared with used engine oil and organic heat transfer oils used respectively in this study. The unused engine oil absorbed 7.8 % more heat compared to water. The difference was due to the compositions of the heat transfer fluids. The salt solutions are made of ions and the water has a few ions while the oils have no ions at all.

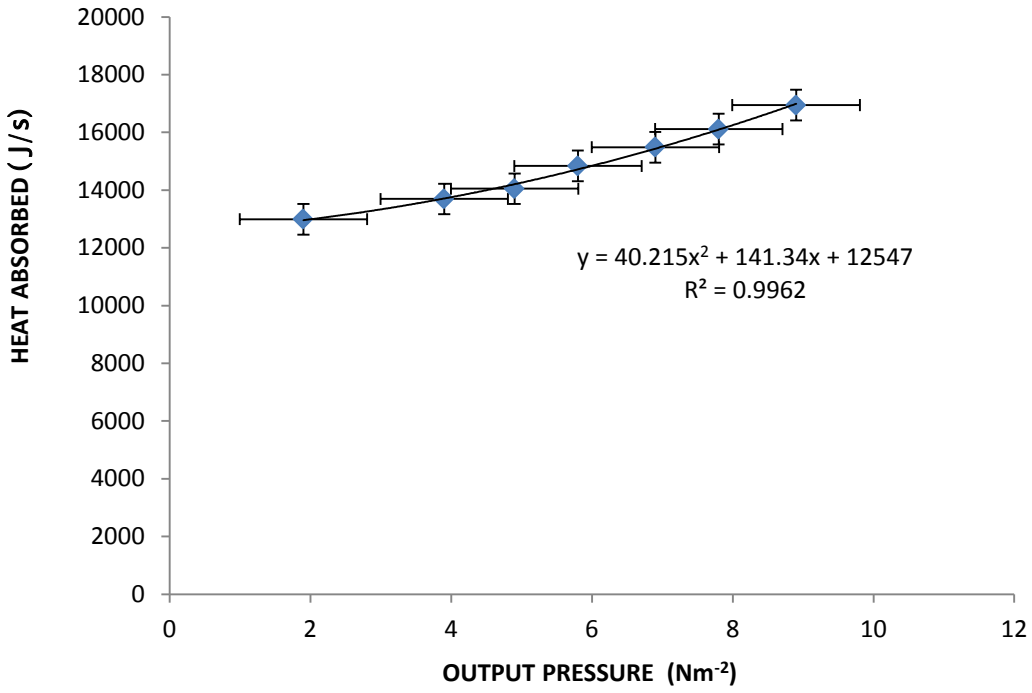

Figure 4. 23: Heat absorbed against output pressure for water on 8.1.2014

Figure 4.24 shows the variation of steam flow rate against time of day for the Vegetable oil 2 that was being fed into the solar concentrator from the reservoir. The steam flow rate increased with the intensity of the solar radiation. The results obtained are in agreement with the fact that solar power intensity increases with time of day and reaches a maximum in the afternoon hence a maximum steam flow rate at that time. The steam flow rate depended on the amount of heat that the heat transfer fluid absorbed from the sun. The variations in the steam flow rate for the different heat transfer fluids was as shown in appendix M. The steam flow rate did not drop immediately the solar intensity reduced since the steam storage system flashed to compensate the discharged steam.

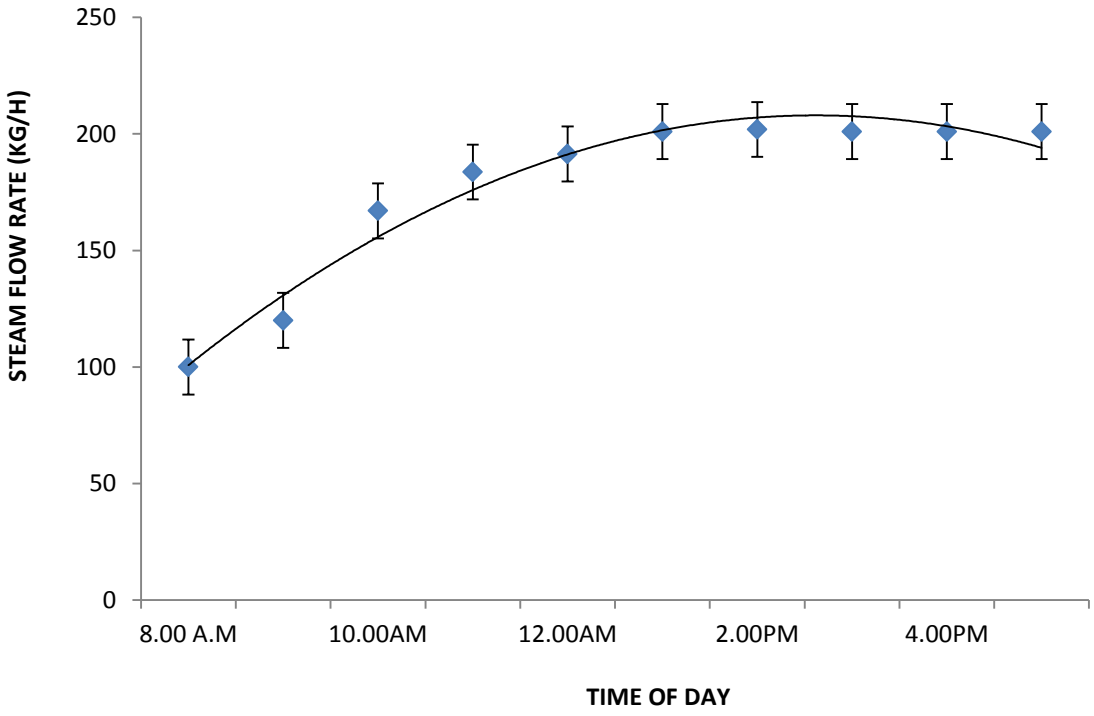

Figure 4. 24: Steam flow rate against time of day for Vegetable oil 2 on 28.2.2014

4.10.10 Solar Thermal Collection Summary

The collector delivered a maximum power of 482.2 W at peak hours. The steam storage system efficiency was obtained as an average of 93.5 % and a thermal capacity of 4.54 $\times$ 10^3 kJ (Kawira *et al.*, 2014). The steam flow rate was obtained as 95.91 kgh^{-1}. Parabolic trough solar concentrators provide a sustainable way of generating power from the sun. Use of concentrated power was noted to be on demand with time (Slocum *et al.*, 2011). In these experiments local heat transfer fluids and technology have been used to generate power. The performance of heat exchanger, steam storage system, turbine and generator represent an attractive means of providing power for off grid areas. However the performance of the organic heat transfer fluids requires improvement in terms of enhancing their ability to transport heat at higher temperatures. In this study, during

direct steam power generation the highest temperature of steam attained was 274 ^{o} C at a pressure of 9.4×10^{6} Nm^{-2} at solar thermal intensity of 1045 Wm^{-2}. The efficiency of the steam storage system was an average of 93.5 % and at a thermal capacity of 4.54×10^{3} kJ. It compared well with other storage system around the world such as Coolidge storage irrigation facility with a thermal capacity of 19.8 GJ and operating at a maximum temperature of 288 ^{o} C. Shenandoa Solar total energy project has thermal capacity of 1.33 GJ and operates at a maximum temperature of 363 ^{o} C. Invapah solar generating facility that uses molten salt and has a storage efficiency of 98 %. The Jonhson and Johnson solar total energy project has a thermal capacity of 29.3 GJ and an efficiency of 96.7 % (Wu *et al.,* 2009). Thermal efficiencies of the heat transfer fluids were 0.89 for 6 M sodium chloride solution, 0.84 for 4 M sodium chloride solution, 0.80 for 2 M sodium chloride solution, 0.78 for water 1, 0.69 for vegetable oil 2, 0.66 for vegetable oil 2, 0.75 for unused vegetable oil and 0.71 for used engine oil (Kawira *et al.,* 2014).

4.11 Receiver Heat Loss

The receiver heat losses were determined and plotted against the temperatures of the heat transfer fluid. Figure 4.25 shows the variation of the heat loss of the receiver against temperatures of operation of 6 M sodium chloride solution passing through the receiver. Figures on heat loss of receiver against operational temperatures of specific heat transfer fluid are found on appendix O. The losses were observed to increase with increase in the temperature of the heat transfer fluid. This was caused by the increase in resistance of steam to absorb more heat at higher temperatures of the heat transfer fluid. The receiver efficiency for this study was obtained as 51.8 %. This compare well with one obtained in a study in South Africa for both evacuated glass shielded receiver and an unshielded receiver which reported peak thermal efficiencies of 53. 8% and 55.2 % respectively (Brooks *et al*., 2006).

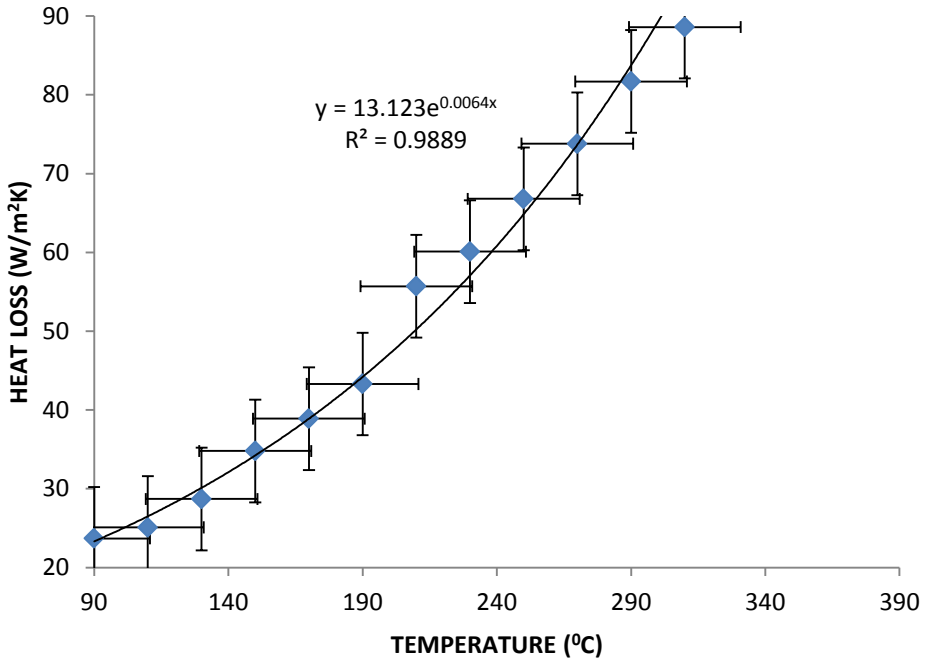

Figure 4. 25: Receiver heat loss for 6M NaCl solution on 24.10.2013

The amounts of heat losses increased with the increase in operation temperatures. Hence for the collector the higher the temperature of the heat transfer fluid passing through the receiver the higher the losses encountered and hence the efficiency of the collector reduced. The heat losses gave the nature of effect the receiver had on the total solar thermal energy collected in that it lowered the amount of useful energy output for the collector.

In summary heat transfer fluids produced turbine average efficiencies of between 51.1 % and 62.5 % with solar power intensities in the range of 700 Wm^{-2} and 1100 Wm^{-2}. The heat transfer fluids studied present alternative and affordable heat transfer fluids compared to the mineral and synthetic heat transfer fluids in the market. They can be used for providing power to off grid areas that are not accessible due to poor terrain.

The solar thermal power generation study involved fabrication by use of materials from local technology. The advantage of methods and materials used in this study is the affordability of both materials and technology. In the previous study the materials used

e.g. steel and the heat transfer fluids used e.g. mineral oil are synthetic and hence not considered affordable since they involve expensive industrial processes.

CHAPTER FIVE

CONCLUSION AND RECOMMENDATIONS

The following are the conclusions and recommendations arrived at from this study.

5.1 CONCLUSIONS

In this study fabrication, characterization and testing of steam storage system, a heat exchanger a direct drive turbine and a three phase power generator was done. Solar thermal collection using the components was done. The collector system was manually tracked in North – South orientation as recommended by (Ecoworld, 2010). The maximum heat absorbed by the heat transfer fluids from the sun was in the range of 4627.2 kJ and 7244.2 kJ per kilogram of water during solar irradiance of 1109 Wm^{-2}. The salt solutions absorbed more heat compared to the other heat transfer fluids and are recommended for solar thermal collection. The maximum power output obtained from the steam formed out of the heat absorbed by the heat transfer fluids was between 284.1 W to 498.3 W. They also achieved higher temperature efficiencies for the hot heat transfer fluids which ranged between 78.1 % and 92.4%. The coiled tube heat exchanger had an effectiveness of 0.91 and the number of heat transfer units was 0.93. It exchanged the heat absorbed by heat transfer fluids with water to make steam to an acceptable extent. The steam storage system was operated in the pressure range of 1.0×10^5 Nm^{-2} and 1.0×10^6 Nm^{-2}. The maximum steam release rate was 12.8 $kgm^{-3}s^{-1}$ at a pressure of 7.9×10^5 Nm^{-2} and solar irradiance of 1109 Wm^{-2}. The largest mean overload corresponding to the maximum steam valve discharge was 40.2 kgh^{-1} for 10 minutes every 65 minutes at a pressure of 5.0×10^5 Nm^2 at a solar irradiance of 956.3 Wm^{-2}. The solar thermal collection without steam storage produced a maximum steam flow rate of 6.1 kgs^{-1} while the maximum steam flow rate with the steam storage system was 7.9 kgs^{-1}. Therefore steam storage systems are recommended in solar power production plants. Coupling of the steam storage system and the heat exchanger increased the capacity of

steam storage to 4.15×10^3 kJ, at maximum temperatures of 249.5 °C and at a pressure of 7.2×10^5 Nm^2. A single stage impulse turbine was fabricated which had an average efficiency of 61.6 % and a maximum power output of 498.2W. A solar dish Stirling engine installed at Sandia National Laboratories produces 25 kW of electricity with a conversion efficiency of 31.25 %. (Sandia National Laboratories, 2004). From this study the turbine fabricated can be used for power production in remote areas.

The generator was capable of producing more power if the number of turns and the size of the magnet was increased depending on the demand and design of collector, steam storage and heat exchanger. The mechanical power applied to the generator was approximated as an average of 2.24×10^4 Js^{-1} and the output frequency was 59.6 Hz. The kilowatts drive input obtained was 0.5 Kw and the average efficiency of the generator was 91.8 %. This compared well with the quoted ones presented in this work. However solar thermal collection could have been enhanced by having more than one turbine stage to ensure more solar thermal energy was converted to power.

The solar thermal characterization and collection was done in solar intensities of the average range 700.0 Wm^{-2} to 1100.0 Wm^{-2}.

The recommended solar thermal collector is the closed collector utilizing 6 M sodium chloride solution since it achieved the highest efficiency under the same conditions in terms of solar thermal heat absorption and efficiency.

5.2 RECOMMENDATIONS

The following are the recommendations hereby given from the study:

1. A study needs to be conducted to improve the ability of the heat transfer fluids to absorb and emit more heat than is represented in this study.
2. The salt solutions were corrosive to some materials used for the heat transfer piping system and anodization of the seamless galvanized pipes should be considered to increase the lifespan of the piping system.
3. The design characteristics of the components need further investigation to increase the efficiency of operation of power generation.
4. A means of improving the precision of the manual tracking system of the solar collector system needs to be found to increase the amount of solar thermal collection.
5. The use of the steam storage system and heat exchanger coupling system requires further design study to enhance the pressures and stresses that bigger plants can withstand.
6. A pilot study on the system is recommended in readiness for commercialization.

REFERENCES

Alghoul, M.A., Sulaiman, M.Y., and Wahab, M.A., (2005). Review of Materials for Solar Thermal Collectors, Malaysia: Emerald Group Publishers, 32 – 201.

ASHRAE, (1998). Methods of Testing to Determine the Thermal Performance. of Solar Collectors. Atlanta: ASHRAE , 1 – 103.

AISI, (2001). Steel Penstocks and Tunnel Liners. Washington DC: AISI, 4 (12), 51 – 106.

ASME, (2002). Pressure Vessel Code – alternate rules. New York: Section VIII, Division 2, 10 – 35.

ASME, (2000b). Pressure vessel Code, Section VIII, Division 2. New York: ASME, 56 – 67.

Arnold, M., (2010). Thermal Solar Plant, Austria: Flowserve Publishers Ltd, 43 – 90.

API, Standard 612 (1995). Special Purpose Steam Turbines for Refinery Services. New York: American Petroleum Institute, 1 – 50.

Akan, K. H., Abdulwahhab, A and Raed A. A. (2007). Design of a Constant Stress Steam Turbine Rotor Blade. Journal of Engineering and Development**,** 11 (3), 76 – 94.

Baker, H., Capelli, P., Kovalev, P., Rish, L., Verette, R., (1996). Washington DC: Shell analysis Manual – 912, 1 – 158.

Bakos, G., Loannidas, I., Tsagas, N., and Seffellis, N., (2001). Design Optimization and Conversion Efficiency Determination of Line Focus Parabolic Trough Solar Collector. *Journal of Applied Energy***, 68** (1), 43 - 50.

Bayon, R., Rojas, E., Valenzuela, L., Zarza, E., Leon, J., (2010). Analysis of the experimental behavior of a 100 kW Latent Heat Storage System for Direct Steam. *Journal of Applied Thermal Engineering,* DOI: 10.1016/j.applthermaleng.2010.07.011. Pp 23 – 31.

Barret, E., Nicholas, C. and Dhar, D., (1986), The Dynamics Analysis of Rotor Bearings Support Compliance Data, New York: Proceeedings of the Fourth International Modal Analysis Conference, 1021 – 1050.

Beckmann, G. and Gilli, V., (1984), Thermal Energy Storage. Berlin: Spriger – Verlag Publishers Ltd, 20 – 135.

Bethel, L., Gans, E., Brown, N. and Lewis, A., (1993), Critical Speeds and the Importance of Stiffness – A Case Study in Design and Testing of a Large Mechanical Drive Steam Turbine to API Standard 612. Texas: Twenty – Second Turbo Machinery Symposium, Turbo Machinery Laboratory, . 678 – 1035.

Bowels, J. E, (1996). Foundation analysis and Design. New York: Mc Grawhill Publishers Ltd, 204 – 278.

Brooks, J., Mills, I. and Harms, T. M., (2006). Performance of a Parabolic Trough Solar Collector. *Journal of solar Engineering*, 17 (3), 73 - 77.

Byung, S., Kun, J., Seung, J., Young, C. and Kyoung, D., (2005). Design Fabrication and Testing of a MEM's Micro Turbine. *Journal of Mechanical Science and Technology*, 19 (2), 682 – 691.

Cecil, H.P. (2011). Thermodynamics of the steam Engine and other Heat Engines, New York: Wiley and Sons Publishers Ltd., 51 – 74.

Chempro, T., (2014). Top – Notch Technology in Production of Oils and Fats. Oil , Austria: refining – ISO – TW, 1 -5.

Chenduran, A., Tharani, S., Chenthooran, G. and Johnson, S., (2004). Design of the `Steam Turbine for Small Scale Power Plant, Fifth Conference Proceedings, Department of Mechanical Engineering, India: University of Peradeniya, 12 – 170.

Church, F., (1987). Steam Turbines, London: Mc Graw Hill Publishers Ltd., 5 – 230.

Cleaveland, T., (2005), Description and Performance of a TRNSYS model of the Solargenix Tracking Power Roof, Orlando: ISES Solar World congress report, 78 (101), 67 - 75.

Collier J.G and Thome J .R (1994). Convective Boiling and Condensation, New York: Mc Graw Hill Publishers Ltd, 10 – 90.

Close, D.J., (1988). Flat Plate Solar Absorbers, Australia: Engineering Section of Common Wealth Scientific and Industrial Research Organization, Proceedings of a Workshop, May 21-27, Report E.D.7, 183 – 249.

Dudley, E., Evans, R., & Mathews, W., (1995). Test Results - Industrial Solar Technology Parabolic Trough Solar Collector, Sandia National Laboratories: SAND 94 – 1117, 1 – 245.

Dunkle, V. and Divovosky, W. (1961). Thermal Radiation Tables and Applications, Australia:

Trans.ASME, 76 - 94.

Duffie, A. and Beckman, A., (2005). Solar Engineering of Thermal Processes, New York: John Wiley and Sons Publishers Ltd, 50 – 274.

Ecoworld, (2010), "*Solar Thermal Energy*," Retrieved from http:// www.ecoworld.com/energy-fuels/solar Accessed 22/12/2009,3.00 a.m.

Ecoworld, (2000), "*solar thermal power*," Retrieved from http://www.ecoworld.com/solarpower/solarsteam.html. Accessed 28.2.2011, 11.30 p.m

Eck, M., Zarza, E., Eickhoff, M., Rheinlander, J., Vanzuela, L., (2003). Applied Research Concerning the Direct Steam Generation in Parabolic Troughs, *Journal of Solar Energy*, 74 (4), 341 - 351.

Ekramian, E., Etemad, S. and Haghshenasfard, M., (2014). Numerical Analysis of Heat Transfer Performance of Flat Plate Solar Collectors, *Journal of Fluid Flow, Heat and Mass Transfer*, 1 **(**1), 38- 42.

NREL, (2000). World Bank Energy Report, Retrieved from http:// www. undp. Org/seed/eap/publications /1999/19.99 a .Accessed 3/1/2010,5.30 p.m.

EEAR, (2008). Technology Characterization: Steam Turbines, USA: Virginia Publishers, 1 -59.

ETSAP, (2013). Thermal Energy Storage, (IRENA), Technology brief EIT, 1 – 90.

Ercan, A., (2006). Storage of Thermal Energy, United Kingdom: Yalcin Abdullah Gogus. Edss Publisher Oxford, 167 – 341.

Eltahir, M. and Mohammed, S., (2012). Designing and testing of a solar parabolic trough system for electricity generation in sudan, Khartoum: Annual Conference of Post Graduate Studies and Scientific Research, Friendship Hall**,** 2 (1), 56 - 71.

Fathollahneyad, H., Tsao, B., Ponnappan, R. and Jacobson, D. (1993). Post Test Corrosion Analysis of High Temperature Thermal Energy Storage Capsules, Journal of Materials Engineering and performance, 2 (1), 125 – 134.

Fre'chette, G., Lee, C. and Arslan, S., (2004). Development of a MEM's based rankine, Cycle Steam Turbine for Power Generation, Project Status. 4TH International workshop on Micro and Nano Technology for Power Generation and Energy Conversion Applications, Japan: 62 – 100.

Ganapathy, V., (1994). Steam Plant Calculations Manual, New York: Marcel Dekker Publishers Inc., 1 – 365.

Gawande, S., Keste, A., Navale, L., Nandgaonkar, M., Sonawane, V. and Ubarhande, N. (2007). Design Optimization of Shell and Tube Heat Exchanger by Vibration Analysis. *Journal of Modern Mechanical Engineering*, 1 (1), 6 - 11.

Geyer, M., Winter, R. and Rizmann, L., (1991), Thermal Storage for Solar Power Plants, Berlin: Van Hull, Springer – Verlag Publishers Ltd., 43 – 154.

Gilbert, P., (1969). US Patent No. US 3452132 A, Process of Steam drawing and annealing, Atlanta: Assigned to Du Point, 1593 – 1658.

Gillet, B. and Moon, E., (1985). Solar Collectors, Holland: Reidel Publishing Company, 1 - 348.

Gould, L., (1988). Analysis of Shells and Plates, New York: Springer – Verlag Publishing Ltd, 1 -102.

Hank, P., Eckhard, L., David, K., Eduard,o Z., Gilbert, C., Randy, G. and Rod, M., (2002). Advances in Parabolic Trough Solar Power Technology, *Journal of Solar Energy Engineering* 11 (24), 109 – 125, 129.74.250.197eee, 56 -74.

Hansson, B. (1972). Physical Data Book in SI Units, Berlin: Pergamon Press, 5-20.

Hewitt, F., (2002). Heat Exchanger Design Hand Book, United Kingdom: Begell House Publishing Ltd, 1 – 113.

Hurtado, P. and Kast, M.,(1984). Experimental Study of Direct in Situ Generation of Steam in a Line Focus Solar Collector. New York: Final Report, NTIS publishers Ltd., 1 – 71.

Incopera, P., Dewitt, P., Bergyman, L. and Laving, S., (2007). Fundamentals of Heat and Mass Transfer, London: Wiley Publishing Ltd, 1 – 125.

Jachen, B., (1996). Steam Turbines – Their Construction, Selection and Operation, Capetown: Proceedings of South African Sugar Technologists Association, 1603 – 1623.

Jawad, H. and Farr, R. (2003). Structural Analysis and Design Process Equipment Vessel Technology, New York: Wiley and Sons Publishing Ltd, 1 – 290

Kaka, C. and Liu, H., (2000). Heat Exchangers: Selection, rating and Thermal Design, Australia: CRC Press, 26 – 154

Kalogirou, S., Lloyd, S. and Ward, J., (1997). Modeling, Optimization and Performance Evaluation of a Parabolic Trough Solar Steam Generation System, *Journal of Solar Energy,* 60 (1), 49 – 59.

Kawira, M., Kinyua, R. and Kamau, J., (2012). Fabrication and Characterization of a prototype parabolic trough solar concentrator for steam production, Nairobi: Msc. Theses, Jomo Kenyatta University of Agriculture and Technology, 45 - 71.

Kawira, M., Kinyua R. and Kamau J., (2012). Fabrication and Characterization of a prototype parabolic trough solar concentrator for steam production, *Journal of Agriculture Science and Technology*, 14 **(**2), 90 – 104.

Kawira, M., Kinyua, R. and Kamau, J., (2014). A Prototype Steam Storage system for Power Production, International *journal of Scientific Engineering and Technology*, 3 (8), 1012 – 1015.

Kawira, M., Kinyua, R. and Kamau, J., (2014). Investigating a Prototype Heat Exchanger for Steam Storage, *IOSR Journal of Applied Physics (IOSR-JAP)*, (6) 4, 70 -80.

Klaus, J., Kruger, D. and Pitz – paal, R., (2008). Solar Thermal Plants – Power and Process Heat, Kohln: Deutsches Zentrum Fir Luft – Und Raumfahrt e.v, D – 51170, 95 – 100.

Kruger, D., Pandian, Y., Hennecke, K. and Schitz, M., (2008). Parabolic Trough Collector Testing in the Frame of the REACT Project, Journal *of Solar Energy* 220 (1), 612 - 618.

Kuppan, T., (2000). Heat Exchanger Design Hand Book, Australia: CRC Press, 65 – 78.

Kearney, D., (2002). Evaluation of molten salt heat transfer fluid in a parabolic trough solar field. Proceedings of the National solar energy conference, Project Over view, New York: NREL – Sandia national Laboratories, 135 – 157.

Kearney, W. and Cohen, E., (1997), Current Experience with the SEGS Parabolic Trough Plants, Cologne: Proceedings of the 8th International Symposium on Solar Thermal Concentrating Technologies, 61 (5), 1301 - 1326.

Kollar, L. and Dulacska, E., (1992). Buckling of Shells, New York: John Wiley and Sons Publishing Ltd., 65 – 128.

Kroger, G., (2004). Air Cooled Heat Exchangers and Cooling Towers, Thermal Flow Performance Evaluation and Design, *Penwell Journal* 1 (1), 1083 – 1098.

Laing, D., Steinmann, D., Ammer, T. and Rither, O., (2006). Solid Media Thermal Storage for Parabolic Trough Power Plants, *Journal of Solar Energy* 80 (10), 1283 - 1289.

Lamberson, J. and Moll, R., (2002), Performance Acceptance Test for a Controlled Extraction Condensing Turbine Generator Drive Superheated Inlet report, New York: Dresser – Rand Co Ltd, 273- 280.

Leyzerovich, A., (2005). Wet Steam Turbines for Nuclear Power Plants. Tusla: Pen Well Books, 111. ISBN 1593700326, 204 - 267.

Maan, H., (1994). Theory and Design of plate and Shell Structures, NewYork: Chapman and Hall Publishing Ltd., 43 – 259.

Medrano, M., Gil, A., Martorrel, I., Potau, X. and Cabeza, L.F., (2010). Thermal Storage Media in Parabolic Trough Technology, New York: Renewable and Sustainable Energy Reviews, 43 – 61.

Minassians, D., Aschenbach, H. and Sanders, R., (2004), Low Cost Distributed Solar Thermal Electric Power Generation, Bellingham: Proceedings of SPIE 5185, Doi: 1117/12.509785, 103 - 320.

Murphy, M. and Kenneth, E., (2001). Steam Generation in Line Focus Solar Collectors, Georgia: A Comparative Assessment of Thermal Performance, Operating Stability and Cost Issues Reprot, SERI/TR- 1311, NREL, 45 – 75.

NREL, (2001). Thermal Energy Storage, Colorado, Universal press, 32 - 71.

O'Brien, R. D., (1988). Fats and Oils. Formulating and Processing for Applications, Pensylvania: Technomic Publishing Company Inc., 761 – 768.

Pacheo, E., Schowalter, S., Kolbe, W. (2002). Development of molten salt heat transfer fluid in a parabolic trough Solar Field, Nevada: Proceedings of National Solar Energy Conference, 1059 – 1093.

Parabola, (2007), Trough Geometric Design, Retrieved from .http://www.bilfoster/2007/112/en. Accessed 24.3.2010, 5.30 a.m

Patrick, P., Todd, O., Robert, T. and Himanshu, T. (2013. Trends and Opportunities in Direct – absorption Solar Thermal Collectors. *Journal of Thermal Science and Engineering Applications*. 5 (2) (021003), 1 - 9.

Pilkington Solar International GmbH, (1999). Survey of Thermal Storage for Parabolic, New Jersey: Universal publishers, 45 – 100.

NREL, *(*2000). Trough Power Plants, Golden: Report prepared for and Published by NREL, NREL /SR- 550 – 27925, CO., 1 – 180.

Sandia Laboratories (2009), Science Encyclopedia, Retrieved from www.Power from the sun. Net/chapter 2.20/3/2010,2.00 a.m.

Pradeep, V., Srinath, T. and Venkatesh, R., (2013). Design, Fabrication and Experimental Testing of Solar Parabolic Trough collector with Automated Mechanism, *International Journal of Research in Aeronautical and Mechanical Engineering*, 1 (4), 37 – 55.

Price, H., Lufert, E. and Kearney, D., (2010). Advances in Parabolic Trough Solar Technology, London: Solar Energy-T ASME Publishers, 3 – 10.

Price, H. and Kearney, D., (1999). Parabolic Trough Technology Roadmap: A Pathway for Sustained Commercial Development and Deployment of Parabolic Trough Technology, Golden: NREL/TP – 550- 24748, NREL, 54 – 78.

Rabl, A., (1985)**.** Active Solar Collector and their Application's, London: Oxford University Press, 67 - 272.

Rai, D., (1987). Solar Energy Utilization, New Dehli: Hama Publishers, 10 – 295.

NREL, (2008), Natural Renewable Energy Laboratory, Retrieved from http://www.Nrel/.Govl. Accessed 25.2.2010, 6.00 a.m

Rogelio, M., Juan, M., Miguel, P., Lourdes, B and Juan, M., (2014). A Novel Modelling of Molten – Salt Heat Storage Systems in Thermal Solar Power Plants, *Journal of Energy and Combustion* 11 (7), 6721 – 6740.

Sandia National Labaratories, (2004). Solar Thermal Energy, Albuquerque: NREL, 50 – 100.

Satos, S., Jovanovic, S., Lang, J. and Spakovscky, Z. (2011), Demonstration of a Palm sized 30 W Air- to – Power Turbine Generator, *Journal of Engineering for Gas Turbines and Power* 133 (10), 1 - 10.

Sarada, K., Jamie, T., Yogi, G., Muhammad, D., Rahman, M., Elias, K. and Stefanakos, M., (2012). Progress in Energy and Combustion Science, *Journal of Thermal Energy Technologies and Systems for Concentrating Power Plants*, 39 (4), 285 - 319.

Saunders, D., (1988). Heat Exchangers, London: Longman, 1 – 98.

Sauro, P., Jiri, J., Kremes, S., (2013). Estimation of Physical Properties of Vegetable oils and Biodiesel using Group Contribution Method, *ISBN* 978-88-95608-23-5, 535 – 540.

Schetz, A. and Fuhs, A. E. (1996). Hand book of Fluid Dynamics and Fluid Machinery, New York. Oxford press, 1028 – 1058.

Singh, P., (1989). Theory and Practice of Heat Exchanger Design, India, Hemisphere Publishing Ltd., 47 – 61.

Shah, R. and Sekuli, D., (2003). Fundamentals of Heat Exchanger Design, New Jersey: John Wiley and Sons, 267 – 315.

Slocum, A., Codd, D., Buongiormo, J., Forsberg, C., McKerrel, T. and Nave, J. (2011). Concentrated Power on Demand. *Journal of Solar Energy* 85 (5), 1519 - 1529.

NREL, (2011). Concentrating solar power Research, Retrieved from "http://www.nrel.gov/csp/lab-capabilities html. Accessed 13/8/2011, 6.30 a.m.

SWERA, (2009). Renewable Energy, Retrieved from http:// www.swera.unep.net. UNEP/Grid-Sioux falls .Accessed 5.5.2010, 11.45 p.m.

World Bank, (2011). Solar Thermal Power Research, Retrieved from http://www.energysaving.nu/solarenergy/thermal.shml. Accessed 23/9/2011, 11.20 p.m.

World Bank (2010). Market Research Report, Retrived from http://www.market research.com/…./2526650.html .Accessed 31.3.2010, 1.00 p.m.

NREL, (2011). Parabolic Steam Power, Retrieved from ‘‘http;//www.nrel.gov/csp/troughnet/market-economics-asses.html. Accessed 4/3/2011, 1.46 p.m

NREL, (1999). Solar Energy Applications, Retrieved from http;/www.energy/env……../p. Accessed 29/6/2010, 5.30 p.m

NREL, (2006). Western governors Association, Clean and Diversified Energy initiative, Retrieved from http://www.West gov.org /wga/initiatives/cdeac/solar.Acessed 28/4/2010,10.45 p.m.

Suhas, S., (1992). Solar Energy, NewDehli: Tata Mc Graw Hill Publishing Co., Ltd, 46 – 187.

SWERA, (2010). Renewable Energy Resources, Retrieved from http://www.swera.com/renewableenergy/powersource.research.com/..Accessed 28.2.2011, 11.30 p.m

Stevenson, N. and William, G., (2001). Elements of Power Systems Analysis, New York: Mc Graw Hill Publishing Ltd., 24 – 98.

Srinivasa, R. G., Haribabu N. and Rao, J., (2014). Heat Transfer Analysis on Shell and Tube Heat Exchangers. *International Journal of Research in Aeronautical and Mechanical Engineering* 2 (1), 11 - 26.

Stine, B. and Harrigan, W., (1985). Solar Energy Systems and Design, New York: John Wiley Publishing Ltd., 101 – 245.

TEMA, (1993). Pressure Vessel Code – alternate rules, Section V, Division 3, New York, TEMA 104 – 156.

Twidel, S., John, W. and Anthony, W., (1986). Renewable Energy Resources, London: ELBSLE and F.N Spon Ltd, 20 – 231.

Umar, S., Mohammad, U., Garba, M., Yahya, H. and Ali, A., (2013). Experimental Performance Evaluation of Paraboilc Trough Concentrator, *International Journal of Environment and Bioenergy* 8 (2), 86 - 93.

Valan, A. and Sornakumart, T., (2006). Performance Characteristics of Parabolic Trough Solar Collector System for Hot Water Generation, International Journal of Energy (7) 2, 138 - 143.

Vera, F., Garcia, R., Gonzalez, J., Cabello, R., Llopis, R., Sanchez, D. and Torrella, E. (2010). A simplified Model for Shell and Tube Heat Exchangers: Practical Application, *Journal of Applied Thermal Engineering* 30 (87), 1231 - 1241.

Vindhya, V., Raj, R., Piyush, S. and Srivastava, K. (2014). Performance Analysis of Shell and Tube Type Heat Exchanger under the Effect of Varied Operating Conditions, *Journal of Mechanical and Civil Engineering* 11 **(**3), 8 – 17.

World Energy Resources (2002). Fossil Fuels, Retrieved from http://undp.org/seed/eap/publications/2001/html. Accessed 13.4.2010, 10.50 p.m

Wang, S. and Wen, J., (2008), An Experimental Investigation of Heat Transfer Enhancement for a Shell and Tube Heat Exchanger, *Journal of Applied Thermal Engineering* 29 (12), 2433 – 24 - 38.

Whitaker, C., (2006). A.C Power Systems Handbook, Boca Raton: F L. Taylor and Francis, 35 - 76. ISBN 9780849340345.

Wu, J., Li, J., Xu, X., Yang, I. and Zhao, F. (2009). Molten Salts/ Ceramic – Foam matrix composites by melt Infiltration Method as Energy Storage Material, Journal *of Wuhan University of Technology* 24 (4), 176 – 298.

Zarza, E., Valunzuela, L., Leon, J., Weyers, H., Eickhoff, M. and Hennecke, K., (2001). The DISS Project: Direct Steam Generation in Parabolic Trough Systems Operations and Mantenance Experience: Update on Status: *Journal of Solar Energy Engineering*. Trans. ASME 124**,** 126 - 133.

APPENDICES

APPENDIX A: LIST OF PLATES

This section consists of two parts which are photographs which were taken during the study and the peer reviewed papers of the work in Journals and conference proceedings. Appendix A shows photographs taken during the fabrication and experimentation process.

Plate 1: Steam storage system before lagging

The designed and fabricated steam storage system was as shown in plate 8. It was tested and used during solar thermal collection. It operated in the pressure range of 1.0×10^5 Nm^{-2} to 1.0×10^6 Nm^{-2}. Steam from the storage system was at higher temperatures and pressure hence use of storage systems in solar thermal production increased the density of power produced from the sun.

Plate 2: Steam storage system testing

The testing of the steam storage system for the temperatures of operation for the vegetable oil 1, vegetable oil 2 and the used engine oil was done using the loop shown in plate 7. The PPR pipes could withstand the steam temperatures and pressures produced. The test pressures were in the range of 1.0×10^5 Nm^{-2} to 5.0×10^5 Nm^{-2} and the maximum test temperatures of operation was 129.8 ° C.

Plate 3: Heat exchanger with copper tube

Plate 9 shows the heat exchanger in the process of fabrication. The coiled copper tube was installed to provide the path of flow of heat transfer fluids. In the shell side water flowed which absorbed the heat from the heat transfer fluid and then turned into steam. It was also used in solar thermal collection as a steam storage system.

Plate 4: Heat exchanger performance test

During the testing of the heat exchanger performance characteristics steam was supplied by the white boiler. Electricity was used to heat water to steam and a thermostat was used to set temperature of the steam from exceeding the test temperature. The steam safety valve at the inlet pipe of the steam exchanger was set so that steam beyond set pressure was left to escape. The PPR pipes withstood temperatures of up to 129.8 ° C.

Plate 5: Turbine blades riveted to shaft

The main parts of the steam turbine consisting of the blades and the shaft are shown in plate 9. The hot fast moving steam from the storage system impinged on the blade at a nozzle angle of

30 °. This caused the shaft to rotate which caused change of magnetic flux linkage in the generator copper coils.

Plate 6: Complete turbine

The complete turbine was as shown. The protruding shaft was bolted to shaft part entering the generator. The steam that exited from the turbine was fed back into the collector where it was reheated. The turbine casing could withstand temperatures of 300 °C and pressures in excess of 1.0×10^6 Nm^{-2}.

Plate 7: Power output measurements

Measurement of power output from the steam generated from the heat transfer fluids was measured using the apparatus shown. Steam from the heat exchanger was discharged in to the turbine which turned a three phase power generator whose power supply was measured as shown.

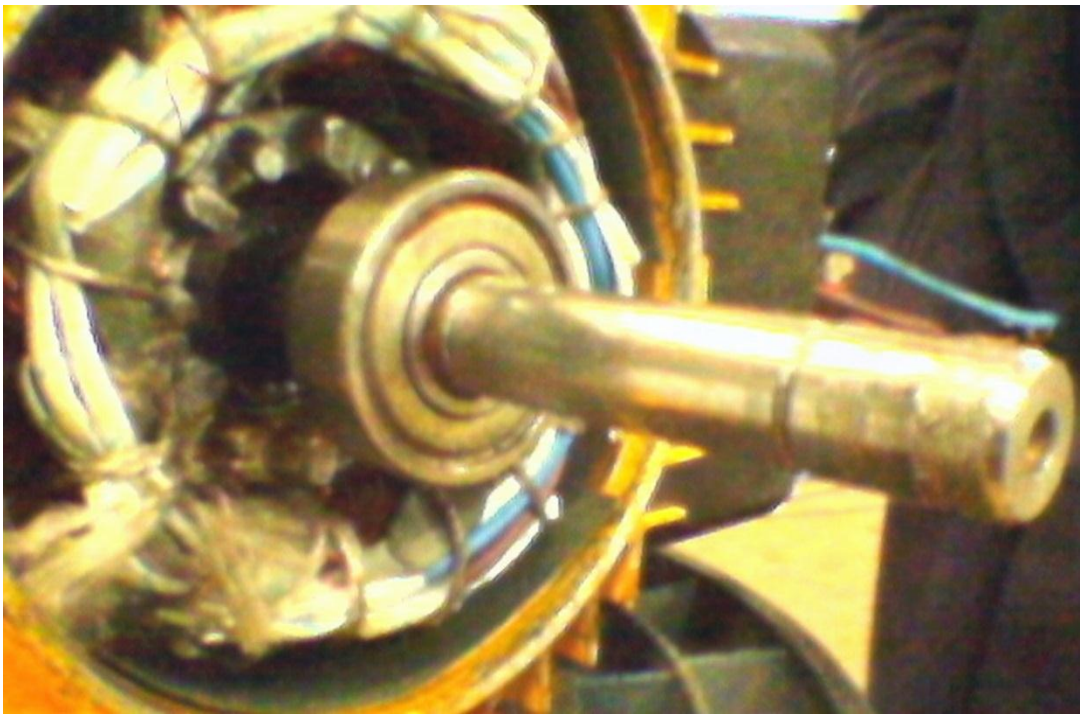

Plate 8: Stator and rotor

The three phase generator consisted of stator made of copper wires. The rotor was a steel metallic shaft rod where a four pole magnet was fixed using glue. The changing magnetic flux produced by the rotating shaft caused a current to flow and a potential difference developed which were measured as shown in plate 7.

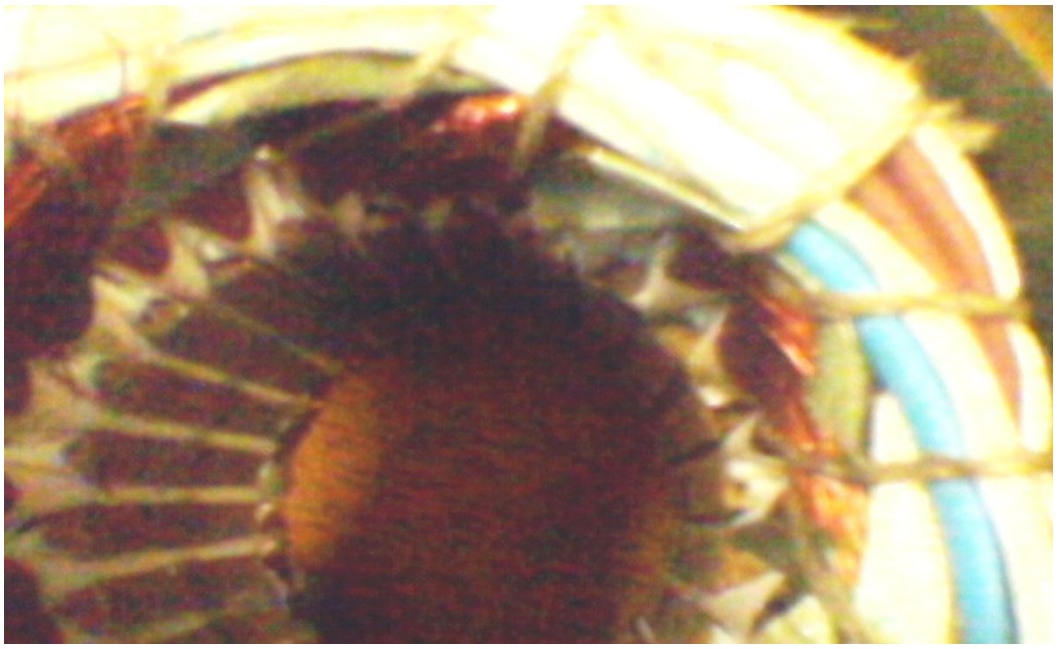

Plate 9: Stator windings

The up and bottom copper windings of the stator were as shown in plate 9. Plastic insulation was used to keep each of the three phases separate.

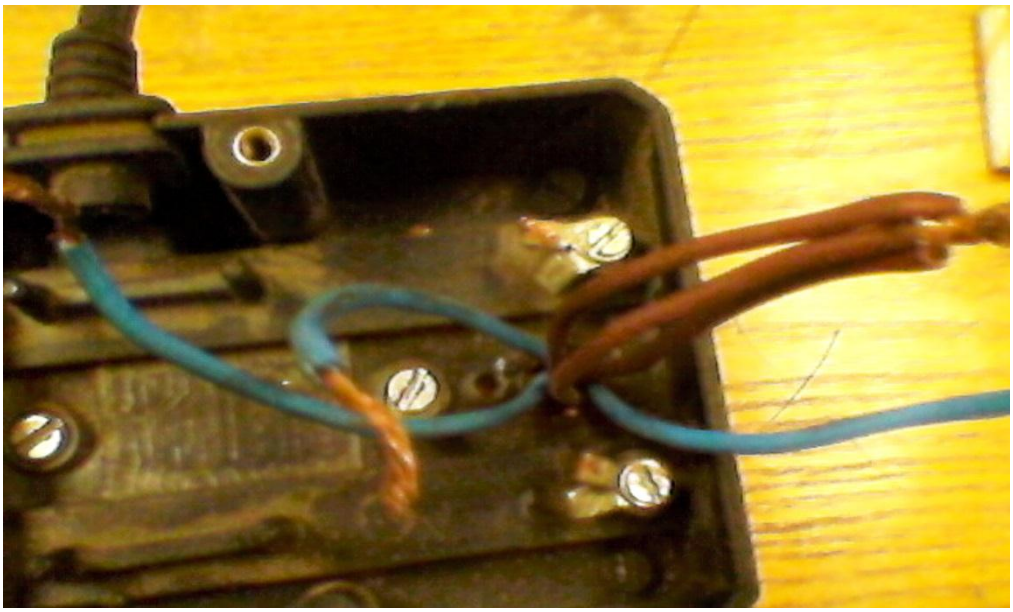

Plate 10: Terminals of three phase power generator

The leads of the three phase generator were externally produced as shown. The electrical leads were connected to a multi meter. The multimeter was current and voltage terminals were connected to the generator. Power was determined using the values of voltage and current read off from the multi meter.

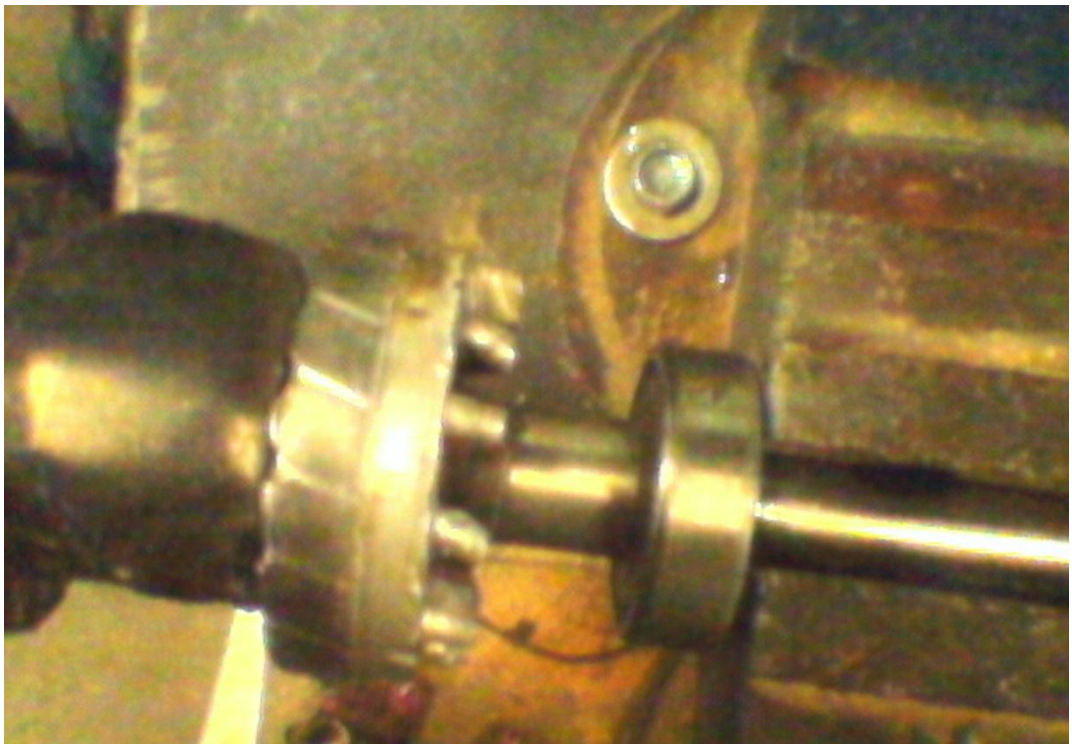

Plate 11: 4 - Pole magnet on shaft

The pole magnet which was fixed on the shaft was as shown in plate 6. The shaft was connected to the generator on one end and to the turbine on the other end. The rotation of the shaft which carries the magnet causes power to be produced by the generator.

Plate 12: Solar thermal collection for vegetable oils

The power generation using vegetable oil 1, vegetable oil 2 and the used engine oil was done using the PPR pipes. This was in order to test if the steam produced by these heat transfer fluids could be passed in the PPR pipes. The vegetable heat transfer fluids and the used engine oil achieved temperatures in the range of 129.5 ° C to 138.7 °C.

Plate 13: Solar thermal collection for salt solutions and unused engine oil

The solar power generation from the unused engine oil and the saline solutions was done using the seamless galvanized pipes. They could withstand pressures in excess of 1.0×10^6 Nm^{-2} and temperatures in excess of 300 °C. Steam generated from the collector was directed into the steam storage system where pressurization took place.

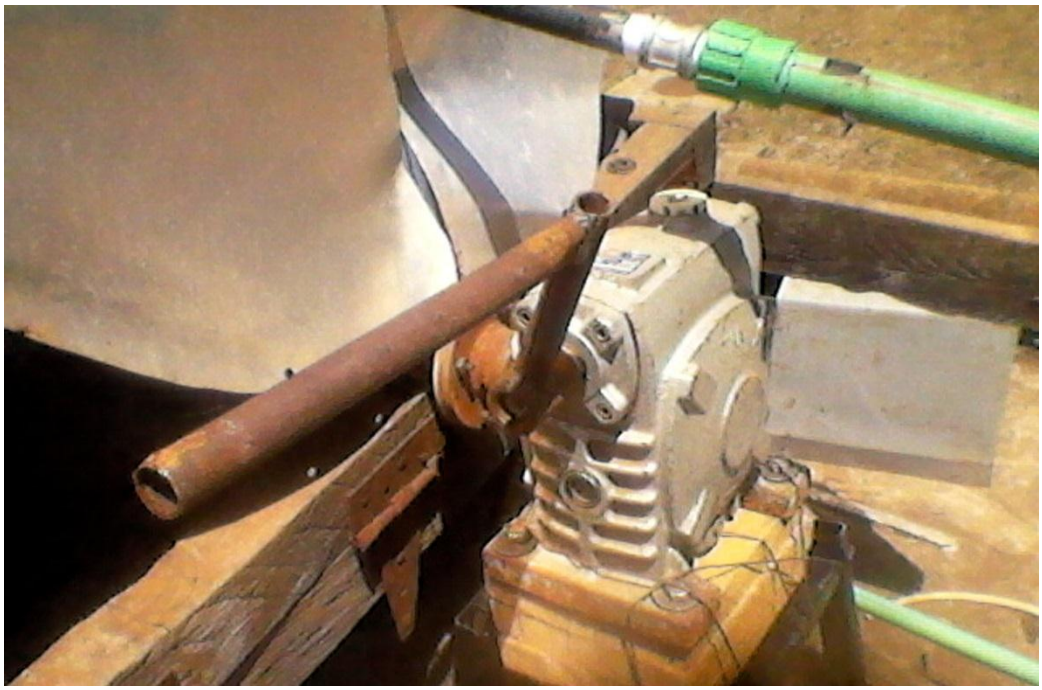

Plate 14: Solar gear tracker

The tracking of the collector to align it to the direct beam from the sun was achieved by use of a solar tracking system that consisted of a gears system and a lever. Turning the lever clockwise manually caused the collector to turn anti clockwise in the north – south orientation. A pin at the plane of the collector was used to ensure that the collector was collecting the direct beam radiation from the sun.

Plate 15: Power source and thermostat for testing loop

During the testing of the collector system, the steam storage system and the heat exchanger steam was generated using electricity from the mains supply. The thermostat was used to set the test temperatures of the heat transfer fluids and water during the various tests. The tests produced the characteristics of the said components before they were used in solar thermal collection.

Plate 16: Solar gear tracker with lever in position during tracking

At solar noon the lever adjustment of the tracker ensured that the collector was aligned to the direct solar beam. This is evident from the shadow cast by the receiver that is perpendicular to the plane of the collector system.

Plate 17: Solar irradiance meter during intensity measurement

Direct solar radiation at the plane of the collector system was measured using a solar radiation meter. The irradiance reached a maximum intensity of 1100 Wm^{-2}. It was recorded and compared with the amount of solar steam generated, power output and the flow rates of the heat transfer fluids used.

Plate 18: Receiver in position during oils solar thermal collection

The fabrication of the solar collector was carried out by lamination of the concentrator with the reflector system after which the receiver system was passed at the focal axis of the concentrator. The test and solar thermal collection of the vegetable heat transfer fluids and the used engine oil was done using the PPR pipes. The receiver was kept in position using very mild steel wires.

Plate 19: Receiver at focal axis of the collector during thermal collection

The receiver was suspended at the focal axis of the collector system. The solar flux from the sun was reflected and focused along the receiver. The heat transfer fluids absorbed the heat from the sun and their temperatures increased. In the heat exchanger the heat absorbed was absorbed by water which turned into steam. The steam was pressurized in a steam storage system before being discharged to the turbine and generator for power production.

APPEDIX B_1: CONFERENCES AND PUBLICATIONS

From the study that was undertaken, three papers were peer reviewed and published and one paper was peer reviewed and presented in a conference. They are as follows:

PUBLICATIONS

1. A paper entitled 'A Prototype Steam Storage System for Power production' was published. ISSN: 227 – 1581 by International Journal of Scientific Engineering and Technology (IJSET). **3** (8), 1 August 2014.
2. A paper entitled 'Investigating a Prototype Heat Exchanger for Steam Storage' was published. E-ISSN: 2278-4861 by IOSR Journal of Applied Physics (IOSR-JAP). **6** (4) ver. II (JUL AUG.2014), PP70 – 80. The paper's digital link (ANED-DDL) is 22.4861/iosr-jap-N06427080 under the website www.aned.us
3. A paper entitled 'A prototype Parabolic Trough Solar Concentrator for Steam Production' was published. ISSN 1561-7645 by Journal of Agriculture Science and Technology (JAGST). **14** (2), 2012.

CONFERENCES

A paper entitled 'Fabrication and Characterization of a Prototype Steam Storage System and Generator for Power Production' in Proceedings of 2014 International Annual Conference on Sustainable Research and Innovation on Wednesday 7th to Friday 9th May 2014 in the African Institute for Capacity Development (AICAD) – Kenya.

APPENDIX B: HEAT EMITTED BY HTfs

Appendix B shows figures on heat emitted by heat transfer fluids with time of day at an average solar power intensity of 998.4 Wm^{-2}

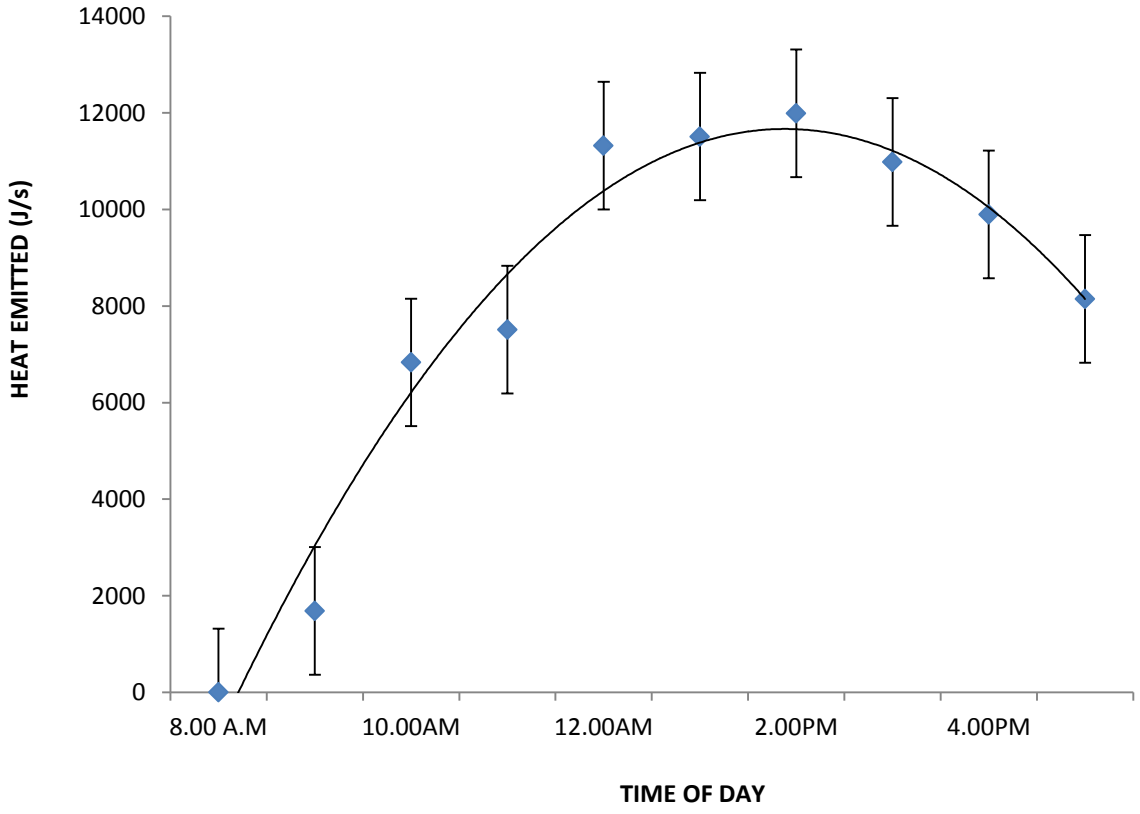

Figure B. 1: Heat emitted by vegetable oil 1 with time of day on 10.1.14

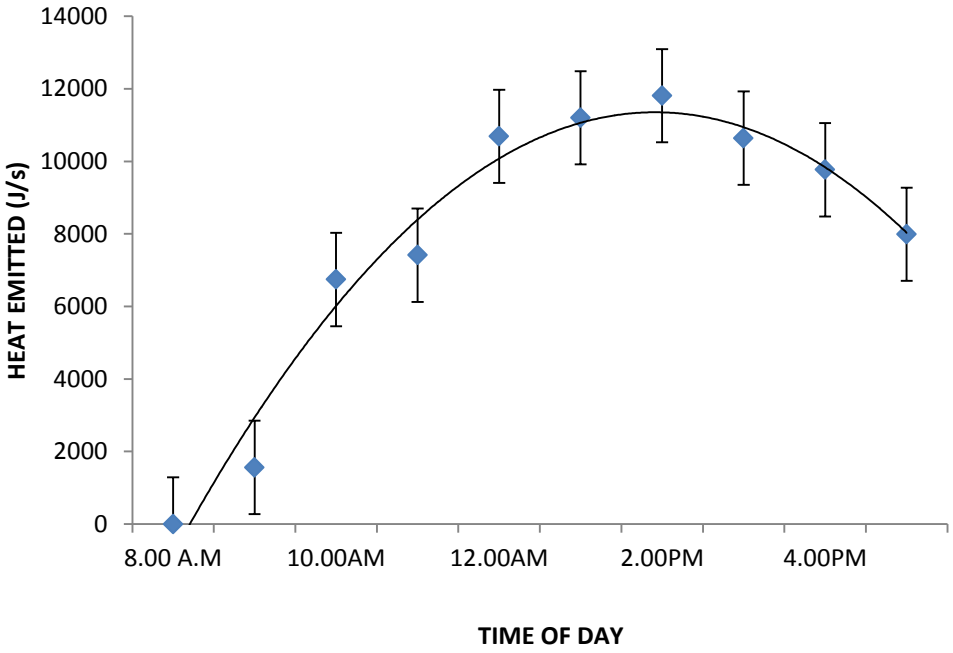

Figure B. 2: Heat emitted by used engine oil with time of day on 11.1.2014

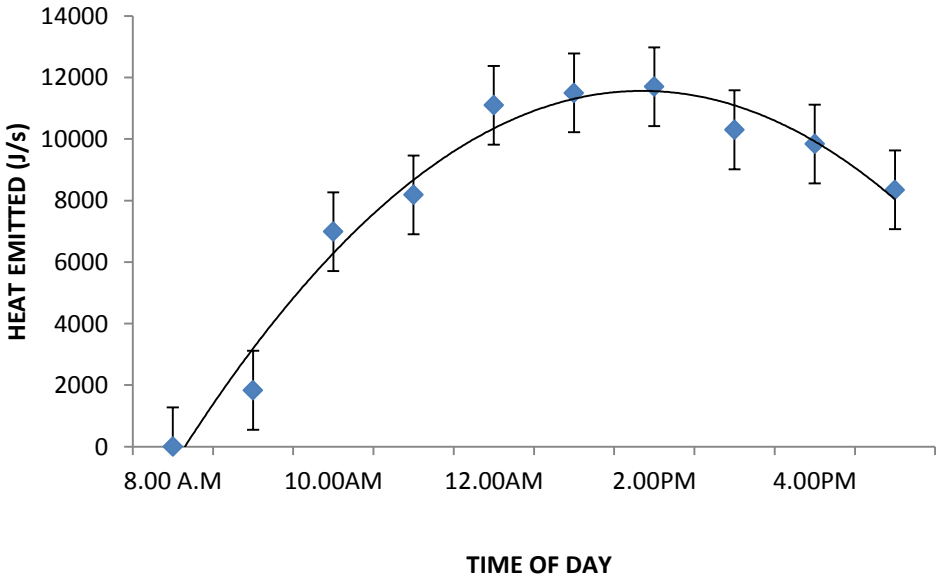

Figure B. 3: Heat emitted by unused engine oil with time of day on 12.1.2014

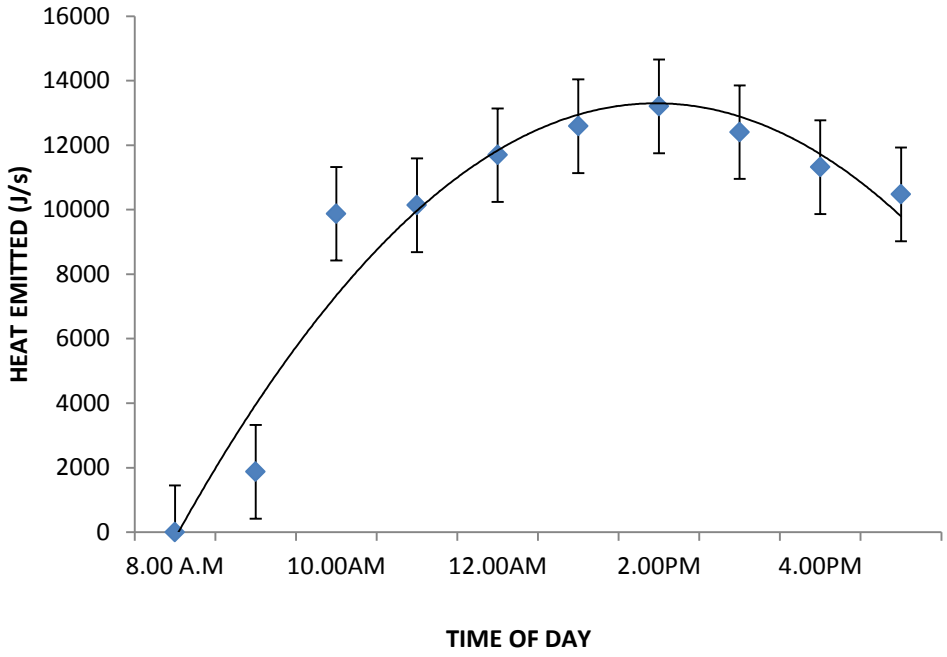

Figure B. 4: Heat emitted by 2M sodium chloride solution with time of day on 13.10.2014

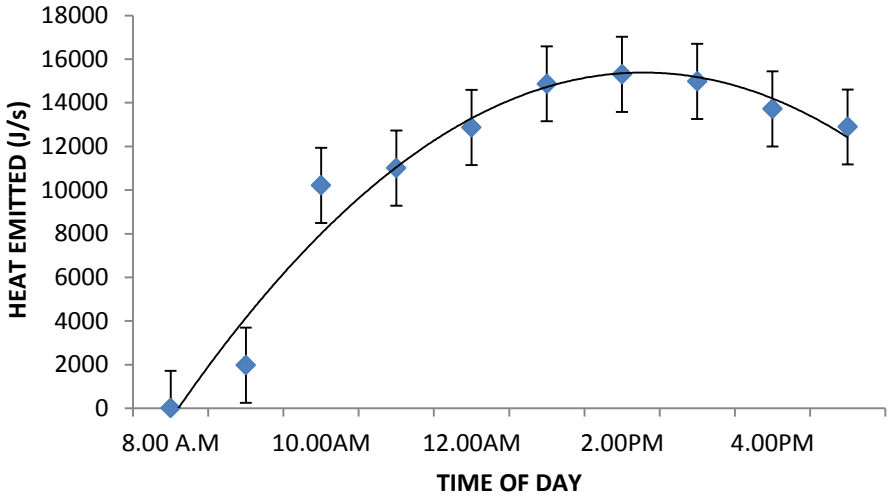

Figure B. 5: Heat emitted by 4M sodium chloride solution with time of day on 14.1.2014

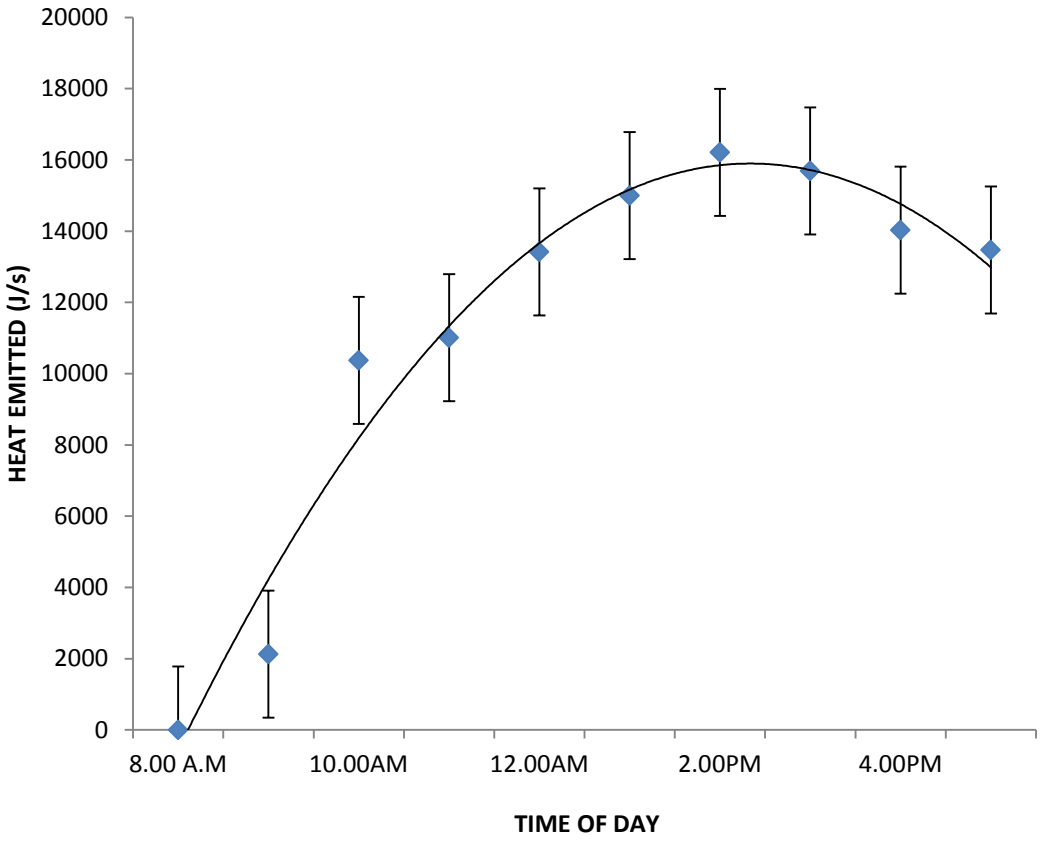

Figure B. 6: Heat emitted by 6M sodium chloride solution with time of day on 15.1.2014

APPENDIX C: HEAT ABSORBED BY HTFs

Appendix C shows figures on heat absorbed by heat transfer fluids with time of day at an average solar power intensity of 1032.3 Wm^{-2}

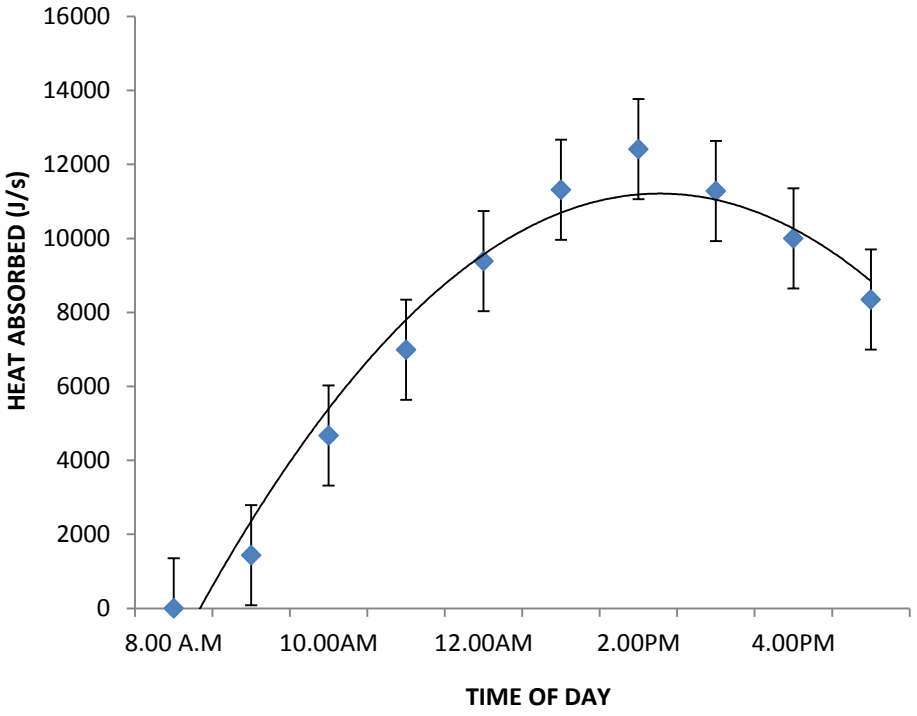

Figure C. 1: Heat absorbed by vegetable oil 1 against time of day on 21.9. 2013

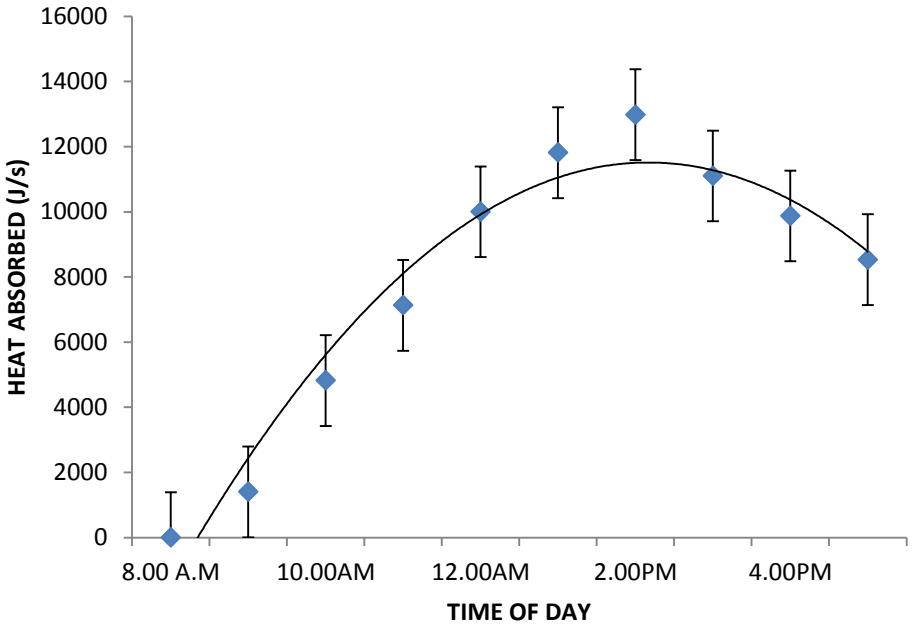

Figure C. 2: Heat absorbed by used engine oil on 20.1.2014

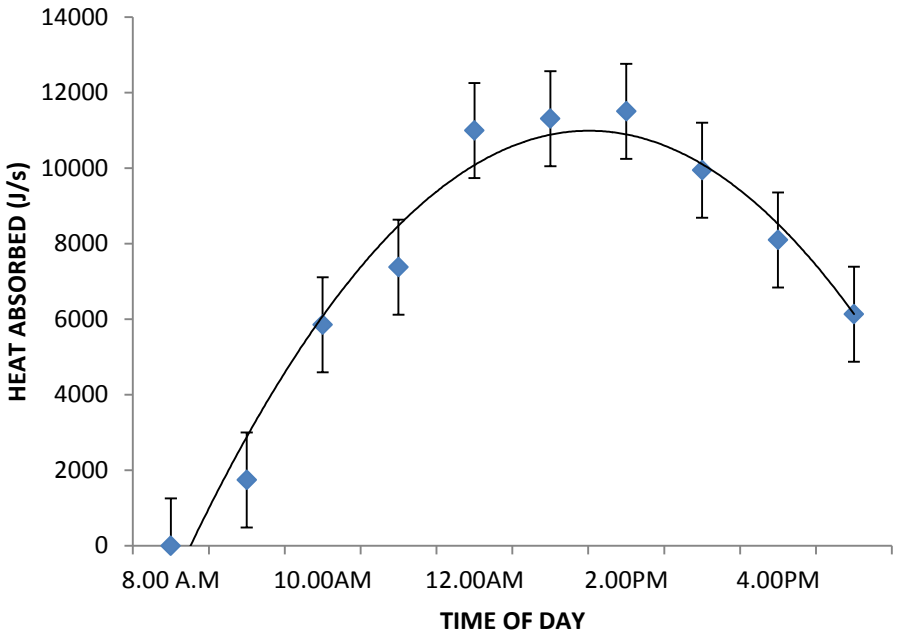

Figure C. 3: Heat absorbed by unused engine oil on 21.1.2014

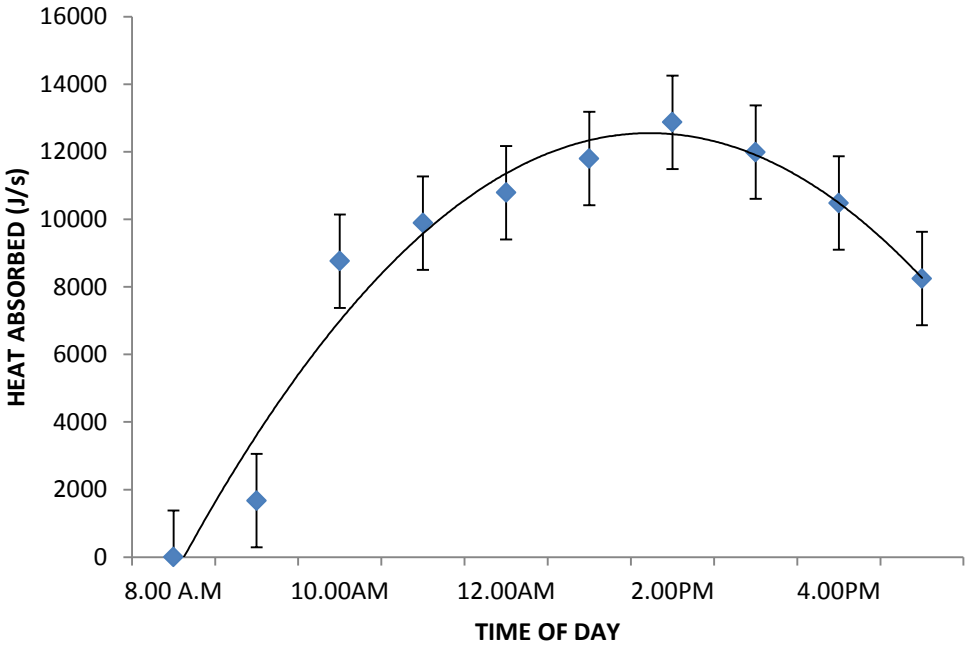

Figure C. 4: Heat absorbed by 2M sodium chloride solution on 22.1.2014

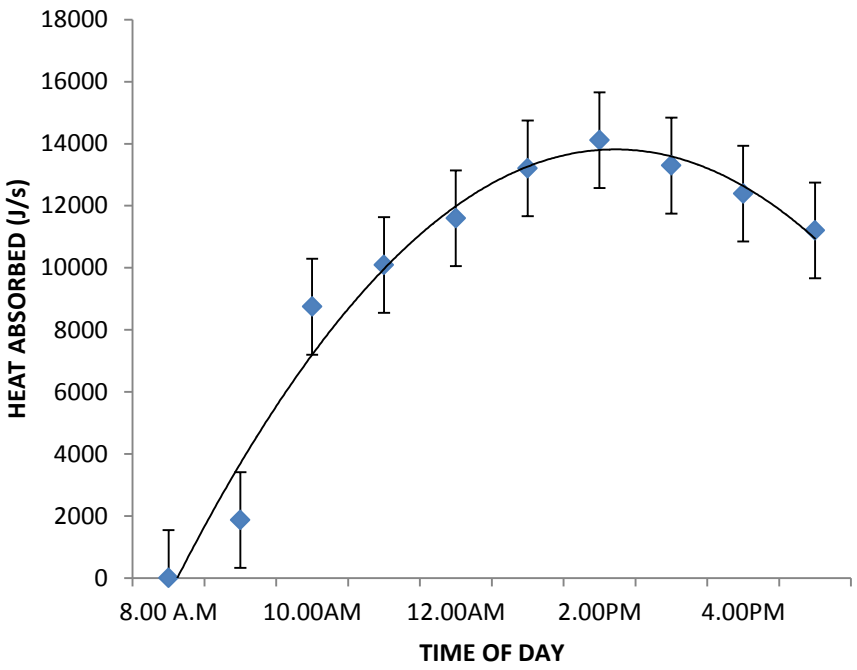

Figure C. 5: Heat absorbed by 4M sodium chloride solution heat transfer fluid on 23.1.2014

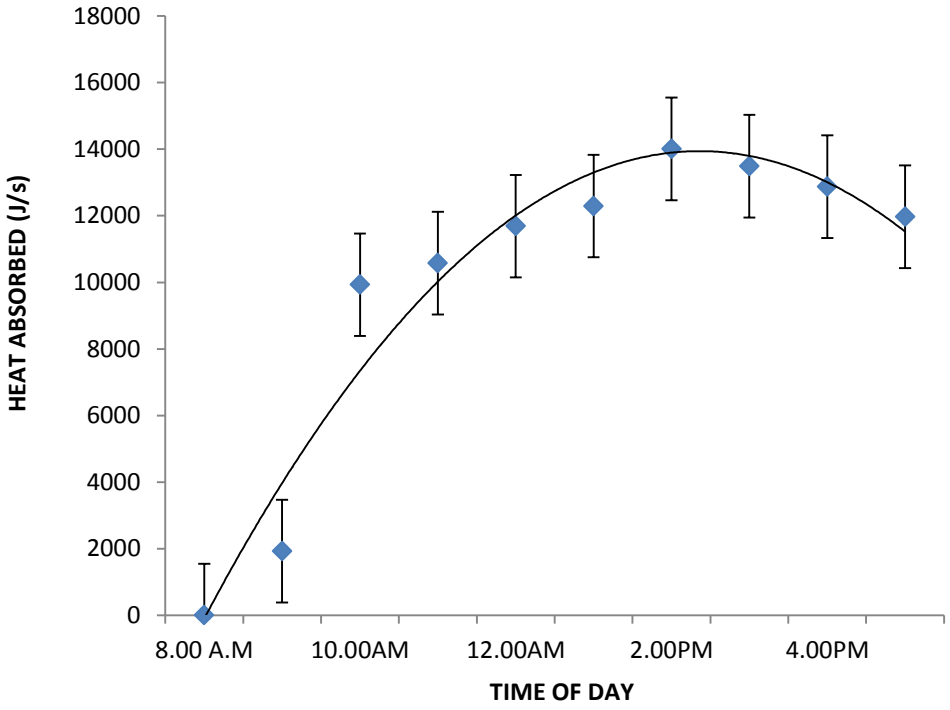

Figure C. 6: Heat absorbed by 6M sodium chloride solution heat transfer fluid on 24.1.2014

APPPENDIX D: HEAT POWER OUTPUT FOR THE HTFs

Appendix D shows figures on heat output against operation pressure of the turbine at an average solar power intensity of 1009.5 Wm^{-2}

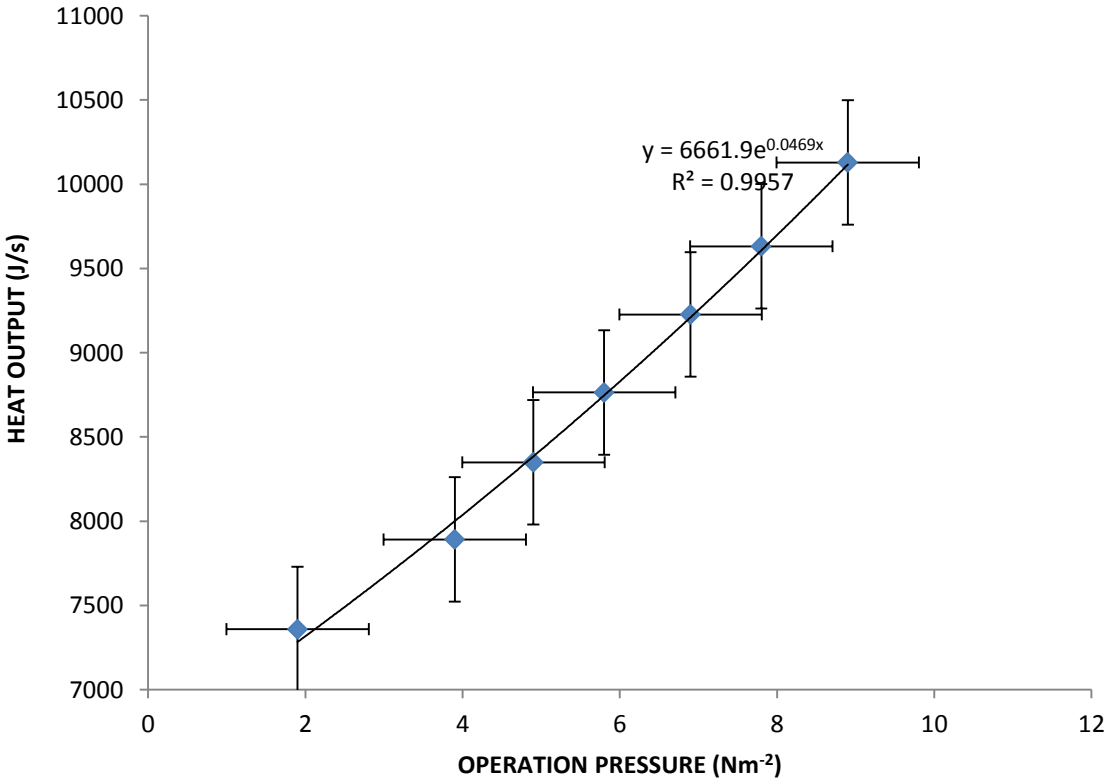

Figure D. 1: Heat output against operation pressure for vegetable oil 1 oil on 10.1.2014

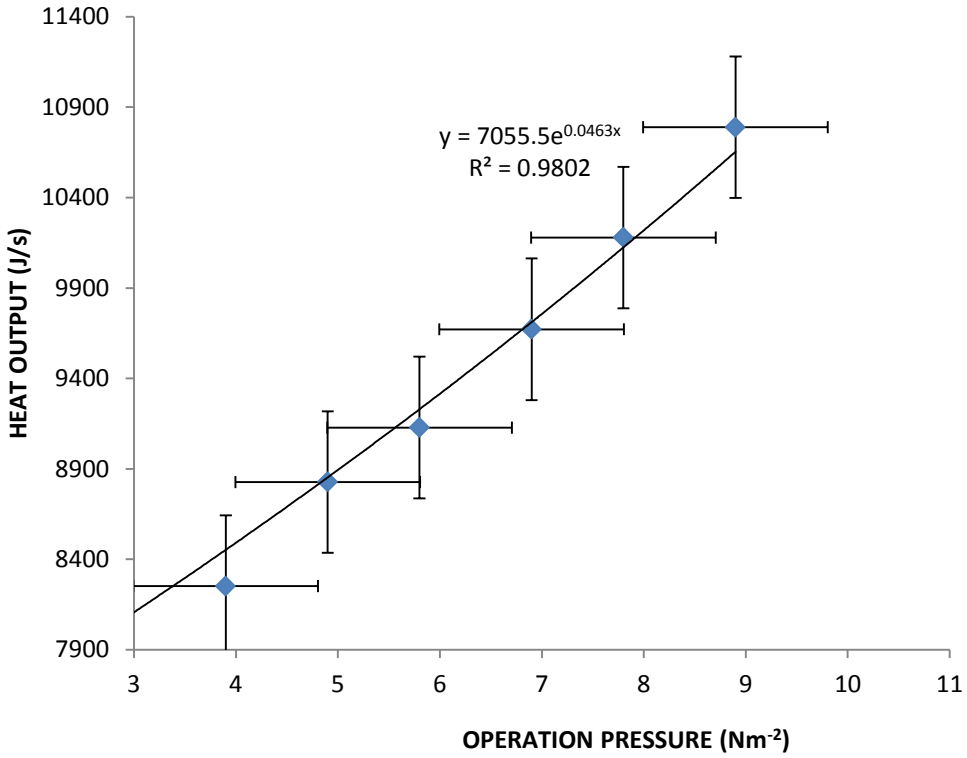

Figure D. 2: Output pressure against operation pressure for unused engine oil on 11.1.2014

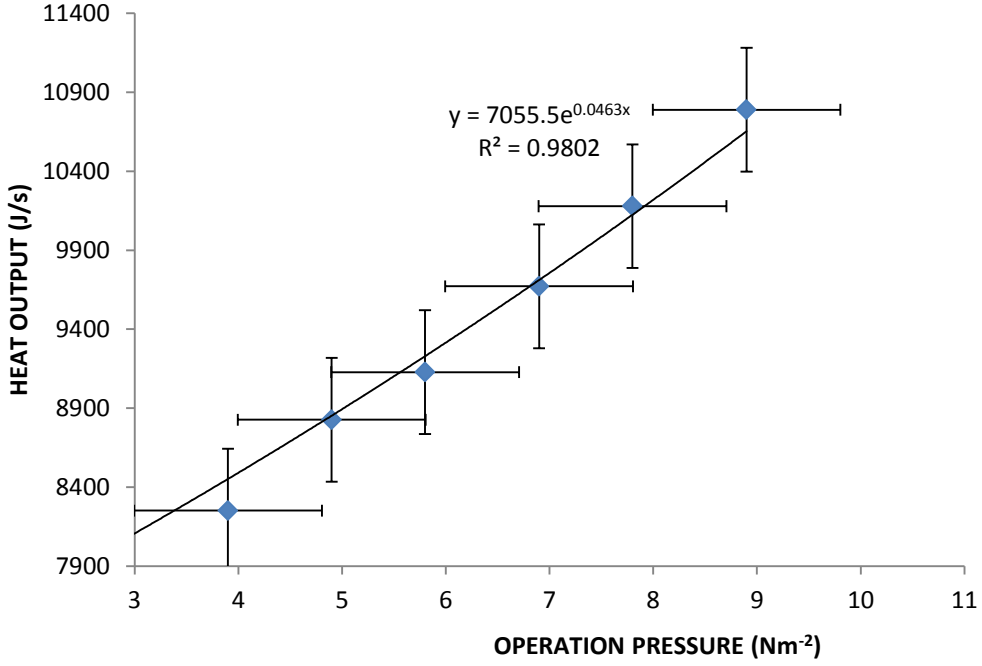

Figure D. 3: Heat output against operation pressure for used engine oil on 12.1.2014

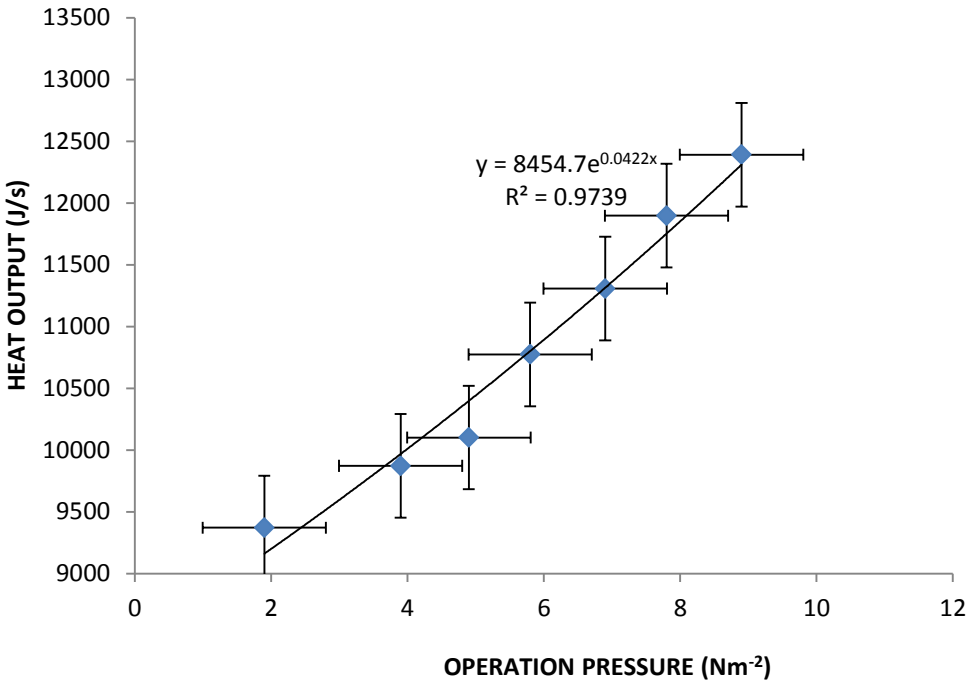

Figure D. 4: Heat output against operation pressure for 2 M salt solution on 13.1.2014

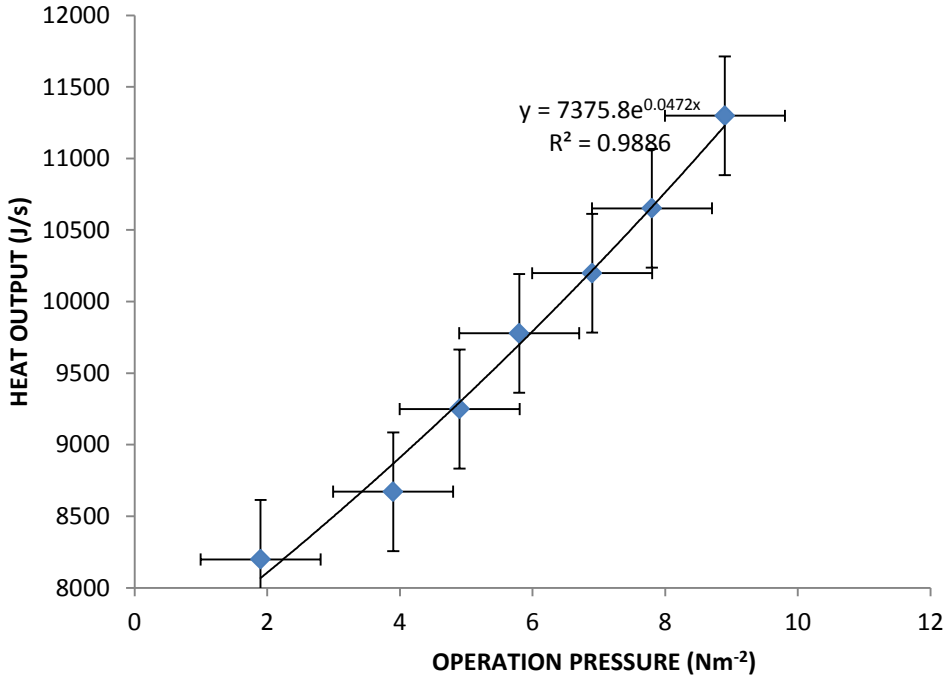

Figure D. 5: Heat output against operation pressure for 4 M salt solution on 14.1.2014

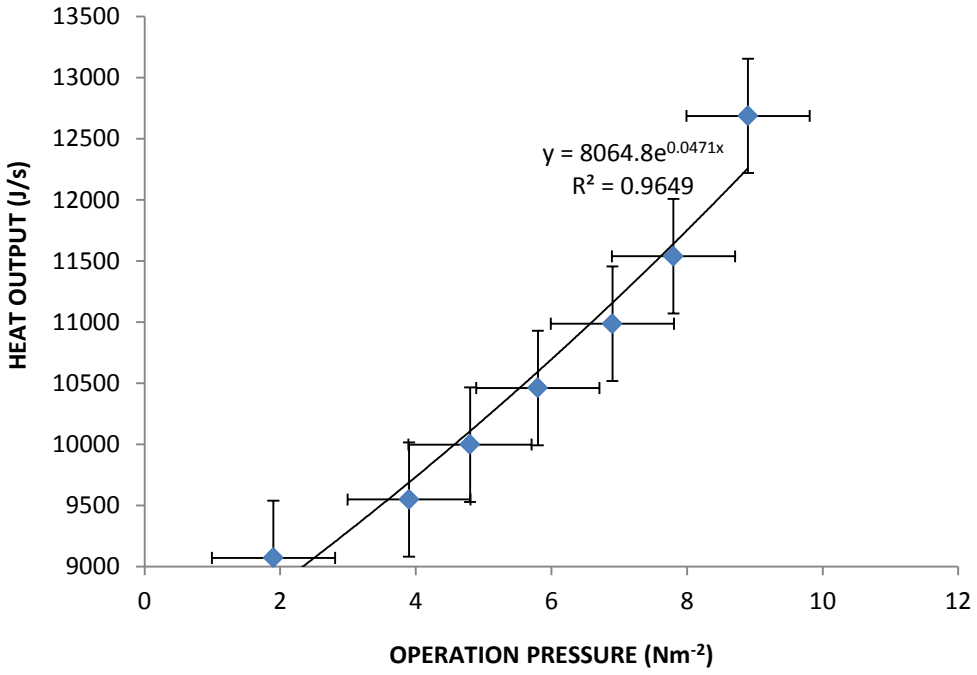

Figure D. 6: Heat output against operation pressure for 6 M salt solution on 15.1.2014

APPENDIX E: POWER OUTPUT AGAINST TIME OF DAY

Appendix E shows power output against time of day for the heat transfer fluids at an average solar power intensity of 1051.6 Wm^{-2}

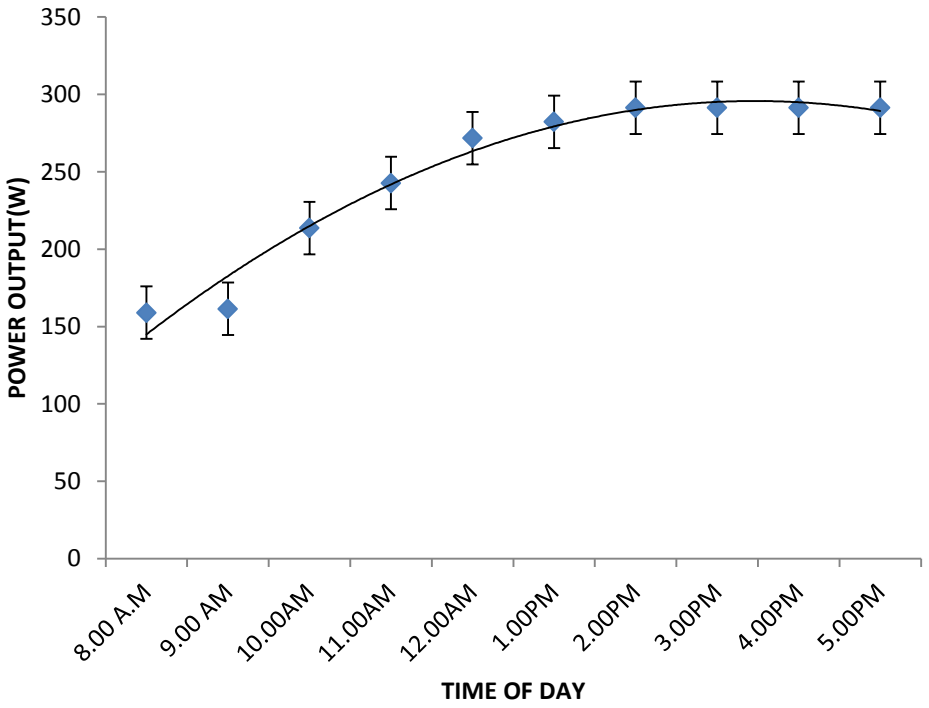

Figure E. 1: Power output against time of day for 4 M sodium chloride solution on 19.1.2014

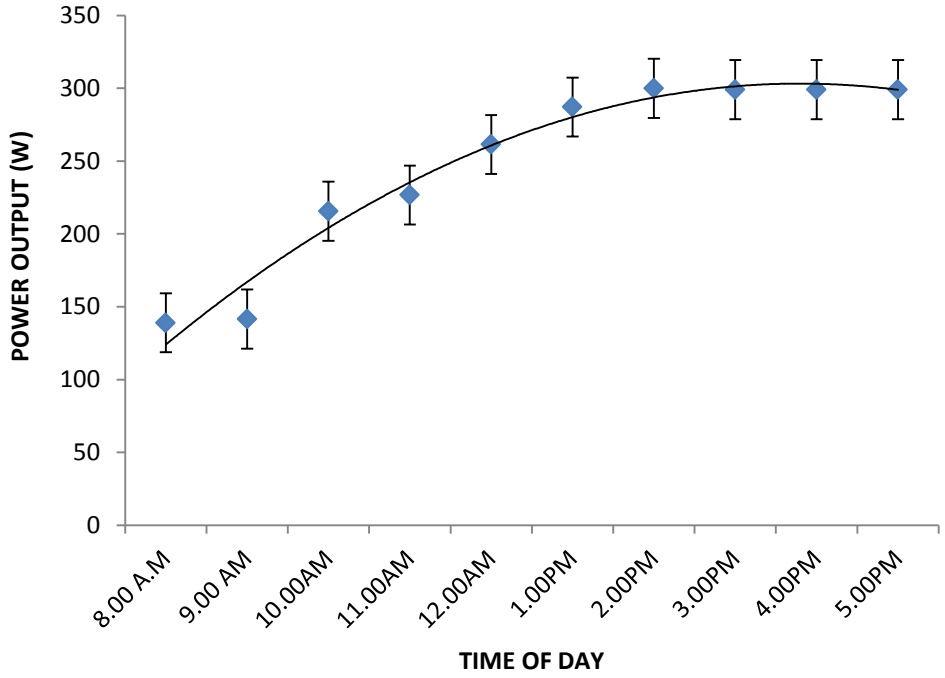

Figure E. 2: Power output against time of day for 2 M sodium chloride solution on 20.1.2014

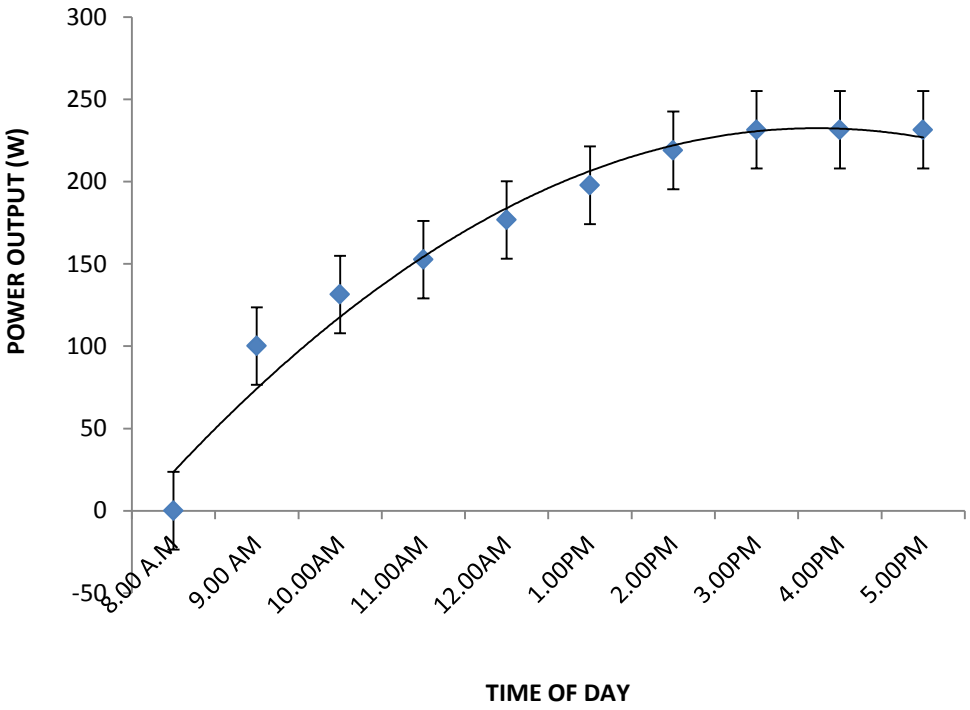

Figure E. 3: Power output against time of day for vegetable oil 1 on 21.1.2014

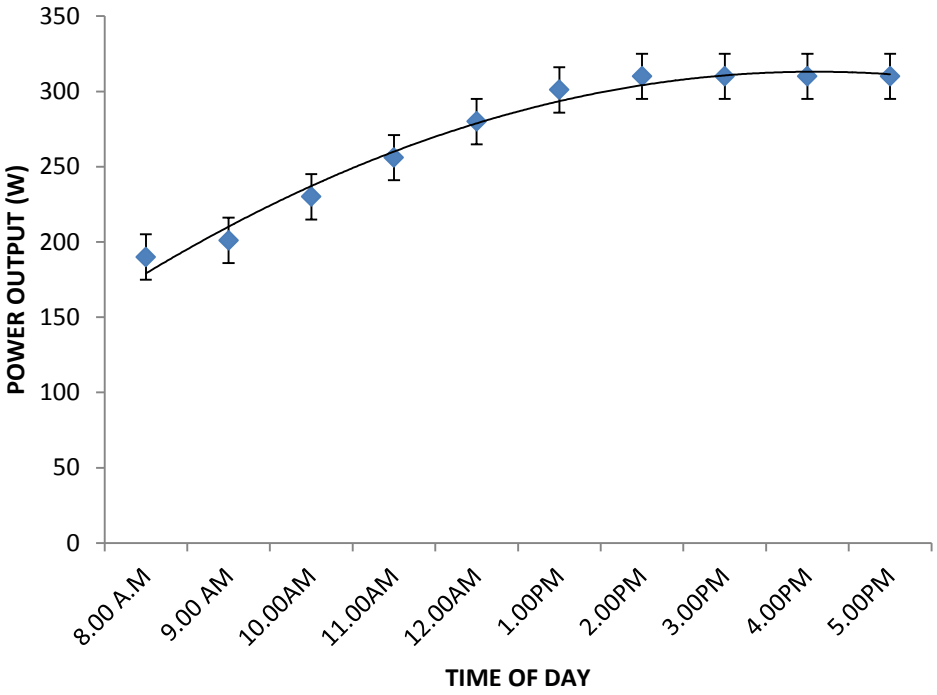

Figure E. 4: Power output against time of day for used engine oil on 22.1.2014

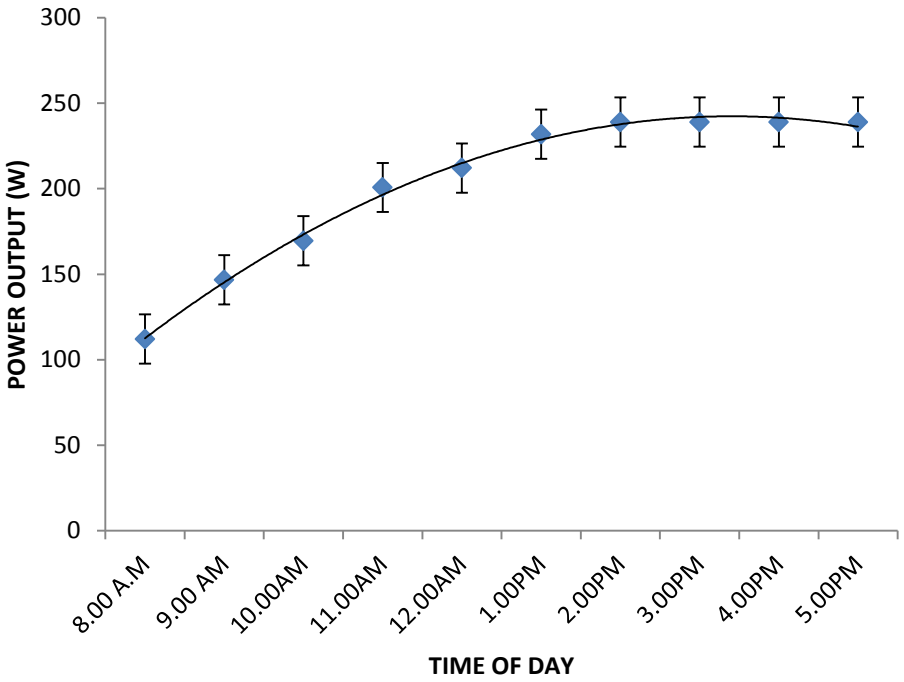

Figure E. 5: Power output against time of day for unused engine oil on 23.1.2014

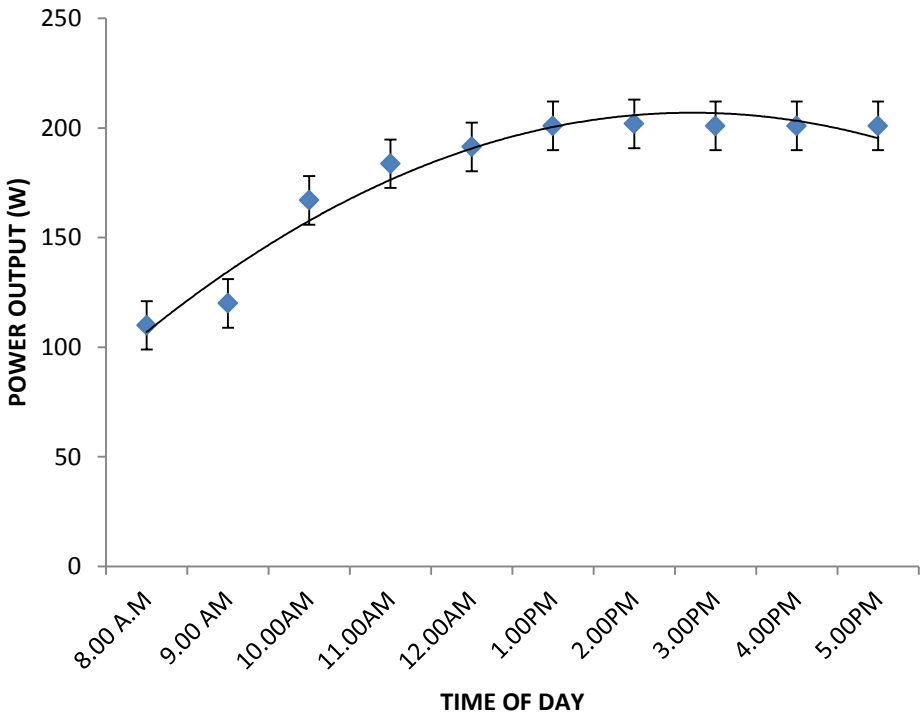

Figure E. 6: Power output against time of day for Vegetable oil 2 on 24.1.2014

APPENDIX F: STEAM FLOW RATE AGAINST POWER

Appendix F shows steam flow rate against power output for the heat transfer fluids at solar power intensity of 1103.1 Wm^{-2}

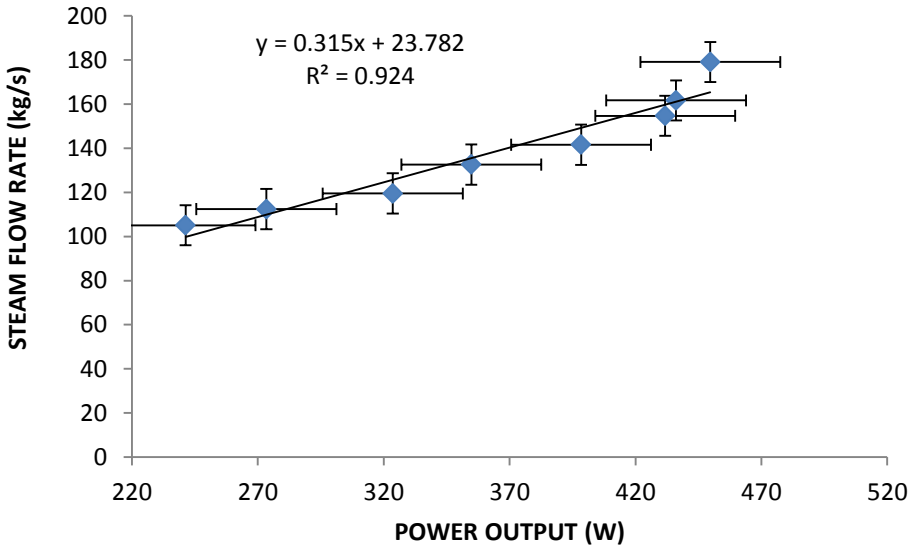

Figure F. 1: Steam flow rate against power output for 4M sodium chloride solution on 19.1.2014

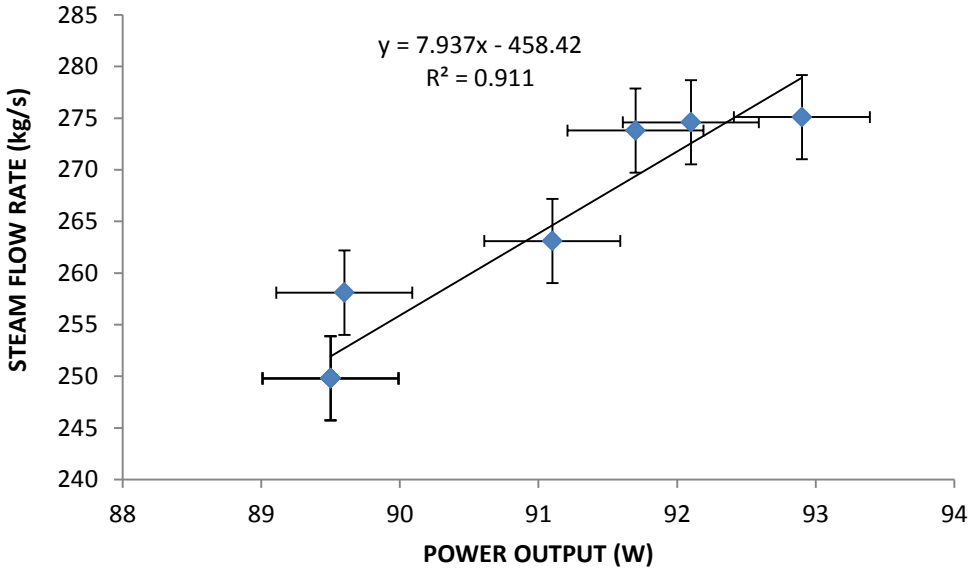

Figure F. 2: Steam flow rate against power output for 2M sodium chloride solution on 20.1.2014

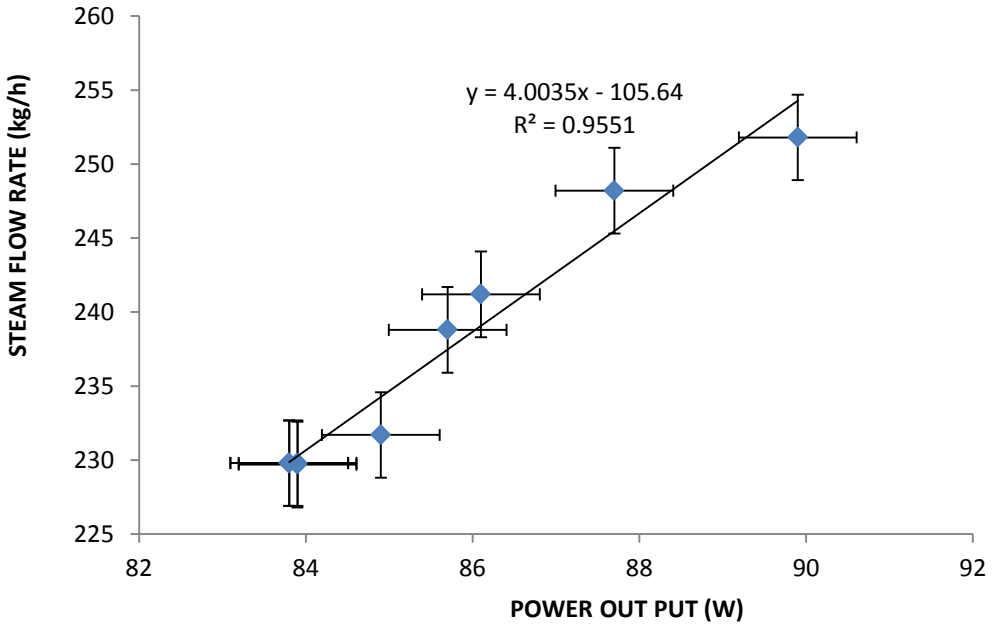

Figure F. 3: Steam flow rate against power output for unused engine oil on 21.1.2014

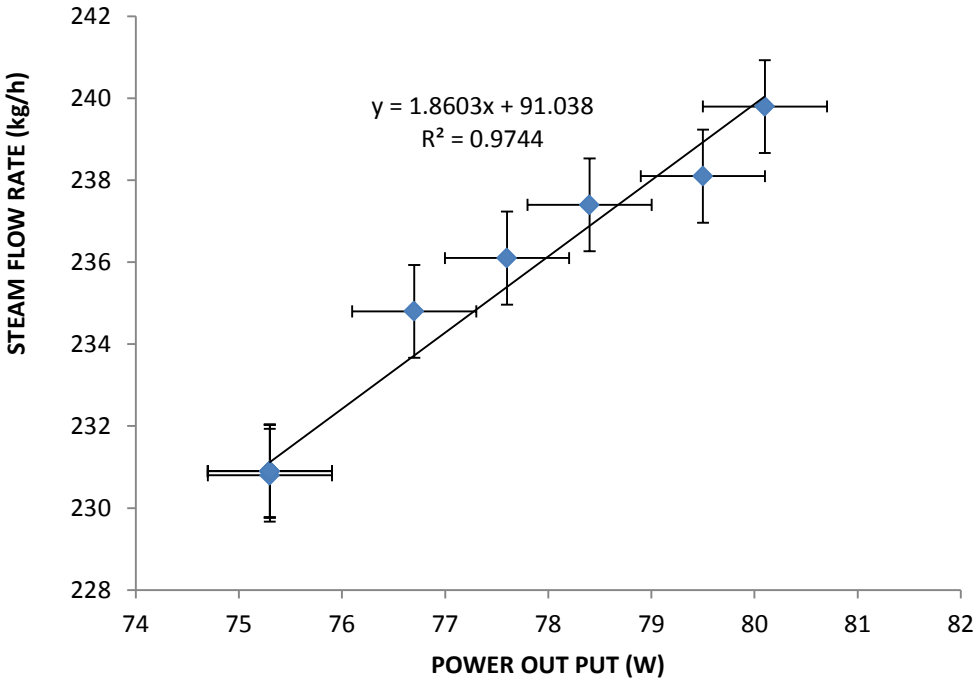

Figure F. 4: Steam flow rate against power output for used engine oil on 22.1.2014

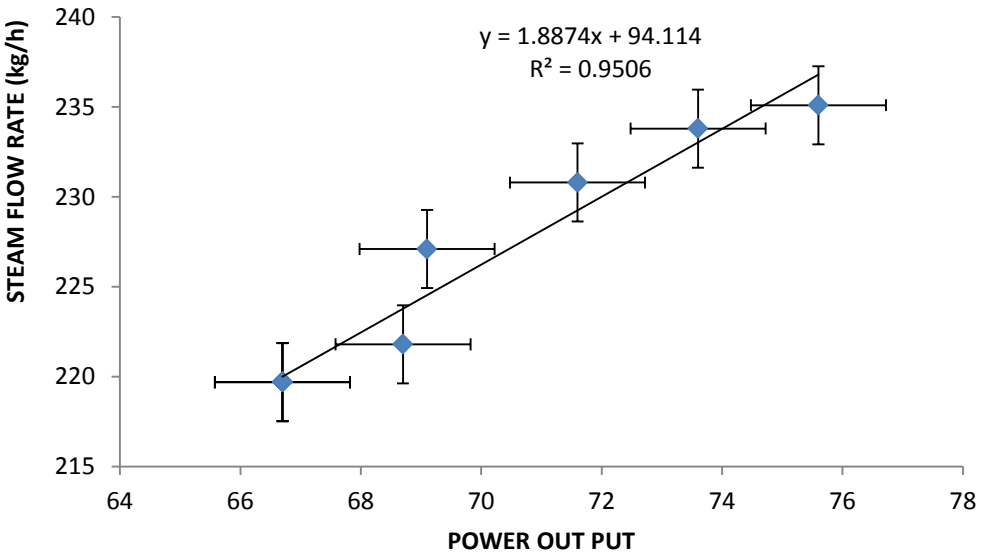

Figure F. 5: Steam flow rate against power output for Vegetable oil 2 on 23.1.2014

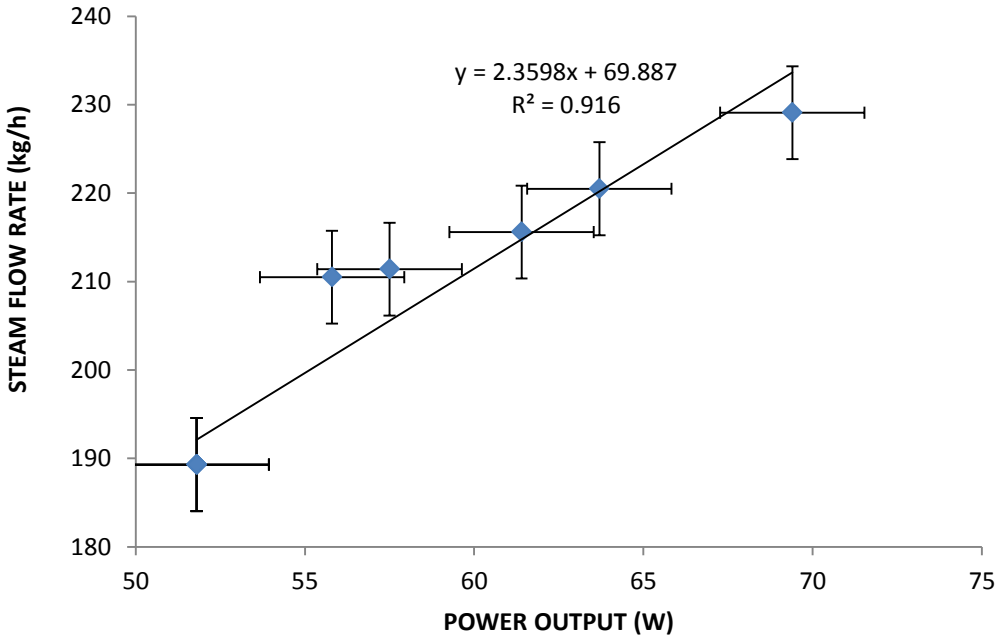

Figure F. 6: Steam flow rate against power output for vegetable oil 1 oil on 24.1.2014

APPENDIX G: CHARACTERIZATION OF COLLECTORS

Appendix G shows characterization of collector with heat transfer fluids at solar power intensities in the range of 923.4 Wm^{-2} to 1152.1 Wm^{-2}

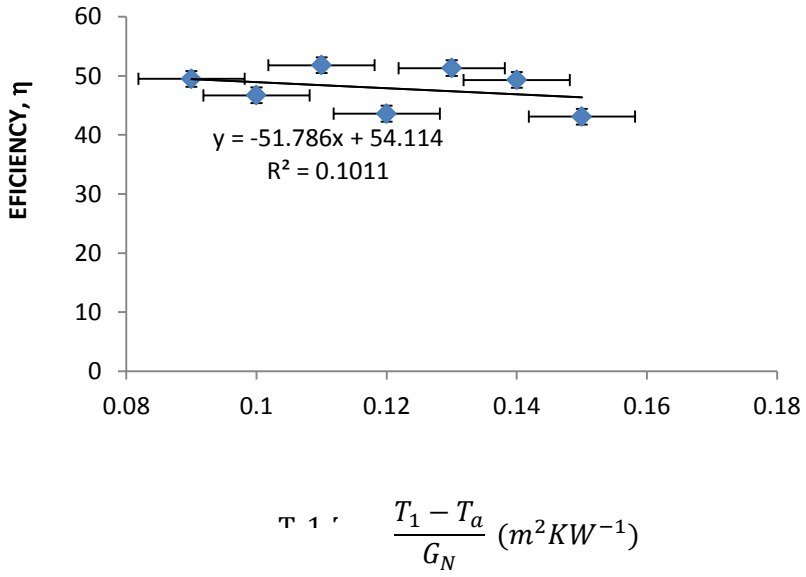

Figure G. 1: Efficiency of open solar concentrator with water on 10.9. 2013

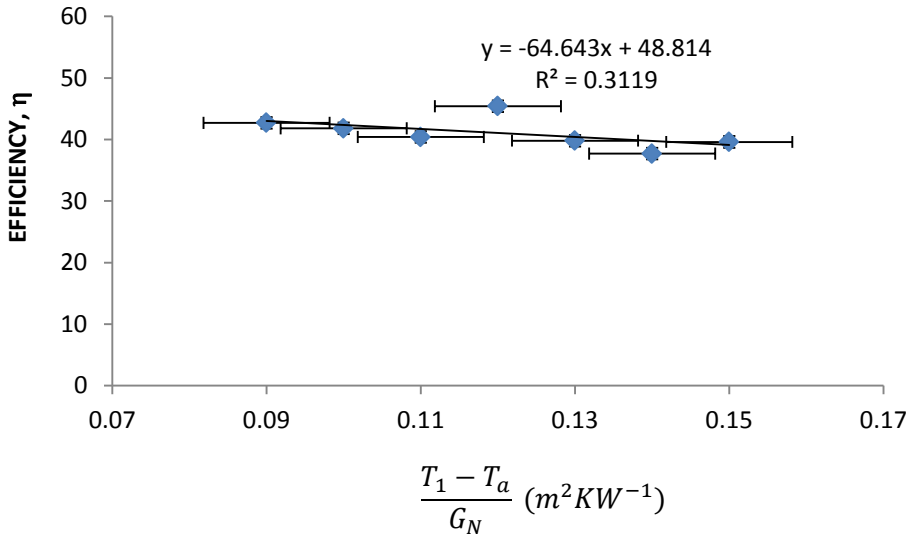

Figure G. 2: Efficiency of closed solar concentrator with Vegetable oil 2 on 11. 9. 2013

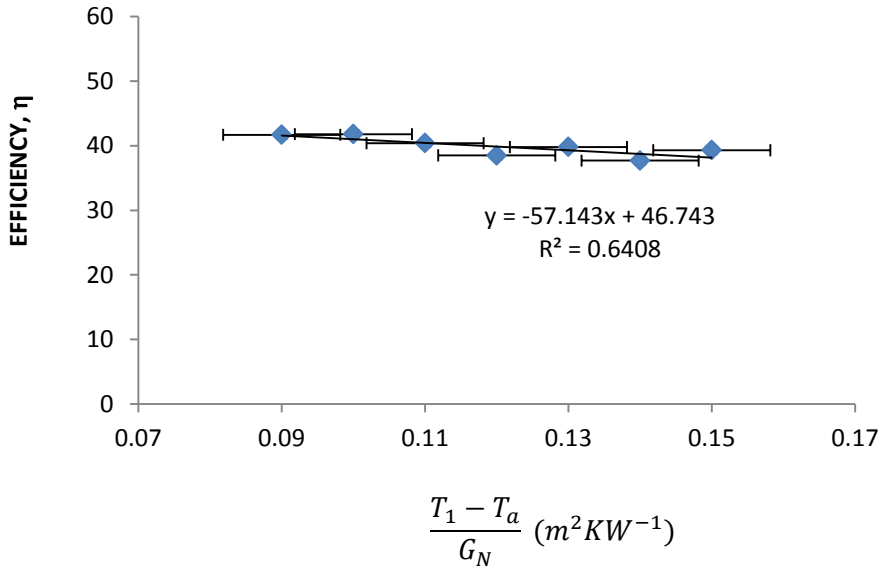

Figure G. 3: Efficiency of open solar concentrator with Vegetable oil 2 on 12. 9. 2013

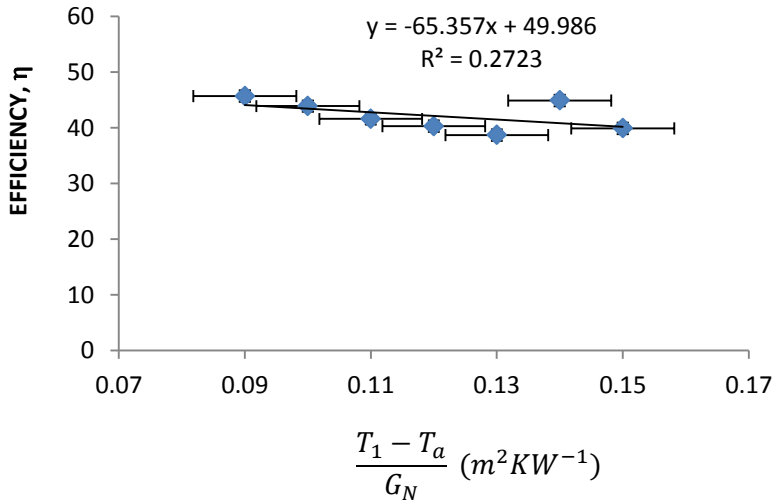

Figure G. 4: Efficiency of closed solar concentrator with vegetable oil 1 oil on 13.9.2013

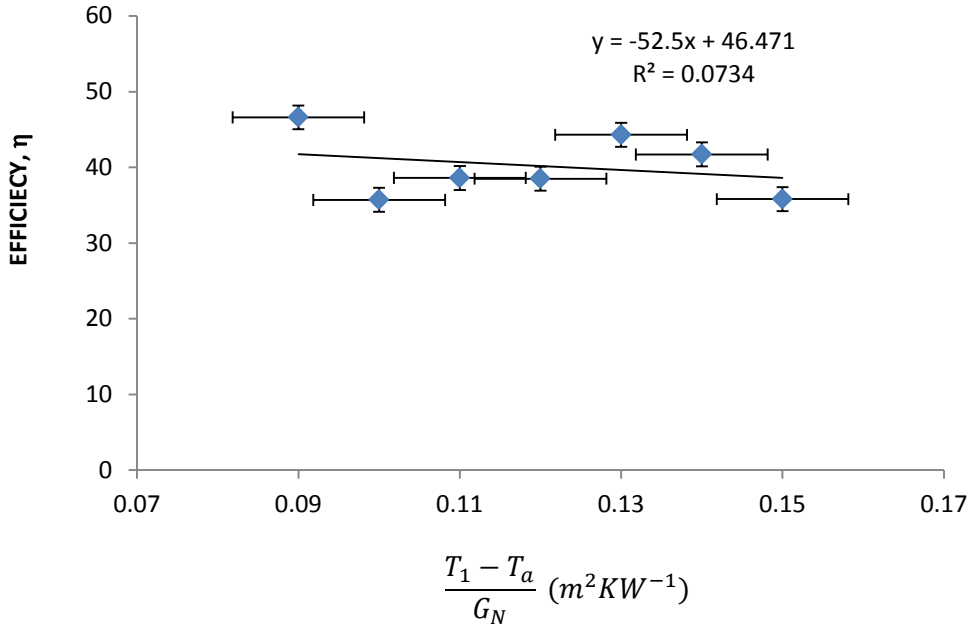

Figure G. 5: Efficiency of open solar concentrator with vegetable oil 1 oil on 14.9.2013

$\frac{T_1 - T_a}{G_N}$ $(m^2K/W$

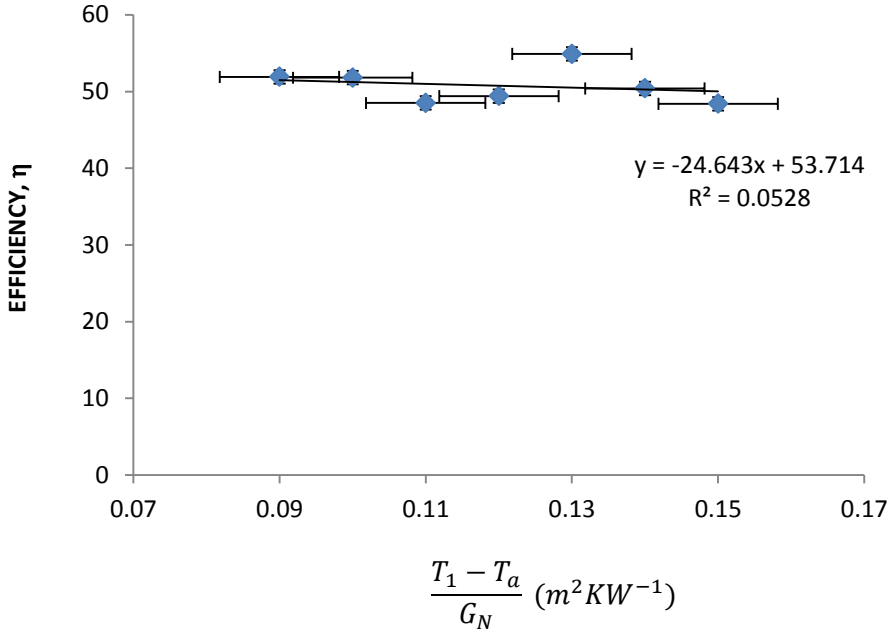

Figure G. 6: Efficiency of closed solar concentrator with used engine oil on 15.9.2013

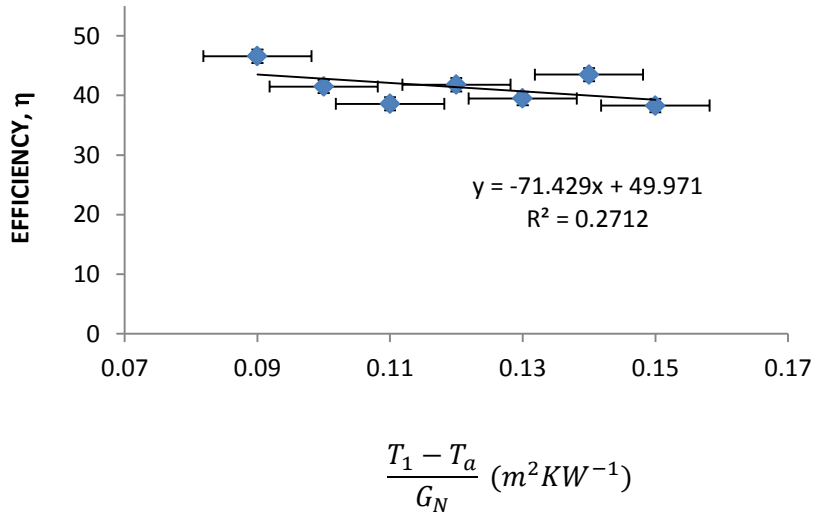

Figure G. 7: Efficiency of open solar concentrator with used engine oil on 16.9.2013

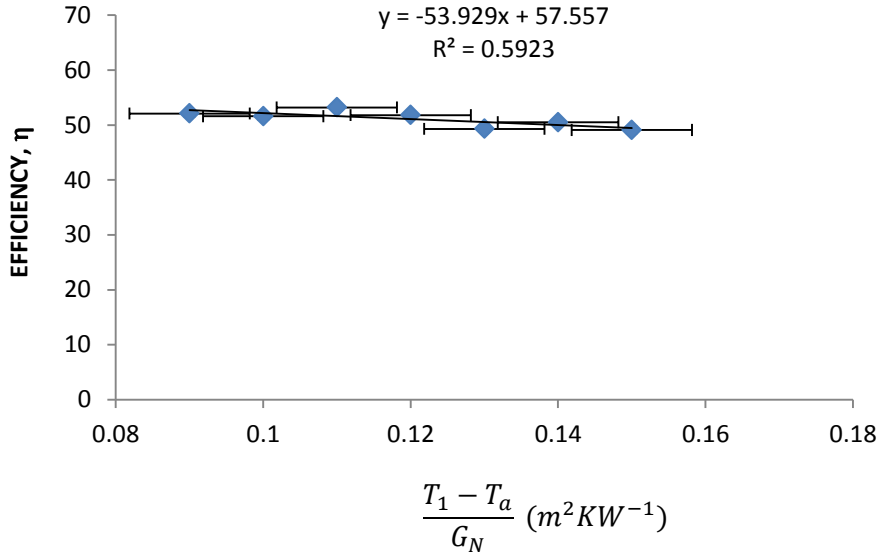

Figure G. 8: Efficiency of closed solar concentrator with unused engine oil on 17. 9. 2013

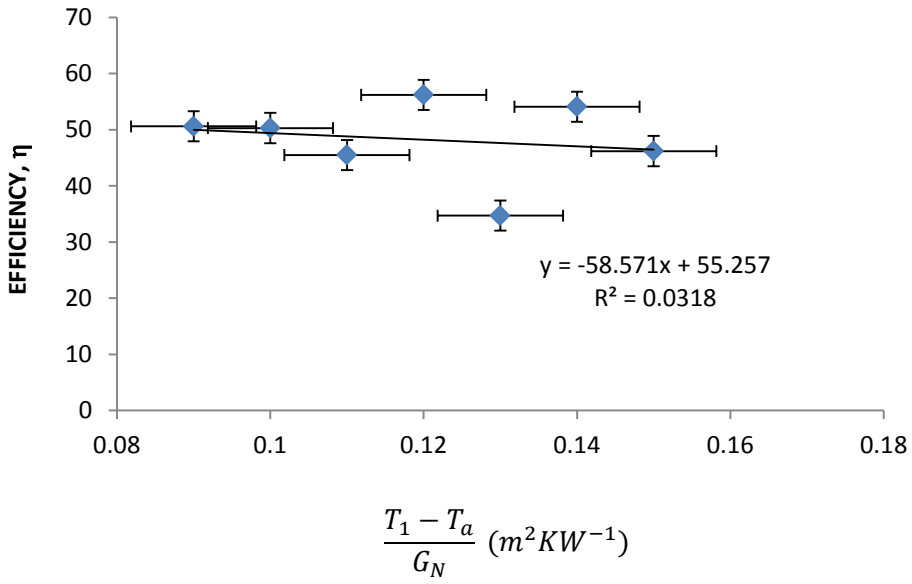

Figure G. 9: Efficiency of open solar concentrator with unused engine oil on 18.9.2013

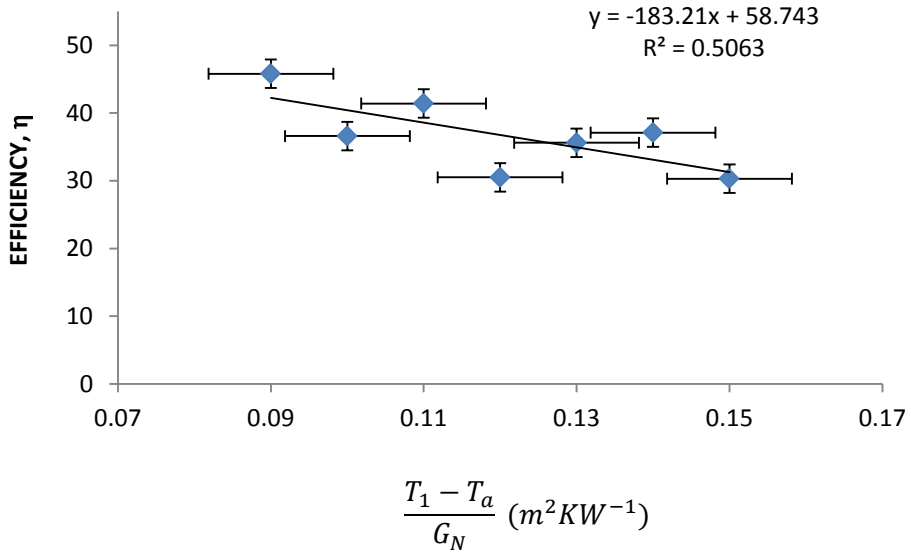

Figure G. 10: Efficiency of closed solar concentrator with 2M sodium chloride solution on 19.9.2013

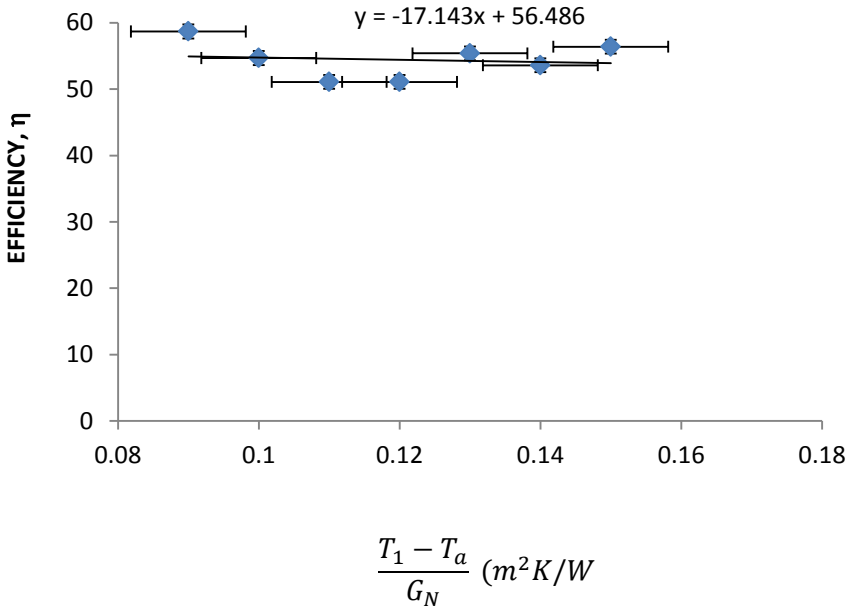

Figure G. 11: Efficiency of open solar concentrator with 2M sodium chloride solution on 20.9.2013

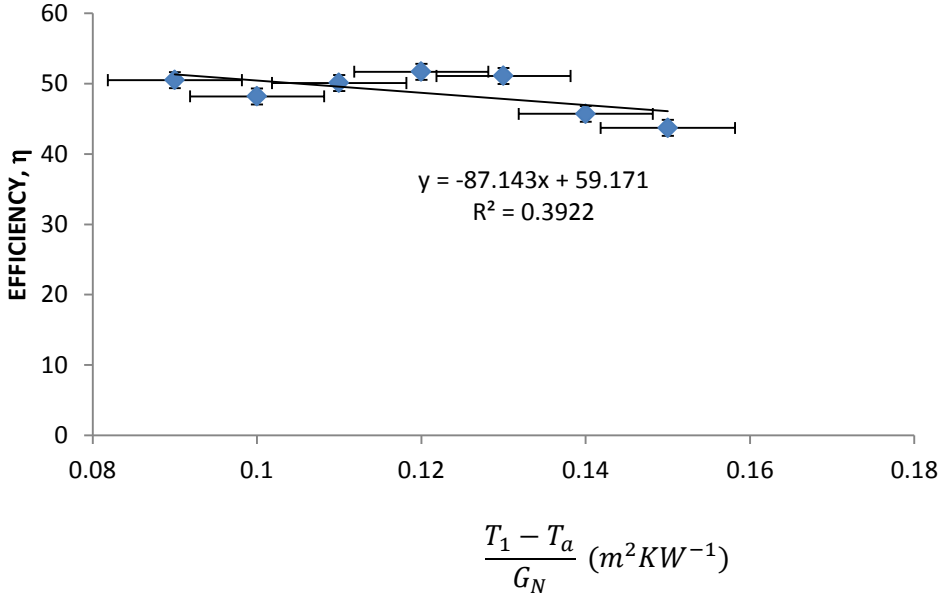

Figure G. 12: Efficiency of closed concentrator with 4M sodium chloride solution on 21.9.2013

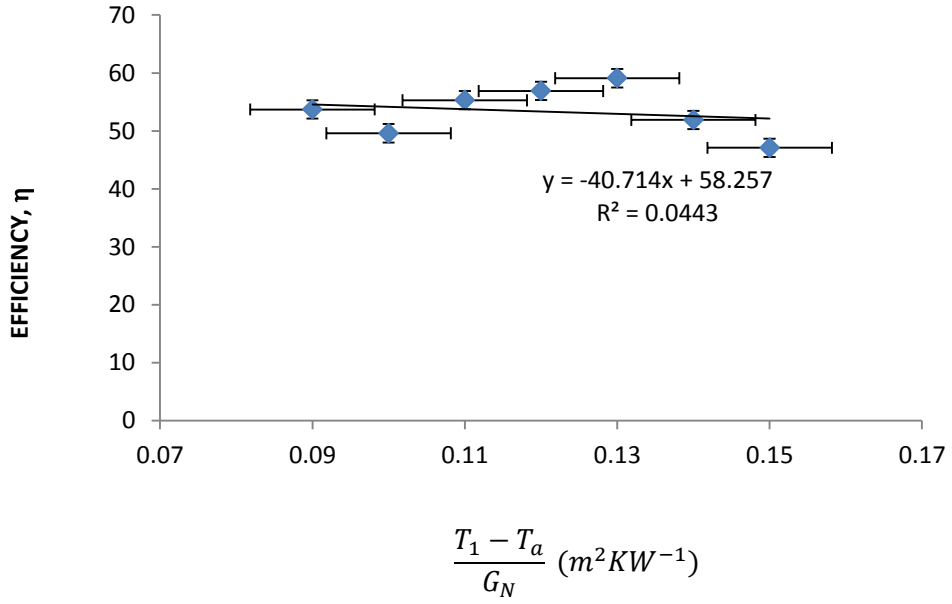

Figure G. 13: Efficiency of open concentrator with 4M sodium chloride solution on 22.9.2013

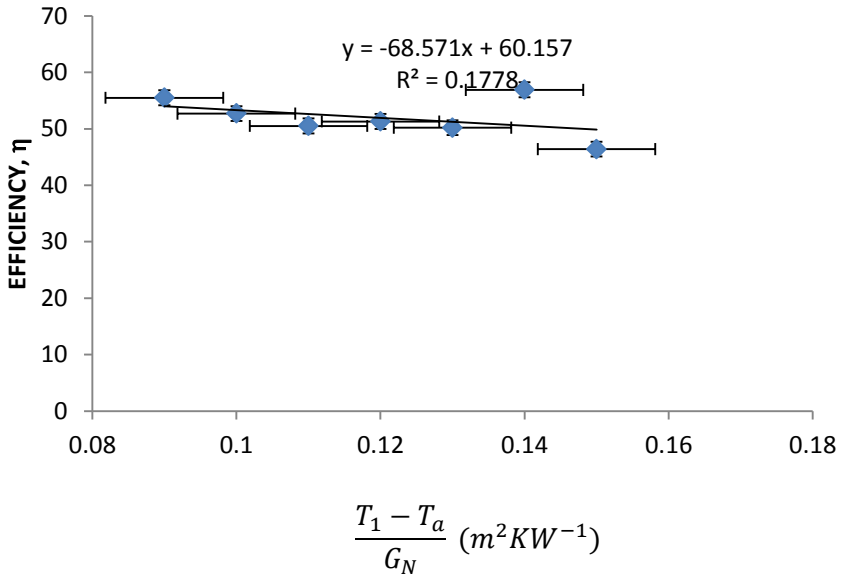

Figure G. 14: Efficiency of closed concentrator with 6M sodium chloride solution on 23.9. 2013

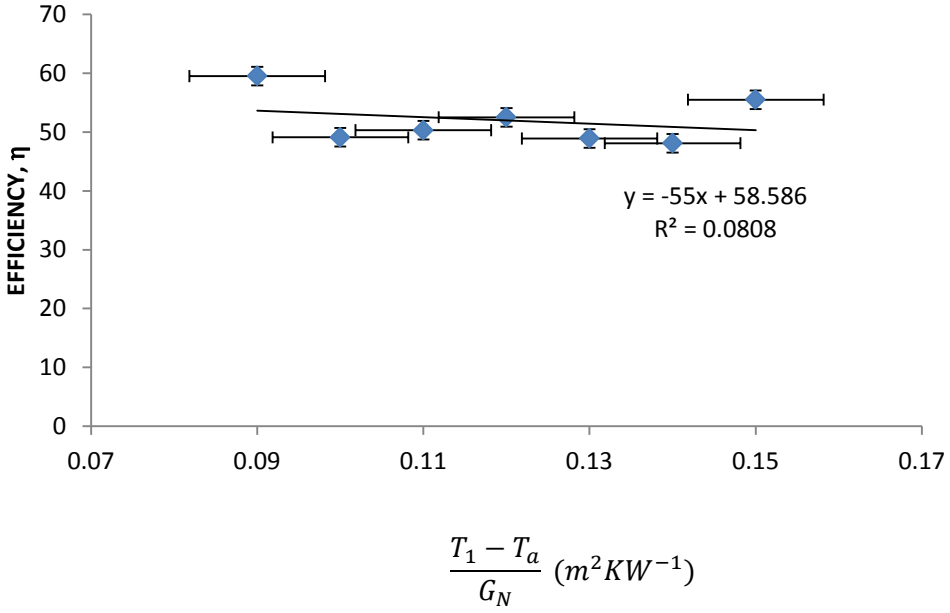

Figure G. 15: Efficiency of open concentrator using 6M sodium chloride solution on 24.9.2013

APPENDIX H: HEAT ABSORBED, PRESSURE AND MASS FLOW RATE FOR HTFs

Tables on appendix H show the heat absorbed, pressure and mass flow rate for the heat transfer fluids with the steam storage system ata an average power intensity of 1068.9 Wm^{-2}

Table H. 1: Heat absorbed, pressure and mass flow rate for Vegetable oil 2 on 24.1.2014

Heat absorbed (J)	**16638.2**	**17140.8**	**17133.9**	**18186.1**	**18397.7**	**18546.1**	**18311.5**	**19489.1**
Pressure × 10^5 (Nm^{-2})	1.0	2.0	3.0	4.0	5.0	6.0	7.0	8.0
Mass flow rate (kgs^{-1})	3.1	3.3	3.7	4.1	4.6	5.1	5.5	5.9

Table H. 2: Heat absorbed, pressure and mass flow rate for vegetable oil 1 on 25.1.2014

Heat absorbed (J)	**16822.2**	**17895.2**	**18157.4**	**18392.5**	**18868.1**	**19307.4**	**19559.2**	**20187.3**
Pressure × 10^5 (Nm^{-2})	1.0	2.0	3.0	4.0	5.0	6.0	7.0	8.0
Mass flow rate	3.1	3.4	3.9	4.1	4.7	5.3	5.8	6.1

(kgs^{-1})

Table H. 3: Heat absorbed, pressure and mass flow rate for used engine oil on 26.1.2014

Heat absorbed (J)	**12789.2**	**14014.6**	**14490.0**	**14705.1**	**14959.2**	**15304.2**	**15592.2**	**15963.2**
Pressure × 10^5 (Nm^{-2})	1.0	2.0	3.0	4.0	5.0	6.0	7.0	8.0
Mass flow rate (kgs^{-1})	2.6	3.0	3.2	3.4	3.8	4.0	4.2	4.3

Table H. 4: Heat absorbed, pressure and mass flow rate for unused oil on 27.1.2014

Heat absorbed (J)	**17044.2**	**17384.6**	**18274.7**	**18408.1**	**19420.1**	**19950.8**	**20565.5**	**250946.1**
Pressure × 10^5 (Nm^{-2})	1.0	2.0	3.0	4.0	5.0	6.0	7.0	8.0
Mass flow rate (kgs^{-1})	3.3	3.7	4.1	4.6	5.0	5.6	5.9	6.4

Table H. 5: Heat absorbed, pressure and mass flow rate for 2 M sodium chloride solution on 28.1.2014

Heat absorbed (J)	**17254.6**	**17879.1**	**18058.5**	**18525.4**	**19546.9**	**19677.7**	**20085.9**	**20248.1**
Pressure × 10^5 (Nm^{-2})	1.0	2.0	3.0	4.0	5.0	6.0	7.0	8.0
Mass flow rate (kgs^{-1})	3.1	3.4	3.7	4.1	4.3	4.9	5.1	5.4

Table H. 6: Heat absorbed, pressure and mass flow rate for 4 M sodium chloride solution

On 29.1.2014

Heat absorbed (J)	**18040.1**	**18421.9**	**18720.8**	**18979.6**	**19546.6**	**19780.1**	**20557.4**	**20735.9**
Pressure × 10^5 (Nm^{-2})	1.0	2.0	3.0	4.0	5.0	6.0	7.0	8.0
Mass flow rate (kgs^{-1})	3.0	3.5	4.1	4.3	4.9	5.4	5.7	6.1

APPENDIX I: HEAT ABSORBED, PRESSURE AND MASS FLOW RATE FOR HTFs

Tables on appendix I show the heat absorbed, pressure and mass flow rate for the heat transfer fluids during solar thermal collection without the steam storage system at average solar power intensity of 1050 Wm^{-2}.

Table I. 1: Variation of heat absorbed, pressure and mass flow rate for Vegetable oil 2 on 8.3.2014

Heat absorbed (J)	**14468.3**	**14905.9**	**14899.2**	**15814**	**15998.7**	**16127.6**	**15923.4**	**16947.0**
Pressure × 10^5 (Nm^{-2})	1.0	2.0	3.0	4.0	5.0	6.0	7.0	8.0
Mass flow rate (kgs^{-1})	2.8	3.1	3.4	3.6	3.7	4.1	4.3	4.5

Table I. 2: Variation of heat absorbed, pressure and mass flow rate for vegetable oil 1 on 9.3.2014

Heat absorbed (J)	**14628.6**	**15561.7**	**15789.4**	**15993.5**	**16407.7**	**16789.0**	**17008.3**	**17554.1**
Pressure × 10^5 (Nm^{-2})	1.0	2.0	3.0	4.0	5.0	6.0	7.0	8.0
Mass flow rate (kgs^{-1})	2.7	3.0	3.4	3.9	4.2	4.7	5.1	5.3

Table I. 3: Variation of heat absorbed, pressure and mass flow rate for used engine oil on 10.3.2014

Heat absorbed (J)	**11121.8**	**12513.7**	**12600.4**	**12787.3**	**13008.5**	**13308.7**	**13561.9**	**13881.6**
Pressure × 10^5 (Nm^{-2})	1.0	2.0	3.0	4.0	5.0	6.0	7.0	8.0
Mass flow rate (kgs^{-1})	2.5	2.8	3.1	3.3	3.6	3.9	4.0	4.1

Table I. 4: Variation of heat absorbed, pressure and mass flow rate for unused oil on 11.3.2014

Heat absorbed (J)	**14821.3**	**15117.8**	**15891.6**	**16007.7**	**16887.2**	**17348.5**	**17883.6**	**18214.4**
Pressure × 10^5 (Nm^{-2})	1.0	2.0	3.0	4.0	5.0	6.0	7.0	8.0
Mass flow rate (kgs^{-1})	2.7	3.0	3.3	3.9	4.3	4.8	5.1	5.3

Table I. 5: Variation of heat absorbed, pressure and mass flow rate for 2 M sodium chloride solution on 12.3.2014

Heat absorbed (J)	**15004.5**	**15547.9**	**15703.3**	**16109.7**	**16997.3**	**17111.2**	**17466.8**	**17607.4**
Pressure × 10^5 (Nm^{-2})	1.0	2.0	3.0	4.0	5.0	6.0	7.0	8.0
Mass flow rate (kgs^{-1})	2.9	3.2	3.7	4.0	4.4	5.1	5.5	5.9

Table I. 6: Variation of heat absorbed, pressure and mass flow rate for 4 M sodium chloride Solution on 14.3.2014

Heat absorbed (J)	**15687.3**	**16019.1**	**16279.3**	**16504.5**	**16997.1**	**17200.9**	**17876.5**	**18031.6**
Pressure × 10^5 (Nm^{-2})	1.0	2.0	3.0	4.0	5.0	6.0	7.0	8.0
Mass flow rate (kgs^{-1})	2.9	3.3	3.9	4.1	4.5	5.3	5.4	6.0

APPENDIX J: OPERATING POINTS FOR HTFs

Appendix J shows tables on operating points of the heat exchanger with heat transfer fluids at solar power intensities of 1076.2 Wm^{-2}

Table J. 1: Operating points for vegetable oil 1 vs water fluids on 5.11.2013

Property	**Hot fluid (vegetable oil 1)**	**Water at ambient temperature fluid (Water)**
Mass flow rate (Kg/s)	5.11	4.6
Volume flow rate (m^3/s)	4.5	4.1
Fluid Pressure (Nm^{-2})	5.0	4.1
Density(Kg/m^3)	1004	0.905
Specific heat, c_p ($Jkg^{-1}{}^oC$)	2500	4170
$T_{2,out}$ **(°C)**	33.60	163.4
$T_{1,out}$ **(°C)**	163.4	23.8

Table J. 2: Operating points for water vs water liquids on 6.11.2013

Property	**Hot Fluid (Water)**	**Water at ambient temperature fluid (Water)**
Mass flow rate (Kg/s)	7.1	6.6
Volume flow rate (m^3/s)	6.7	6.1
Fluid Pressure (Nm^{-2})	5.0	5.0
Density (Kg/m^3)	1000	1000
Specific heat, c_p	4180	4180
$T_{2,out}$ **(°C)**	31.8	274.8
$T_{1,out}$ **(°C)**	274.8	22.4

Table J. 3: Operating points for used engine oil vs water on 7.11.2013

Property	**Hot fluid (Used engine oil)**	**Water at ambient temperature fluid (Water)**
Mass flow rate (Kg/s)	7.5	7.0
Volume flow rate (m^3/s)	6.1	6.3
Fluid Pressure (Nm^{-2})	5.0	5.0
Density (Kg/m^3)	800	1000
Specific heat, c_p	2500	4180
$T_{2,out}$ **(°C)**	33.9	238.7
$T_{1,out}$ **(°C)**	237.8	22.7

Table J. 4: Operating points for unused engine oil vs water on 8.11.2013

Property	**Hot fluid (Used engine oil)**	**Water at ambient temperature fluid (Water)**
Mass flow rate (Kg/s)	7.4	6.3
Volume flow rate (m^3/s)	6.5	5.8
Fluid Pressure (Nm^{-2})	5.0	5.0
Density (Kg/m^3)	1025	1000
Specific heat, c_p	5200	4180
$T_{2,out}$ **(°C)**	32.7	260.1
$T_{1,out}$ **(°C)**	268.1	321.4

Table J. 5: Operating points for 2 M sodium chloride solution vs water on 9.11.2013

Property	**Hot fluid (2M salt solution)**	**Water at ambient temperature fluid (Water)**
Mass flow rate (Kg/s)	7.4	6.3
Volume flow rate (m^3/s)	6.5	5.8
Fluid Pressure (Nm^{-2})	5.0	5.0
Density (Kg/m^3)	1050	1030
Specific heat, c_p	3980	1000
$T_{2,out}$ **(^{o}C)**	32.7	260.1
$T_{1,out}$ **(^{o}C)**	268.1	21.4

Table J. 6: Operating points for 4 M sodium chloride solution vs water on 10.11.2013

Property	**Hot fluid (4M salt solution)**	**Water at ambient temperature fluid (Water)**
Mass flow rate (Kg/s)	7.7	6.5
Volume flow rate (m^3/s)	6.4	5.9
Fluid Pressure (Nm^{-2})	5.0	5.0
Density $(Kg/m3)$	1030	1000
Specific heat, c_p	3910	3910
$T_{2,out}$ **(^{o}C)**	34.4	273.1
$T_{1,out}$ **(^{o}C)**	274.8	22.5

Table J. 7: Operating points for 6 M sodium chloride solution vs water on 11.11.2013

Property	**Hot fluid (6M salt solution)**	**Water at ambient temperature fluid (Water)**
Mass flow rate (Kg/s)	8.0	7.1
Volume flow rate (m^3/s)	7.5	6.5
Fluid Pressure (Nm^{-2})	5.0	5.0
Density (Kg/m^3)	1030	1000
Specific heat, c_p	3850	3850
$T_{2,out}$ **(°C)**	36.8	278.9
$T_{1,out}$ **(°C)**	279.9	23.4

APPENDIX K: SOLAR HEAT ABSORBED BY HTFs

Appendix K shows tables on heat absorbed from the sun by the heat transfer fluids at solar power intensity of an average of 1108 Wm^{-2}

Table K. 1: Heat absorbed by Vegetable oil 2 on 25.1.2014

Pressure$\times 10^5$ **Nm^{-2}**	**Q (J)**	**Mass flow rate (kg/s)**	**Mass of steam (kg)**
2.0	15320.9	3.5	6.8
4.0	16100.4	4.0	7.1
6.0	16540.6	4.5	7.3
8.0	17305.5	5.0	7.7
10.0	18403.6	5.5	8.1

Table K. 2: Heat absorbed by vegetable oil 1 on 26.1.2014

Pressure10^5 **Nm^{-2}**	**Q (J)**	**Mass flow rate (kg/s)**	**Mass of steam (kg)**
2.0	15978.3	3.5	7.0
4.0	16507.1	4.0	7.3
6.0	17202.4	4.5	7.6
8.0	17995.5	5.0	7.9
10.0	18600.3	5.5	8.2

Table K. 3: Heat absorbed by used oil on 27.1.2014

Pressure10^5 **Nm**$^{-2}$	**Q(J)**	**Mass flow rate (kg/s)**	**Mass of steam (kg)**
2.0	12987.4	3.5	5.7
4.0	13101.7	4.0	5.8
6.0	13507.8	4.5	6.0
8.0	14001.6	5.0	6.2
10.0	14304.6	5.5	6.3

Table K. 4: Heat absorbed by unused engine oil on 28.1.2014

Pressure10^5 **Nm**$^{-2}$	**Q(J)**	**Mass flow rate (kg/s)**	**Mass of steam (kg)**
2.0	15697.6	3.5	6.9
4.0	16471.4	4.0	7.3
6.0	17891.7	4.5	7.9
8.0	18568.0	5.0	8.2
10.0	19207.7	5.5	8.4

Table K. 5: Heat absorbed by 2 M salt solution on 29.1.2014

Pressure10^5 **Nm**$^{-2}$	**Q(J)**	**Mass flow rate (kg/s)**	**Mass of steam (kg)**
2.0	15987.7	3.5	7.1
4.0	16689.4	4.0	7.4
6.0	17453.1	4.5	7.7
8.0	17999.5	5.0	8.0
10.0	18505.6	5.5	8.1

Table K. 6: Heat absorbed by 4 M sodium chloride solution on 30.1.2014

Pressure10^5 **Nm**$^{-2}$	**Q(J)**	**Mass flow rate (kg/s)**	**Mass of steam (kg)**
2.0	16405.8	3.5	7.3
4.0	16998.4	4.0	7.5
6.0	17527.3	4.5	7.6
8.0	18491.4	5.0	8.2
10.0	18974.2	5.5	8.4

Table K. 7: Heat absorbed by 6 M sodium chloride solution on 31.1.2014

Pressure 10^5 **Nm**$^{-2}$	**Q(J)**	**Mass flow rate (kg/s)**	**Mass of steam (kg)**
2.0	16896.5	3.5	7.5
4.0	17568.1	4.0	7.8
6.0	18453.9	4.5	8.2
8.0	19107.7	5.0	8.5
10.0	19608.5	5.5	8.7

APPENDIX L: PRESSURE DROP RATIO AGAINST THE STEAM FLOW RATE FOR HTFs

Appendix L shows figures on pressure drop ratio against the steam flow rate produced by the heat transfer fluids at solar power intensities of 1013.2 Wm^{-2}.

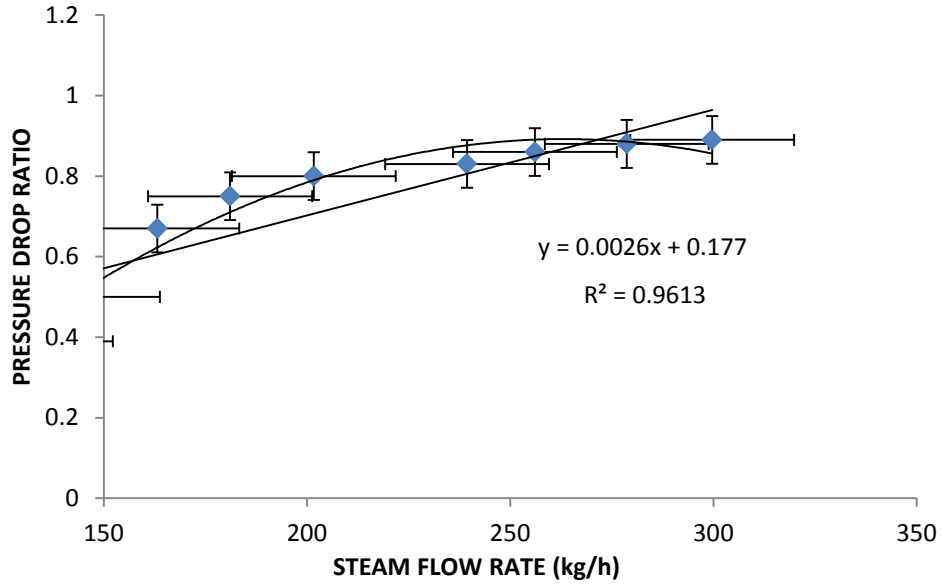

Figure L. 1: Pressure drop against steam flow rate for Vegetable oil 2 on 6.2.2014

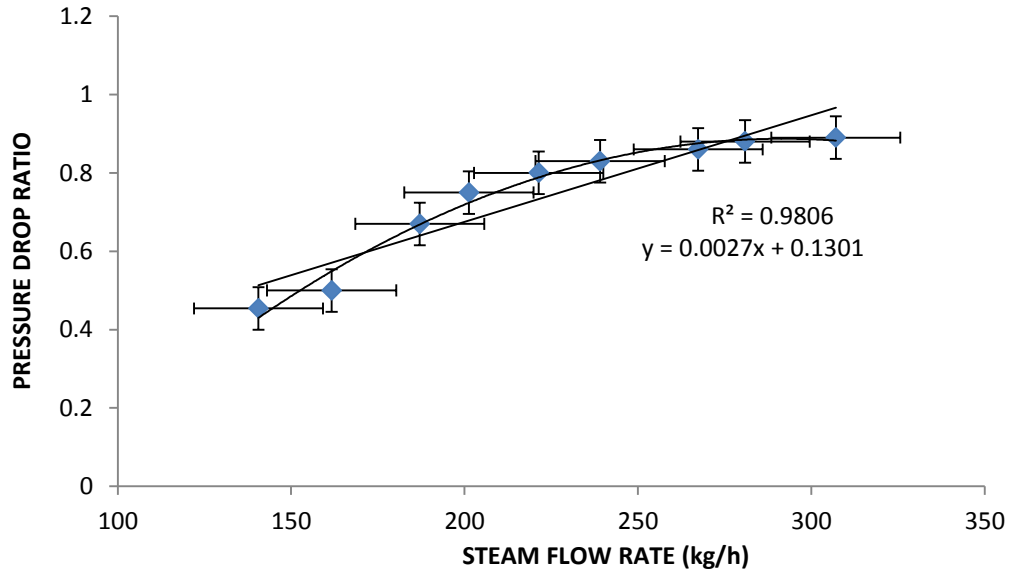

Figure L. 2: Pressure drop against steam flow rate for vegetable oil 1 oil on 7.2.2014

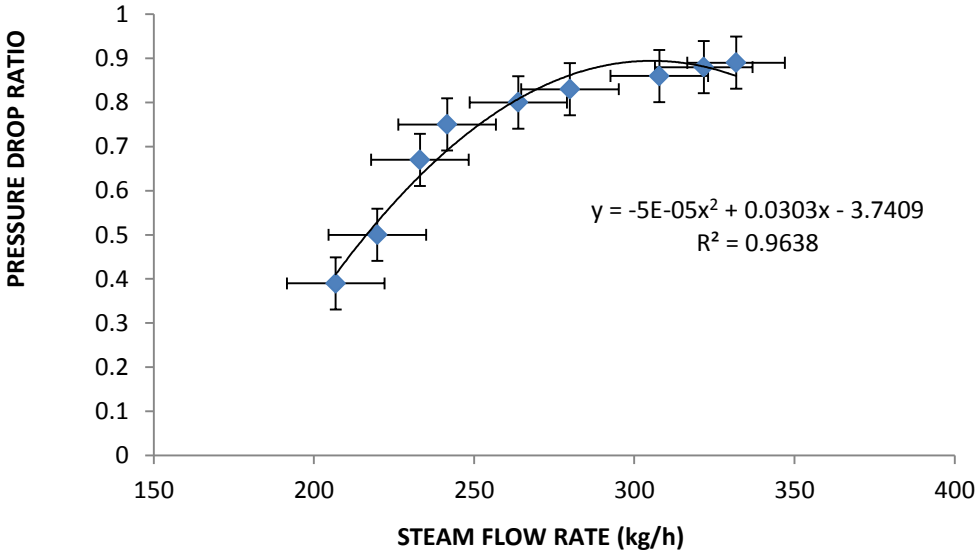

Figure L. 3: Pressure drop against steam flow rate for unused engine oil 8.2.2014

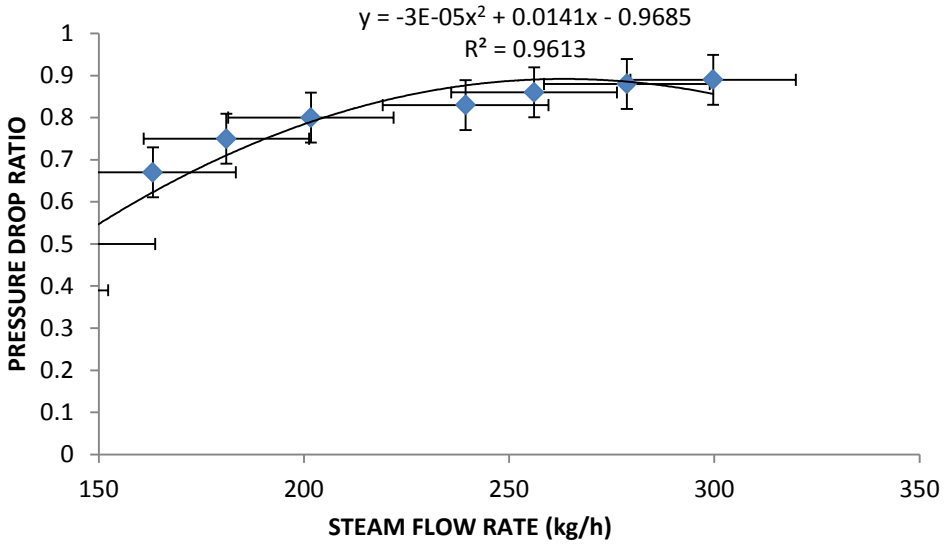

Figure L. 4: Pressure drop against steam flow rate for used engine oil on 9.2.2014

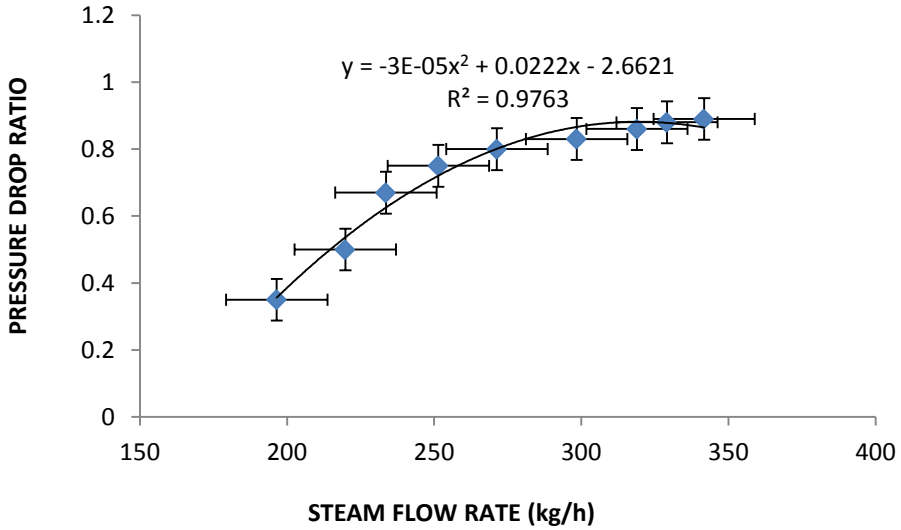

Figure L. 5: Pressure drop against steam flow rate for 2M sodium chloride solution on 10.2.2014

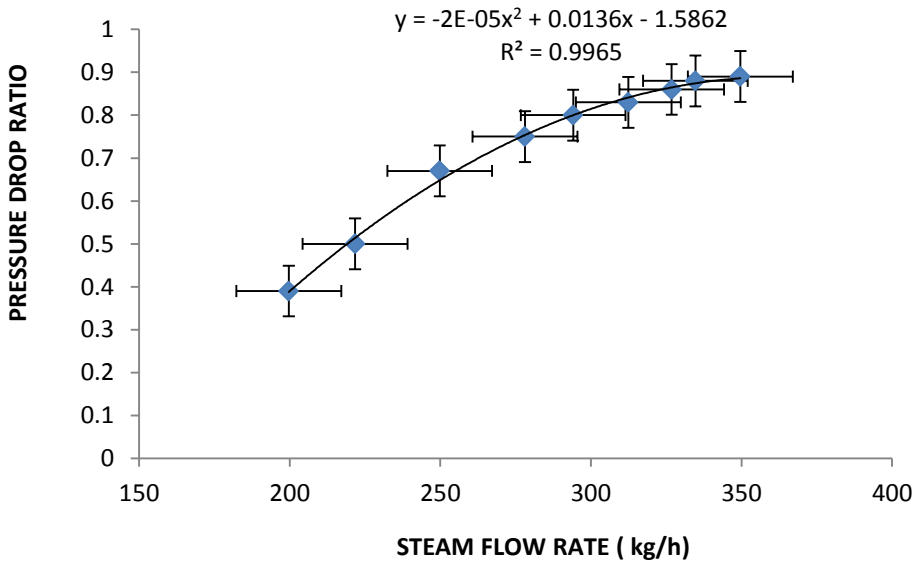

Figure L. 6: Pressure drop against steam flow rate for 4M sodium chloride solution on 11.2.2014

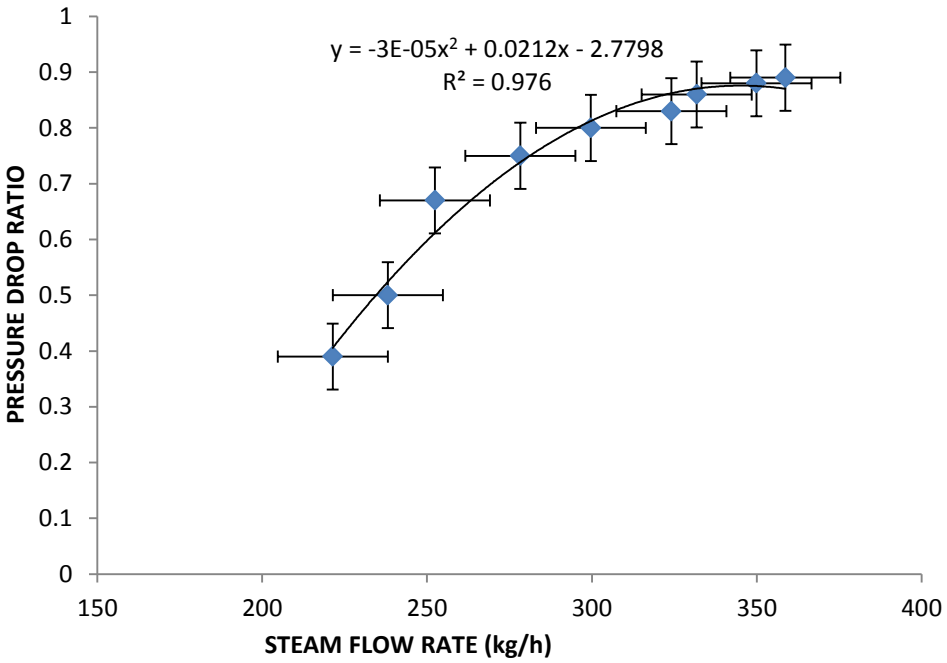

Figure L. 7: Pressure drop against steam flow rate for 6M sodium chloride solution 12.2.2014

APPENDIX M: HEAT OUTPUT AGAINST OUTPUT PRESSURE FOR HTFs

Appendix M shows the heat output against output pressure for the heat transfer fluids at solar power intensities of an average of 907 Wm^{-2}

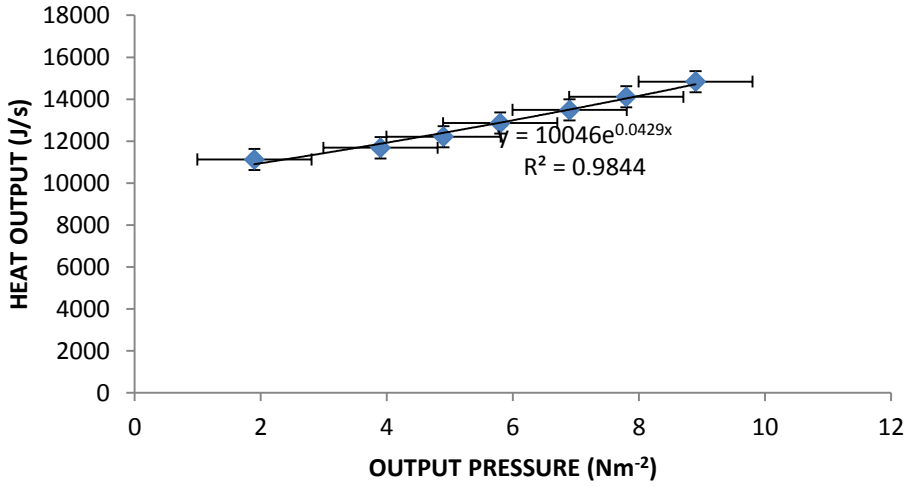

Figure M. 1: Heat absorbed against output pressure for Vegetable oil 2 on 20.2.2014

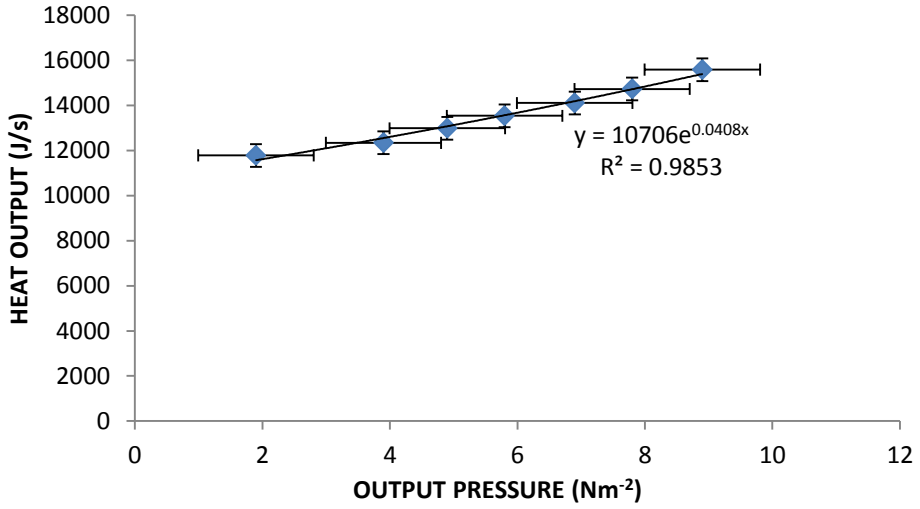

Figure M. 2: Heat absorbed against output pressure for vegetable oil 1 oil on 21.2.2014

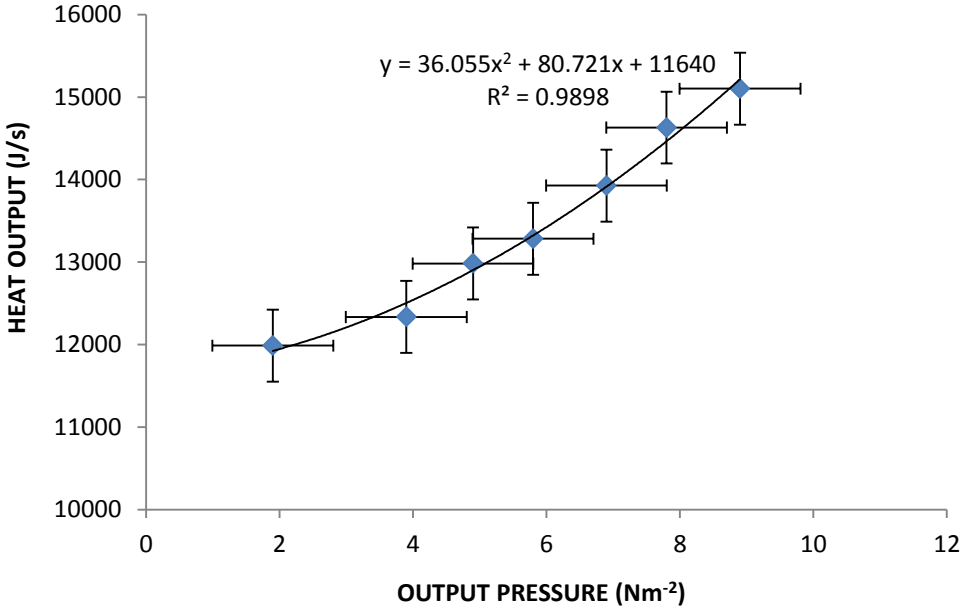

Figure M. 3: Heat absorbed against output pressure for used engine oil on 22.2.2014

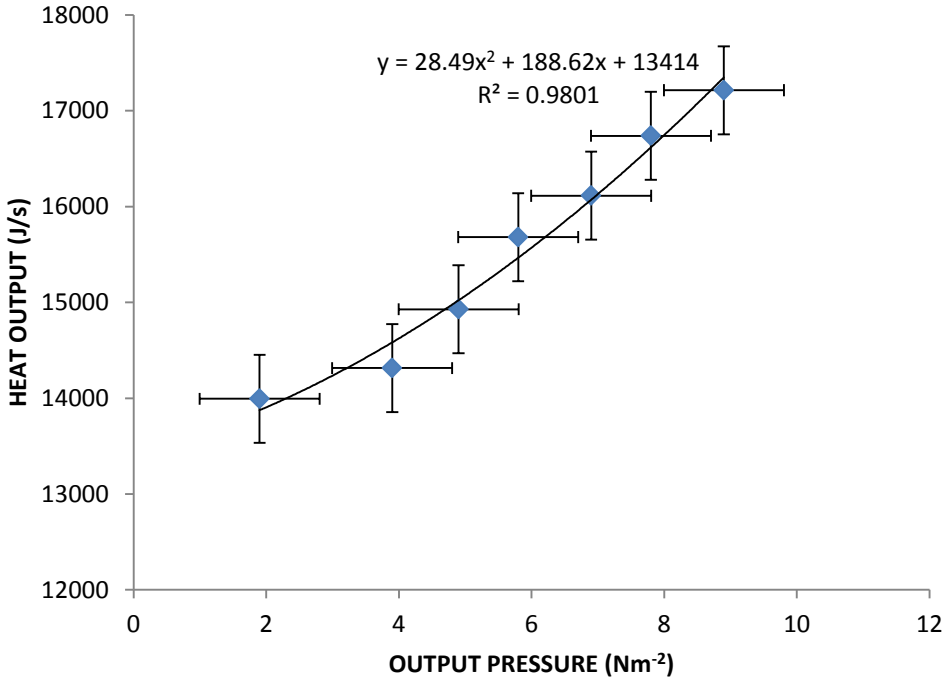

Figure M. 4: Heat absorbed against output pressure for unused engine oil on 23.2. 2014

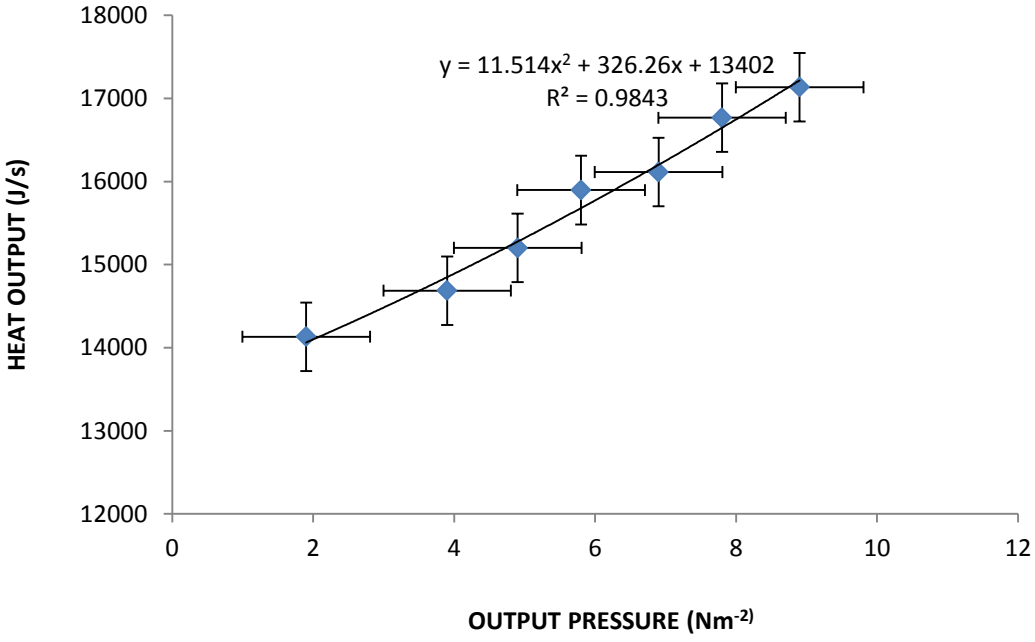

Figure M. 5: Heat absorbed against output pressure for 2M sodium chloride solution on 24.2.2014

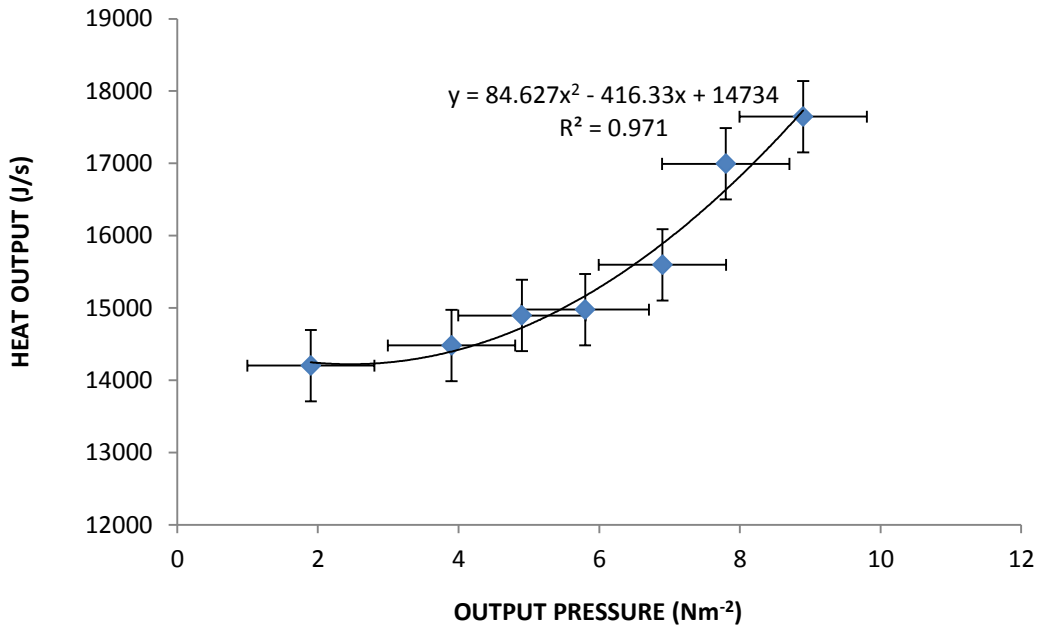

Figure M. 6: Heat absorbed against output pressure for 4Msodium chloride solution on 25.2.2014

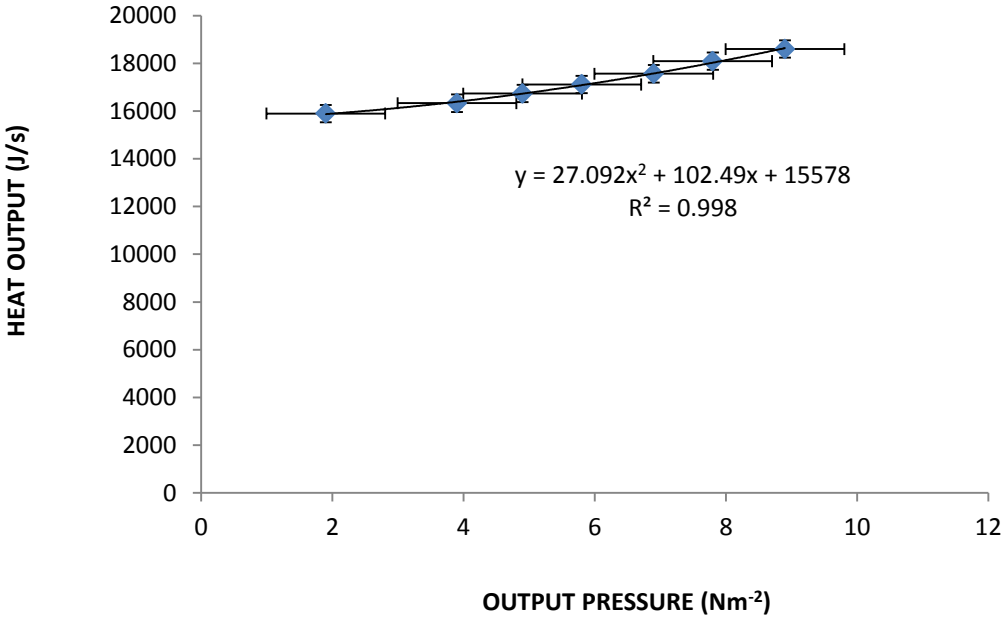

Figure M. 7: Heat absorbed against output pressure for 6M sodium chloride solution on 26.2.2014

APPENDIX N: STEAM FLOW RATE WITH TIME OF DAY FOR HTFs

Appendix N shows the steam flow rate with time of day for the heat transfer fluids at solar power intensities of an average of 1038.2 Wm^{-2}

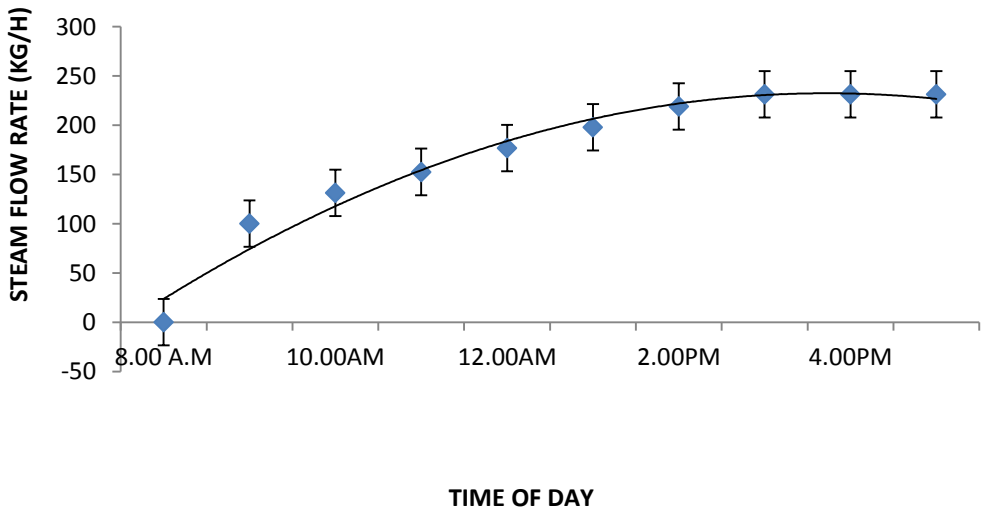

Figure N. 1: Steam flow rate against time of day for vegetable oil 1 oil on 28.2.2014

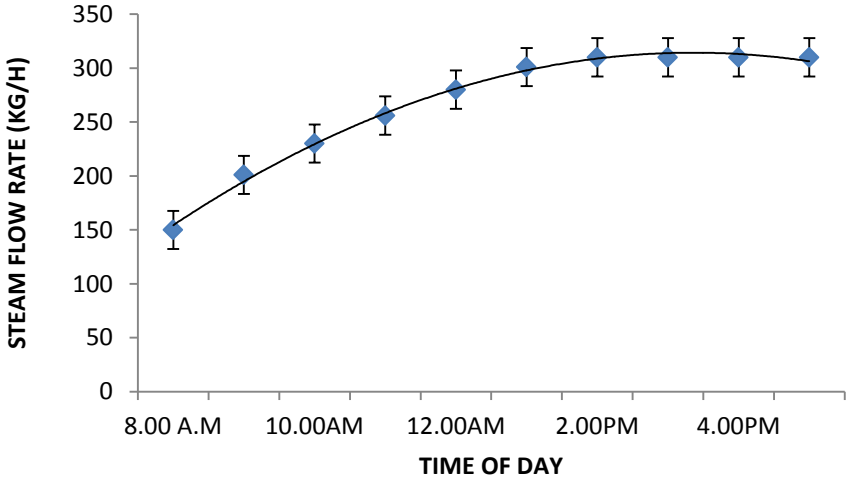

Figure N. 2: Steam flow rate for used oil against time of day for used engine oil on 1.3.2014

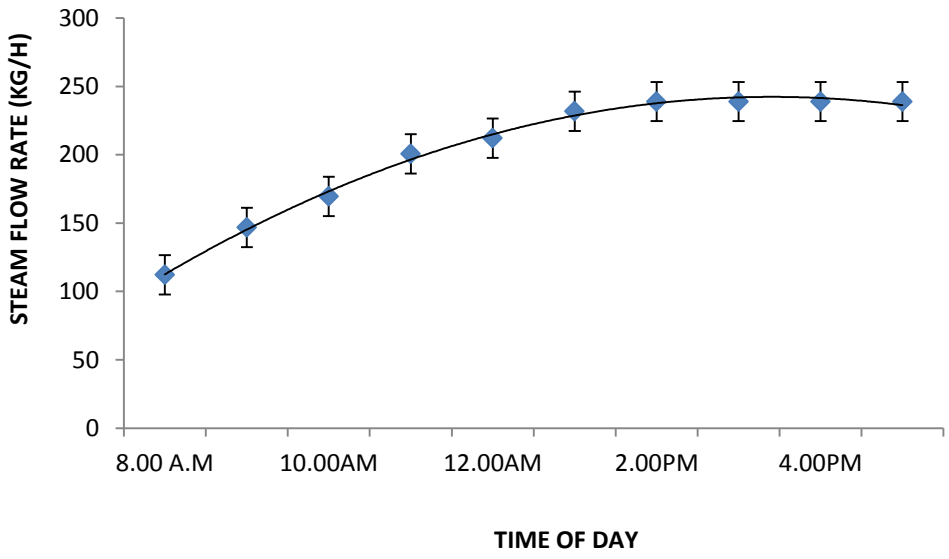

Figure N. 3: Steam flow rate against time of day for unused engine oil on 2.3.2014

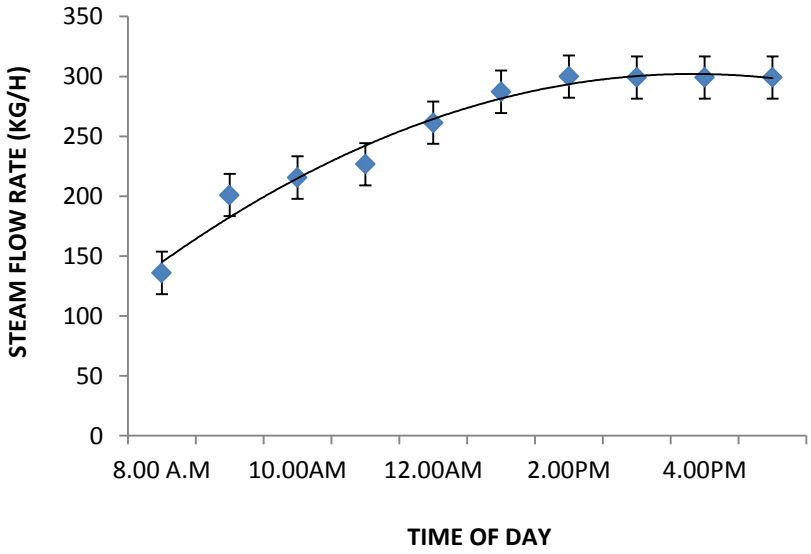

Figure N. 4: Steam flow rate against time of day for 2M sodium chloride solution on 3.3.2014

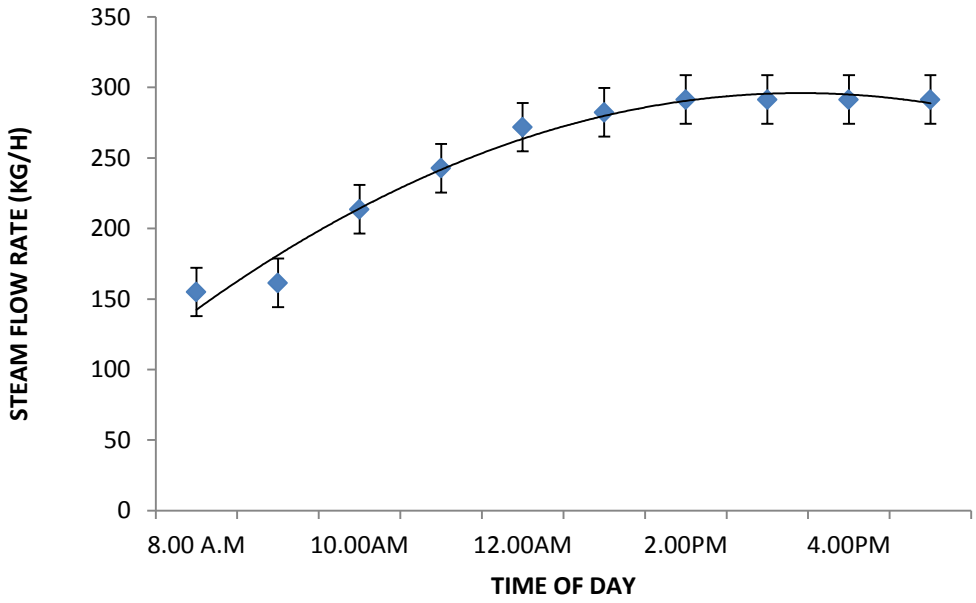

Figure N. 5: Steam flow rate against time of day for 4M sodium chloride solution on 4.3.2014

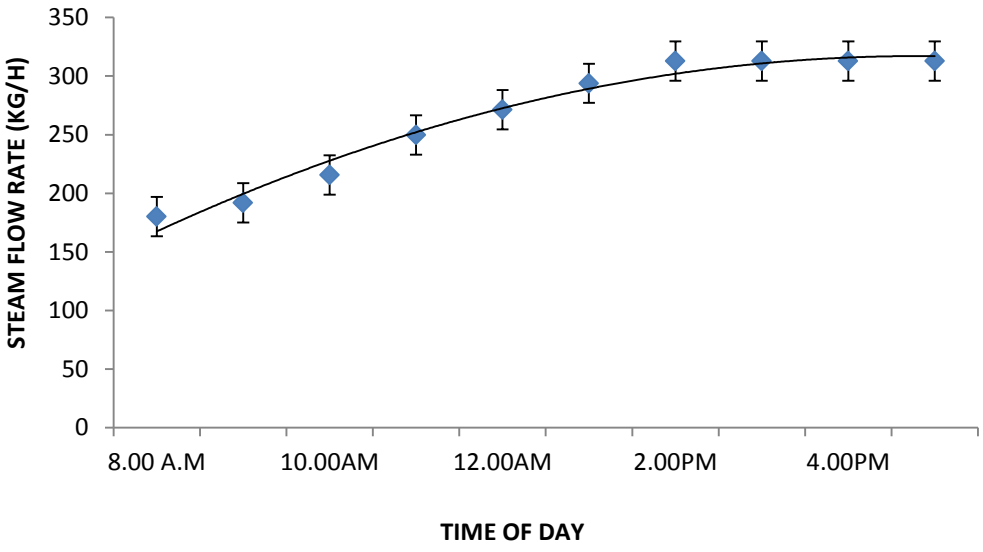

Figure N. 6: Steam flow rate against time of day for 6M sodium chloride solution on 5.3.2014

APPENDIX O: HEAT LOSS FOR THE ABSORBER PIPE

Appendix O shows the heat loss for the absorber pipe with temperature of the heat transfer fluids.

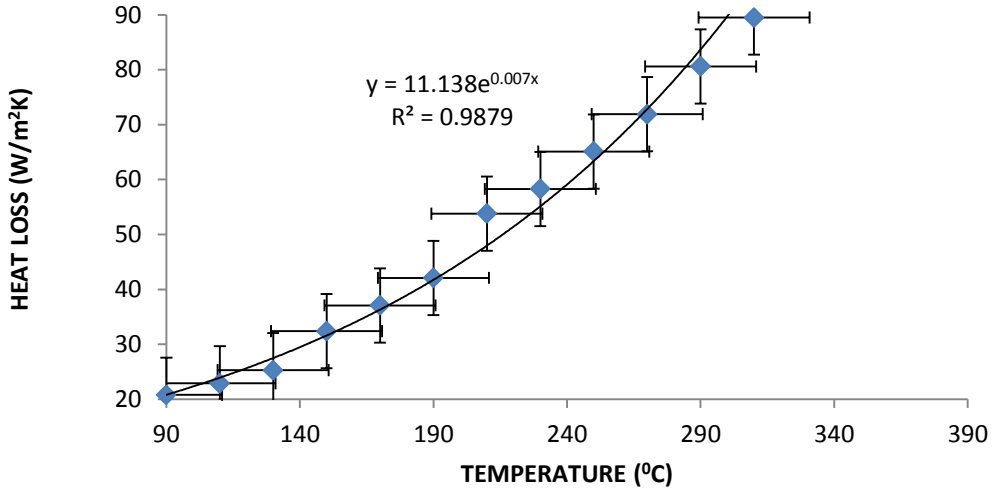

Figure O. 1: Receiver heat loss for 4M sodium chloride solution on 25.10.2013

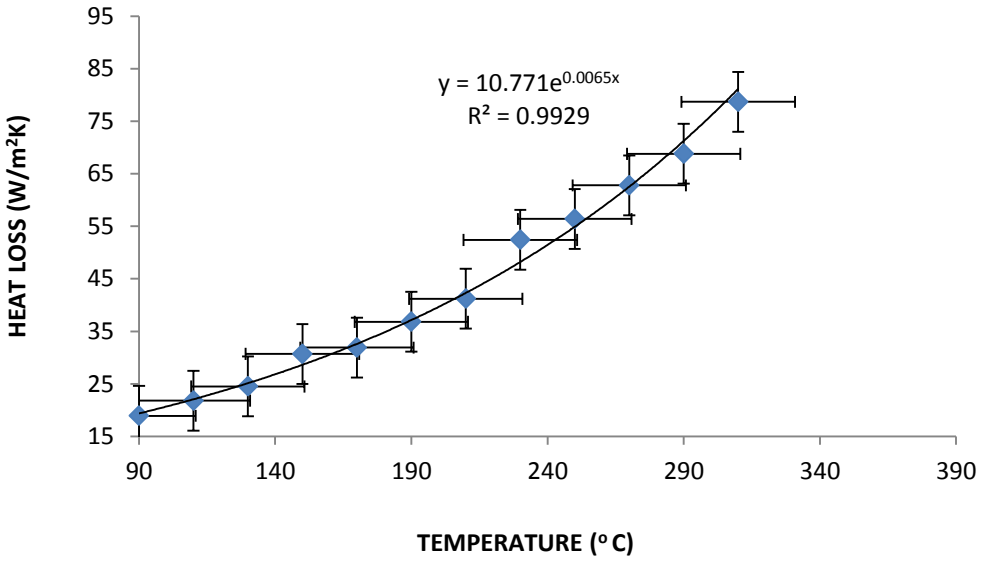

Figure O. 2: Receiver heat loss for 2M sodium chloride solution on 26.10.13

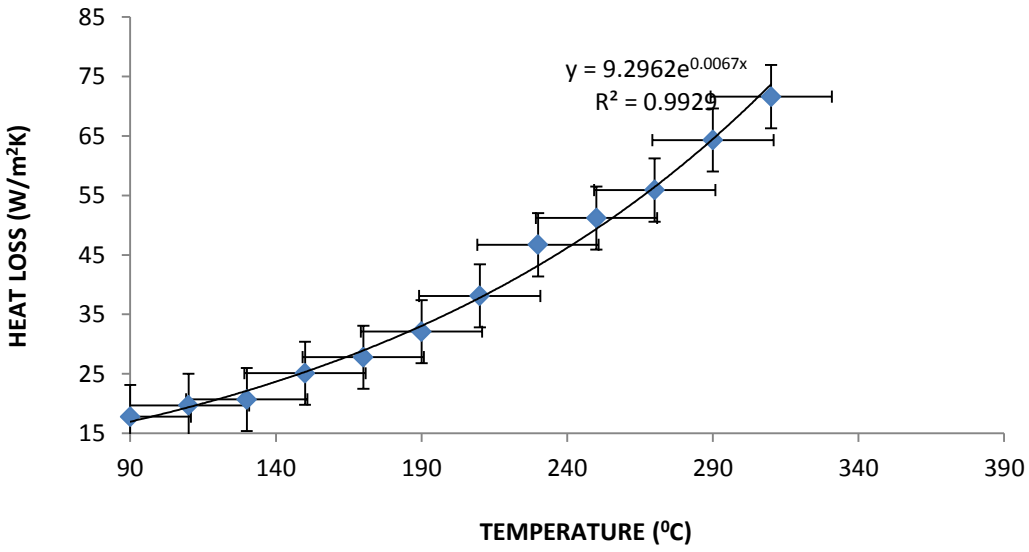

Figure O. 3: Receiver heat loss against operation temperature for unused engine oil on 27.10.13

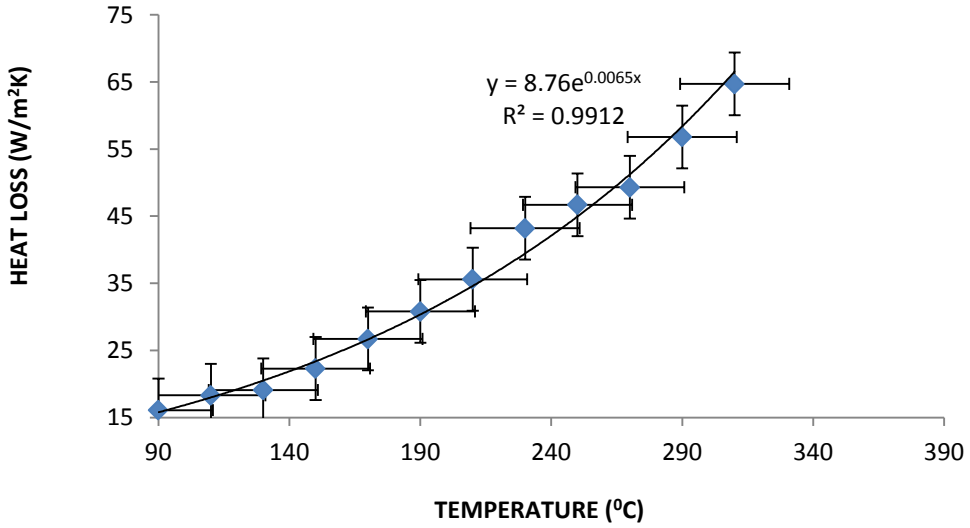

Figure O. 4: Receiver heat loss against operation temperature for used engine oil 28.10.13

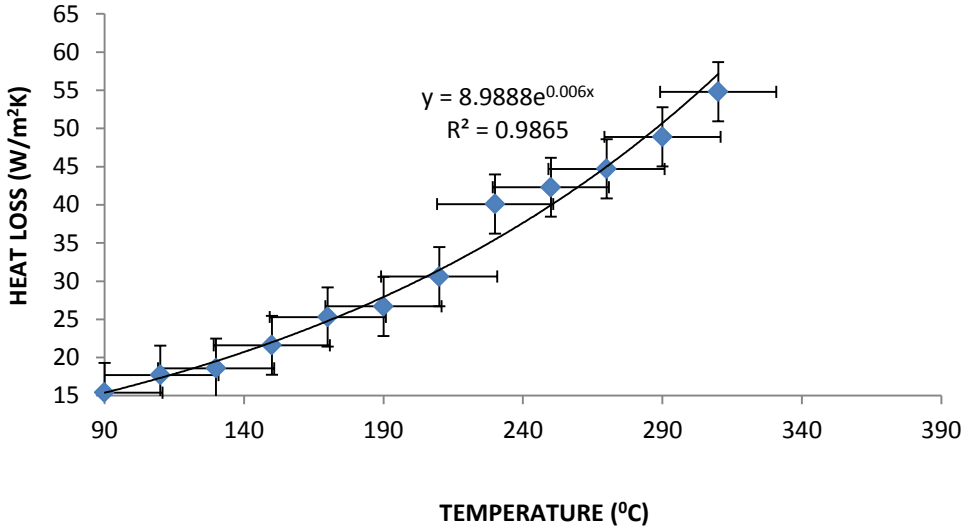

Figure O. 5: Receiver heat loss for Vegetable oil 2 on 29.10.13

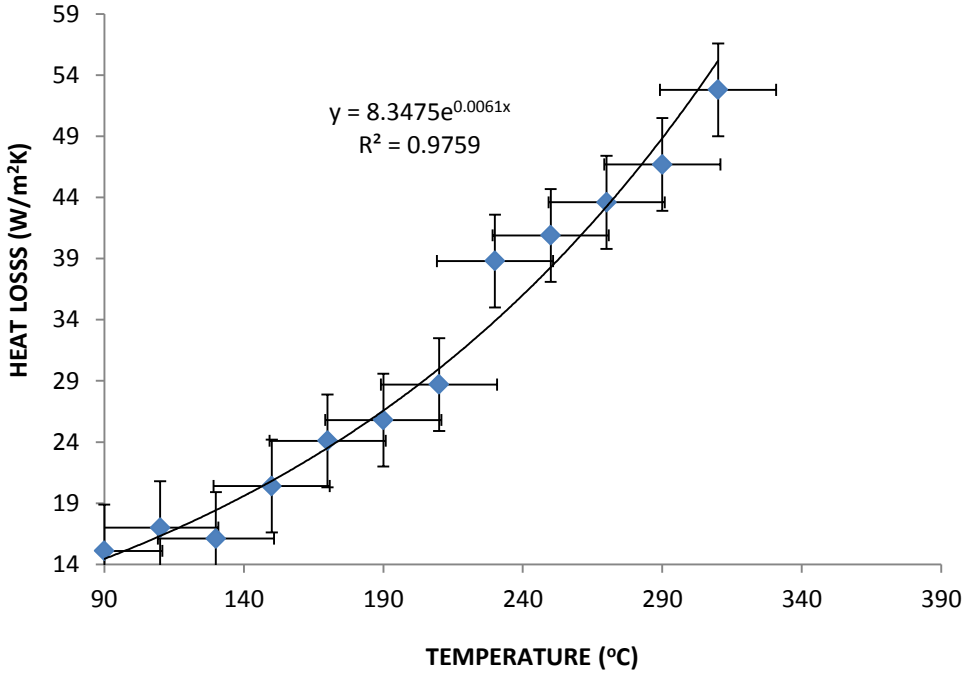

Figure O. 6: Receiver heat loss for against temperature of operation of vegetable oil 1 on 30.10.2013

APPENDIX P: THE AUTO CAD DESIGN FIGURES

Appendix P shows the Auto Cad design figures for the solar collector, turbine rotor and blades, steam storage system, shell and coiled tube heat exchanger.

Figure P. 1: Design and Fabrication of Steam Storage System

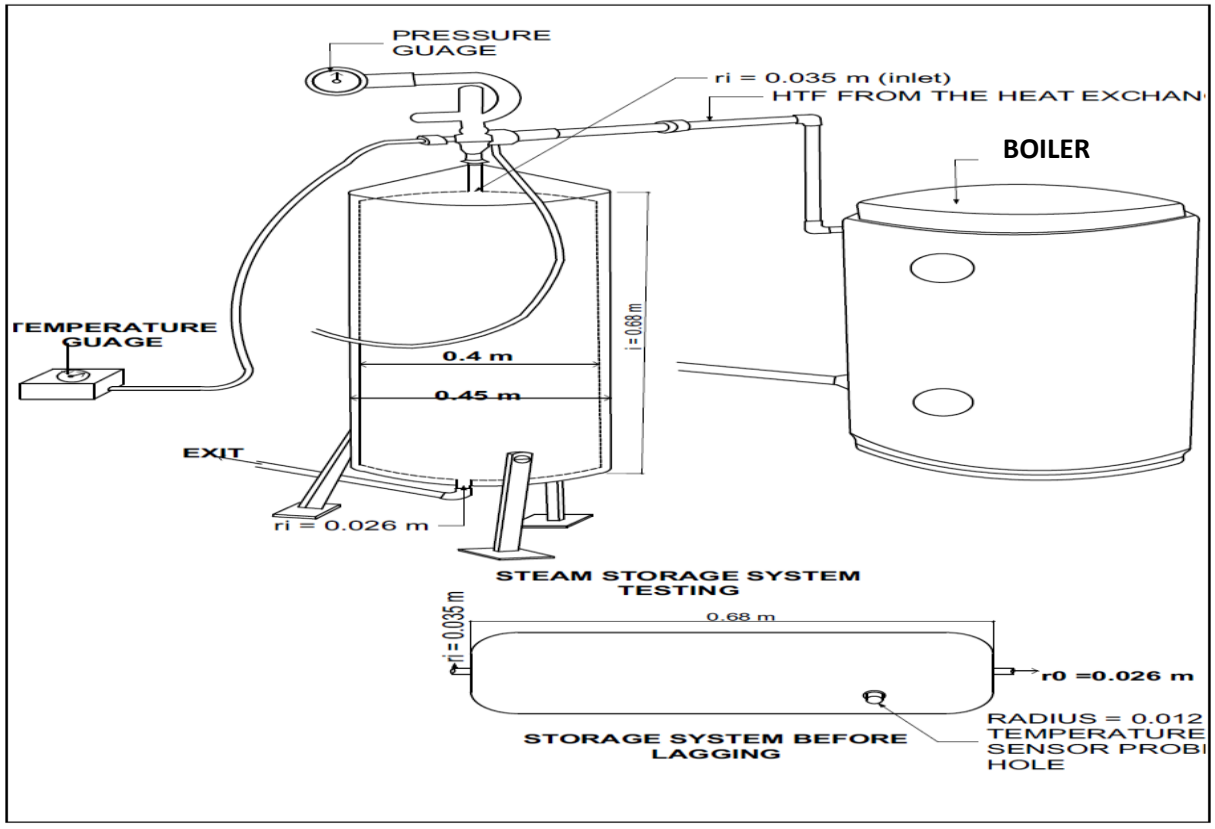

Figure P. 2: Design and Fabrication of Shell and Tube Heat Exchanger

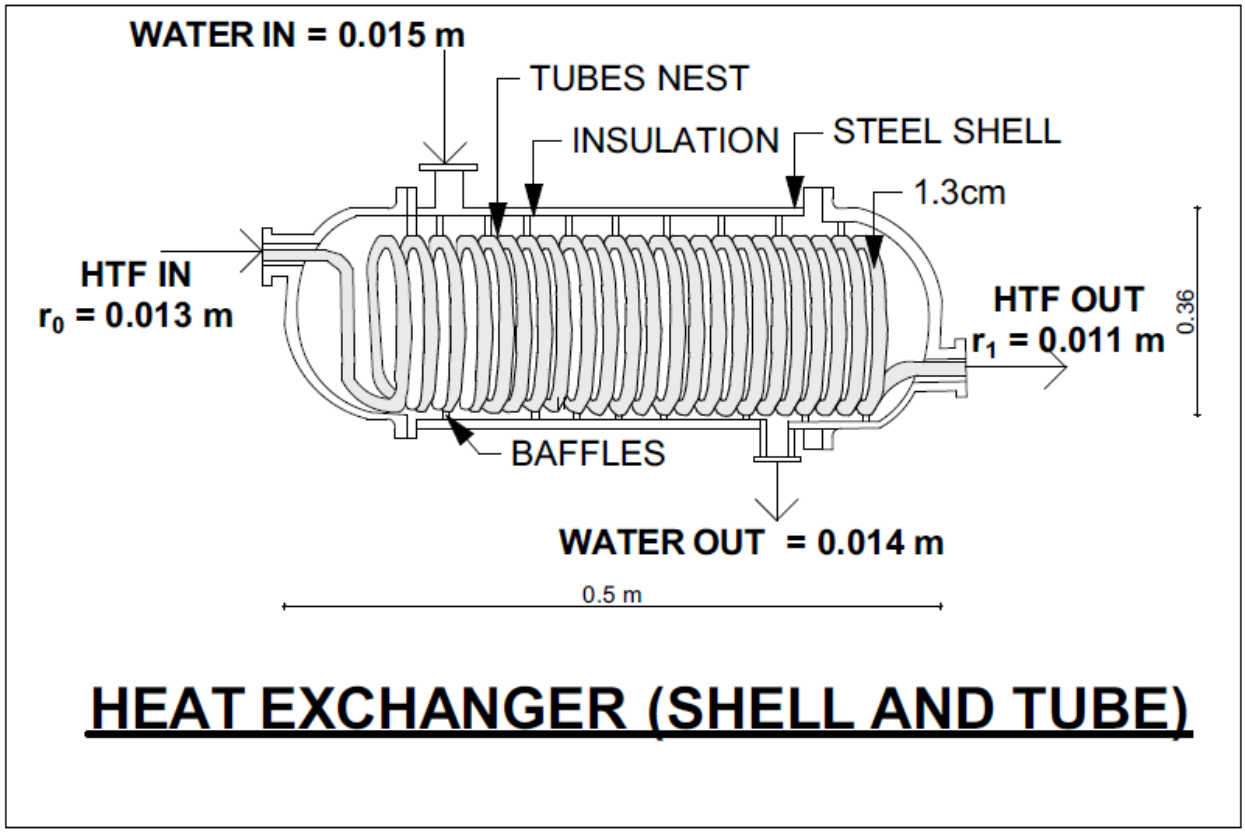

Figure P. 3: Design and Fabrication of Rotor and Blades

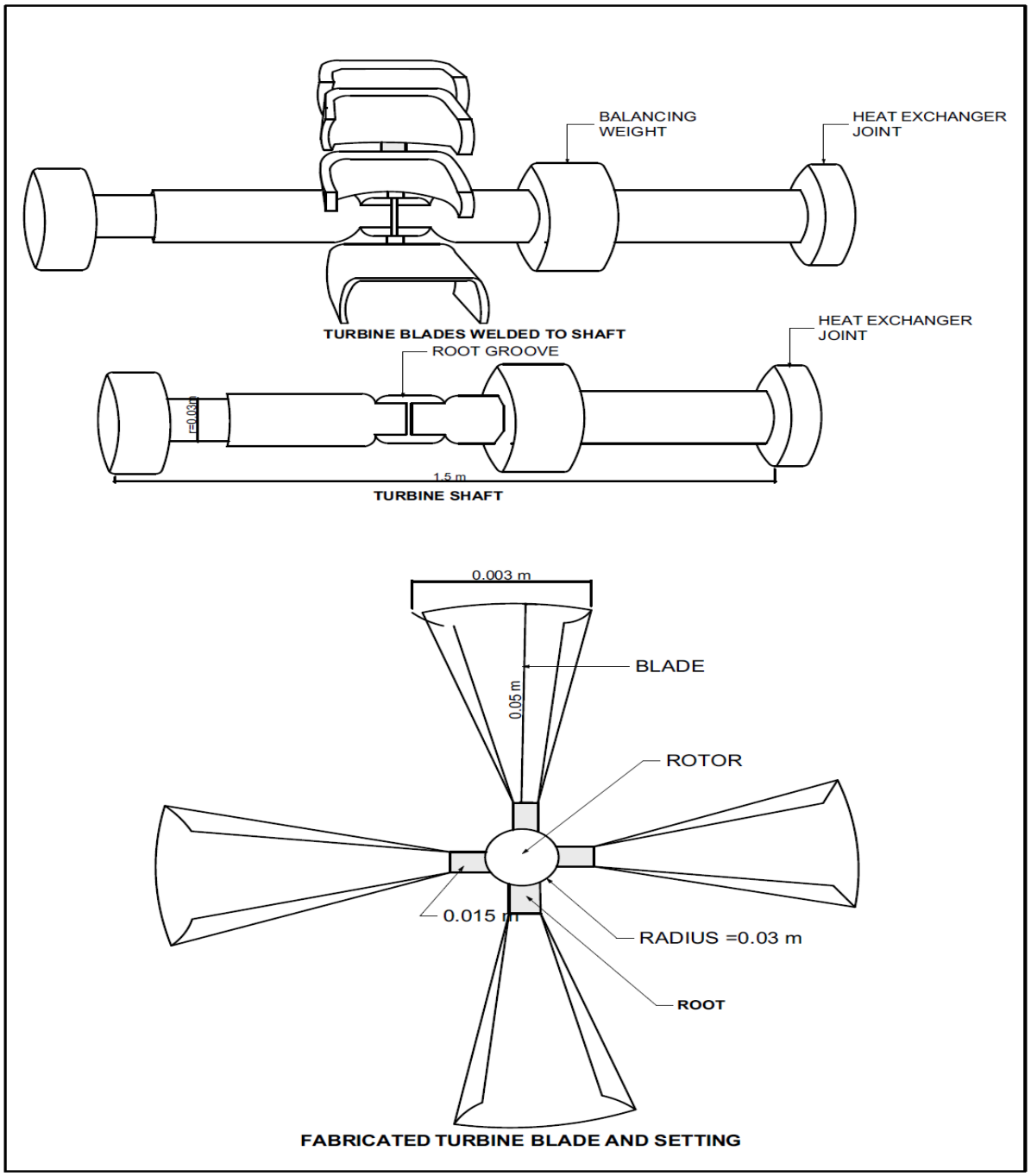

Figure P. 4: Solar Collector Design and Fabrication